Transition Metal Complexes of Novel Phenanthroline Derivatives and their Antibacterial Activity

A thesis submitted to the National University of Ireland in fulfilment of the requirements for the degree of

Doctor of Philosophy

By

Muhib Ahmed, B.Sc.

Department of Chemistry,
Faculty of Science and Engineering,
Maynooth University,
Maynooth,
Co. Kildare,
Ireland.

January 2019

Research Supervisors: Dr Denise Rooney and Dr Malachy McCann

Head of Department: Dr Jennifer McManus

Table of Contents

^{1}H NMR Spectral Data from Stability Testing of **4.2a1**, **4.2a1**, **4.2a1** 261

Declaration of Authorship

I have read and understood the Departmental policy on plagiarism.

I declare that this thesis is my own work and has not been submitted in any form for another degree or diploma at any university or other institution of tertiary education.

Information derived from the published or unpublished work of others has been acknowledged in the text and a list of references is given.

Signed _____ Date _____

Muhib Ahmed

Dedication

I dedicate this to you

Tayyaba and Maqbool Ahmed

Thank you

Acknowledgments

I would like to sincerely thank my two supervisors Dr Denise Rooney and Dr Malachy McCann. You both have constantly supported me throughout my PhD and have always been available to offer me guidance, support and reassurance. I have learned so much from the both of you and I could not have asked for better mentors. Thank you both for your friendship, patience, advice and encouragement all of which made this possible for me. I am also very appreciative of our collaborators; Professor Andre Luis Souza do Santos and Professor Maria Cristina Lourenco for the anti-TB screening, Professor Kevin Kavanagh for allowing me to carry out antimicrobial testing in his lab, Professor Brendan Twamley and Professor Vickie McKee for carrying out the X-ray crystallography work.

I would like to express my gratitude toward the Chemistry Department. My thanks to the previous head of department, Dr John Stephens, and the present head of department, Dr Jennifer McMannus, for affording me the opportunity to work in this amazing department. A special mention also to the academic staff and the technicians for providing help with various equipments during the course of this project. I would also like to thank Maynooth University for awarding me the Pat & John Hume scholarship to complete this PhD. A big thank you to Noel, the guardian angel of the Chemistry Department.

For all of the postgraduate, past and present, thank you all very much for the friendship, the banter, the cakes, the gifts and the supportive chats. Without you all this journey would not have been so enjoyable. I wish you all the best in the future.

Finally, I would like to thank my parents, Tayyaba and Maqbool Ahmed, my siblings, Talha, Razi, Faeza and Wafi, and ofcourse my wife, Aliya. The sacrifices you have all made to support me through the last few years are countless. Thank you, thank you, *THANK YOU*…

Abbreviations

AIDS = acquired immunodeficiency syndrome

ALP = alkaline phosphatase

bs = broad singlet

C. albicans = *Candida albicans*

C. perfingens = *Clostridium perfringens*

CAP = covalently attached protein

CDC = centre of disease control and prevention

CHN% = carbon, hydrogen, nitrogen %

cnge = cyanoguanidine

COSY = correlation spectroscopy

d = doublet

DCM = dichloromethane

dd = doublet of doublet

dH2O = deionised water

DHFR = dihydrofolate reductase

DMSO = dimethyl sulfoxide

DNA = deoxyribonucleic acid

dppn = benzo[*i*]dipyrido[3,2-*a*:2’,3’-*h*]quinoxaline

dppz = dipyrido[3,2-*a*:2',3'-*c*]phenazine

dpq = dipyrido[3,2-*d*:2',3'-*f*]quinoxaline

E. coli = *Escherichia coli*

EDG = electron donating group

EDTA = ethylenediaminetetraacetic acids

EE = ethisterone

EPS = extracellular polymeric substrances

ES = ethynylestradiol

ESI = electron spray ionisation

EtOH = ethanol

EtOAc = ethyl acetate

EWG = electron withdrawing group

ExPEC = extraintestinal pathogenic *E. coli*

FAAS = Flame Atomic Absorption Spectroscopy

FAS = fatty acid synthase

FDA = food and drug agency

G. mellonella = *Galleria mellonella*

HDT = host-directed therapy

HIV = human immunodeficiency virus

HMBC = heteronuclear multiple bond correlation

HPLC = high performance liquid chromatography

HRMS = high resolution mass spectroscopy

HSQC = Heteronuclear single quantum coherence spectroscopy

HUS = haemolytic uremic syndrome

IC = inhibitory concentration

IMP = integral membrane protein

INH = isoniazid

IR = infrared

L. lactis = *Lactococcus lactis*

LC-MS = liquid chromatography-mass spectrometry

LD = lethal dose

LP = lipoprotien

LPS = lipopolysaccharide

LTA = lipoteichoic acid

m = multiplet

M. tb = *Mycobacterium tuberculosis*

MATE = multidrug and toxic compound extrusion

MDR = multidrug resistant

MDR-TB = multidrug resistant tuberculosis

MeCN = acetonitrile

meimzH = methylimidazole

MeOH = methanol

MFS = major facilitator superfamily

MIC = minimum inhibitory concentration

MM = minimal growth media

mp = melting point

MRI = magnetic resonance imaging

MRSA = methicilin resistant Staphylcoccus aureus

MS = mass spectrometry

NAD = nicotinamide adenine dinucleotide

NAIP = 2-(naphthalen-1-yl)-1*H*-imidazo[4,5-*f*][1,10]phenanthroline

NAT = *N*-acetyltransferase

neocuprine = 2,9-dimethyl-1,10-phenanthroline

NMR = nuclear magnetic resonance

OD = optical density

oda = octanedioic acid

OMP = outer membrane protein

P. aeruginosa = *Pseudomonas aeruginosa*

PBP = penicillin binding protein

PBS = phosphate buffer solution

PDR = pan-drug resistant

phen = 1,10-phenanthroline

phendiol = 1,10-phenanthroline-5,6-diol

ppm = parts per million

R = resistant

RNA = ribonucleic acid

RND = resistance modulation division

ROS = reactive oxygen species

s = singlet

S. aureus = *Staphylococcus aureus*

S. pyrogenes = *Streptococcus pyrogenes*

SI = selectivity index

SMR = small multidrug resistant

SOD = superoxide dismutase

t = triplet

TA = teichoic acid

TB = tuberculosis

tdda = 3,6,9-trioxaundecanedioic acid

tip = 2-thiophenimidazo[4,5-f][1,10]phenanthroline

TOF = time of flight

tu = thiourea

UV-Vis = ultraviolet-visible spectroscopy

VRE = vancomycin resistance enterococci

WHO = world health organisation

WTA = wall teichoic acid

XDR = extensive-drug resistant

YEPD = yeast extract peptone dextrose

Abstract

Illnesses caused by microbial species, such as *Mycobacterium tuberculosis* (*M. tb*) are one of the leading the causes of mortality worldwide[1]. The emergence of drug-resistant strains of microbes has led to an urgent demand of novel antibiotics. Derivatives of 1,10-phenanthroline (**phen**) and their metal complexes have been shown to possess antimicrobial effects[2].

The first part of research carried out in this study involves synthesis and characterisation of oxazine-based derivative of **phen** and its Ag(I), Cu(II) and Mn(II) complexes. The antimicrobial effects of this ligand and its metal complexes were studied using a Gram-positive (*Staphylococcus aureus)* and Gram-negative (*Escherichia coli*) bacteria and a fungal (*Candida albicans*) strain. In addition, lipophilic derivatives of the oxazine-based **phen** derivatives and its Cu(II) complexes were also prepared, characterised and screened against Gram-positive bacterial strain. The toxicity of all of these ligands and their complexes was also studied using the greater wax moth larvae *Galleria mellonella*. The Cu(II) complexes were the most active towards the Gram-positive bacteria and the increase in lipophilicity, up to a certain point, displayed an increase in antibacterial activity of the ligand and its Cu(II) complex. The Ag(I) complex was the most active towards the fungal strain. The compounds tested did not display promising activity towards the Gram-negative bacterial strain. All compounds tested were well tolerated by *Galleria mellonella*.

Second part of this research focuses on targeting *M. tb* by derivatising isoniazid (**INH)** through Schiff base condensation. A **phen**-based hybrid of **INH** is prepared and complexed to Ag(I), Cu(II) and Mn(II) metal ions and the ligand and metal complexes were characterised. The antimycobacterial activity of this ligand and its metal complexes was studied against a drug susceptible and three drug resistant strains of *M. tb*. The broad-range antimicrobial activity of this ligand and its metal complexes was also studied against Gram-positive (*Staphylococcus aureus*), Gram-negative (*Pseudomonas aeruginosa*) and fungal (*Candida albicans*). The toxicity of these compounds toward the mammalian cell line A549 was also examined. All of the compounds generated displayed promising antimycobacterial activity towards all

strain of *M. tb* and presented SI values >10. The Ag(I) complexes displayed excellent broad range antimicrobial activity.

Chapter 1

Introduction

Chapter Structure

This chapter has been designed with the intention of introducing key concepts upon which the scientific work is based. The aim of this chapter is to acquaint the reader with the clinical relevance of bacterial infections and how to tackle these infections by modification of **phen** to form potent antibacterial agents and to enhance their activity via metal complexation to offer multiple modes of action to achieve antibacterial activity. The chapter is composed of three main sections:

1. Bacteria, bacterial infections and current treatments: This involves an introduction to the microorganisms known as bacteria, their classification as Gram-positive and Gram-negative with the use of Gram-staining, and the mechanical structural differences between these two classes. *Mycobacteria* (which cannot be classified by the Gram staining method) is also introduced. Examples of bacteria belonging to each class, infections caused by these bacteria, the current treatments employed in the clinical settings to treat these illnesses, and the emergence of resistance to these antibiotics is also discussed.
2. Antibacterial activity of metal complexes: An overview of research published on antibacterial activity of Cu(II), Ag(I), Mn(II) metal ions, and their complexes is outlined. The antibacterial activity of **phen**, its derivatives, and their respective metal complexes is summarised along with the mechanisms of action employed by these metal complexes.
3. *Mycobacterium tuberculosis* and anti-tubercular agents: An introduction to *M. tb* is given along with the current regime of first-line drugs utilised to target tuberculosis. The remainder of the section is focused on **INH** (a potent first-line drug), its mechanism of action, the development of resistance by *M. tb* towards **INH**, and strategies utilised to modify **INH** *i.e.* Schiff-base formation and metal complexation, to overcome isoniazid resistance. The antimycobacterial activity of **phen**, its derivatives, and their metal complexes is also outlined along with the antimycobacterial mode of action of one derivative of **phen**.

1.1 Bacteria, Bacterial Infections and Current Treatments

1.1.1: Introduction to Bacteria

1.1.1.1: Bacteria

Bacteria belong to prokaryotic microorganism domain and are considered to be amongst the earliest organisms to appear on earth[3]. These microorganisms are the most diverse and abundant form of life on earth, with billions of bacterial cells in nearly every square meter of soil, water and air[4]. Over the millennia these simple unicellular organisms have evolved to inhabit even the harshest of environments and can be found in acidic hot springs, radioactive waste[5], and deep portions of the earth's crust.

Bacterial cells are usually 0.5 – 5.0 µm in length, about one tenth of eukaryotic cells, and can adopt a number of morphologies depending on their environment, cell wall and cytoskeleton[6]. The most common shapes of bacteria are spherical, called *cocci*, or rod-shaped, called *bacilli*, or spirals, called *spirilla* if they are rigid or *spirochetes* if they are flexible[7]. Though many bacterial cells exist as single cells; some can grow as doublets (such as *Neisseria*), or chains (such as *streptococci* which causes strep throat), or clusters in the shape of grapes (such as *staphylococci* which causes food poisoning), and even further complicated structures.

1.1.1.2: Applications of Bacterial Organisms

Due to their vast diversity and biological functions, bacteria play vital roles in a myriad of industrial, environmental, medical, and research processes:

- In the food industry bacteria such as *Lactococcus lactis* are used to make dairy products such as buttermilk, yogurt, and cheese via fermentation. Through the same process, many food products can be preserved in their pickled form[8].

- In the sewage industry bacteria are used for bioremediation: biological cleansing of the environment. Bacteria break down organic and inorganic matter in the sewage through both aerobic and anaerobic processes[9]. Under aerobic conditions, bacteria are responsible for nitrification and phosphorus removal[10], and under anaerobic conditions bacteria removes nitrates from sewage via reduction of nitrates to dinitrogen gas[11].

- Recent studies have shown that certain bacterial species can also be used to clean up oil spills[12]. In the same way, different strains of bacteria are utilised to recover precious metals such as gold and palladium and are now even being considered for bioremediation of radioactive waste[13].

- In the environment bacteria act as decomposers, digesting organic remains via biochemical reactions necessary for the ecosystem to provide important nutrients such as the products from the nitrogen cycle and the carbon cycle[3].

- Due to the ability of certain bacteria to grow at exponential rates with relative ease, genetic engineering and molecular biology has developed methods to alter bacterial DNA for the purpose of researching the results of gene modification. These techniques can be exploited to produce beneficial natural products such as insulin, growth factors and antibodies[14].

With other living organisms, bacteria can form symbiotic relationships which can be: 1) mutualistic, where both organisms benefit *e.g:* release of vitamins K and B_{12} from bacteria in human intestines; 2) commensalistic, where only one organism benefits *e.g: Streptococcus pyogenes* in the nose favours the bacteria without causing harm to the host; 3) parasitic, where one organism benefits but harms the other organism *e.g: Vibrio cholera*e causes cholera[15].

Though the majority of bacterial species can be used for our benefit, pathogenic bacteria have once again recently become a cause for major concern worldwide. With the discovery of multidrug resistant (MDR) strains of bacteria such as methicillin-resistant *Staphylococcus aureus* (MRSA), multidrug resistant *Mycobacterium tuberculosis* (MDR-TB), “pan-resistant” strains of *Pseudomonas*

aeruginosa and *Acinetobacter baumanii*, there is an immediate necessity for development of novel therapeutics[16].

1.1.2: Classification of Bacteria by Use of Gram Stain

1.1.2.1: Cell Envelope and Gram Stain

One of the key components of the bacterial cell envelope (the cell wall and associated membranes) is peptidoglycan, a polymer of β 1→4 linked derivatised sugars, *N*-acetyl-D-glucosamine, and amino acid, *N*-acetylmuranic acid, extensively cross-linked by short peptide bridges[17,18]. Peptidoglycan helps maintain the structural shape of the cell, providing strength, rigidity, and osmotic stability. Depending on the thickness of this peptidoglycan layer, the bacterial cell can either retain or lose the crystal violet dye, a technique developed by Hans Christian Gram to distinguish between bacterial cells[19]. Gram-positive bacteria, such as *Staphylococcus aureus* (*S. aureus*), have a peptidoglycan layer of 30 – 100 nm in thickness[20] which retains the crystal violet dye. On the other hand, Gram-negative bacteria have a peptidoglycan layer of 2 – 3 nm thickness[21] and are not capable of retaining the dye. Most bacteria can be categorized into either of the two classes as Gram-positive or Gram-negative based on the outcome of this test.

The structural differences between the cell envelope of Gram-positive and negative bacteria can be seen in **Figure 1**.

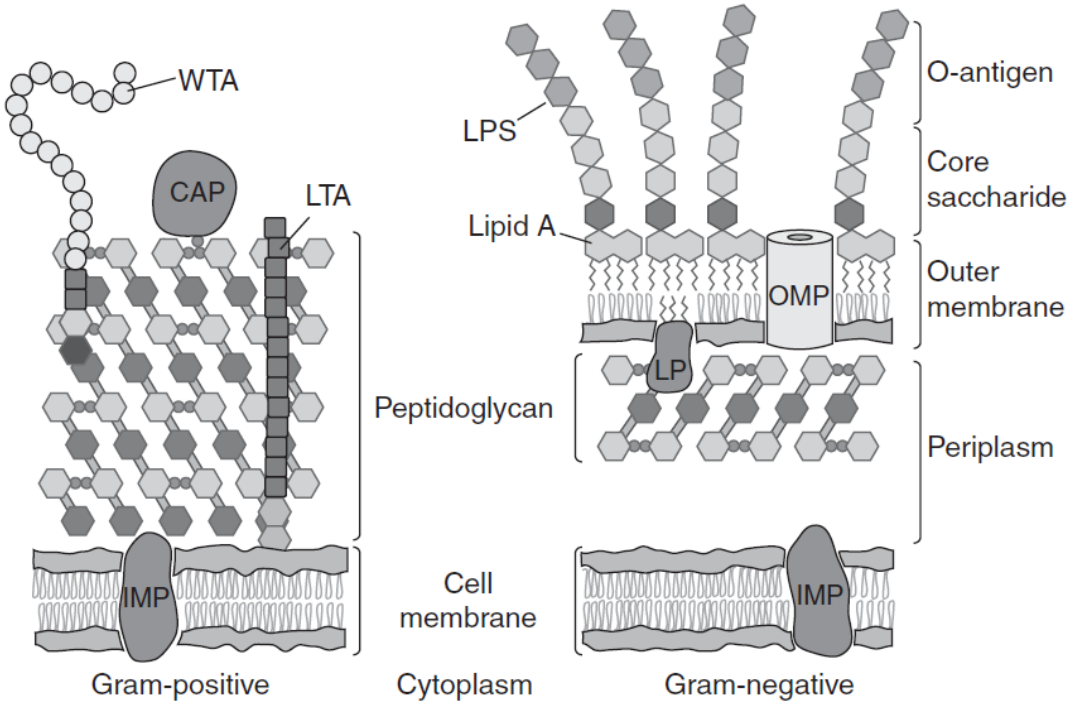

Figure 1: Structural components of Gram-positive and Gram-negative bacterial cell envelop[20]: CAP (covalently attached protein); IMP (integral membrane protein); LP (lipoprotein); LPS (lipopolysaccharide) LTA (lipoteichoic acid); OMP (outer membrane protein); WTA (wall teichoic acid).

1.1.2.2: Gram-positive Bacteria: *Staphylococcus aureus* (*S. aureus*)

Due to their thicker mesh of peptidoglycan layer, Gram-positive bacteria are structurally very strong (**Figure 1**). During the Gram-stain test, once the crystal violet dye precipitates inside the cell it can no longer exit the cell during the decolourization stage due to the small pore size of the peptidoglycan mesh[19]. Embedded in the peptidoglycan layers are teichoic acid (TA) which are acidic polymers of glycerol phosphate, ribitol phosphates or glucosyl phosphates[17]. These TAs can be found either in the peptidoglycan, known as wall teichoic acids (WTA) extending perpendicularly to the cell wall, or appended onto the cell membrane, known as lipoteichoic acids (LTA)[20]. These TAs serve the Gram-positive cells in many different essential biological functions, majority of which can be classified as: 1) protection; 2) biomolecule regulation and; 3) binding to receptors and surfaces[22].

The presence of the phosphate groups of the WTA and LTA provide an anionic net charge, leading them to be described as "continuum of anionic charge"[20]. Due to this, they regulate the cationic uptake by actively binding to the cations[23], which then in

turn effects the rigidity and porosity of the cell wall. Cationic peptides have been shown to selectively disrupt biological functions of bacterial cell versus mammalian cells due to their ability to bind to the inherent anionic nature of bacterial cell walls[24]. By the same token, it can be postulated that cationic metallodrugs could also target bacterial cell due to their cationic nature[25]. Interestingly, modifications of the TAs via insertion of amino acids (D-alanine) or other cationic biomolecules to lower the overall anionic net charge have been observed to lead to resistance to cationic antibiotics such as vancomycin[26]. Furthermore, due to the lipophobic nature of the TAs, the bacterial cells gain resistance towards highly lipophilic antibacterial fatty acids, such as those released from the human skin and thus allowing Gram-positive bacteria to thrive on human skin[27].

S. aureus belongs to the staphylococci genus which are Gram-positive cocci bacteria that form grape-like clusters (**Figure 2**) due to their ability to grow in multiple planes[3]. They are non-motile and can be found on the skin, the nasal cavity, the lower reproductive tract of women, and the respiratory tract of ~30% healthy humans[28,29]. Although these bacteria exist in a commensal relationship with humans, they are classified as pathogens due to their ability to form colonies and infect both immuno-competent and immune-depressant hosts[30].

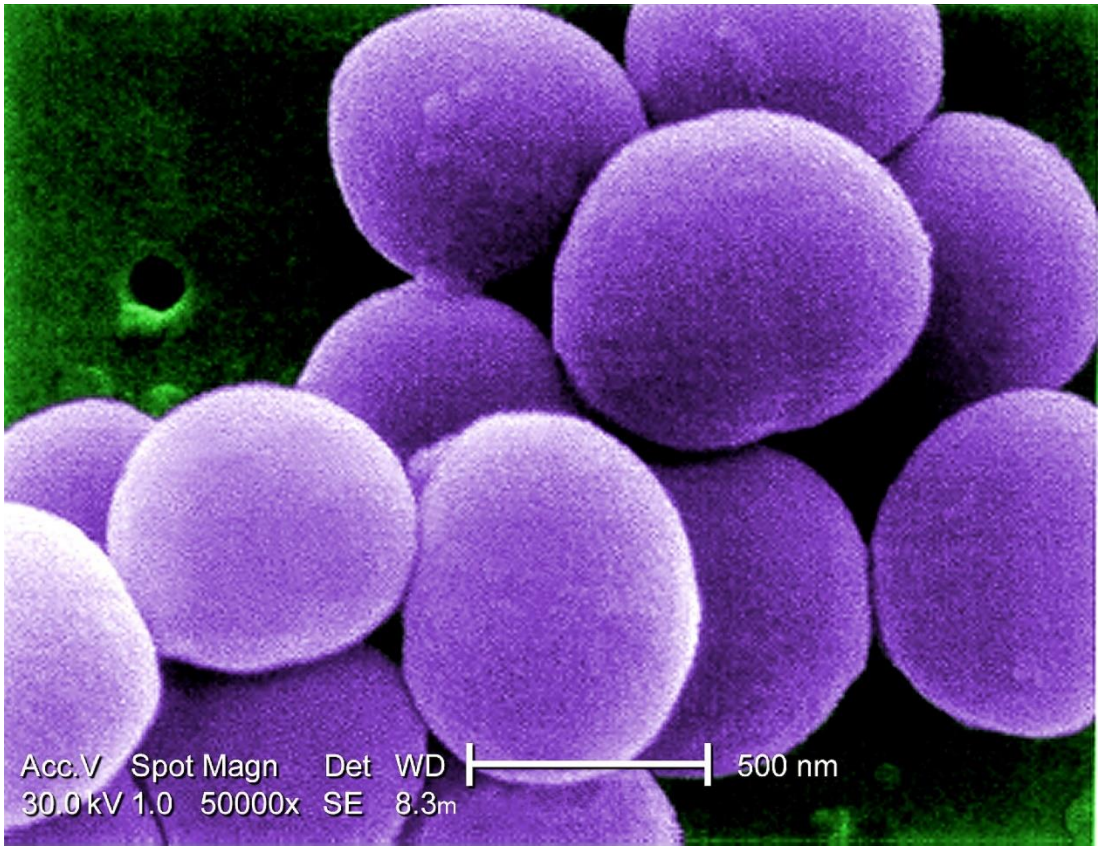

Figure 2: Morphology of S. aureus[3]

In the majority of cases, *S. aureus* is prevented from causing infections by the skin and mucous membrane. However, if these are breached (by cuts, surgery or trauma) and the bacteria is allowed to enter through these cavities then it can lead to abscess lesion or septicaemia once it enters the blood or lymphatic channels[31,32]. Diseases caused by *S. aureus* typically can be categorized into[33]:

- Food poisoning.
- Bacteremia: blood stream infections such as ineffective endocarditis, septic arthritis that are considered life-threatening.
- Skin Infections: these include impetigo, boils and soft-tissue infections. In young children staphylococcal scalded skin syndrome, caused by exfoliative toxins of *S. aureus,* is a major concern and causes major damage to the epidermal layer of the skin[34].

- Bone infections: bone-joint or metal-biomaterials in the body can be infected by *S. aureus* to lead to serious and even life threatening conditions such as osteomyelitis[35].
- Implant Infection: The outermost surface of the *S. aureus* is embedded with adhesins which adhere to proteins found in plasma and extracellular matrix. Due to this, *S. aureus* is a major cause of concern because of its ability to form biofilms on implants leading to serious infections[30].

Since *S. aureus* can be found on healthy humans in such a high abundance, it is no surprise that this opportunistic pathogen becomes such a grievous threat in environments such as hospitals where there is an abundance of immuno-depressant patients. Furthermore, due to the gathering of such various strains of *S. aureus* present concurrently, the formation of antibiotic-resistant strains of the bacteria is also very likely[36]. This is further supported by the fact that *S. aureus* is the second biggest contributor to nosocomial infections[37].

The treatment for mild *S. aureus* infections is to prescribe penicillin which is from the family of β-lactams (**Figure 3**) and acts on the disruption of peptidoglycans by binding to penicillin-binding proteins (PBPs) and thus inhibiting cell wall synthesis. However, in the majority of cases the effect of penicillin is greatly reduced due to the emergence of penicillin resistance strains that produce β-lactamase. Due to this, the majority of β-lactam containing antibiotics have been rendered inefficient against *S. aureus*. Furthermore, the most troublesome strain of *S. aureus* is the methicillin-resistant strain MRSA as it produces a specific PBP, the PBP2′ which allows the synthesis of the cell wall in the presence of β-lactam antibiotics[38].

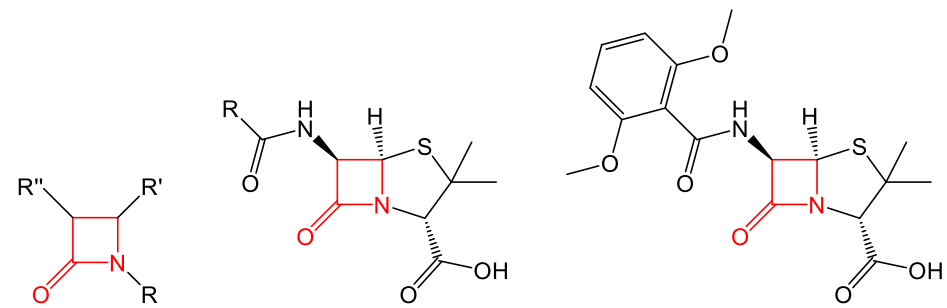

ß-lactam ring **penicillin** **methicillin**

Figure 3: chemical structure of β-lactam based antibiotics

Currently, vancomycin (**Figure 4**) is the drug prescribed for MRSA infections and it inhibits the peptidoglycan cross-linkage formation by binding to amino acids found in the peptidoglycan layers[30]. However, with the ability to form resistance to antibiotics that *S. aureus* possesses, it is no surprise then that there are already reported cases of vancomycin resistant strains of *S. aureus*[39]. Furthermore, in the majority of cases genes responsible for the resistance mechanism can be found on the plasmids. This leads to rapid spread of resistance to other bacteria, and therefore it is only a matter of time before the resistance to vancomycin becomes a common issue[40].

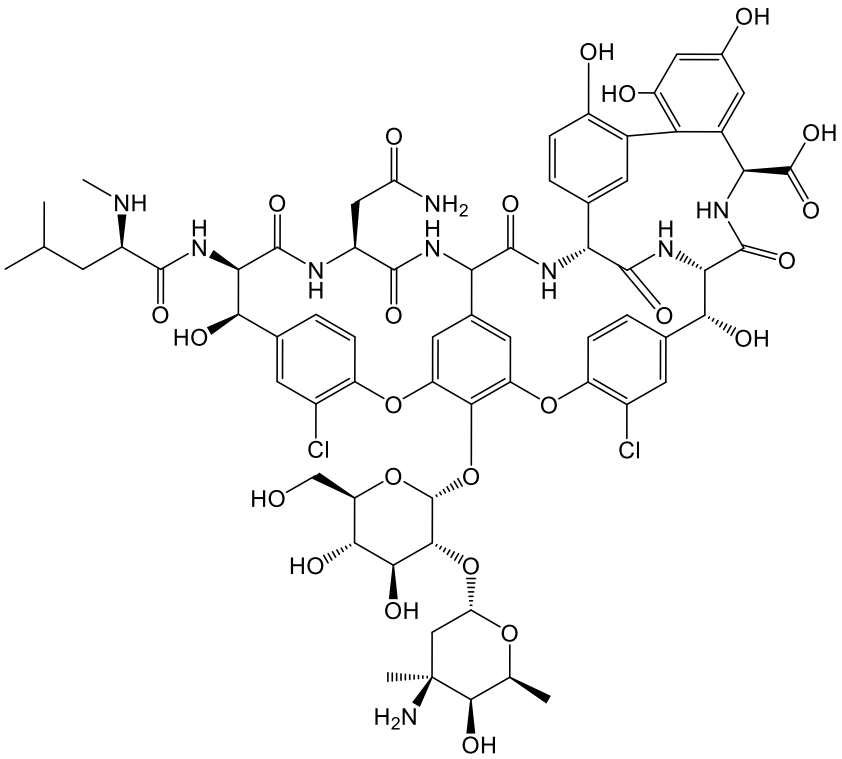

vancomycin

Figure 4: structure of vancomycin

1.1.2.3: Gram-negative Bacteria: *Escherichia coli*

Gram-negative bacteria possess a thinner peptidoglycan layer without the presence of TAs and yet, their cell envelope is even more complicated (**Figure 1**). There are

three main components of a Gram-negative cell envelop: 1) The outer membrane (OM); 2) the peptidoglycan layer and; 3) the inner membrane (IM)[20].

The OM consists of, in most cases, an outer layer of lipopolysaccharides (LPS) and an inner layer of bilayer phospholipids. The OM serves to provide a protective layer of resistance towards the host-defence by inhibiting the effects of lysozymes, β-lysins, and various white blood cell proteins[41]. Additionally it acts as a strong permeability barrier, regulating the influx of dangerous substances such as hydrophobic antibiotics[42]. The LPS consist of the polysaccharide O-antigen, an oligosaccharide core, and fatty acid chains appended onto a phosphorylated glucosamine disaccharide which is an endotoxin known as lipid A[43]. The LPS fragments are also what make the Gram-negative bacteria more toxic towards human as the release of lipid A, following the lysis of the bacterial cell envelope causes fever, diarrhoea and possibly a fatal endotoxic shock. Furthermore, the LPS layer is more abundant in fatty acid chains than the typical phospholipid bilayer of the bacterial cell and thus it can be considered much more hydrophobic in nature. The anionic phosphoric terminals also bind very strongly to divalent cations, leading to formation of cross-bridges with neighbouring LPS molecules[44]. Due to the formation of these hydrophobic cross-bridges, the OM of Gram-negative bacteria inherently possess resistance towards hydrophobic antibiotics. However, chelating agents such a ethylenediaminetetraacetic acids (**EDTA**) which can compete for the LPS bound cation lead to severe disruption of the OM and allow for antibiotics to damage the cell organelles[45].

In addition to the LPS and the bilayer phospholipids, the OM also contains proteins. Some of the OM transmembrane proteins (Omps), such as porins, OmpF and OmpC are responsible for the passive diffusion of small molecules such as sugars, nucleosides, amino acids, phophates, and other essential ions across the OM[42]. Due to the ability of small hydrophilic molecules to pass through porins, it is no surprise then that antibiotics such as β-lactams are allowed to pass through the OM using these channels[46]. However, in recent studies there are two major ways in which antibiotic resistance has occurred by alteration of porin channels: 1) loss/reduction in the number or replacements of porin channels which allow for antibiotic diffusion

and; 2) alteration of channels to reduce permeability[47]. This combined with the fact that LPS offer resistance towards hydrophobic antibiotics is one of the reasons why the OM is such an excellent protective barrier.

The OM is appended onto the peptidoglycan layer by the Braun's lipoprotein[48], and the peptidoglycan layer is somewhat similar to the Gram-positive layer but much thinner and lacking in TAs. The peptidoglycan layer is also suspended in an aqueous cellular compartment known as the periplasm which is sandwiched between the OM and the IM. The periplasm is the evolutionary advantage of Gram-negative bacteria, assisting in the undertaking of important functions such as protein transport, sequestration of toxic enzymes, peptidoglycan synthesis, and resistance to cationic antimicrobial peptides[49].

The final layer of the cell envelope of the Gram-negative bacterium is the IM. The IM is a phospholipid bilayer housing proteins necessary for energy production, lipid biosynthesis, protein secretion, and transport[20]. With the combination of properties of these components, the cell envelope of Gram-negative bacteria possesses an intrinsic resistance towards antibiotics to a much greater extent than Gram-positive bacteria. However, this alone is not the only factor attributing to the resilience of the Gram-negative bacteria as the half-equilibrium times, *i.e* the time taken for the concentration of antibiotics in the periplasm to reach >50% of the extracellular concentrations, are 10-30 seconds for many species[50]. Many recent studies have shown that the extra intrinsic resistance of Gram-negative bacteria can be attributed to the multiple-drug efflux pumps[51]. Efflux pumps are made up of various individual protein components, spanning the cell envelope, and have been known to pump toxic molecules from the cell into the surrounding environment and can be found in both Gram-positive and Gram-negative bacteria[20,52].

Efflux pumps can be categorized into 5 types depending on the number of membranes they transverse, their energy source, the substrates they efflux and the components they possess (**Figure 5**). The four pumps are known as the major facilitator superfamily (MFS), adenosine triphosphate binding cassette superfamily (ABC), the small multidrug resistance family (SMR), and the multidrug and toxic compound extrusion family (MATE), pump substrates across IM and can be found in

both Gram-negative and Gram-positive bacteria[53]. The fifth efflux pump type is the resistance-nodulation-devision (RND) and is a tripartite complex (three protein component) that traverses both the IM and OM, can be found only in the Gram-negative bacteria. The RND efflux pumps are responsible for the projection of harmful substances from the cytosol and periplasmic membrane into the surrounding media outside the OM[54], and have been found to be associated with causing resistance towards multiple antibiotics[55]. Due to the abilities of these multicomponent pumps to excrete drugs outside the OM, these pumps work synergistically with the OM barrier of the Gram-negative cell envelope to lower the periplasmic and cytoplasmic concentrations of harmful substances by out-pacing the spontaneous influx of these substances[51].

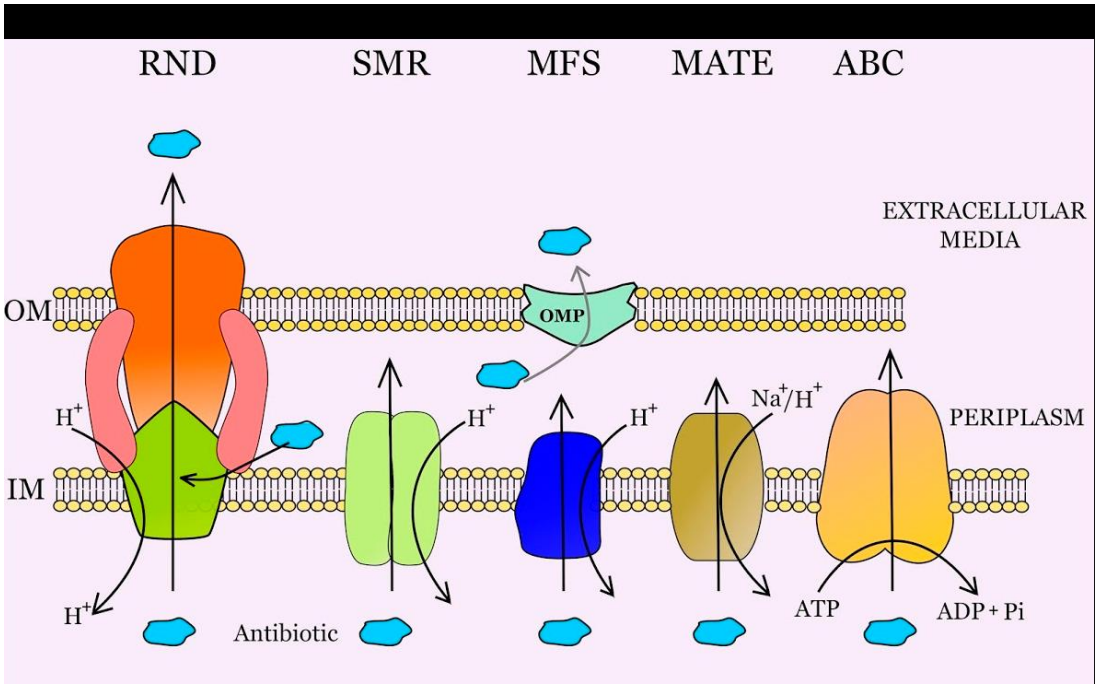

Figure 5: The main types of efflux pumps[55].

Escherichia coli (E. coli) is classified as a Gram-negative bacterium that can be found in the lower intestine of healthy humans as a commensal bacterium. Although most strains of this bacteria are non-threatening and can even provide benefits to healthy humans such as production of vitamins and the prevention of colonisation of other harmful anaerobic microbes, some strains can be pathogenic and even lead to life-threatening conditions. It is the most commonly studied bacteria and its strains can be divided up into 3 main categories[56]: 1) commensal: these are found as part of the

gut flora and they only cause infection in the case of abdominal damage; 2) diarrhoeagenic: these cause diarrhoea; 3) extraintestinal pathogenic *E. coli* (ExPEC): these are capable of surviving under sterile conditions of extraintestinal sites and these are the main cause of extraintestinal infection. Some of the common illnesses associated with *E. coli* infections include acute inflammation, diarrhoea, epididymo-orchitis, hemorrhagic colitis, myositis, neonatal meningitis, osteomyelitis, septicaemia, urinary tract infections, and some fatal illnesses such as haemolytic uremic syndrome (HUS) and thrombotic thrombocytopenic purpurea[56,57]. From a public health point of view, the O157:H7 strain is possibly of the greatest concern. This strain produces a toxin known as SHIGA toxin which causes destruction of red blood cells, leading to complications in the blood filtration system in the kidney and causing HUS[58].

1.1.2.4: Gram-variable Bacteria: *Mycobacterium tuberculosis*

Gram-variable bacteria are a group of bacteria that cannot be conclusively classified as Gram-positive or Gram-negative by the Gram stain method. This group of bacteria are known as *Corynebacterineae*, and consist of clinically relevant pathogens such as *M. tb* and some from *Nocardia* family[20]. These bacteria are referred to as acid-fast bacteria due to their resistance to the decolourization step carried out by alcohol and/or acid wash.

The resistance towards the acid/alcohol decolourization process can be attributed to the structure of the cell envelope of these bacteria. Just like Gram-positive bacteria, acid-fast bacteria are encapsulated by a cytoplasmic membrane with a thick peptidoglycan layer attached. However, unlike Gram-positive bacteria, these bacteria have arabinogalactam polysaccharides covalently linked to the peptidoglycan mesh and further mycolic acids attached to the arabinoglalactam via esterification[59]. These mycolic acids are extremely lipophilic and give the outer layer of the cell envelope a waxy appearance. In addition, these mycolic acids give these acid-fast bacteria an OM (unlike Gram-positive bacteria), however, this OM is symmetrical and significantly different from the OM of Gram-negative bacteria[60].

Due to the presence of characteristics from both Gram-positive and Gram-negative cell envelop, the classification of acid-fast bacteria can be quite difficult by use of the Gram stain alone. An alternative staining method known as the Ziehl-Neelsen stain is used. This staining method utilises Carbol Fuchsin as a staining agent which stains all strains of bacteria. However, when the cells are treated acid/alcohol solution, it is retained only by acid-fast bacteria due to their thick, waxy lipid layer.

An example of acid-fast bacteria is *M. tb*, which is the causative agent of tuberculosis (TB). Introduction to this pathogen, the antibiotics used for treatment of TB, emergence of resistance, and strategies to overcome resistance are outlined in **Section 1.3**.

1.1.3: Current Antibacterial Agents and Emergence of Resistance

1.1.3.1: Antibacterial Agents

Currently, bacterial illnesses can be combated with drugs known as antibiotics. Antibiotics can be bactericidal, whereby they kill the bacteria, or bacteriostatic, where they stop the bacteria from growing. Antibiotics typically target the bacterial cell via any of 5 strategies: 1) DNA synthesis, 2) RNA synthesis, 3) protein synthesis, 4) cell wall synthesis and, 5) intermediary metabolism[61]. Currently prescribed antibiotics can be categorized into the following classes (**Figure 6**)[62]:

1. **Aminoglycosides**: These broad-spectrum antibiotics are made up of aminated sugars appended onto a dibasic cyclitol by glycosidic linkages. Their mode of action is to bind to prokaryotic ribosome and thus prevent bacterial protein synthesis[63]. These agents pass through the OM of Gram-negative bacteria by disrupting the Mg^{2+} cross-bridges of the LPSs.
2. **β-lactams**: antibiotics from this family inhibit the formation of the peptidoglycan cross-linked network by inhibiting PBPs. Antibiotics containing β-lactams can be be placed into four categories: carbapenems, cephalosporins, monobactams, penicillins. Of these four the carbapenems

are the most potent broad-spectrum agents against Gram-positive and Gram-negative bacteria. These are often the last resort treatment. They bind to multiple PBPs and inhibit their function[64].

3. **Fluoroquinolones**: These antibiotics belong to the quinolones class and their mode of action for their antibacterial activity relies on the quinolone to bind to the DNA complex, preventing it from unwinding and duplicating[61].

4. **Glycopeptides**: The primary target for these antibiotics (such as vancomycin (**Figure 4**)) is the inhibition of the bacterial cell wall formation by inhibiting the peptidoglycan biosynthesis[65].

5. **Macrolides**: These drugs contain a macrocyclic lactone ring of 12 or more elements and are used against bacterial infections caused by Gram-positive bacteria. These drugs inhibit protein synthesis by binding to a ribosomal subunit and thus leading to a halt in the growth of the cell[66].

6. **Oxazolidinones**: These relatively new antimicrobial agents have shown great activity toward even methicillin-resistant strains of bacteria. They inhibit the initiation of protein synthesis by binding to the 50S ribosomal subunit[67].

7. **Polypeptides**: These peptides, for example dactomycin, have displayed activity against both Gram-positive and Gram-negative bacteria. They inhibit the transfer of cytoplasmically produced peptidoglycan precursors to bactoprenol pyrophosphate[68].

8. **Rifamycins**: Rifamycins are composed of an aromatic scaffold bridged at nonadjacent positions by an aliphatic chain to give rise to basket like molecular structure e.g. rifampicin (**Figure 18**). These antibacterials bind to the RNA polymerase to inhibit the DNA-dependent RNA synthesis[69].

9. **Sulfonamides**: These broad-spectrum antibiotics of low toxicity and high potency act by disrupting the folic acid synthesis within the bacterial cell[70].

10. **Tetracyclines**: These broad-range antibiotics exhibit antibacterial activity against a number of Gram-positive and Gram-negative bacterial species by inhibiting protein synthesis[71].

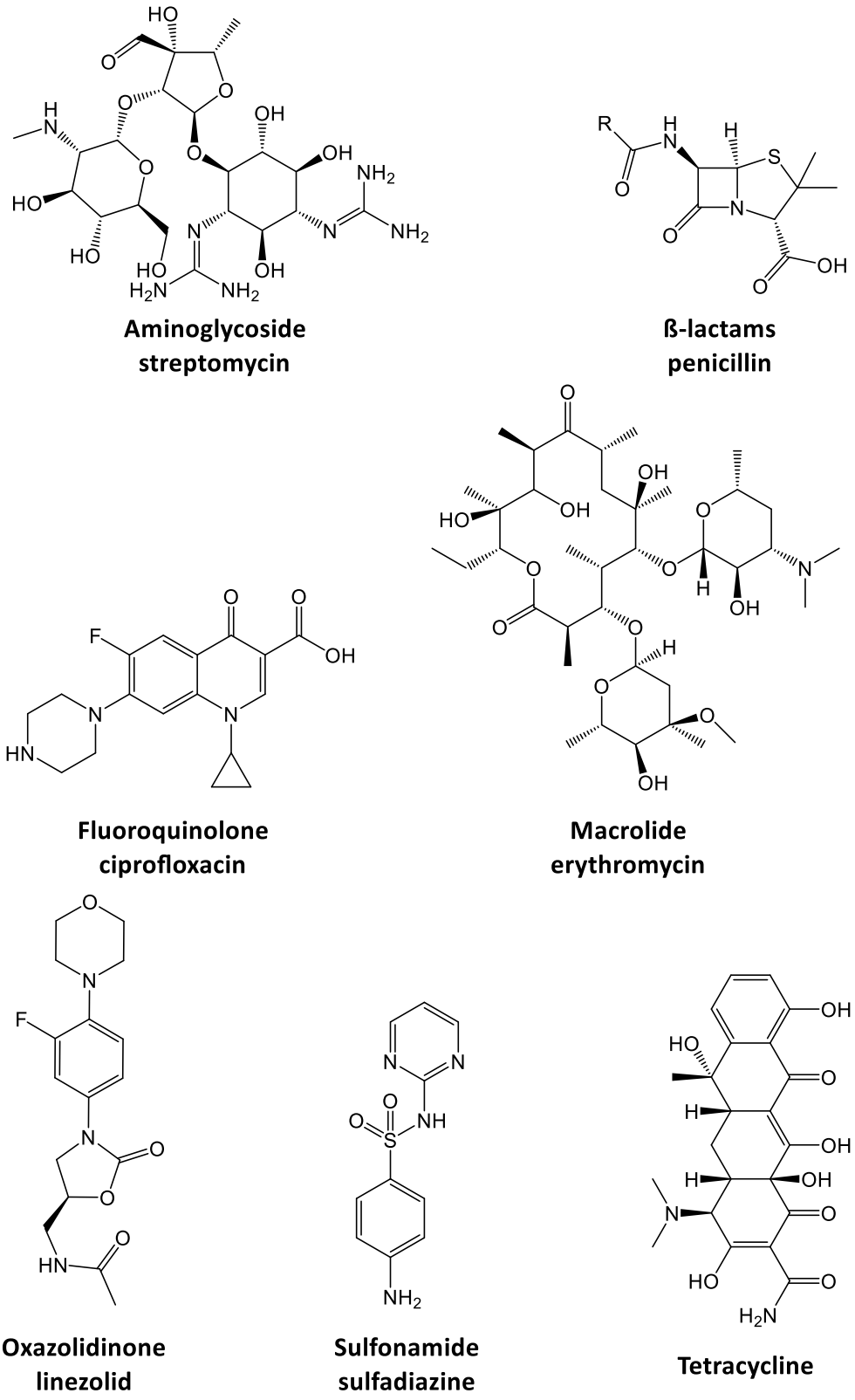

Figure 6: Chemical structure of common clinical antibiotics

Modern antibiotics were first introduced in 1943 with the Food and Drug Association (FDA) approval of penicllin, although Sir Alexander Flemming had discovered it in 1928 and already began studying its therapeutic activity. Even though the

introduction of this “magic bullet” initiated the “antibiotic era” where infectious diseases that had been the leading cause of mortality world-wide for centuries could now finally be controlled, unfortunately, even as early as 1942 there were reports of penicillin-resistant *Staphylococcus* strains observed in patients[72]. Faced with the challenge of eradicating infectious illnesses, there were great strides made to tackle any new microbial infections including the antibiotic resistant strains. Unfortunately, with the discovery and development of each antibiotic, the discovery of a resistant strain soon followed, even to the extent that there exists a resistant strain for nearly all antibiotics (**Figure 7**)[73]. As an example from Gram-positive bacteria, MRSA has been a cause for concern worldwide. In America, it alone is responsible for more deaths than HIV/AIDS, Parkinson’s disease, emphysema, and homicide combined[73].

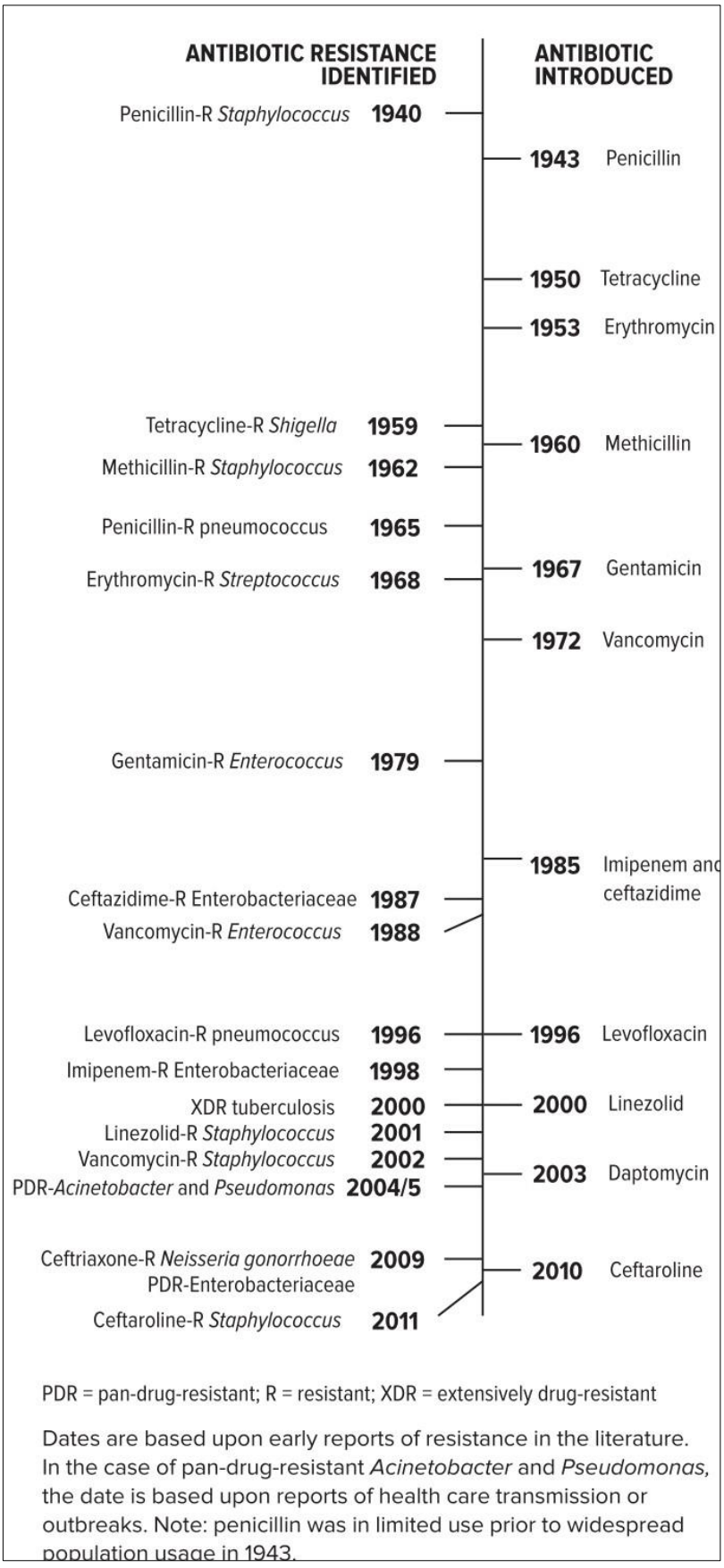

Figure 7: Timeline of development of antibiotics and the discovery of resistant strains[73].

1.1.3.2: Development of Resistance towards Antibiotics

The resistance of microbial species to a harmful substance is a natural process, required by the bacteria for survival. However, accelerated emergence of antibiotic resistance in the clinical setting can be ascribed to the following factors: 1) over use and misuse of antibiotics; 2) use of antibiotics extensively in the agricultural industry; 3) transmission of resistance from intrinsically resistant species[74]. Once there exists at least one bacterium capable of resisting the effects of the antibiotic, it will survive while the susceptible bacterial cells will die. This bacterium can then reproduce to propagate the antibiotic-resistance mechanism and disseminate it to other bacteria[75].

The actual mechanisms employed by resistant strains of bacteria at the cellular level can be classified into three major categories depending on the antibiotics and their respective mode of action[76]:

1. **Reduced antibiotic intake and increase efflux**: many resistant forms of bacteria will modify their cell envelope to prevent the antibiotic from reaching its substrate. There are generally two mechanisms involved with this strategy:
    a. Reduced permeability: for example, the loss/reduction/modification of porin channels to prevent the uptake of antibiotics[77].
    b. Increased efflux: as mentioned in the **Section 1.1.2.3,** the emergence of efflux pumps and in particular multidrug efflux pumps have resulted in decreased intracellular concentrations of antibiotics.
2. **Deactivation of the antibiotic**: By changing the chemical structure of the antibiotic, the resistant bacterial strains can often completely deactivate the antibiotic. Bacteria can do this by:
    a. Modification of the antibiotic: for example, acylation of **INH** to produce a deactivated form of the antibiotic (**Section 1.3.1.2).** Other methods include: phosphorylation and adenylation[78].

b. Destruction of the pharmacophore of the antibiotic: by degrading the active functional group of the antibiotic, the resulting derivative can no longer have a potent effect. An example of this is the β-lactamase that cleaves the amide bond of β-lactams and thus deactivating the antibiotic[78].

3. **Modification of the target site/molecule:** By altering the target of the antibiotic, the antibiotic can no longer carry out a detrimental function to the bacteria or prevent biochemical functions necessary for cell survival. The target can be protected[79] or modified[80].

The formation of biofilms by bacterial population, homogeneous or heterogeneous, is another mechanism employed by microbes to form protective measures against antibiotics and other harmful substances. Biofilms can be defined as a consortium of microorganisms implanted in a self-produced extracellular matrix, composed of extracellular polymeric substances (EPS), adhered to either an abiotic or biotic surface[81]. Biofilms can be found in everyday surfaces, *e.g.* formation of plaque on the enamel of teeth[3], and are a major cause of concern in clinical setting for causation of infections. These infections can be device-related, where the implantation of a device such as catheters or prosthetics provide the surface for biofilm formation, or non-device related, such as the formation of biofilms on surfaces like teeth leading to illnesses like periodontitis[82].

Biofilm formation occurs in 4 generalized steps depicted in **Figure 8**: 1) adherence of planktonic cell to an inert surface, 2) multiplication of the immobile adhered cell, 3) maturation of the biofilm architecture and, 4) dispersion of the microbial cell from the biofilm, and with the final step, the dispersed cells are released to form further biofilms[83]. The formation of biofilms offer resistance to the bacterial cell from various antibiotics[84] and can be attributed to the following factors[85]:

- Reduced permeability: The EPS of the biofilm forms a matrix of proteins, polysaccharides, DNA molecules, RNA, lipids, ions, and water[84]. Antibiotics are often retained in this matrix and can no longer effectively penetrate into the bacterial cell.

- Environmental factors within biofilm: The subterranean layers of the biofilm possess characteristic environmental factors such as lack of oxygen, pH changes, deactivating enzymes, etc. Under these physiological changes, certain antibiotics are rendered ineffective.
- Phenotype Diversity: Due to the diversity of the bacterial colonies, and the fact that gene transfer is an occurring phenomenon within biofilms, genes responsible for defence mechanisms such as efflux pumps are easily transmitted between the various bacterial cells, leading to formation of resistance in the overall population.
- Persister cells: Within biofilms, there exist a population of cells that are metabolically inert in that they don't grow and hence require less nutrients. Furthermore, they enhance their defensive mechanisms toward harmful agents which in turn leads to reducing their effectiveness towards these cells. In addition, once the planktonic cells within the biofilm are effected by the antibiotics, these persister cell replicate and regenerate the biofilm population[83].

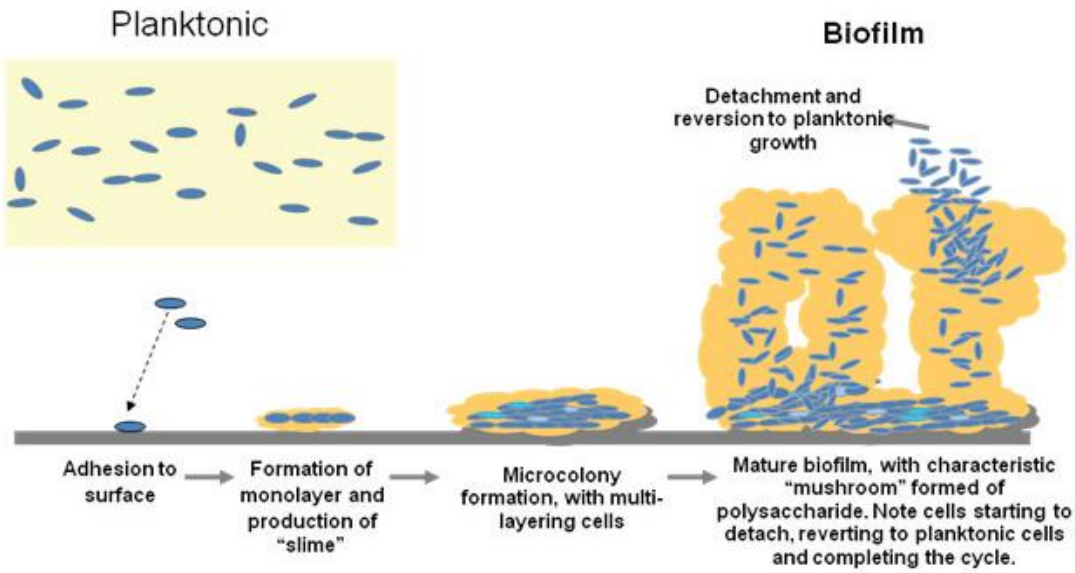

Figure 8: The four stages of biofilm formation[84]

1.2: Antibacterial Activity of Metal Complexes

1.2.1: Metals in Medicine

Metals have been utilised for their medicinal activity for over 5000 years[86]. The birth of inorganic medicinal chemistry is attributed to the discovery of the arsenic-based therapeutic agent for treatment of syphillis, named salvarsan. This was discovered by Paul Ehrlich in his vision of producing a "*magic bullet*", which can selectively target pathogenic cells over healthy human cells[87]. Despite this, it was the discovery of *cis*-platin by Barnett Rosenberg as a successful anticancer agent which heralded the boom of metal-based drugs in clinical applications. Nowadays, metal-based complexes are being investigated for their applications in[87–90] : 1) anticancer agents (Pt(II/IV), with investigation into anticancer activity exhibited by V(IV), Nb(V), Mo(II), Fe(II/III), Ge(IV), Sn (IV), Cu(II), Ag(I) and Ru(II/III)); 2) antiarthritic agents (Au(I)); 3) antiulcer agents (Bi(V)); 4) antimicrobial agents (As(II), Ag(I), Zn(II), Cu(II), Ni(II), Fe(II/III), Mn(II) and Co(II)); 5) antidiabetics (V(IV)); 6) antiviral agents (Co(III), Hg(II)); 7) cardiovascular treatment (Fe(II), Mn(II), Ru(II)); 8) psycho-therapeutics (Li(I)); 9) photodynamic therapy (Sn(IV), Lu(III)); and 10) radiopharmaceuticals (Tc(V)) MRI contrast agent (Gd(III)).

Application of metals in medicinal chemistry is derived from the biological importance of metals in the functions of life[90]. For example, Fe and Mn ions are essential components of haemoglobin and chlorophyll respectively. Metal ions of Zn, Cu, Fe and Mn are found in proteins, functioning as metalloenzymes where the catalytic activity of these enzymes is paramount on the presence of the metal centres. These metals are also the target for quite a few organic drugs/prodrugs, that either inhibit the functions of these metals or utilise their activity to form active therapeutic agents[88]. Often the presence of these metals at the wrong place, at the wrong concentration, can also lead to detrimental effects for the life-cycle of the cell. For these reason, incorporation of metals by way of coordination to suitable ligands often leads to significant therapeutic biological activity and offers various modes of action against illnesses[91].

1.2.1.1: Copper and its Complexes as Antibacterial Agents

Copper (Cu) exists predominantly in biological systems in either Cu(I) or Cu(II) oxidation states and is involved in critical biological enzymatic functions such as those of superoxide dismutase (SOD), cytochrome *c* oxidase, tyrosinase, and more[92]. Although excessive levels of Cu can be detrimental to human health, it is still more tolerable than the majority of transition metals, making it an excellent candidate for metal complexes designed as therapeutics. Indeed, copper complexes have been reported for their anticancer[93], anti-inflammatory[94], antibacterial[95], DNA intercalation[96], nuclease mimetic[97], SOD mimetic[98], antifungal[99], and radiopharmaceutical applications[92,100].

Certain biochemical processes associated with the presence of copper can be employed for their therapeutic activity. Copper is involved in disruption of metalloproteins[101], generation of reactive oxygen species (ROS)[102], disruption of membrane integrity[103,104], carrier of charged species[105], etc. It is no surprise then that the use of copper by macrophages as a form of "brass dagger" to expose microbes to excess copper is a defence mechanism employed by hosts for antibacterial effects[106]. The effect of excess copper can lead to reduction of the pathogenic effect of bacteria, for example in *S. aureus,* virulence factors are reduced and the ability to form biofilms is significantly reduced due to copper stress[107].

Although copper is an essential metal required for the cell cycle, even by bacteria, it has to be carefully regulated due to its toxicity highlighted above. Bacteria can cause the sequestration of copper, use enzymes for detoxification and employ efflux mechanism for the homeostasis of copper found inside and outside the cell[108]. Due to this, metal complexes of copper are of major interest as a delivery method to allow for the passage of the metal through the bacterial cell envelope and possibly to important targets such as DNA.

The formation of an active metal complex could be carried out with the use of a ligand which possess biological activity as well as a ligand which does not possess biological activity. In the case where the ligand does not possess any therapeutic activity, the function of the ligand could be to facilitate the uptake of the metal ion by the cell[109]. In this case, the lipophilic ligand masks the non-lipophilic nature of the

metal and allows the passage of the metal through the lipophilic cell envelope and at the same time prevents the sequestration of the metal ion by the anionic groups found in the cell envelope and enzymes. In the case where the metal complex is formed through chelation with a biologically active ligand, the metal could serve either or both of the following purposes:

1. mask any of the non-lipophilic functional groups of the ligand through complexation: An example of such can be seen with the enhanced activity of some sulfamides when complexed to Cu(II) compared to the free sulfamides[110]. In this case, the active form of the sulfamides are the anionic form, which encounter difficulties when permeating through the cell envelop. However, with metal complexation, this anionic functionality is masked and allowed to permeate into the cell[91].

2. work with the ligand in a synergistic fashion, where the activity of the ligand and the metal being expressed in tandem leads to greater effects than the activity of each individually combined. An example of such is the $[Cu(\mathbf{phen})_2]^{2+}$ complex, where the **phen** ligand binds the complex to the DNA in an intercalative fashion and the Cu(II) ion is responsible for the DNA nuclease activity of the metal complex[97].

Using metal complexation to mask the lipophobic groups and enhance the lipophilicity of the complex to facilitate the uptake of either the metal or the ligand is based upon Overtone's concept of cell permeability and Tweedy's chelation theory[111]. Overtone's rule states that: "entry of any molecule into a cell is governed by its lipid solubility"[112], based on the hypothesis that the cell wall consists of lipophilic components and thus, the greater the lipophilicity of an agent, the greater is its ability to permeate across the cell wall. Since the cationic metal struggles to permeate through the cell wall according to Overtone's rule, Tweedy's chelation theory states that the polarity of the metal ion can be reduced by complexing the metal to a lipophilic ligand.

1.2.1.2: Silver and its Complexes as Antibacterial Agents

The antimicrobial activity of silver has been known as far back as 300 BC, and its selective toxicity towards microbial cells as opposed to mammalian cells made it a focus in the late 1800s as a potential antimicrobial agent[113]. Although the use of silver displayed promising results, it was replaced by the advent of even less toxic antibiotics such as penicillin in the 1940s. With the emergence of MDR strains of bacteria, the majority of these antibiotics are being rendered ineffective. However, silver continues to display sufficient efficacy towards the sensitive and resistant strains that are now plaguing the clinical setting[114]. Although resistanance towards silver has been observed[115], the instances where this is the case are very rare and indeed a benefit of using silver on top of its broad-spectrum antimicrobial activity[116] is that it is observed that the development of resistance towards silver is generally much more difficult[117].

Currently in the market, silver has found its greatest use in the burn wound care for its antimicrobial actions (**Figure 9**). Silvadene is the commercial name of a silver sulphadiazine cream, made from complexation of silver to a sulphonamide, which had been prescribed, up until recently, as a topical antibiotic to prevent infection on burn wounds[118]. Following this success, the use of silver extended to broad application such as the use of silver-coated vascular and urinary catheters as well as other medical devices[116]. In addition, due to it antimicrobial action, the incorporation of silver into textiles designed towards athletic activities has also been researched.

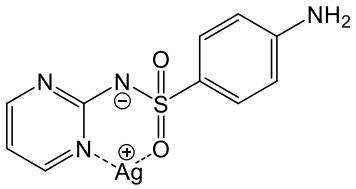

Silver sulfadiazine

Figure 9: Silver complex for burn wound care

The antimicrobial activity of silver is derived from its cationic form Ag(I)[119] and due to silver being a noble metal (E^0 = +0.8V), it only releases a very small amount of the biologically active ionic form. For this reason, silver salts have been the form to be administered for the desired therapeutic action with $AgNO_3$ being the most common

salt to be used[116]. Different salts of silver possess different solubility profile, for example $AgNO_3$ is very soluble where as AgCl is sparingly soluble in aqueous media. With these varying solubility profiles, the effect of silver can be tuned for different purposes while administrating it as a therapeutic agent. For example, AgCl is used in antibacterial spray possessing a lower concertation of silver, whereas $AgNO_3$ is applied to treat burn wounds.

The antimicrobial activity of Ag(I) can be attributed to its initial interaction with the cell membrane. Ag(I) is described as a soft Lewis acid that binds strongly to P and S donor ligands, however it also has the ability to bind to N and O donor ligands. Due to this, Ag(I) is capable of binding to almost any molecule of biological significance[113]. Once the free silver ion is in solution, it binds to essential side chains containing disulphide, amino, imidazole, carbonyl, and phosphate residues, leading to the disruption of the cell wall[114]. Indeed, it has been shown that when *S. aureus* was treated with $AgNO_3$, release of intracellular proteins was observed, demonstrating that silver leads to an increase in permeability of the cell wall[120]. Once inside the cell membrane, Ag(I) binds to essential enzymes, proteins, intracellular membranes, nuclear membrane, RNA, and DNA through the free amino, thiol, and phosphate groups, leading to disruption of essential biochemical processes, defective respiratory pathways, and inhibition of RNA and DNA replication[121].

Due to the significant antimicrobial activity of Ag(I), it has been widely used for formation of metal complexes, an example of which has already been given in silver sulfadiazine. In general, silver metal complexes formed through Ag-O and Ag-N bonds tend to possess a broader range of activity when compared to Ag-S and Ag-P bonded complexes[122]. Indeed, in the case where the ligand used has no biological function/activity, the antimicrobial activity of the metal complex has been attributed to the ease by which the ligand can be replaced by a biological ligand found within the targeted microbial cell[123]. In the case where silver(I) complex of H_2aspartic acid, Hglycin, Haspargine and H_2salicyclic acid were synthesised and tested for their antimicrobial activity, the free ligands were shown to possess no significant activity[123]. However, the metal complexes exhibited antimicrobial activity comparable to the activity of $AgNO_3$, suggesting that the ligand acts only as a carrier

of the silver ion to the biological target whereupon reaching this target, the ligand is replaced by the strong metal-donor interaction of the P and S donor groups normally found in biomolecules.

1.2.1.3: Manganese and its Complexes as Antibacterial Agents

Manganese, due to its numerous oxidation states (II, III, IV), is essential for important biological functions for life[124]. Due to its redox activity, it serves an important role in redox-reaction based enzymes such as ribonucleotide reductase, which is responsible for synthesis of ribonucleotides, and deoxyribonucleotides, peroxidase, Mn-SOD, and catalase[125]. The metal salts and metal complexes of manganese have been reported to show catalytic activity for epoxidation of olefins[126], flame retardants[127], biomedical applications[128], MRI (magnetic resonance imaging) contrast agents[129], and as an antiradical agent[130]. Manganese metal complexes have been studied for their antibacterial activity for quite some time and although the simple metal salts of manganese have been shown to possess little to no antibacterial activity, manganese metal complexes have been shown to possess moderate to good antibacterial activity[128]. In one study, Mn(II) metal complexes showed higher antibacterial activity towards Gram-negative strains compared to Gram-positive strain[131], while in other studies the final Mn(II) complex was reported to possess significantly higher antibacterial activity than the ligand and the metal salt[132,133], and another group reported the higher antibacterial activity as well as higher DNA cleavage ability of the Mn(II) complex compared to the free ligand and salt[134].

1.2.1.4: Antibacterial Activity of Bio-conjugate Compounds and their Metal Complexes

Recently, there has been focus placed on the development of derivatives incorporating bioactive molecules necessary for cell function. As such folic acid, which is involved in synthesis of nucleotides, dipeptides, and fatty acid, which are essential components of the cell wall, have been reported to be appended onto curcumin, a therapeutic agent with established antitumor, antibacterial, antiviral,

and antifungal illnesses[135]. The results reported from the biological screening of these derivatives display excellent inhibitory effects against both Gram-positive and -negative bacteria with the folate derivative possessing minimum inhibitory concentration (MIC) as low as 0.09 μM. As an example of similar **phen** based bioconjugates, recently Cu(II) complexes containing steroid-derived **phen** chelates were published[136] (**Figure 10**). The biological screening of these Cu(II) complexes displayed excellent *in vitro* and *in vivo* inhibitory action towards *S. aureus* with MIC values as low as 1.5 μM and 17.5 μM against *S. aureus* and MRSA respectively.

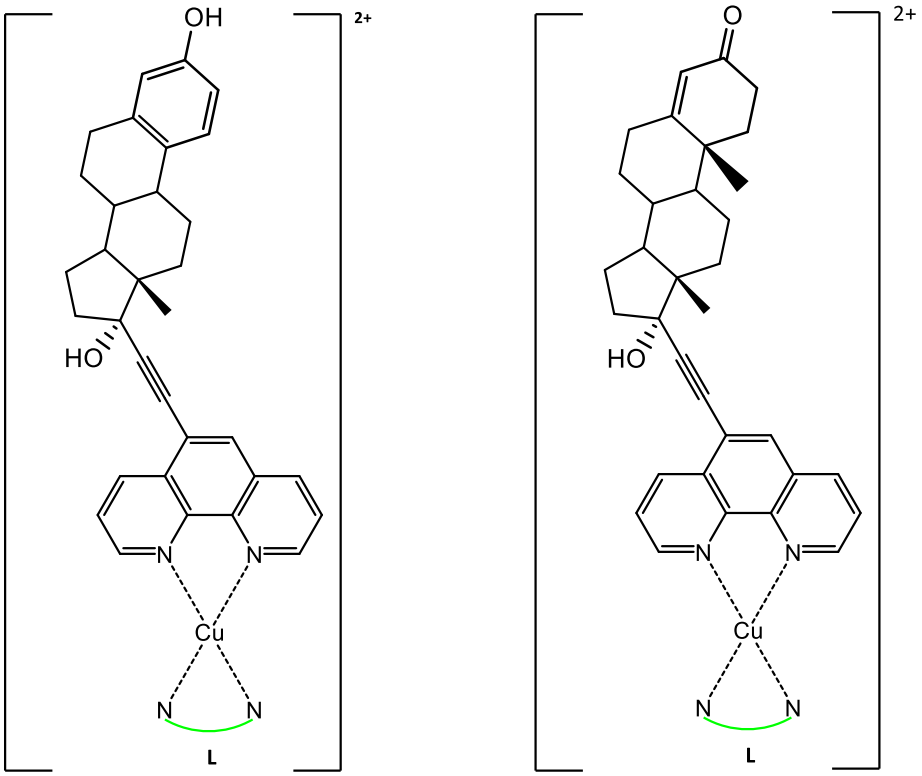

L =

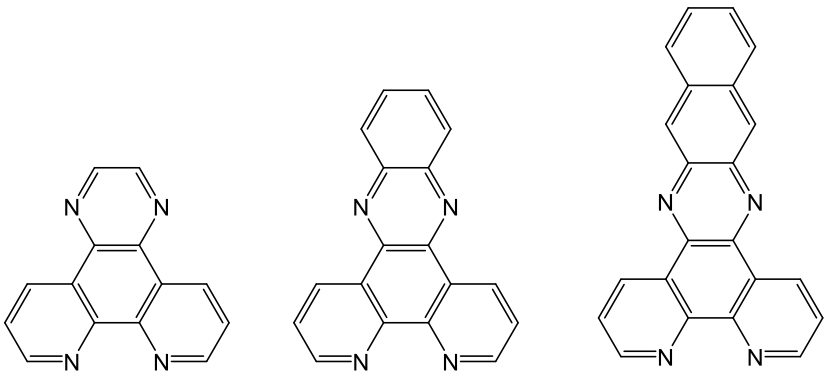

*Figure 10: structures of **phen** based bioconjugates and their Cu(II) complexes. **ES** = ethynylestradiol. **EE** = ethisterone. **dpq** = dipyrido[3,2-d:2',3'-f]quinoxaline. **dppz** = dipyrido[3,2-a:2',3'-c]phenazine. **dppn** = benzo[i]dipyrido[3,2-a:2',3'-h]quinoxaline.*

Following the same concept as above, amino acids have also gained popularity as possible bioactive components which can be appended onto other therapeutic agents. Metals, especially Cu(II), bound to amino acids have been established to possess DNA binding and cleavage activity[137]. In addition, a study of Cu(II) and Co(II)

complexed onto methionine, phenylalanine, valine, leucine and histidine showed that these complexes exhibit antibacterial activity towards *Bacillus cereus* and *Micrococcus luteus* at 10^{-4} M ranges[138]. In addition, amino acids have been complexed to metal ions to form heteroleptic complexes containing other ligands of biological importance. In particular, **phen** and its derivatives have been used as ligands in heteroleptic complexes containing amino acids for their studies into DNA binding, cleaving and anti-tumour activity[137,139–141]. Furthermore, amino acid appended derivatives of potent DNA intercalators such as thiazol orange[142] and ferrocene-appended Cu(II)-**phen** complex[143] (**Figure 11**) were shown to possess promising DNA cleavage capabilities upon irradiation with visible light, making them interesting candidates for further investigations as photodynamic therapy agents. The free amine functional group of amino acids have also made them excellent substrates for Schiff-base condensation reactions with suitable therapeutic agents.

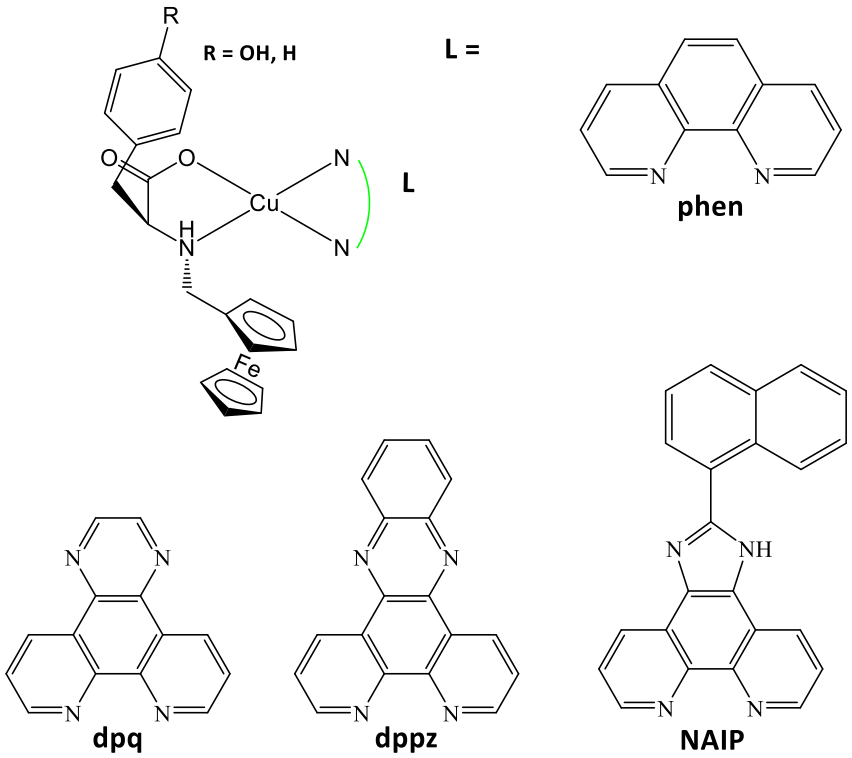

*Figure 11: amino acid derived ferrocene phototoxic Cu(II) complexes. **NAIP** = 2-(naphthalen-1-yl)-1H-imidazo[4,5-f][1,10]phenanthroline*

A broad range of amino acids were utilised in imine formation via Schiff-base condensation with cinnamaldehyde, a natural antimicrobial agent[144]. The biological

screening of these imines against *E. coli* and *S. aureus* revealed the L-tyrosine derivative presenting enhanced activity against *E. coli* compared to cinnamaldehyde and ciprofloxacin and various derivative being more active than these two controls against *S. aureus*. A further improvement upon Schiff-base imines containing amino acids could be made via complexation of these new derivatives to metal centres. Zahid H. Chohan reported biological activity of Schiff-base products of glycine, alanine, phenylalanine, methionine and cysteine reacted with salicylaldehyde and their metal complexes of Co(II), Cu(II), N(II) and Zn(II)[145]. These ligands and their metal complexes were screened against a broad spectrum of Gram-negative and Gram-positive bacteria, displaying significant antibacterial activity against all strains with two of the Zn(II) complexes possessing MIC_{80} values of 0.08 µM and 0.04 µM against *P. aeruginosa* and *S. typhi* respectively.

In another report, the Schiff-base derivatives formed by reaction of tyrosine, alanine and glycine with indole-3-carboxaldehyde were complexed to Co(II), Cu(II) and Ni(II)[146]. These ligands and their metal complexes exhibited antibacterial activity against *S. aureus, E. coli, Klebsiellapneumonae, Proteus vulgarus,* and *P. aeruginosa*.

Manganese (III) complexes containing ligands derived from Schiff-base condensation of N-(2-hydroxy-1-naphthalidiene) with glycine, alanine, phenylalanine, histidine and tryptophan have also been reported for their biological screening against *S. aureus, E. coli*, *B. polymxa* and *C. albicans*[147]*.* Although the complexation of these ligands to the Mn(III) metal centre led to a reduction in their antibacterial activity, the ligand themselves however possessed inhibitory effects.

1.2.2: Antibacterial Activity of 1,10-phenanthroline, its Derivatives and Their Metal Complexes

The structural features of **phen** (**Figure 12**) has earned it much deserved attention from researchers in all areas of medicinal chemistry. Its three fused aromatic rings make it perfectly planar, offer it hydrophobicity and allow it to be an excellent candidate to be a DNA intercalator. Its basic nitrogens are perfectly stationed at the 1 and 10 position allowing it be an excellent bidentate ligand, forming a stable

chelation ring. Due to these properties, **phen** and its metal complexes have been studied for their anti-tumour[148], anti-viral[149], anti-fungal[150] and antibacterial activity[2]. **Phen** is able to coordinate to an array of metal ions, allowing it to be administered for therapeutic activity as either: 1) a metal complex where it facilitates the uptake of the metal ion into the target cell and thus has synergistic therapeutic effect along with its activity as well as that of the metal ion[111], or; 2) it could also be administered as a free ligand where it is believed that it sequesters essential metal ions necessary for cell function and thus lead to inhibition of important biological pathways or degradation of biological organelles[151].

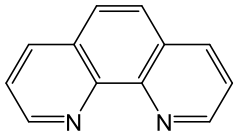

1,10-phenanthroline
phen

*Figure 12: structure of **phen***

The antibacterial activity of **phen**, its derivatives, and their metal complexes was the undermining focus of the extensive screening carried out by Dwyer and co-workers against a broad spectrum of Gram-positive and Gram-negative bacterial species[2]. As a result of their studies, they reported the antibacterial activity of hydrochloride salts and quaternary salts of **phen** and its derivatives against *M. tb, S. aureus, streptococcus pyogenes, clostridium perfringens*. The bacteriostatic activity of **phen** was reported to be 63 µM, a moderate value, against *M. tb* and *S. aureus* with lesser activity towards the other species. Additionally, it was generally noticed that the addition of methyl groups to increase the lipophilicity of the molecule lead to an increase in activity and in the case of 3,5,6,8-tetramethyl-1,10-phenenathroline a 30-fold increase in bacteriostatic effect was observed against *M. tb*. Although they screened their compounds against Gram-negative bacteria, they did not report any results for their study, stating that the overall activity of these compounds was much lower against these strains, a trend which commonly occurs in lipophilic antibiotics and possible explanations have been given in **Section 1.1.2.3**.

1.2.2.1: Antibacterial Activity of 1,10-phenanthroline-5,6-dione

Spurred by the promising results outlined above, researchers have attempted to modify **phen** in various ways to enhance its efficacy. Possibly the most well-known of these derivatives is the oxidised derivative 1,10-phenanthroline-5,6-dione (**3.1**) (**Figure 13**) which possess the *O,O'*-quinonoid functional group to provide further chelation or redox capabilities.

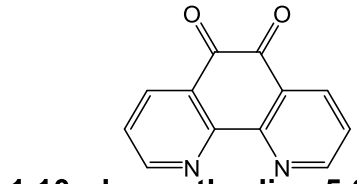

1,10-phenanthroline-5,6-dione
3.1

Figure 13: structure of 1,10-phenanthroline-5,6-dione

3.1 and its metal complexes have been utilised as intermediates in synthetic chemistry and as catalyst for essential oxidations of amines[152]. Unsurprisingly however, their most efficient application is in medicinal chemistry, with the metal-free as well as the metal-coordinated **3.1** being substantially more effective than **phen**. When tested against *E. coli, P. aeruginosa* and *S. aureus* the MIC_{50} value range for **3.1** and **phen**, respectively, are reported as: *E. coli*: 15-22 µM and >555 µM; *P. aeruginosa*: 15-22 µM and 416-555 µM; *S. aureus*: 30-45 µM and 278-416 µM[153]. Against the yeast *C. albicans* the reported MIC_{50} values are 13.9 µM for **phen** and 2.9 µM for **3.1** and similar results are obtained for anti-tumour screening, demonstrating that the added *O,O'*-quinonoid functionality provides the **phen** scaffold enhanced potency. A possible explanation to this enhanced activity can be deduced from the electrochemical behaviour of **phen** compared to **3.1**. Whereas **phen** does not display any electrochemical activity in the potential region of +1000 to -1000 mV, the electrochemical analysis of **3.1** displays half-wave potential values of -471 mV and -1042 mV[151]. This ability of **3.1** to undergo redox reactions allows it to disturb essential cellular functions as well as generating lethal by-products[151].

1.2.2.2: 1,10-phenanthroline Derivatives with Extended Aromaticity

An alternative method for improvement in the activity of **phen** is to attach aromatic rings onto the backbone, increasing it aromaticity. An example of such derivatives is **dppz**, formed by carrying out Schiff-base condensation between 1,2-diaminobenzene and **3.1**. Utilizing **dppz** as a ligand, it was shown that [Ru(**bb$_7$**)(**dppz**)]$^{2+}$ (**Figure 14**) possessed inhibitory activity against Gram-positive bacteria at 2 μg/ml and at 8 μg/ml against Gram-negative bacteria[154].

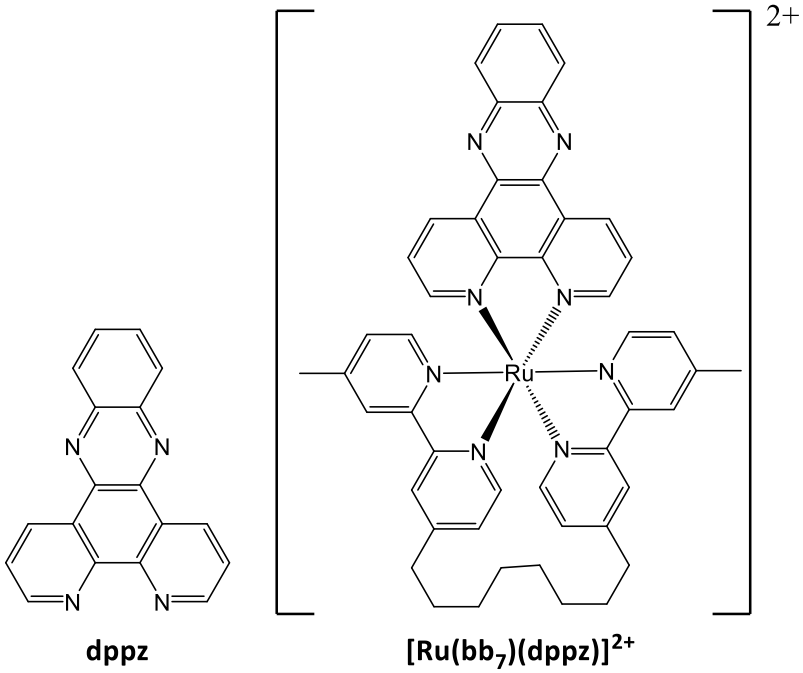

*Figure 14: structure of **phen** derivative **dppz** with extended aromaticity and its Ru(II) complex for tested for antibacterial activity*

The same complex containing neocuproine (2,9-dimethyl-1,10-phenanthroline), which was shown to be more active than the **phen** equivalent, only inhibited bacterial growth at 8 μg/ml and >32 μg/ml concentrations for Gram-positive and negative strains respectively[155]. Although the metal complexes containing this ligand exhibit excellent activity against bacterial strains, the ligand itself has been shown to possess non-existent antibacterial activity even at concentrations >200 μg/ml against *E. coli* and *B. subtilis*[148]**.**

1.2.2.3: Antibacterial Activity of Metal Complexes of 1,10-phenanthroline and its Derivatives

The therapeutic activity of **phen** and it metal complexing capability leading to enhancing its activity had been studied as early as 1955[156]. However, as stated in **Section 1.2.2** it was actually the work of Dwyer, published in 1969 which displayed the excellent antimicrobial activity of **phen**, its ligands and its metal salts of Cu(II), Fe(II), Ni(II) and Ru(II)[157]. It was reported that although **phen** and its derivatives exhibited excellent bacteriostatic activity, with certain ligands possessing activities at MIC values as low as 1.9 µM against *M. tb*, certain metal complexes exhibited MIC values as low as 0.032 µM against *M. tb*, 1.9 µM against *S. aureus*, and 4 µM against *S. pyogenes* amongst other strains of bacteria. Although these metal complexes display promising results against Gram-positive bacteria, it was noted that their activity towards Gram-negative bacteria was negligible.

Though Dwyer's results led to further antibacterial screening of **phen**, its derivatives and their metal complexes, it was the results published by Sigman in 1979 which displayed **phen**-based metal complexes as one of the most desirable therapeutic agents. Sigman observed that $[Cu(\mathbf{phen})_2]^{2+}$, in the presence of a reducing agent, mimics DNA nuclease activity, a hallmark for anticancer activity. Since these reports, **phen** based metal complexes have been reported for their anticancer[158], broad-range antibacterial[159], antiparasitic[160] and antifungal activity[161].

Metal complexes of **phen** and its derivatives possess two inherent advantages:

1. the hydrophobic **phen** ligand possess basic nitrogens at 1 and 10 position, leading to a stable 5-member chelation ring, making it an excellent chelator which mask the hydrophilic nature of the bioactive metal centres and,
2. the ability of any noncoordinated **phen** to interact with metal ions from essential enzymes and proteins, disrupting biological functions and making labile metal complexes bimodal in their therapeutic activity.

Furthermore, once inside the cell, **phen** based metal complexes can employ various different modes of actions:

- **DNA binding and/or DNA damage:** DNA is an excellent target for any therapeutic to prevent further spread of infectious/disease cells and inhibition of essential cellular processes, leading to cell death. The **phen** ligand being completely planar due to its extended aromaticity possess excellent DNA intercalative properties[102] and coupled with a metal centre/metal complex (Ag(I), Cu(I), Cu(II), Co(II), Dy(III), Ni(II), Co(III), Mn(III), Pd(II), Pt(II), Fe(III), Y(III) and Zn(II)), it can possess enhanced intercalative action, alternative DNA binding modes and DNA cleaving activity[111].

  Keene and Grant have reported the synthesis and antibacterial screening of mono-, di-, tri- and tetra-nuclear Ru(II) complexes containing **phen**, its lipophilic derivatives and di-bipyridyl linkers connected via lipophilic alkyl chains of varying lengths[159] (**Figure 15**).

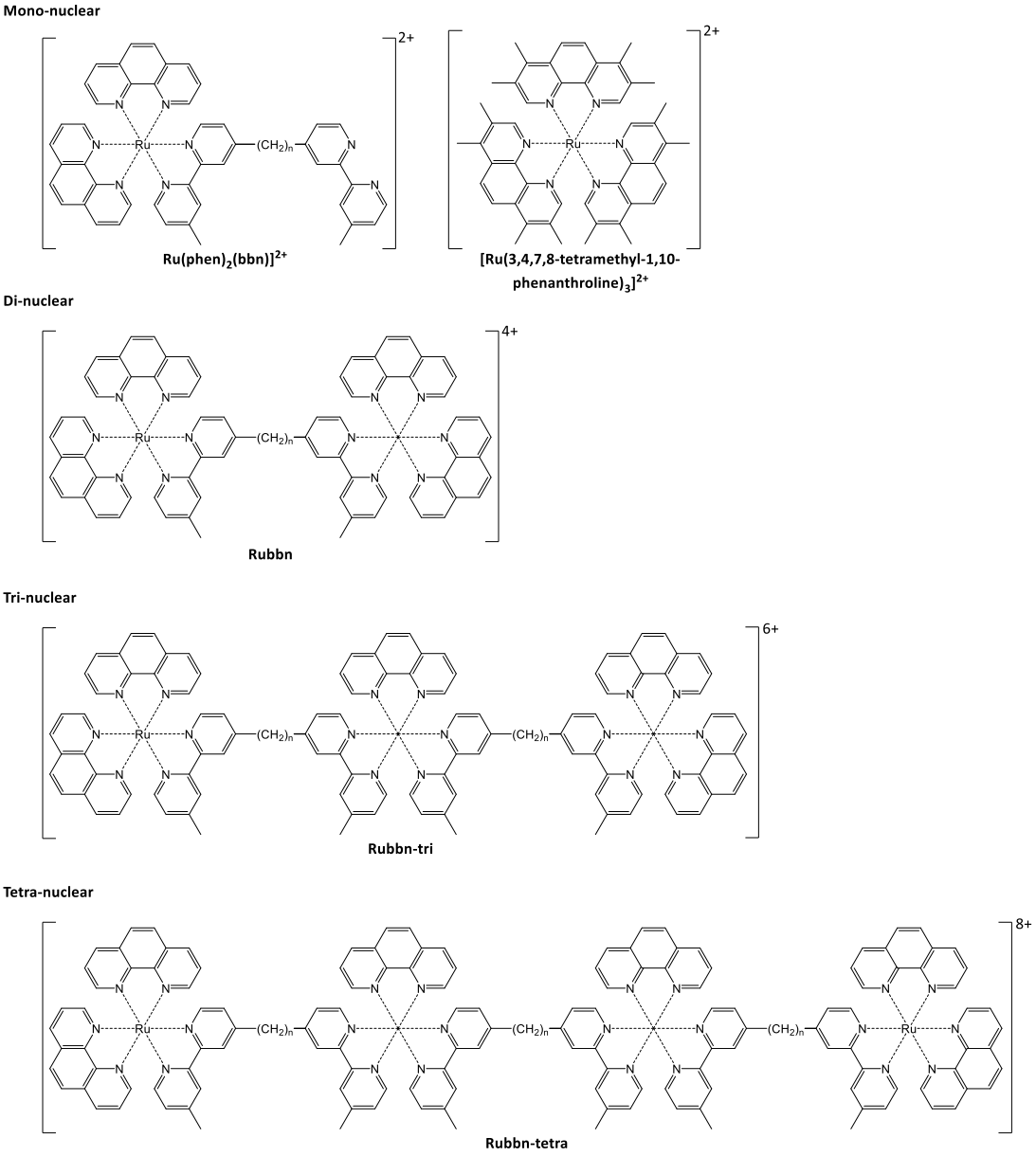

*Figure 15: Structure of mono, di, tri, and tetra **phen**-based Ru complexes*

They report that although the mono-nuclear complexes exhibit antibacterial activity, their effects were limited and the complexes were far less active when compared to clinically used drugs. In comparison, the di-nuclear complexes were far more potent against Gram-positive, Gram-negative, and MRSA and vancomycin resistant enterococci (VRE) strains. In addition, the study into their uptake by bacterial cells revealed that their influx to the bacterial cell is an energy-dependant process and that these complexes lead to severe permeabilisation of the bacterial cell envelope[162]. Upon formation of the tri- and tetra- nuclear complexes, these researchers discovered that

some of these complexes of higher nuclearity exhibited antibacterial activity up to four times higher than their dinuclear counterparts. Although the mode of action of these complexes is not fully understood, it is postulated that these complexes exhibit their activity through their interaction with DNA as they have been shown to interact with DNA and cause DNA damage.

Metal complexes of known antibacterials whose mode of action involves targeting DNA have also been reported. **Lomefloxacin** belongs to the quinolone family, which target DNA replication, enzyme gyrase and topisomerase[163], and is clinically employed as an antibacterial agent. Its binary copper(II) complex exhibit enhanced DNA binding capabilities, however, the complex itself is unstable at physiological conditions[164]. The incorporation of **phen** to this complex to form the ternary complex (**Figure 16**) demonstrates higher stability, DNA binding capabilities through intercalative interactions, DNA nuclease activity, and an alternative cellular uptake of the complex compared to the metal free quinolone[165–167].

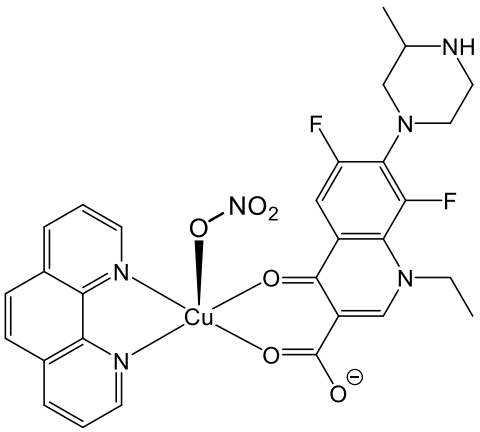

[Cu(lomefloxacin)(NO_3)(phen)]

*Figure 16: Structure of [Cu(**lomefloxacin**)(NO_3)(**phen**)]*

- **Cell wall damage:** The di-nuclear ruthenium complexes (**Figure 15**) were not only shown to target DNA but also permeabilise bacterial cell envelope. A similar result was also reported from the effect of $[Ru(\textbf{phen})_2(\textbf{tip})]^{2+}$ (**Figure 17**), where **tip** = 2-thiophenimidazo[4,5-f][1,10]phenanthroline, which caused cytoplasmic leakage via disruption of cell membrane and also induced DNA and RNA damage as part of its antibacterial activity[168].

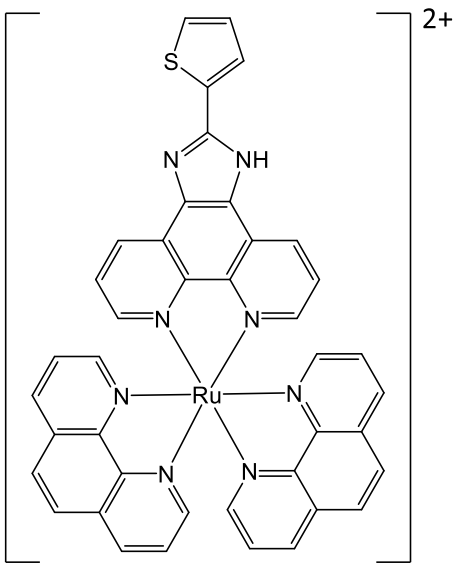

$[Ru(phen)_2(tip)]^{2+}$

Figure 17: Structure of $[Ru(\textbf{phen})_2(\textbf{tip})]^{2+}$

Cu(II) and Pt(II) complexes containing **phen** and its substituted derivatives along with 1S,2S- and 1R,2R-diaminocyclohexane co-ligands were tested for their broad range antibacterial activity[169]. It was found that the copper complexes were most active against *S. aureus* whereas the platinum complexes were found to be selective towards *E. coli*. To test for the difference in selectivity by the two metal complexes, the two most active complexes from each metal centre ($[Cu(\textbf{4,7-diphenyl-phen})(A_L)]^{2+}$ $[Pt(\textbf{phen})(\textbf{A}_L)]^{2+}$ where $\textbf{A}_L$ = with 1S,2S- and 1R,2R-diaminocyclohexane) were studied for their cell wall permeabilisation activity against *S. aureus* and *E. coli*. The results from this study suggest that the copper complexes cause severe permeabilisation of the *S. aureus* cell wall, however, the platinum complexes do not disrupt the cell wall permeability of *E. coli*.

- **Reactive Oxygen Species (ROS) generation:** The intracellular generation of ROS can lead to oxidative stress within the cell and lead to cell death (apoptosis)[170]. The highly reactive species produced during ROS generation can interact with proteins, membranes, lipids, and nucleic acid within the cell. The interaction of these macromolecules with ROS, such as the $^{\bullet}OH$ radical, can lead to protein-protein cross-linkage, cell membrane damage, inactivation of membrane-bound enzymes, DNA damage, and DNA-protein

cross-linkage. Metal complexes containing **phen** have been thoroughly reported for their ROS generation ability which contributes to their antimicrobial activity[171].

- **Enzyme inhibition:** metal-free **phen** can lead to enzyme inhibition via sequestration of essential metals found within the enzyme structure. On the other hand, as mentioned above, the presence of a redox-active metal centre-complex can lead to formation of ROS which can also inhibit enzymes. As such metal-**phen** complexes have been widely studied for their enzyme inhibition activity. In a study, it was shown that metal-free **phen** and its Cu(II) complexes ($[Cu(\mathbf{phen})(\mathbf{meimzH})(H_2O)_2]^{2+}$ and $[Cu(\mathbf{phen})(\mathbf{cnge})(H_2O)(NO_3)_2]$ (where **meimzH** = methylimidazole; **cnge** = cyanoguanidine) inhibit the alkaline phosphatase (ALP) enzyme, leading to antibacterial activity[172,173]. The metal-free **phen** demetalated the ALP enzyme by removal of Zn^{2+} ions, whereas the enzyme inhibitory action of the copper complexes was attributed to ligand-substitution mechanism involving the ALP enzyme.

  The antibacterial activity of $[Cu(2,9\text{-dimethyl-}1,10\text{-phenanthroline})_2]NO_3$ was shown to be associated with its ability to inhibit a bacterial enzyme[174]. Upon further study into the uptake of this metal complex, these researchers discovered that the hydrophobic ligand acted as a carrier, facilitating the transport of the copper ion into the bacterial cytoplasm which in turn led to enzyme inhibition.

1.3: *Mycobacterium Tuberculosis* and Anti-tubercular Agents

1.3.1: *Mycobacterium Tuberculosis* and Clinical Drugs

Mycobacterium tuberculosis (*M. tb*) is the bacterium responsible for causing tuberculosis, or consumption. Tuberculosis (TB) has plagued the human society for millennia with the earliest records for human infection being observed in Egyptian mummies and Egyptian art[175]. It is hypothesised that the origin of *Mycobacterium* can be traced as far back as 150 million years ago[176]. Although its symptoms have been well documented since the ancient Greeks, the cause of this affliction eluded the medical society and therefore, it is of no surprise that *M. tb* may have led the count of deaths amongst microbial infections until the discovery of its cure[177]. Due to the lack of understanding of etiology of TB, the physicians of the pre-1880s could do little more than to prescribe fresh air and a healthy diet to tackle this illness. It was not until 1882 that Robert Koch isolated the bacillus responsible for TB and studied its contagious characteristics. He published his research in the *Berliner Klinische Wochenschrift* journal[178]. For his work, he was deservedly awarded the Nobel Prize in 1905 and due to his development of *M. tb* etiology, researchers began the search for agents to target this bacterium. The first of such agents was streptomycin which was discovered by Albert Schatz, a PhD student of the Nobel Laureate Abraham Waksman. This discovery heralded the development of further antibiotics which lead to a refinement of treatment regime to tackle TB. Although this has led to effective TB control in developed countries, the underdeveloped countries cannot handle the cost of implementing these strategies. According to the World Health Organisation (WHO) there were 10.4 million people who developed TB, 1.7 million deaths and 490,000 reported cases of multidrug-resistant TB (MDR-TB) in 2016[179]. In addition, it was also reported that 95% of TB death occur in low and middle income countries, and it is estimated that 33% of the global population is infected with the latent form of TB.

1.3.1.1: Current Treatment for Tuberculosis

The current treatment for TB consists of administrating a cocktail of at least four of the five first-line drugs: isoniazid (**INH**), rifampacin, pyrazinamide, ethambutol and streptomycin (**Figure 18**) available for anti-TB treatment. If the pathogen is susceptible to **INH** and rifampicin, the patient can be treated with the above drugs. However, the bacterium causing the infection can be resistant to **INH** or/and rifampicin. In this case, the treatment requires second-line drugs: ciprofloxacin, moxifloxacin, *p*-aminosalicylic acid, kanamycin, capreomycin, amikacin. These drugs can be categorized by their mode of action[180]:

- **Fatty acid biosynthesis inhibitors**: **INH**, pyrazinamide, ethionamide.
- **Arabinogalactam and peptidoglycan biosynthesis inhibitors:** ethambutol.
- **Protein synthesis inhibitors**: streptomycin, kanamycin, amikacin, capreomycin.
- **DNA-based process inhibitors**: rifampicin

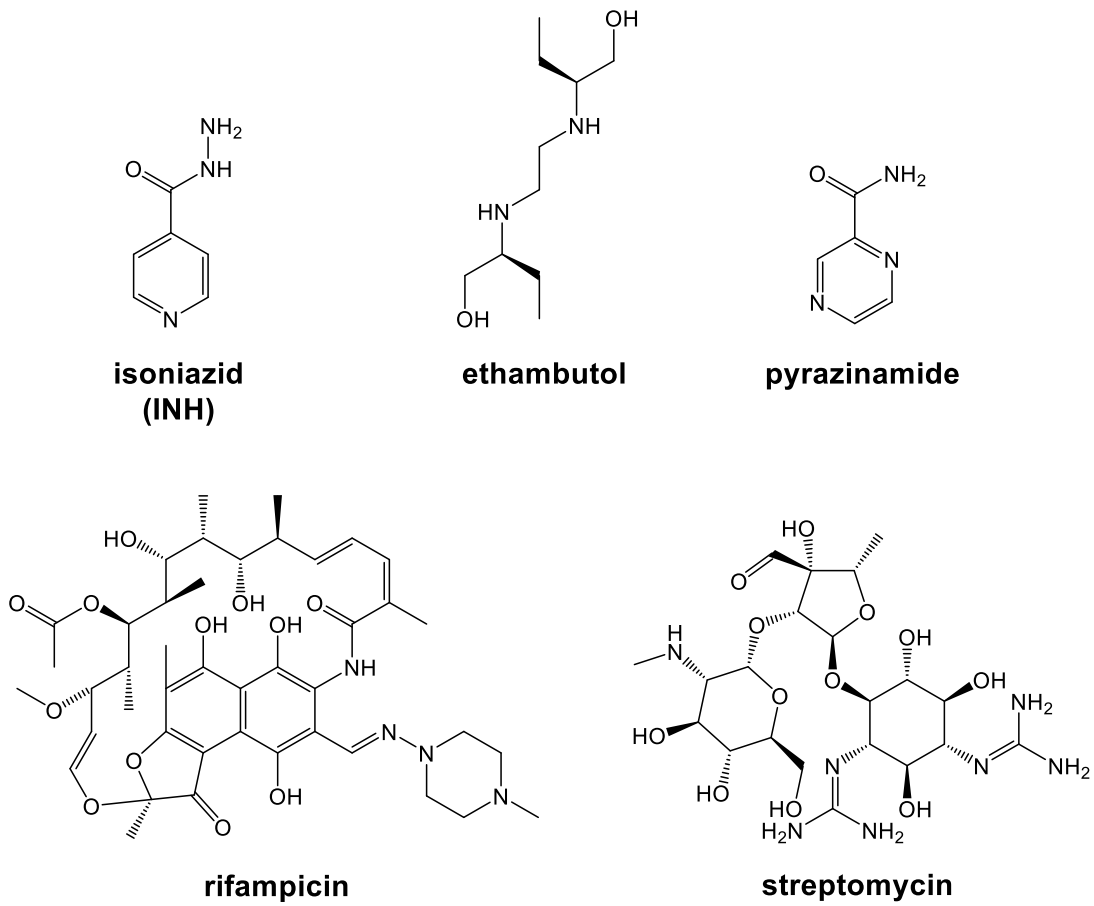

Figure 18: Current drugs used as first-line treatment for TB

The current standard protocols from various organisations such a CDC (centre for disease control) and WHO for treatment of **INH** and rifampicin susceptible TB suggest administration of 4 of the 5 first-line drugs for the first 2 months which subdues the active bacterial infections, and then administrating **INH** and rifampicin for further 4-7 months to fully eradicate any slow growing latent bacterial cells[181]. The long and tedious regime does not only pose various difficulties for the patient in absolute compliance to the treatment, but also poses side-effects such as hepatoxicity, often forcing the clinician to terminate the treatment prematurely[182]. This further complicates the treatment of TB patients as failure to adhere to the treatment would lead to survival of bacterial cells which then develop resistance (acquired resistance) towards the administered drugs and lead to relapse of the patient and, in this case, rendering at least one of the first-line drugs ineffective[183]. In addition, these first-line drugs may encounter primary resistance, where a patient has developed drug-resistant TB without being previously treated by any anti-TB drug[184].

The emergence of resistance, both primary and acquired, has led to the global threat of multidrug resistant bacteria which are resistant to either or both **INH** and rifampicin, the most effective of the first-line drugs. Globally, 5% of TB cases are expected to be MDR-TB and treatment of these cases require the administration of second-line drugs over a period of 12-24 months[183]. Alongside being significantly more expensive, these second-line drugs also lead to a greater range of severe side-effects.

Due to the emergence of resistance towards majority of the currently available anti-TB drugs, one strategy for tackling this issue is to synthetically modify the current therapeutics with the aims of producing agents of higher efficacy with novel modes of action. In this regard, **INH** has received the most attention due to its effective mode of activation and mode of action.

1.3.1.2: Mode of Action of INH and Mechanisms of Resistance by Tuberculosis

INH is a prodrug which requires *in vivo* activation through KatG, an enzyme within *M. tb* which catalyses the electron-transfer reaction responsible for the formation of the active drug[185]. Due to the complexity of the many faceted mechanism of **INH**, it is currently unknown the exact biological pathways affected by **INH** leading up to its anti-TB activity. However, it is well known that in the presence of KatG, **INH** is converted to produce an isonicotinic radical which binds to NADH to produce an **INH**-NAD adduct. This adduct then subsequently binds to and inhibits enoyl-acyl carrier protein reductase, inhA, which then inhibits the synthesis of mycolic acid required for mycobacterial cell wall synthesis[186] (**Figure 19**). Although it has been recently shown that **INH**-NAD/NADP adducts can act as inhibitors of dihydrofolate reductase (DHFR), which is essential for nucleic acid biosynthesis, and therefore affect a range of cellular pathways, it is generally accepted that the major mode of action is through inhibition of cell wall biosynthesis. The inhibition of DHFR alongside the production of other side-products of **INH** activation leading to alteration of biochemical pathways facilitate the antimycobacterial effect of **INH** in a synergistic manner[187,188].

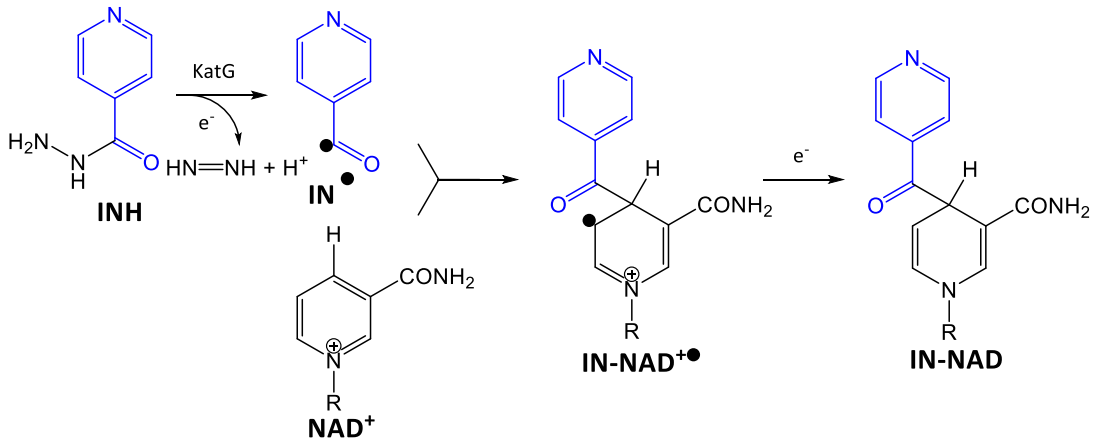

*Figure 19: Mode of activation of **INH** with all of the key radical species*[186]

Although **INH** acts as an effective agent against *M. tb*, resistance towards **INH** was observed in the clinical setting soon after its introduction as a therapeutic[189]. Amongst various other genes, it has been identified that deletion or mutation of *katG, inhA, kasA, ndh,* or *oxyr-aphC* genes play essential roles in leading to **INH** resistance[190]. The major contributor of these is the deletion/mutation of *katG* gene, which is responsible for the presence of KatG. Alteration of this gene is responsible for roughly 50% of **INH**-resistant strain of TB[191]. In addition, **INH** can be metabolized by acetylation at the -NH_2 group, caused by *N*-acetyltransferase (NAT) enzyme, leading a decrease in serum concentration and activity as well as presenting hepatoxicity effects[192]. With these two strategies employed by *M. tb* to render **INH** ineffective, there has been considerable attention on modification of **INH** to overcome these two issues.

1.3.2: Strategies to Overcome Resistance towards Isoniazid

1.3.2.1: Incorporation of Effective Pharmacophores

Due to the highly effective nature of anti-mycobacterial activity of **INH**, it has been chemically modified in various ways to generate more efficacious agents. One strategy includes the incorporation of an other effective pharmacophore into **INH** hybrids to generate compounds with additional modes of action attributed to the pharmacophore attached[193]. A recent review by Y.-Q. Hu *et al* outlines the anti-TB

screening results of **INH** hybrids incorporating azoles, pyrazoline, pyrrole, triazine, azetidinone, thiazolidinone, isatin, quino(xa)line, furoxan, cinnamic acid as well as other biologically active pharmacophores[194] (**Figure 20**). Although these hybrids exhibit excellent anti-TB activity towards **INH** susceptible strain, in majority of the cases their activity towards the **INH** resistant strain are not reported. Furthermore, their respective modes of action are yet to be studied.

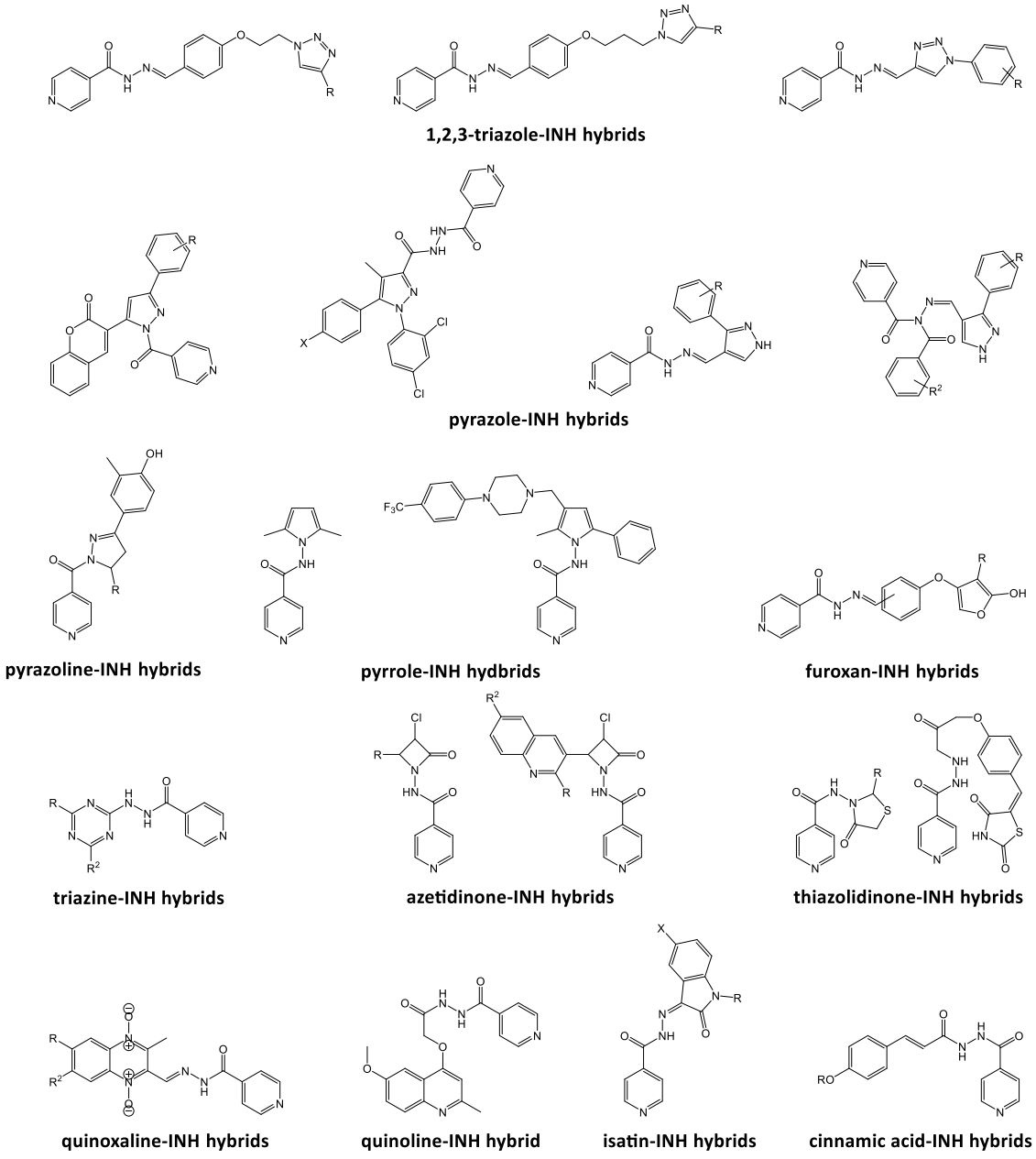

*Figure 20: effective pharmacophore-**INH** hybrids*

1.3.2.2: Metal Complexation of INH

Metal complexes of **INH** have also attracted much attention since the discovery of excellent activity exhibited by the anionic complex, $[Fe(CN)_5(\mathbf{INH})]^{3-}$, towards a **INH** susceptible and resistant strain[195]. This strategy to complex a metal centre to the **INH** molecule derives its roots from the hypothesis that Cu(II) and Fe(III) facilitate the KatG enzyme in the formation of **INH**-NAD adduct via oxidation and may also provide an alternative pathway to accessing this adduct in the absence of KatG[188,196]. Additionally, it has been shown that the presence of Mn(II) also catalyses the formation of IN-NAD adduct both in the presence and absence of KatG[196].

Upon carrying out further mechanistic studies on the anti-TB action of $[Fe(CN)_5(\mathbf{INH})]^{3-}$, it was discovered that this complex inhibits the **INH**-resistant 121V mutant InhA enzyme. Furthermore, the deactivation of this enzyme can occur in the absence of NAD^+ or NADH as well as KatG catalase peroxidase enzyme, suggesting that this complex can be used to target **INH**-resistant strains that resist the mode of action of **INH** by mutation or deletion of KatG. Additionally, the **INH**-free analogue$[Fe(CN)_6]^{3-}$ did not inhibit the InhA enzyme in the presence or absence of NADH[197], demonstrating that the **INH** ligand is required for the activity of $[Fe(CN)_5(\mathbf{INH})]^{3-}$. Upon further investigation, the activity of $[Fe(CN)_5(\mathbf{INH})]^{3-}$ was compared to that of the ruthenium analogue, $[Ru(CN)_5(\mathbf{INH})]^{3-}$, which is of similar size and charge but differs from its iron counterpart in its electrochemical nature. Whereas the Fe(II) complex can be easily oxidised, the Ru(II) complex is more stable towards electrochemical processes. Based upon these results, these researchers proposed that the Fe(II) complex acts as a "self-activating metallodrug" in which the **INH** ligand is activated to give the **IN$^\bullet$** radical through inner-sphere electron transfer from the ligand to the Fe(II) metal centre, leading to the **INH** activation in the absence of KatG (**Figure 21**).

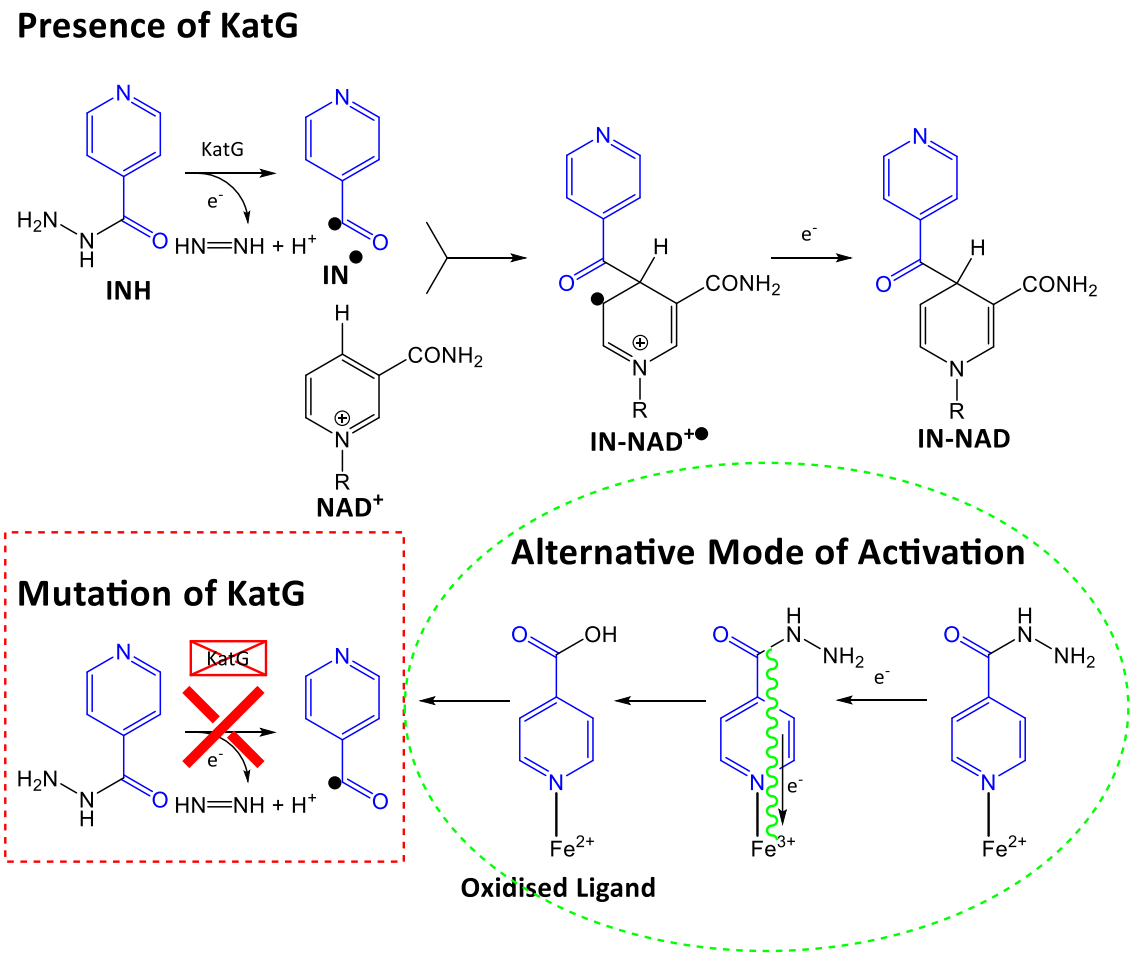

*Figure 21: Alternative mode of action of **INH**[191]*

These preliminary studies demonstrate that $[Fe(CN)_5(\mathbf{INH})]^{3-}$ could be a potent metallodrug and in addition, the toxicity of this compound towards mammalian HL60 leukaemia and MCF-7 breast cancer cells indicate that it is far less toxic towards mammalian cells than it is towards mycobacterial cells. In fact, the selectivity index (SI) calculated for this compound (by dividing IC_{50} (for mammalian cells) by MIC (for TB cells)) is reported to be >125 which is far larger than the acceptable SI value (>10) for further drug development in the pre-clinical stage according to the "Hugo Laboratory" drug-development pipeline[198]. Further studies reporting the stability of this complex in physiological environment, its *in vivo* activity towards *M. tb,* and its *in vivo* tolerance in various animal models demonstrate that this complex is a very promising potential therapeutic and it has since been tested in pre-clinical evaluations[191,199].

Although studies on this metallodrug had presented promising results as a therapeutic agent, a recent study has shown that this drug does in fact depend on the presence of KatG[200]. These researchers tested the inhibitory capabilities of this complex against various **INH**-resistant MDR-TB clinical isolates containing mutation most commonly found in the *katG* gene. The results from these testing as well as further testing carried out on genetically modified strains, demonstrate that this complex displays MIC values up to 64 times higher than those reported for tests carried out on **INH** susceptible strain[201]. The fact that in each of these strains, it was the KatG enzyme that was affected, these researchers conclude that KatG is essential for the activation of this complex for it inhibitory effect. In addition, the self-activating mechanism of this complex was examined in the same study by studying the activity of this complex in infected murine macrophages, a strategy previously used to study the effect of this complex in intracellular environment[202]. The lack of activity exhibited by this complex suggest that the intracellular environment does not permit the self-activation of this complex. Due to the results reported in this study, the anticipated use of this compound to target **INH**-resistant strains needs to be re-evaluated.

Other metal complexes containing **INH** as a ligand were reported in 2013 by Poggi *et al* who synthesised Cu(II) and Co(II) complexes[203]: $[Cu(\mathbf{INH})(H_2O)]SO_4.2H_2O$ and $[CoCl(\mathbf{INH})_2(H_2O)]Cl.2\frac{1}{2}H_2O$. These complexes exhibited MIC values of 2.2 µM and 0.41 µM for the Cu(II) and Co(II) complexes respectively. In addition, when tested for their cytotoxicity towards VERO cells (ATCC CCL81) and 'macrophage' J774A.1 mouse cell lines (ATCC TIB-67), these complexes exhibited IC_{50} values far larger than their MIC values against MTB $H_{37}Rv$ (ATCC 27294), giving rise to SI values of 80.1 and 2631.6 for the Cu(II) and Co(II) complex respectively. It is important to note that the Co(II) complex not only displays MIC value as low as that of **INH** but also, it is very well tolerated by mammalian cells, making it a promising candidate for further studies.

1.3.2.3: Isoniazid Derived Hydrazones

An approach to enhance the activity of **INH** towards resistant strains of mycobacteria is to protect the –HN-**NH_2** terminal of **INH** from being acetylated by the NAT enzyme and hence reducing the rate of metabolization of **INH**. For this purpose, **INH** has been coupled to various functional groups by Schiff base condensation reaction or amide coupling[204,205]. An added benefit of forming such coupled products is the increase in lipophilicity, a strategy that has been used in attempts to enhance the uptake of therapeutic agents by focusing on increasing diffusion across the lipid membrane[193,206]. Indeed then it is no surprise that hydrazones of **INH** were shown to be active against *M. tb* even as early as 1954. In their study to use hydrazone formation of 106 carbonyl compounds (ketones and aldehydes) to yield crystalline structures, Sah *et al* were able to generate the hydrazones of these compounds and show that majority of the resulting hydrazones displayed anti-TB activity greater than that of streptomycin and similar to that of **INH**[207].

In two review articles published by Rollas and Mathew[208,209], the authors describe the synthesis and antimycobacterial activity of various Schiff-base derived hydrazones of **INH**, the majority of which inhibit bacterial growth of **INH** sensitive *M. tb* H_{37}Rv strain at concentrations below 3 μg/ml. The most active of these compounds (**Figure 22**) incorporates a pyrrole derivative[210], a precursor to other drugs such as Tolmetin, Lipitor and Toradol. This compound exhibits its antimycbacterial effect at dosage below 0.1 μg/ml and possess SI value >100.

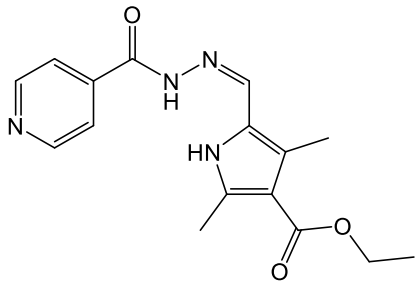

*Figure 22: Schiff-base pyrrole derivative of **INH***

1.3.3: 1,10-phenanthroline Based Metal Complexes as Antimycobacterial Agents

1.3.3.1: Antitubercular Activity of 1,10-phenanthroline and its Metal Complexes

Phen and its derivatives have been shown to be effective therapeutics for a myriad of illnesses as has been covered in **Section 1.2**. In their comprehensive antimicrobial activity studies of **phen**, its derivatives, and their metal complexes, Dwyer *et al* demonstrated that **phen** inhibits mycobacterial growth at 63 μM dosage, with the tetramethyl derivative exhibiting bacteriostatic action at 1.9 μM dose. In addition, these researchers also established that metal complexes (Cu(II), Fe(II), Ni(II) and Ru(II)) of **phen** and its derivatives exhibit enhanced activities upon complexation when compared to the free ligands[157].

Since then, many different complexes incorporating the **phen** ligand have been synthesised and screened for their anti-TB activity. In 2018 McCarron *et al* reported the synthesis and the biological screening of various Mn(II) metal complexes and salts, as well as similar Cu(II) complexes, against two clinically relevant *M. tb* strains, mammalian A549 cell line, epithelial VERO cell line, and *G. mellonella* larvae model[211]. The most active of the 9 compounds synthesised and tested was the dinuclear double salt $[Mn_2(\mathbf{oda})(\mathbf{phen})_4(H_2O)_2][Mn_2(\mathbf{oda})(\mathbf{phen})_4(\mathbf{oda})_2].4H_2O$ (where **oda** = octanedioic acid) (**Figure 23**), which exhibited anti-TB activity against $H_{37}Rv$ and CDC1551 strains at 0.47 μM and 0.15 μM respectively, with SI value being calculated against these strains to give 325 (against VERO), 445 (against A459) and 1017 (against VERO), 1347 (against A549) respectively. Although a Cu(II) analogue of this metal salt was not reported, a similar dinuclear salt, $[Cu_2(\mathbf{oda})(\mathbf{phen})_4](ClO_4)_2.2.76H_2O.EtOH$, was reported and interestingly it presented MIC values against $H_{37}Rv$ and CDC1551 strains at 12.68 μM and 1.15 μM respectively. With the SI values being <1 against all cell lines, it can be clearly seen that the nature of the metal centre plays an essential role in activity and efficacy of a metal complex. In addition, it was further reported that the similar Mn(II) and Cu(II) complexes, $\{[Mn(\mathbf{tdda})(\mathbf{phen})_2]3H_2O.EtOH\}_n$ and $\{[Cu(\mathbf{tdda})(\mathbf{phen})_2]3H_2O.EtOH\}_n$ {where **tdda** =

3,6,9-trioxaundecanedioic acid), were synthesised and exhibit vastly different biological profiles. Although not as active as the dinuclear double salt the mononuclear {[Mn(**tdda**)(**phen**)$_2$]3H$_2$O.EtOH}$_n$ exhibited anti-TB activity at MIC < 1.02 µM with SI values up to 467. In comparison, the Cu(II) equivalent exhibited anti-TB activity at 13.48 µM against H$_{37}$Rv and 1.01 µM against CDC1551, with SI values <8.

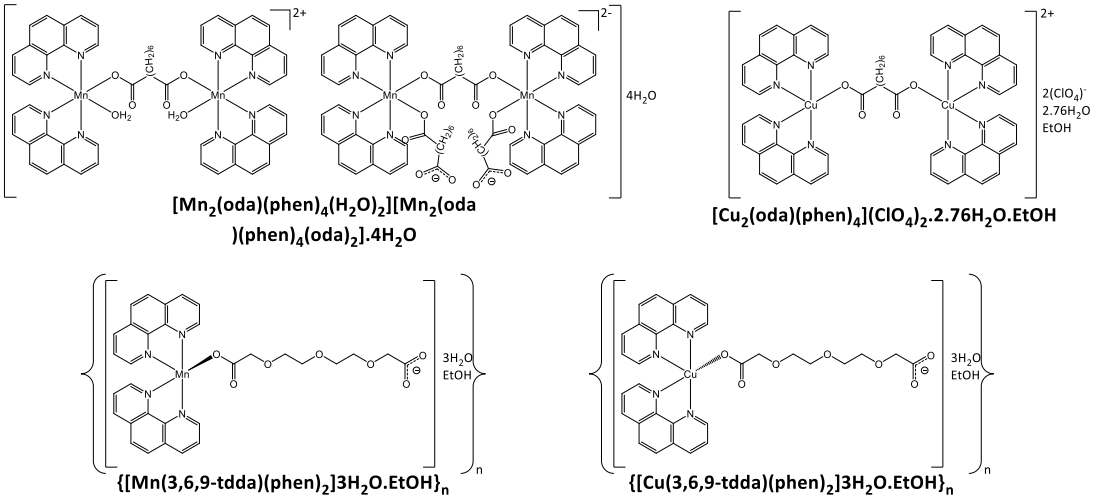

*Figure 23: structure of [Mn$_2$(**oda**)(**phen**)$_4$(H$_2$O)$_2$][Mn$_2$(**oda**)(**phen**)$_4$(**oda**)$_2$].4H$_2$O and related complexes*

In 2013 Hoffman *et al* reported the synthesis of Co(II) and Cu(II) mono- and di-nuclear metal complexes incorporating **phen** ligands and the pyrophosphate ligand. The addition of the pyrophosphate ligands was made to produce both mono- or di-nuclear neutral complexes, whereupon these pyrophosphate ligands would act as water-solublising agents generating metal complexes with hydrophilic cores to hydrophobic exterior scaffold generated by the **phen** ligands[212]. Upon generating {[Co(**phen**)$_2$]$_2$(µ-P$_2$O$_7$)} and {[Cu(**phen**)]$_2$(µ-P$_2$O$_7$)}, and their mono-nuclear analogues [Co(**phen**)$_2$(H$_2$P$_2$O$_7$)] and [Cu(**phen**)(H$_2$O)(H$_2$P$_2$O$_7$)], their antimycobacterial activity was studied against drug susceptible strains *M. tb* Erdman ATCC 35801, *M. tb* H$_{37}$Rv and *M. tb* HN878, as well as the drug resistant strain MDR *M. tb* ATCC 49967. Against *M. tb* H$_{37}$Rv strain it was observed that the mono-nuclear Co(II) complex was the most active, exhibiting antibacterial activity at MIC value of 2.05 µM, whereas its Cu(II) analogue only displayed antibacterial activity at MIC value of 71.53 µM. In the case of these two mono-nuclear complexes, the Co(II) complex was the far more potent agent with an excellent SI value of 142.28, when compared to the SI value of 1.82 possessed by the Cu(II) analogue. More importantly, the di-nuclear complexes

both presented excellent MIC values against the MDR *M. tb* ATCC 49967 strain, with Co(II) exhibiting activity at 2.41 µM and the Cu(II) at 2.8 µM. Just as with the mono-nuclear complexes, it was the Co(II) di-nuclear complex which was more efficacious, possessing an SI value of 233.8, compared to the SI value of 4.786 exhibited by the Cu(II) analogue.

The antibacterial activity of Ag has been known and studied for over a century. It is no surprise then that the incorporation of Ag(I) in a **phen** metal complex could be a logical approach to target *M. tb*. Segura *et al* reported in 2014 the synthesis and anti-mycobacterial screening of dinuclear Ag(I) complexes containing **phen**, **bipy** and thiourea (**tu**) ligands[213]. The three complexes synthesised: [{Ag(**phen**)(µ-**tu**)}$_2$](NO$_3$)$_2$, [{Ag(**phen**)(µ-**tu**)}$_2$](CF$_3$SO$_3$)$_2$ and [{Ag(**bpy**)(µ-**tu**)}$_2$](NO$_3$)$_2$ (**Figure 24**); were tested against *M. tb* and their toxicity towards J774 macrophages was measured. The study reports that although the metal-free **phen** ligand as well as the starting metal salts possess some anti-TB activity at MIC values of 12.8 µM, 34.2 µM and 27.1 µM for **phen**, AgCF$_3$SO$_3$ and AgNO$_3$ respectively, the Ag(I) complexes are far more active with MIC values of 4.7 µM and 7.3 µM for [{Ag(**phen**)(µ-**tu**)}$_2$](NO$_3$)$_2$] and [{Ag(**phen**)(µ-**tu**)}$_2$](CF$_3$SO$_3$)$_2$] respectively. Although these complexes possess promising anti-TB activity, their capability to serve as therapeutic agents is hindered by their toxicity towards the J774 macrophages, giving rise to SI values of 0.46 and 4.48 for for [{Ag(**phen**)(µ-**tu**)}$_2$](NO$_3$)$_2$] and [{Ag(**phen**)(µ-**tu**)}$_2$](CF$_3$SO$_3$)$_2$] respectively. Interestingly, despite the **bpy** ligand being active at MIC value of 119 µM, its Ag metal complex, [{Ag(**bpy**)(µ-**tu**)}$_2$](NO$_3$)$_2$], does not exhibit any substantial anti-TB activity.

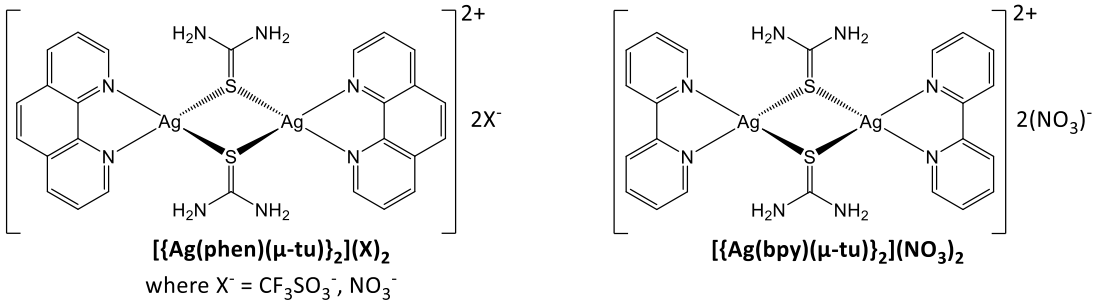

*Figure 24: structure of Ag-**phen** and Ag-**bpy** complexes as anti-TB agents*

1.3.3.2: Antimycobacterial Mode of Action of 5-nitro-1,10-phenanthroline

The modes of action of **phen**-based ligands and their metal complexes toward inhibition of cell growth and functions have been outlined in **Section 1.2.2.3.** Although these mechanisms can be utilised by **phen**-based ligands and metal complexes, specific derivatives can lead to bacteria-specific mode of action which leads to antibacterial activity. Recently, Kidwai *et al* published a report outlining the dual mode action utilised by the 5-nitro-1,10-phenanthroline (**5-n-p**) derivative to carry out its antimycobacterial activity[214]. The study identified **5-n-p** as a possible lead compound for further anti-TB testing and attempted to generate spontaneous resistant mutants towards this agent. Upon successfully cultivating such mutants, a subsequent whole-genome sequence revealed that the resistance arose from mutation in *fibB* gene which is responsible for coding F_{420} coenzyme L-glutamate ligase which plays a role in biosynthesis of coenzyme F_{420}.

Further studies carried out by these researchers revealed that **5-n-p** may act as a prodrug within mycobacteria, being activated by F_{420}-dependent reductase. Indeed, upon characterisation of metabolites of **5-n-p** within mycobacteria by LC-MS revealed the presence of **phen** and 5-amino-1,10-phenanthroline. In addition, the activity of both of these metabolites by themselves is lower than that of **5-n-p**, suggesting that the higher activity of the latter can be associated with the activation of this prodrug. Upon further analysis it was revealed that this prodrug inhibits the biosynthesis of mycolic acid through inhibition of fatty acid synthase I (FAS-I) pathways, a mode of action similar to the clinical pro-drug **INH** which inhibits FAS-II pathway.

Additional mechanistic studies revealed that an additional mode of action which can be utilised by **5-n-p** is its ability to induce autophagy in macrophages. Autophagy is described as a self-degradative process essential for recycling of nutrients from biomolecules and structures such as aggregated proteins, damaged organelles and dead cells for the reuse of these nutrients at critical stages of development and in response to nutrient stress[215]. Therefore, autophagy is proposed to be a survival mechanism which can also be utilised for elimination of intracellular pathogens. This

ability of **5-n-p** makes it a possible candidate for further studies as an agent for host-directed therapy (HDT), a strategy which utilises the innate immune response for protection against pathogens. Although, the nitro- functional group is essential for the promising anti-mycobacterial activity exhibited by **5-n-p**, the versatility possessed by **phen** derivative such as this one makes these derivatives promising candidates as therapeutic agents against the growing concern caused by *M. tb*.

1.4: Outline of the Thesis

Building upon the information presented in this chapter, the work discussed in this thesis aim to examine methodologies to target microbial infections. **Chapter 2** consists of synthesis and characterisation of novel oxazine-based **phen** ligands and their metal complexes. These ligands and their metal complexes were screened for their antibacterial activity. **Chapter 2** also consists of synthesis and characterisation of a **phen**-**INH** hybrid ligand, formed through Schiff base condensation, and its metal complexes. With the help of our collaborators, this hybrid and its metal complexes were screened against four strains of drug susceptible and drug resistant strains of *M. tb* and various microbial strains. **Chapter 3** consists of the discussion of synthesis and characterisation of the oxazine-based **phen** ligands, their metal complexes and their biological profile is also discussed. **Chapter 4** gives the discussion of the synthesis and characterisation of the **phen**-**INH** hybrid and its metal complexes. The antimycobacterial activity of these compounds are also discussed in **Chapter 4**.

Chapter 2

Experimental

2.1: Introduction

This chapter can be broken down into 4 sections: **2.2**, **2.3**, **2.4**, and **2.5**. These section outline the synthesis of various starting material, and the use of these starting materials for the formation various biologically active ligands and then the subsequent metal complexation of these ligands with metal salts. **Section 2.2** details the instrumentation and the materials used throughout the synthesis and characterisation of all of the chemicals that were synthesised. **Section 2.3** gives the synthetic protocols utilised for the synthesis, isolation and purification of starting materials **3.1, 3.2a-h**, and the synthesis of the oxazine-based ligands (**3.3a-g**) and their metal complexes (**3.5a-e**). The synthesis of pyrido-type by-products (**3.4a-c**) is also given. **Section 2.4** outlines the synthesis of hydrazone-based product **4.1** formed by reaction of **3.1** and **INH**, the complexation of **4.1** to Ag(I), Mn(II) and Cu(I) metal salts. The isolation of degredation products (**4.3a-b**) of **4.1** is also given as well as attempted synthesis of **4.3a** through conventional azo-coupling reaction.

Biological screening of compounds **3.3a-e** as well as their metal **3.5a-e** were also carried out in Professor Kevin Kavanaghs laboratory in Maynooth University. The methodology, materials, and instrumentations utilised are also given in **Section 2.5**.

2.2: Instrumentations and Materials

2.2.1: Instrumentations

The NMR (Nuclear Magnetic Resonance) spectra were recorded on a Bruker Avance spectrometer operating at 500 MHz for ^{1}H nucleus and 126 MHz for the ^{13}C nucleus. The probe temperature was maintained at 25 °C. Residual solvent peaks were used as internal standard. Chemical shifts are given in ppm and coupling constants are given in Hz. Multiplicity is denoted as follows: s (singlet), bs (broad singlet) d (doublet), t (triplet), dd (doublet of doublets), m (multiplet). Proton and carbon signals were assigned with the aid of DEPT experiments and 2-D NMR experiments COSY, HSQC, HMBC.

IR (Infrared) spectra were recorded on a Perkin Elmer Spectrum 100 FT-IR spectrometer. Solid samples were finely ground with dry KBr and pressed between two dies using 9 tonnes of pressure. All spectra were obtained within the region of 4000-400 cm^{-1}.

High Resolution Mass Spectrometry (HRMS) analysis was carried out at Maynooth University and University of Bath. In Maynooth University, ESI (electrospray ionization) mass spectra were collected on an Agilent-L 1200 Series coupled to a 6210 Agilent Time-of-Flight (TOF) equipped with both a positive and negative electrospray source. In University of Bath, the HPLC-ESI-TOF analysis was conducted using an electrospray time-of-flight (MicrOTOF) mass spectrometer (Bruker Daltonik GmbH, Bremen, Germany), which was coupled to an Agilent HPLC stack (Agilent, Santa Clara, CA, United States) consisting of Agilent G1312A binary pump with G1329A autosampler and G1316A column oven.

The elemental analysis (CHN%) was carried out on a FLASH EA 1112 Series Elemental Analyser with Eager 300 operating software. Magnetic moment measurements were carried out on a Johnson Matthey Magnetic Susceptibility Balance with $Hg[Co(SCN)_4]$ used as the standard. The UV-Vis analysis was carried out on Perkin Elmer Lambda 35 UV-Vis Spectrometer.

The Flame Atomic Absorption Spectroscopy (FAAS) analysis was carried out on a Perkin Elmer AAnalyst 200. The setup was equipped with a double-beam optical system, hollow cathode lamp and acetylene and air gas based nebulizer. A copper specific lamp (Hollow Cathod Lamp: Cu. Part Number: 5UN Cu-A. Serial Number: B22133) was used. Standards were prepared from commercial 1 mg/ml Cu in 2 to 5% HNO_3 standard solution. 25mL of the standard solution was diluted with 5% HNO_3 to produce a 1 L solution of 25 ppm standard stock solution. The standard stock solution was diluted to produce 6.25, 12.5 and 16 and 25 ppm standard solutions. Each of these standards were used to generate a standard curve by plotting copper concentration (ppm) vs absorbance (**Figure 25**).

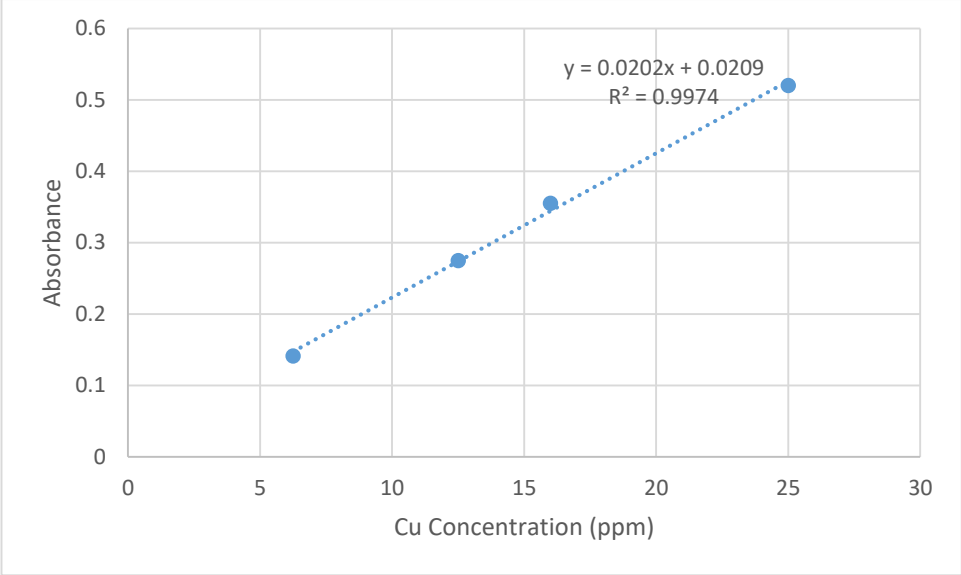

Figure 25: the relationship between copper concentration and absorbance (FAAS)

The HPLC (High Performance Liquid Chromatography) spectra were extracted from LC-MS studies that were performed on an Agilent Technologies 1200 Series instrument consisting of a G1322A Quaternary pump and a G1314B UV detector (254 nm) coupled to an Advion Expression L Compact Mass spectrometer (ESI) operating in positive mode. Separations were performed on a Waters Xbridge OST 2.5 µm, 4.6 x 50 mm column (C18) operating at a flow rate of 0.2 mL min-1. Separations were performed using a mobile phase of 0.1% formic acid in water (Solvent A) and 0.1% formic acid in acetonitrile (Solvent B) and a linear gradient of 0-100% B over 30 min.

2.2.2: Chemicals and Material

The following chemicals were purchased either from Sigma Aldrich, Fluorochem, Across Organics, and TCI (Tokyo Chemical Industry) and used without any further purification:

1,10-phenanthroline, $KBrO_3$, L-tyrosine, L-phenylalanine, *p*-nitro-L-phenylalanine, acetyl chloride, N-methylmorpholine, trimethylamine, pyridine, isonicotinic acid hydrazide, hydrazine monohydrate, Pd/C (10% loading), *p*-tolouene sulfonic acid, $Ag(ClO_4)$, $Ag(BF_4)$, $Ag(NO_3)$, $Cu(ClO_4)_2.6H_2O$, $Cu(BF_4)_2.xH_2O$, $Mn(ClO_4)_2.6H_2O$, $Mn(NO_3)_2.6H_2O$, Copper standard solution (for FAAS) 1 mg/ml Cu in 2 to 5% HNO_3.

Nutrient broth and Phosphate Buffered Saline (PBS) were obtained from Sigma Aldrich and prepared according to the manufacturer's instructions. Minimal Growth Media (MM) was made by dissolving glucose (2% w/v), Yeast Nitrogen Base without amino acid (0.17% w/v), and ammonium sulfate (0.5% w/v) in dH_2O. Yeast Extract Peptone Dextrose (YEPD) media composed of glucose (2% w/v), bacteriological peptone (2% w/v), and yeast extract (1% w/v).

2.3: Synthesis of Oxazine-based Phenanthroline Derivatives and their Metal Complexes

2.3.1: Synthesis of 1,10-phenanthroline-5,6-dione (3.1):

Following a reported procedure[216], 1,10-phenanthroline (2.000 g, 11.10 mmol) was dissolved in 24 mL of 60% H_2SO_4. To this, $KBrO_3$ (2.039 g, 12.21 mmol) was added in small portions over a period of 30 min. The solution was allowed to stir for 20 h at 30 °C. The resulting clear deep red solution was poured over 300 g of ice and neutralised using saturated NaOH solution. The desired product was then separated using DCM and recrystallized from MeOH. The final product was filtered, washed with 3 x 20 ml portions of MeOH and dried under vacuum.

Yield: 1.889 g, 81%

mp: 260-261 °C

MS: Calculated *m/z* for: $(M+H)^+$ 211.0502; Found: $(M+H)^+$ 211.0507; Difference (ppm): 2.42

IR (KBr, cm^{-1}): 3061, 1686, 1577, 1560, 1459, 1414, 1315, 1292, 1205, 1115, 1010, 924, 816, 807, 739, 667, 613, 539.

^{1}H NMR ($CDCl_3$, 500 MHz): **δ** 9.12 (dd, *J* = 4.8, 2.1 Hz, 2H), 8.51 (dd, *J* = 8.1, 2.1 Hz, 2H), 7.60 (dd, *J* = 8.1, 4.8 Hz, 2H)

^{13}C NMR ($CDCl_3$, 126 MHz): **δ** 178.6 (**C**=O), 156.4, 152.9, 137.3, 128.1, 125.6.

2.3.2: Synthesis of L-α-amino Esters 3.2a-h:

R	R'	product
-OH	CH_3	**3.2a**
-OH	C_3H_7	**3.2b**
-OH	C_6H_{13}	**3.2c**
-OH	C_8H_{17}	**3.2d**
-OH	$C_{12}H_{25}$	**3.2e**
-H	CH_3	**3.2f**
-H	C_3H_7	**3.2g**
$-NO_2$	C_2H_5	**3.2h**

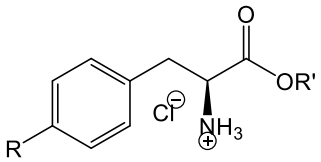

3.2a-h

*Figure 26: structure of L- α-amino ester **3.2a-h***

General Synthesis: The synthesis of the L-α-amino esters (**Figure 26**) was carried out by appropriate modifications of a reported synthesis[217]. Acetyl chloride (4.352 mL, 60.99 mmol) was added to a cold alcohol solution. To this, L- α-amino acid (11.04 mmol) was added and the resulting clear colourless solution was refluxed for 3 h. The resulting solution was filtered and then reduced, if possible, to 10 mL on a rotary evaporator. The product was precipitated via addition of 400 mL diethyl ether. The resulting white solid was filtered and washed with 3 x 50 mL portions of diethyl ether and dried under vacuum. All products **3.2a-h** were synthesised by following this protocol. Any modification required for the synthesis of any of the products are given below.

2.3.2A: <u>L-tyrosine methyl ester hydrochloride</u> (3.2a): L-tyrosine (2.000 g) was added to a MeOH solution (56 mL, 1.4 mol) containing acetyl chloride.

<u>Yield</u>: 2.403 g, 94%

<u>mp</u>: 190-192 °C

<u>MS</u>: Calculated *m/z* for: $(M+H)^+$ 196.0968; Found: $(M+H)^+$ 196.0971; Difference (ppm): 1.50

<u>IR (KBr, cm^{-1}):</u> 3342, 2882, 1744, 1614, 1592, 1515, 1449, 1397, 1349, 1225, 1108, 1060, 991, 935, 866, 840, 732, 599, 514.

^{1}H NMR (DMSO-d6, 500 MHz): **δ** 9.55 (s, 1H, O**H**), 8.67 (s, 3H, $^+$N**H$_3$**), 7.01 (d, *J* = 8.5 Hz, 2H, Ar**H**), 6.74 (d, *J* = 8.5 Hz, 2H, Ar**H**), 4.12 (dd, *J* = 7.8, 5.6 Hz, 1H, α**H**), 3.65 (s, 3H, -OC**H$_3$**), 3.09 (dd, *J* = 14.1, 5.6 Hz, 1H, β**H**), 3.00 (dd, *J* = 14.1, 7.8 Hz, 1H, β**H**).

^{13}C NMR (DMSO-d6, 126 MHz): **δ** 170.0 (**C**=O), 157.2 (**C**-OH), 130.8 (Ar**C**), 124.9 (Ar**C**), 115.9 (Ar**C**), 53.9 (α**C**), 52.9 (-O**C**H$_3$), 35.6 (β**C**).

2.3.2B: L-tyrosine propyl ester hydrochloride (3.2b): L-tyrosine (2.000 g) was added to a 1-propanol solution (103 mL, 1.4 mol) containing acetyl chloride.

Yield: 2.666 g, 93%

mp: 156-158 °C

MS: Calculated *m/z* for: $(M+H)^+$ 224.1281; Found: $(M+H)^+$ 224.1289; Difference (ppm): 3.60

IR (KBr, cm^{-1}): 3293, 2879, 1743, 1615, 1593, 1517, 1446, 1385, 1357, 1232, 1105, 1058, 989, 932, 839, 729, 616, 509.

^{1}H NMR (DMSO-d6, 500 MHz): **δ** 9.51 (s, 1H, O**H**), 8.66 (s, 3H, $^+$N**H$_3$**), 7.08 – 6.93 (m, 2H, Ar**H**), 6.78 – 6.69 (m, 2H, Ar**H**), 4.13 (dd, *J* = 7.8, 5.6 Hz, 1H, α**H**), 4.01 (t, *J* = 6.5 Hz, 2H, -OC**H$_2$**), 3.11 (dd, *J* = 14.1, 5.6 Hz, 1H, β**H**), 2.97 (dd, *J* = 14.1, 7.8 Hz, 1H, β**H**), 1.61 – 1.40 (m, 2H, C**H$_2$**), 0.81 (t, *J* = 7.0 Hz, 3H, C**H$_3$**).

^{13}C NMR (DMSO-d6, 126 MHz): **δ** 169.6 (**C**=O), 157.2 (**C**-OH), 130.8 (Ar**C**), 124.9 (Ar**C**), 115.8 (Ar**C**), 67.4 (-O**C**H$_2$), 53.9 (α**C**), 35.7 (β**C**), 21.7 (**C**H$_2$), 10.6 (**C**H$_3$).

2.3.2C: L-tyrosine hexyl ester hydrochloride (3.2c): L-tyrosine (2.000 g) was added to a 1-hexanol solution (75 mL, 0.6 mol) containing acetyl chloride. The solution was heated to 100˚C for 3 h and hot-filtered. The product was precipitated via addition of 400 mL petroleum ether, filtered and washed with 5 x 50 mL portions of hot petroleum ether. The product was dried under vacuum.

Yield: 2.965 g, 89%

mp: 163-164 °C

MS: Calculated *m/z* for: $(M+H)^+$ 266.1751; Found: $(M+H)^+$ 266.1762; Difference (ppm): 4.30

IR (KBr, cm^{-1}): 3294, 2953, 1739, 1614, 1591, 1517, 1446, 1387, 1356.34, 1231, 1115, 1056, 981, 942, 875, 844, 729, 614, 504.

^{1}H NMR (DMSO-d6, 500 MHz): **δ** 9.50 (s, 1H, O**H**), 8.64 (s, 3H, $^+$N**H₃**), 7.11 – 6.93 (m, 2H, Ar**H**), 6.76 – 6.67 (m, 2H, Ar**H**), 4.13 (dd, *J* = 7.8, 5.6 Hz, 1H, α**H**), 4.08 – 4.01 (m, 2H, -OC**H₂**), 3.10 (dd, *J* = 14.1, 5.6 Hz, 1H, β**H**), 2.95 (dd, *J* = 14.1, 7.8 Hz, 1H, β**H**), 1.54 – 1.41 (m, 2H, C**H₂**), 1.33 – 1.13 (m, 6H, 3 x C**H₂**), 0.86 (t, *J* = 7.0 Hz, 3H, C**H₃**).

^{13}C NMR (DMSO-d6, 126 MHz): **δ** 169.7 (**C**=O), 157.2 (**C**-OH), 130.8 (Ar**C**), 124.9 (Ar**C**), 115.8 (Ar**C**), 65.9 (-O**C**H_2), 53.9 (α**C**), 35.7 (β**C**), 31.3 (**C**H_2), 28.3 (**C**H_2), 25.3 (**C**H_2), 22.4 (**C**H_2), 14.4 (**C**H_3).

2.3.2D: L-tyrosine octyl ester hydrochloride (3.2d): L-tyrosine (2.000 g) was added to a 1-octanol solution (75 mL, 0.48 mol) containing acetyl chloride. The same procedure as L-tyrosine hexyl ester hydrochloride preparation was followed.

Yield: 3.095 g, 85%

mp: 169-171 °C

MS: Calculated *m/z* for: $(M+H)^+$ 294.2064; Found: $(M+H)^+$ 294.2063; Difference (ppm): -0.30

IR (KBr, cm^{-1}): 3296, 2923, 1739, 1614, 1585, 1517, 1446, 1387, 1357, 1232, 1114, 1057, 977, 942, 877, 845, 731, 614, 505.

^{1}H NMR (DMSO-d6, 500 MHz): **δ** 9.44 (s, 1H, O**H**), 8.58 (s, 3H, $^+$N**H₃**), 7.14 – 6.92 (m, 2H, Ar**H**), 6.79 – 6.65 (m, 2H, Ar**H**), 4.13 (dd, *J* = 7.8, 5.6 Hz, 1H, α**H**), 4.09 – 4.00 (m, 2H, -OC**H₂**), 3.09 (dd, *J* = 14.1, 5.6 Hz, 1H, β**H**), 2.96 (dd, *J* = 14.1, 7.8 Hz, 1H, β**H**), 1.55 – 1.42 (m, 2H, C**H₂**), 1.35 – 1.14 (m, 10H, 5 x C**H₂**), 0.87 (t, *J* = 7.0 Hz, 3H, C**H₃**).

^{13}C NMR (DMSO-d6, 126 MHz): **δ** 169.6 (**C**=O), 157.2 (**C**-OH), 130.8 (Ar**C**), 124.9 (Ar**C**), 115.8 (Ar**C**), 65.9 (-O**C**H_2), 53.9 (α**C**), 35.8 (β**C**), 31.7 (**C**H_2), 29.0 (**C**H_2), 28.9 (**C**H_2), 28.3 (**C**H_2), 25.7 (**C**H_2), 22.5 (**C**H_2), 14.4 (**C**H_3).

2.3.2E: L-tyrosine dodecyl ester hydrochloride (3.2e): L-tyrosine (2.000 g) was added to a 1-dodecanol solution (75 mL, 0.34 mol) containing acetyl chloride. The solution was heated to 100 °C and stirred for 3 h. The solution was hot-filtered while maintaining the temperature of the glassware above 35 °C. The product was precipitated by addition of 400 mL of petroleum ether, filtered and washed with multiple portions of heated petroleum ether. The product was dried under vacuum.

Yield: 3.408 g, 80%

mp: 166-168 °C

MS: Calculated *m/z* for: $(M+H)^+$ 350.2690; Found: $(M+H)^+$ 350.2707; Difference (ppm): 5.00

IR (KBr, cm^{-1}): 3287, 2917, 1740, 1614, 1592, 1517, 1446, 1386, 1357, 1235, 1118, 1058, 983, 942, 877, 845, 730, 622, 509.

^{1}H NMR (DMSO-d6, 500 MHz): **δ** 9.44 (s, 1H, O**H**), 8.59 (s, 3H, $^+$N**H$_3$**), 7.04 – 6.98 (m, 2H, Ar**H**), 6.75 – 6.69 (m, 2H, Ar**H**), 4.13 (dd, *J* = 7.8, 5.6 Hz, 1H α**H**), 4.08 – 4.01 (m, 2H, -OC**H$_2$**), 3.09 (dd, *J* = 14.1, 5.6 Hz, 1H, β**H**), 2.96 (dd, *J* = 14.1, 7.8 Hz, 1H, β**H**), 1.54 – 1.42 (m, 2H, C**H$_2$**), 1.32 – 1.16 (m, 18H, 9 x C**H$_2$**), 0.86 (t, *J* = 7.0 Hz, 3H, C**H$_3$**).

^{13}C NMR (DMSO-d6, 126 MHz): **δ** 169.6 (**C**=O), 157.2 (**C**-OH), 130.8 (Ar**C**), 124.9 (Ar**C**), 115.8 (Ar**C**), 65.9 (-O**C**H_2), 53.9 (α**C**), 35.7 (β**C**), 31.8 (**C**H_2), 29.5 (**C**H_2), 29.5 (**C**H_2), 29.5 (**C**H_2), 29.4 (**C**H_2), 29.2 (**C**H_2), 29.1 (**C**H_2), 28.3 (**C**H_2), 25.7 (**C**H_2), 22.6 (**C**H_2), 14.4 (**C**H_3).

2.3.2F: L-phenylalanine methyl ester hydrochloride (3.2f): L-phenylalanine (1.817 g) was added to a MeOH solution (56 mL, 1.4 mol) containing acetyl chloride.

Yield: 2.087 g, 94%

mp: 155-157 °C

MS: Calculated *m/z* for: $(M+H)^+$ 180.1019; Found: $(M+H)^+$ 180.1024; Difference (ppm): 2.80

IR (KBr, cm^{-1}): 3477, 2847, 1747, 1584, 1497, 1448, 1242, 1085, 1062, 991, 935, 748, 702, 627, 474.

^{1}H NMR (DMSO-d6, 500 MHz): **δ** 8.80 (s, 3H, $^{+}$N**H$_3$**), 7.36 – 7.23 (m, 5H, Ar**H**), 4.23 (dd, *J* = 7.8, 5.6 Hz, 1H, α**H**), 3.65 (s, 3H, -OC**H$_3$**), 3.23 (dd, *J* = 14.1, 5.6 Hz, 1H, β**H**), 3.11 (dd, *J* = 14.1, 7.8 Hz, 1H, β**H**).

^{13}C NMR (DMSO-d6, 126 MHz): **δ** 169.8 (**C**=O), 135.3 (Ar**C**), 129.9 (Ar**C**), 129.0 (Ar**C**), 127.7 (Ar**C**), 53.8 (α**C**), 52.9 (-O**C**H$_3$), 36.3 (β**C**).

2.3.2G: L-phenylalanine propyl ester hydrochloride (3.2g): L-phenylalanine (1.817 g) was added to a 1-propanol solution (103 mL, 1.4 mol) containing acetyl chloride.

Yield: 2.548 g, 95%

mp: 150-151 °C

MS: Calculated *m/z* for : $(M+Na)^+$ 230.1151; Found: $(M+Na)^+$ 230.1151; Difference (ppm): -0.20

IR (KBr, cm^{-1}): 3470, 2833, 1743, 1593, 1509, 1443, 1234, 1083, 1057, 982, 928, 743, 702, 642, 483.

^{1}H NMR (DMSO-d6, 500 MHz): **δ** 8.91 (s, 3H, $^{+}$N**H$_3$**), 7.34 – 7.23 (m, 5H, Ar**H**), 4.18 (dd, *J* = 7.8, 5.6 Hz, 1H, α**H**), 4.00 – 3.92 (m, 2H, -OC**H$_2$**), 3.30 (dd, *J* = 14.1, 5.6 Hz, 1H, β**H**), 3.08 (dd, *J* = 14.1, 7.8 Hz, 1H, β**H**), 1.52 – 1.37 (m, 2H, C**H$_2$**), 0.76 – 0.71 (m, 3H, C**H$_3$**).

^{13}C NMR (DMSO-d6, 126 MHz): **δ** 169.5 (**C**=O), 135.4 (Ar**C**), 129.8 (Ar**C**), 128.9 (Ar**C**), 127.6 (Ar**C**), 67.4 (-O**C**H$_2$), 53.8 (α**C**), 36.4 (β**C**), 21.7 (**C**H$_2$), 10.6 (**C**H$_3$).

2.3.2H: 4-nitro-L-phenylalanine ethyl ester hydrochloride (3.2h): *p*-nitro-L-phenylalanine (2.312 g) was added to a EtOH solution (82 mL, 1.4 mol) containing acetyl chloride.

Yield: 2.680 g, 93%

mp: 187-188 °C

MS: Calculated *m/z* for: $(M+H)^+$ 239.1026; Found: $(M+H)^+$ 239.1030; Difference (ppm): 1.50

IR (KBr, cm^{-1}): 3460, 2822, 1736, 1605, 1525, 1506, 1447, 1349, 1246, 1059, 1013, 746, 702, 648, 483.

^{1}H NMR (DMSO-d6, 500 MHz): **δ** 8.89 (s, 3H, $^+$N**H$_3$**), 8.20 (d, *J* = 8.6 Hz, 2H, Ar**H**), 7.61 (d, *J* = 8.6 Hz, 2H, Ar**H**), 4.33 (dd, *J* = 7.8, 5.6 Hz, 1H, α**H**), 4.18 – 4.06 (m, 2H, OC**H$_2$**), 3.41 (dd, *J* = 14.1, 5.6 Hz, 1H, β**H**), 3.27 (dd, *J* = 14.1, 7.8 Hz, 1H, β**H**), 1.10 (t, *J* = 7.0 Hz, 3H).

^{13}C NMR (DMSO-d6, 126 MHz): **δ** 169.0 (**C**=O), 147.3 (Ar**C**), 143.7 (Ar**C**), 131.5 (Ar**C**), 123.9 (Ar**C**), 62.3 (-O**C**H$_2$), 53.2 (α**C**), 35.9 (β**C**), 14.3 (**C**H$_3$).

2.3.3: Synthesis of alkyl-2-(4-R-phenyl)-2*H*-[1,4]oxazino[2,3-*f*][1,10]phenanthroline-3-carboxylate (3.3a-h, Figure 27):

R	R'	product
-OH	CH_3	**3.3a**
-OH	C_3H_7	**3.3b**
-OH	C_6H_{13}	**3.3c**
-OH	C_8H_{17}	**3.3d**
-OH	$C_{12}H_{25}$	**3.3e**
-H	CH_3	**3.3f**
-H	C_3H_7	**3.3g**

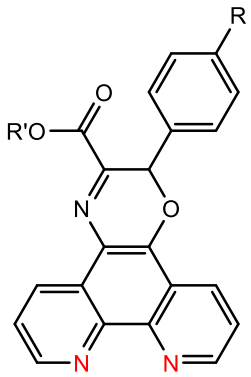

3.3a-g

*Figure 27: structure of alkyl-2-(4-R-phenyl)-2H-[1,4]oxazino[2,3-f][1,10]phenanthroline-3-carboxylate (**3.3a-g**)*

General Synthesis: L-α-amino ester hydrochloride salt (1.00 mmol) was dissolved in 25 mL of DMSO and to this solution, *N*-methylmorpholine (0.121 mL, 1.10 mmol) was added. The solution was heated to 75˚C while being constantly stirred and **3.1** (0.210 g, 1.00 mmol) was then added to give a bright yellow solution. After constant stirring at 75˚C for 24 h, a clear bright orange solution was observed and mixed with 125 mL of DCM. The organic layer was washed with 5 x 125 mL portions of H_2O and then dried over $MgSO_4$. The resulting DCM solution was condensed to dryness on a rotary evaporator to give the crude product. If a syrup was observed at this point, further washings with H_2O would be required to separate out the DMSO. The dried contents of the flask were then heated in 15 mL MeOH and allowed to stand overnight. The

resulting bright yellow crystalline solid was filtered, washed with 3x 20 mL portions of MeOH and dried under vacuum.

2.3.3A: methyl-2-(4-hydroxyphenyl)-2*H*-[1,4]oxazino[2,3-*f*][1,10]phenanthroline-3-carboxylate (3.3a): 3.2a (0.232 g) was reacted with **3.1** according to the general method.

Yield: 0.173 g, 45%

mp: decomp. @ 250 °C

MS: Calculated *m/z* for: $(M+H)^+$ 386.1135; Found: $(M+H)^+$ 386.1144; Difference (ppm): 2.20

IR (KBr, cm^{-1}): 3283, 2946, 1711, 1609, 1587, 1514, 1503, 1439, 1354, 1258, 1174, 1131, 1060, 1018, 982, 971, 920, 806, 741, 679, 632.

^{1}H NMR (DMSO-d6, 500 MHz): **δ** 9.72 (s, 1H, O**H**), 9.13 (dd, *J* = 4.3, 1.8 Hz, 1H, Phen**H**), 9.04 (dd, *J* = 4.3, 1.8 Hz, 1H, Phen**H**), 8.89 (dd, *J* = 8.3, 1.8 Hz, 1H, Phen**H**), 8.61 (dd, *J* = 8.3, 1.8 Hz, 1H, Phen**H**), 7.85 (dd, *J* = 8.3, 4.3 Hz, 1H, Phen**H**), 7.80 (dd, *J* = 8.3, 4.3 Hz, 1H, Phen**H**), 7.23 – 7.18 (m, 2H, Ar**H**), 6.72 – 6.63 (m, 2H, Ar**H**), 6.59 (s, 1H, β**H**), 3.90 (s, 3H, -OC**H$_3$**).

^{13}C NMR (DMSO-d6, 126 MHz): **δ** 163.1 (**C**=O), 159.2 (**C**-OH), 152.0 (Phen**C**), 150.2 (α**C**), 149.1 (Phen**C**), 146.8 (Phen**C**), 142.7 (Phen**C**), 138.9 (Phen**C**-O), 131.4 (Phen**C**), 130.3 (Phen**C**), 129.4 (Ar**C**), 126.5 (Phen**C**-N), 125.3 (Ar**C**), 124.6 (Phen**C**), 124.3 (Phen**C**), 122.2 (Phen**C**), 121.7 (Phen**C**), 116.3 (Ar**C**), 72.5 (β**C**), 53.4 (-O**C**H_3).

2.3.3B: propyl-2-(4-hydroxyphenyl)-2*H*-[1,4]oxazino[2,3-*f*][1,10]phenanthroline-3-carboxylate (3.3b): 3.2b (0.260 g) was reacted with **3.1** according to the general method.

Yield: 0.169 g, 41%

mp: decomp. @ 230 °C

MS: Calculated *m/z* for: $(M+H)^+$ 414.1448; Found: $(M+H)^+$ 414.1440; Difference (ppm): -2.08

IR (KBr, cm^{-1}): 3443, 2973, 1734, 1610, 1592, 1516, 1500, 1434, 1379, 1351, 1313, 1286, 1254, 1239, 1223, 1172, 1133, 1073, 1021, 969, 925, 831, 742, 678, 632.

^{1}H NMR (DMSO-d6, 500 MHz): **δ** 9.74 (s, 1H, O**H**), 9.12 (dd, *J* = 4.3, 1.8 Hz, 1H, Phen**H**), 9.03 (dd, *J* = 4.3, 1.8 Hz, 1H, Phen**H**), 8.88 (dd, *J* = 8.3, 1.8 Hz, 1H, Phen**H**), 8.59 (dd, *J* = 8.3, 1.8 Hz, 1H, Phen**H**), 7.85 (dd, *J* = 8.3, 4.3 Hz, 1H, Phen**H**), 7.79 (dd, *J* = 8.3, 4.3 Hz, 1H, Phen**H**), 7.22 – 7.19 (m, 2H, Ar**H**), 6.69 – 6.66 (m, 2H, Ar**H**), 6.57 (s, 1H, β**H**), 4.30 – 4.21 (m, 2H, -OC**H$_2$**), 1.75 – 1.64 (m, 2H, C**H$_2$**), 0.91 (t, *J* = 7.5 Hz, 3H, C**H$_3$**).

^{13}C NMR (DMSO-d6, 126 MHz): **δ** 162.6 (**C**=O), 159.2 (**C**-OH), 151.9 (Phen**C**), 150.6 (α**C**), 149.1 (Phen**C**), 146.8 (Phen**C**), 142.7 (Phen**C**), 138.9 (Phen**C**), 131.4 (Phen**C**), 130.3 (Phen**C**), 129.4 (Ar**C**), 126.5 (Phen**C**-N), 125.5 (Ar**C**), 124.6 (Phen**C**), 124.2 (Phen**C**), 122.1 (Phen**C**), 121.7 (Phen**C**), 116.3 (Ar**C**), 72.7 (β**C**), 67.7 (-O**C**H_2), 21.9 (**C**H_2), 10.6 (**C**H_3).

2.3.3C: hexyl-2-(4-hydroxyphenyl)-2*H*-[1,4]oxazino[2,3-*f*][1,10]phenanthroline-3-carboxylate (3.3c): 3.2c (0.302 g) was reacted with **3.1** according to the general method.

Yield: 0.173 g, 38%

mp: 208-209 °C

MS: Calculated *m/z* for: $(M+H)^+$ 456.1918; Found: $(M+H)^+$ 456.1940; Difference (ppm): 4.80

IR (KBr, cm^{-1}): 3425, 2961, 1707, 1607, 1583, 1513, 1503, 1434, 1380, 1341, 1327, 1290, 1260, 1172, 1134, 1073, 1022, 956, 929, 840, 742, 684, 635.

^{1}H NMR (DMSO-d6, 500 MHz): **δ** 9.70 (s, 1H, O**H**), 9.12 (dd, *J* = 4.3, 1.8 Hz, 1H, Phen**H**), 9.03 (dd, *J* = 4.3, 1.8 Hz, 1H, Phen**H**), 8.88 (dd, *J* = 8.3, 1.8 Hz, 1H, Phen**H**), 8.58 (dd, *J* = 8.3, 1.8 Hz, 1H, Phen**H**), 7.84 (dd, *J* = 8.3, 4.3 Hz, 1H, Phen**H**), 7.78 (dd, *J* = 8.3, 4.3 Hz, 1H, Phen**H**), 7.21 – 7.17 (m, 2H, Ar**H**), 6.69 – 6.66 (m, 2H, Ar**H**), 6.57 (s, 1H, β**H**),

4.33 – 4.24 (m, 2H, -OC**H₂**), 1.69 – 1.63 (m, 2H, C**H₂**), 1.31 – 1.23 (m, 6H, 3 x C**H₂**), 0.86 – 0.83 (m, 3H, C**H₃**).

^{13}C NMR (DMSO-d6, 126 MHz): **δ** 162.7 (**C**=O), 159.4 (**C**-OH), 152.1 (Phen**C**), 150.8 (α**C**), 149.2 (Phen**C**), 147.0 (Phen**C**), 142.9 (Phen**C**), 139.0 (Phen**C**-O), 131.5 (Phen**C**), 130.4 (Phen**C**), 129.6 (Ar**C**), 126.7 (Phen**C**-N), 125.6 (Ar**C**), 124.7 (Phen**C**), 124.3 (Phen**C**), 122.3 (Phen**C**), 121.9 (Phen**C**), 116.4 (Ar**C**), 72.9 (β**C**), 66.4 (-O**C**H_2), 31.4 (**C**H_2), 28.5 (**C**H_2), 25.6 (**C**H_2), 22.6 (**C**H_2), 14.5 (**C**H_3).

2.3.3D: octyl-2-(4-hydroxyphenyl)-2*H*-[1,4]oxazino[2,3-*f*][1,10]phenanthroline-3-carboxylate (3.3d): 3.2d (0.330 g) was reacted with **3.1** according to the above method.

Yield: 0.169 g, 35%

mp: 213-215 °C

MS: Calculated *m/z* for: $(M+H)^+$ 484.2231; Found: $(M+H)^+$ 484.2240; Difference (ppm): 1.86

IR (KBr, cm^{-1}): 3435, 2925, 1739, 1609, 1594, 1578, 1517, 1501, 1432, 1375, 1314, 1277, 1238, 1173, 1137, 1071, 1022, 944, 930, 839, 818, 742, 676, 631.

^{1}H NMR (DMSO-d6, 500 MHz): **δ** 9.70 (s, 1H, O**H**), 9.12 (dd, *J* = 4.3, 1.8 Hz, 1H, Phen**H**), 9.03 (dd, *J* = 4.3, 1.8 Hz, 1H, Phen**H**), 8.87 (dd, *J* = 8.3, 1.8 Hz, 1H, Phen**H**), 8.57 (dd, *J* = 8.3, 1.8 Hz, 1H, Phen**H**), 7.83 (dd, *J* = 8.3, 4.3 Hz, 1H, Phen**H**), 7.78 (dd, *J* = 8.3, 4.3 Hz, 1H, Phen**H**), 7.22 – 7.18 (m, 2H, Ar**H**), 6.69 – 6.65 (m, 2H, Ar**H**), 6.57 (s, 1H, β**H**), 4.34 – 4.24 (m, 2H, -OC**H₂**), 1.71 – 1.63 (m, 2H, C**H₂**), 1.33 – 1.20 (m, 10H, 5 x C**H₂**), 0.87 – 0.82 (m, 3H, C**H₃**).

^{13}C NMR (DMSO-d6, 126 MHz): **δ** 162.5 (**C**=O), 159.3 (**C**-OH), 151.9 (Phen**C**), 150.6 (α**C**), 149.1 (Phen**C**), 146.9 (Phen**C**), 142.7 (Phen**C**), 138.9 (Phen**C**-O), 131.4 (Phen**C**), 130.2 (Phen**C**), 129.4 (Ar**C**), 126.5 (Phen**C**-N), 125.4 (Ar**C**), 124.6 (Phen**C**), 124.2 (Phen**C**), 122.1 (Phen**C**), 121.7 (Phen**C**), 116.2 (Ar**C**), 72.7 (β**C**), 66.2 (-O**C**H_2), 31.6 (**C**H_2), 29.04 (**C**H_2), 29.01 (**C**H_2), 28.4 (**C**H_2), 25.8 (**C**H_2), 22.5 (**C**H_2), 14.4 (**C**H_3).

2.3.3 E: dodecyl-2-(4-hydroxyphenyl)-2*H*-[1,4]oxazino[2,3-*f*][1,10]phenanthroline-3-carboxylate (3.3e): 3.2e (0.386 g) was reacted with **3.1** according to the general method.

Yield: 0.167 g, 31%

mp: 172-174 °C

MS: Calculated *m/z* for: $(M+H)^+$ 540.2857; Found: $(M+H)^+$ 540.2857; Difference (ppm): -1.10

IR (KBr, cm^{-1}): 3430, 2923, 1737, 1711, 1610, 1590, 1516, 1503, 1487, 1464, 1433, 1377, 1322, 1285, 1238, 1171, 1130, 1072, 1021, 956, 840, 810, 739, 677, 631.

^{1}H NMR (DMSO-d6, 500 MHz): **δ** 9.70 (s, 1H, O**H**), 9.11 (dd, *J* = 4.3, 1.8 Hz, 1H, Phen**H**), 9.02 (dd, *J* = 4.3, 1.8 Hz, 1H, Phen**H**), 8.87 (dd, *J* = 8.3, 1.8 Hz, 1H, Phen**H**), 8.56 (dd, *J* = 8.3, 1.8 Hz, 1H, Phen**H**), 7.82 (dd, *J* = 8.3, 4.3 Hz, 1H, Phen**H**), 7.76 (dd, *J* = 8.3, 4.3 Hz, 1H, Phen**H**), 7.21 – 7.18 (m, 2H, Ar**H**), 6.69 – 6.66 (m, 2H, Ar**H**), 6.56 (s, 1H, β**H**), 4.34 – 4.22 (m, 2H, -OC**H₂**), 1.68 – 1.62 (m, 2H, C**H₂**), 1.33 – 1.09 (m, 18H, 9 x C**H₂**), 0.78 (t, *J* = 6.9 Hz, 3H, C**H₃**).

^{13}C NMR (DMSO-d6, 126 MHz): **δ** 162.5 (**C**=O), 159.3 (**C**-OH), 151.9 (Phen**C**), 150.5 (α**C**), 149.0 (Phen**C**), 146.9 (Phen**C**), 142.8 (Phen**C**), 138.8 (Phen**C**-O), 131.3 (Phen**C**), 130.2 (Phen**C**), 129.4 (Ar**C**), 126.5 (Phen**C**-N), 125.4 (Ar**C**), 124.4 (Phen**C**), 124.1 (Phen**C**), 122.1 (Phen**C**), 121.7 (Phen**C**), 116.2 (Ar**C**), 72.7 (β**C**), 66.2 (-O**C**H_2), 31.7 (**C**H_2), 29.5 (**C**H_2), 29.5 (**C**H_2), 29.4 (**C**H_2), 29.4 (**C**H_2), 29.2 (**C**H_2), 29.0 (**C**H_2), 28.4 (**C**H_2), 25.8 (**C**H_2), 22.5 (**C**H_2), 14.3 (**C**H_3).

2.3.3F: methyl 2-phenyl-2*H*-[1,4]oxazino[2,3-*f*][1,10]phenanthroline-3-carboxylate (3.3f): 3.2f (0.215 g) was reacted with **3.1** according to the general method. The desired product could not be isolated by the work-up given previously. A small amount of solid was precipitated via dropwise addition of diethyl ether. The impure product could be observed in the NMR spectra of this solid.

MS: Calculated *m/z* for: $(M+H)^+$ 370.1186; Found: $(M+H)^+$ 370.1192; Difference (ppm): 1.57

(impure) ^{1}H NMR (DMSO-d6, 500 MHz): **δ** 9.06 (dd, *J* = 4.3, 1.8 Hz, 1H, Phen**H**), 8.95 (dd, *J* = 4.3, 1.8 Hz, 1H, Phen**H**), 8.76 (dd, *J* = 8.3, 1.8 Hz, 1H, Phen**H**), 8.51 (dd, *J* = 8.3, 1.8 Hz, 1H, Phen**H**), 7.75 – 7.69 (m, 2H, Phen**H**), 7.38 – 7.35 (m, 2H, Ar**H**), 7.26 – 7.24 (m, 3H, Ar**H**), 6.63 (s, 1H, β**H**), 3.91 (s, 3H, -OC**H$_3$**).

(impure) ^{13}C NMR (DMSO-d6, 126 MHz): **δ** 163.1, 151.9, 149.7, 149.1, 146.8, 142.7, 138.8, 135.3, 131.3, 130.2, 130.1, 129.5, 127.4, 126.3, 124.5, 124.1, 122.2, 121.4, 72.4, 53.5.

2.3.3G: propyl 2-phenyl-2*H*-[1,4]oxazino[2,3-*f*][1,10]phenanthroline-3-carboxylate (3.3g): 3.2g (0.244 g) was reacted with **3.1** according to the general method. Once the DCM was removed under vacuum, the remaining solid precipitate was heated in a minimum amount of $CHCl_3$, filtered and allowed to stand. A bright yellow precipitate was observed.

Yield: 0.011 g, 3%

mp: 152-153 °C

MS: Calculated *m/z* for: $(M+H)^+$ 398.1499; Found: $(M+H)^+$ 398.1500; Difference (ppm): 0.30

IR (KBr, cm^{-1}): 3433, 2971, 1706, 1711, 1582, 1500, 1489, 1430, 1322, 1249, 1132, 1058, 1019, 973, 800, 738.

^{1}H NMR (DMSO-d6, 500 MHz): **δ** 9.13 (dd, *J* = 4.3, 1.8 Hz, 1H, Phen**H**), 9.03 (dd, *J* = 4.3, 1.8 Hz, 1H, Phen**H**), 8.85 (dd, *J* = 8.3, 1.8 Hz, 1H, Phen**H**), 8.63 (dd, *J* = 8.3, 1.8 Hz, 1H, Phen**H**), 7.84 (dd, *J* = 8.3, 4.3 Hz, 1H, Phen**H**), 7.80 (dd, *J* = 8.3, 4.3 Hz, 1H, Phen**H**), 7.43 – 7.38 (m, 2H, Ar**H**), 7.33 – 7.29 (m, 3H, Ar**H**), 6.71 (s, 1H, β**H**), 4.33 – 4.24 (m, 2H, -OC**H$_2$**), 1.75 – 1.67 (m, 2H, C**H$_2$**), 0.91 (t, *J* = 7.5 Hz, 3H, C**H$_3$**).

^{13}C NMR (DMSO-d6, 126 MHz): **δ** 162.5, 152.1, 150.4, 149.2, 146.9, 142.8, 138.8, 135.5, 131.4, 130.3, 130.1, 129.6, 127.5, 126.6, 124.6, 124.3, 122.2, 121.5, 72.6, 67.8, 21.9, 10.7.

2.3.4: Synthesis of alkyl 4-(4-R-phenyl)-7-oxo-7*H*-pyrido[4,3,2-*de*][1,10]phenanthroline-5-carboxylate (3.4a-c, Figure 28):

R	R'	product
-H	CH_3	**3.4a**
-H	C_3H_7	**3.4b**
$-NO_2$	C_2H_5	**3.4c**

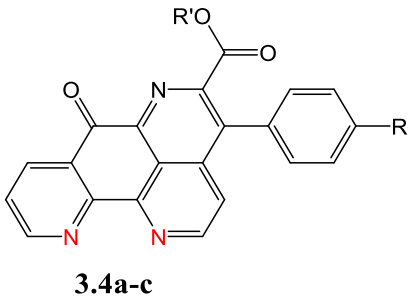

3.4a-c

*Figure 28: structure of alkyl 4-(4-R-phenyl)-7-oxo-7*H*-pyrido[4,3,2-*de*][1,10]phenanthroline-5-carboxylate (**3.4a-c**)*

2.3.4A: methyl 7-oxo-4-phenyl-7*H*-pyrido[4,3,2-*de*][1,10]phenanthroline-5-carboxylate (3.4a): 3.2f (0.215 g) was reacted with **3.1** according to the general method (**Section 2.3.3**). Once the DCM was removed under vacuum, the crude product was dissolved in 3 mL of MeOH and to this solution 5 mL of EtOAc was added. The solution was allowed to crystallise in the freezer to give bright yellow crystals.

Yield: 0.026 g, 7%

mp: decomp. @ 230 °C

MS: Calculated *m/z* for $C_{22}H_{13}N_3O_3$: $(M+Na)^+$ 390.0849; Found: $(M+Na)^+$ 390.0863; Difference (ppm): 3.59

IR (KBr, cm^{-1}): 3434, 1729, 1678, 1578, 1439, 1376, 1280, 1258, 1234, 1202, 1167, 1002, 702, 676, 607.

^{1}H NMR (DMSO-d6, 500 MHz): **δ** 9.12 – 9.09 (m, 1H, Phen**H**), 9.02 (d, *J* = 5.9 Hz, 1H, Phen**H**), 8.62 (dd, *J* = 7.9, 1.6 Hz, 1H, Phen**H**), 7.82 (dd, *J* = 7.9, 4.6 Hz, 1H, Phen**H**), 7.69 – 7.60 (m, 4H, Phen**H** + 3Ar**H**), 7.51 – 7.46 (m, 2H, Ar**H**), 3.70 (s, 3H, -OC**H$_3$**).

^{13}C NMR (DMSO-d6, 126 MHz): **δ** 181.0 (**C**=O), 166.7 (**C**=O), 155.3 (Phen**C**), 151.7 (Phen**C**), 150.7 (Phen**C**), 149.0 (Phen**C**), 147.5 (α**C**), 146.4 (Phen**C**=N), 138.5 (Phen**C**), 135.9 (Phen**C**), 135.4 (Ar**C**), 133.5 (β**C**), 130.2 (Ar**C**), 129.7 (Ar**C**), 129.4 (Phen**C**), 129.2 (Ar**C**), 126.6 (Phen**C**), 120.8 (Phen**C**), 119.8 (Phen**C**), 53.1 (-O**C**H$_3$).

2.3.4B: propyl 7-oxo-4-phenyl-7*H*-pyrido[4,3,2-*de*][1,10]phenanthroline-5-carboxylate (3.4b): 3.2g (0.244 g) was reacted with **3.1** according to the general method (**Section 2.3.3**). Once the DCM was removed under vacuum, the crude product was dissolved in warm diethyl ether. The solution was allowed to cool. The desired product precipitated as a yellow solid during evaporation of diethyl ether. It was filtered and air dried.

Yield: 0.073 g, 18%

mp: decomp. @ 230 °C

MS: Calculated *m/z* for: $(M+Na)^+$ 418.1162; Found: $(M+Na)^+$ 418.1164; Difference (ppm): 0.5

IR (KBr, cm^{-1}): 3434, 1728, 1676, 1579, 1441, 1378, 1281, 1259, 1232, 1200, 1169, 1001, 705, 679, 606.

^{1}H NMR (DMSO-d6, 500 MHz): **δ** 9.15 – 9.14 (m, 1H, Phen**H**), 9.07 (d, *J* = 5.9 Hz, 1H, Phen**H**), 8.66 (dd, *J* = 7.9, 1.6 Hz, 1H, Phen**H**), 7.85 (dd, *J* = 7.9, 4.6 Hz, 1H, Phen**H**), 7.71 – 7.62 (m, 4H, Phen**H** + 3Ar**H**), 7.53 – 7.47 (m, 2H, Ar**H**), 4.06 (s, *t* = 6.5 Hz, 2H, -OC**H$_2$**), 1.37 (dt, *J* = 7.3, 6.5 Hz, 2H, C**H$_2$**), 0.70 (t, *J* = 7.3 Hz, 3H, C**H$_3$**).

^{13}C NMR (DMSO-d6, 126 MHz): **δ** 181.1 (**C**=O), 166.5 (**C**=O), 155.3 (Phen**C**), 151.8 (Phen**C**), 149.1 (Phen**C**), 148.0 (Phen**C**), 146.6 (α**C**), 146.6 (Phen**C**=N), 138.5 (Phen**C**), 136.0 (Phen**C**), 135.0 (Ar**C**), 133.6 (β**C**), 130.3 (Ar**C**), 129.8 (Ar**C**), 129.5 (Phen**C**), 129.3 (Ar**C**), 126.6 (Phen**C**), 120.9 (Phen**C**), 119.8 (Phen**C**), 67.58 (-O**C**H$_2$), 21.6 (**C**H$_2$), 10.6 (**C**H$_3$).

2.3.4C: ethyl 4-(4-nitrophenyl)-7-oxo-7*H*-pyrido[4,3,2-*de*][1,10]phenanthroline-5-carboxylate (3.4c): 3.2h (0.262 g) was reacted with **3.1** according to the general method. The crude product was dissolved in 10 mL EtOH and allowed to stand in the freezer overnight. The bright red precipitate formed was filtered, washed with 3 x 10 mL portions of cold EtOH and dried under vacuum.

Yield: 0.132 g, 30%

mp: > 250 °C

MS: Calculated *m/z* for: $(M+Na)^+$ 449.0856; Found: $(M+Na)^+$ 449.0878; Difference (ppm): 4.89

IR (KBr, cm^{-1}): 3429, 2927, 1723, 1683, 1598, 1581, 1505, 1345, 1291, 1204, 1104, 859, 709.

^{1}H NMR (DMSO-d6, 500 MHz): **δ** 9.15 (dd, *J* = 4.6, 1.8 Hz, 1H, Phen**H**), 9.07 (d, *J* = 5.9 Hz, 1H, Phen**H**), 8.67 (dd, *J* = 7.9, 1.8 Hz, 1H, Phen**H**), 8.53 – 8.45 (m, 2H Ar**H**), 7.86 (dd, *J* = 7.9, 4.6 Hz, 1H, Phen**H**), 7.83 – 7.78 (m, 2H, Ar**H**), 7.61 (d, *J* = 5.9 Hz, 1H Phen**H**), 4.19 (q, *J* = 7.1 Hz, 2H, -OC**H$_2$**), 1.04 (t, *J* = 7.1 Hz, 3H, C**H$_3$**).

^{13}C NMR (DMSO-d6, 126 MHz): **δ** 181.1 (**C**=O), 165.6 (**C**=O), 155.4 (Phen**C**), 151.7 (Phen**C**), 150.8 (Phen**C**), 149.3 (Phen**C**), 148.4 (Ar**C**), 147.3 (α**C**), 146.8 (Phen**C**=N), 141.0 (Ar**C**), 138.5 (Phen**C**), 136.1 (Phen**C**), 134.10 (β**C)** 131.8 (Ar**C**), 129.5 (Phen**C**), 126.7 (Phen**C**), 124.2 (Ar**C**), 120.8 (Phen**C**), 119.7 (Phen**C**), 62.3 (-O**C**H_2), 14.0 (**C**H_3).

2.3.5: Metal Complexation of 3.2a-e:

2.3.5A1: [Ag(3.3a)$_2$](ClO$_4$).2MeOH.H$_2$O (3.5a1):

A 10 mL MeOH solution of $AgClO_4$ (0.027 g, 130 μmol) was added to a stirred heated 40 mL MeOH suspension of **3.3a** (0.100 g, 260 μmol). The resulting clear yellow solution was refluxed in the absence of light for 2 h to give a yellow suspension. The resulting bright yellow precipitate was filtered, washed with 3 x 20 mL portions of MeOH, and dried under vacuum.

Yield: 0.097 g, 70%

CHN (%): Calculated $[Ag(C_{22}H_{15}N_3O_4)_2](ClO_4).2MeOH.H_2O$:

Carbon, 52.11; Hydrogen, 3.80; Nitrogen, 7.93. Found: Carbon, 52.05; Hydrogen, 3.52; Nitrogen, 8.00

MS: Calculated *m/z* for $[Ag(C_{22}H_{15}N_3O_4)_2]^+$: $(M)^+$ 877.1171; Found: $(M+H)^+$ 877.1198; Difference (ppm): 3.08

IR (KBr, cm^{-1}): 3424, 1714, 1611, 1596, 1509, 1435, 1346, 1260, 1173, 1098, 1032, 809, 734, 622.

^{1}H NMR (DMSO-d6, 500 MHz): **δ** 9.75 (s, 2H, O**H**), 9.13 (dd, *J* = 4.5, 1.6 Hz, 2H, Phen**H**), 9.07 – 9.01 (m, 4H, Phen**H**), 8.77 (dd, *J* = 8.3, 1.6 Hz, 2H, Phen**H**), 8.04 – 7.93 (m, 4H, Phen**H**), 7.30 – 7.19 (m, 4H, Ar**H**), 6.71 – 6.68 (m, 4H, Ar**H**), 6.66 (s, 2H, β**H**), 3.93 (s, 6H, -OC**H$_3$**).

^{13}C NMR (DMSO-d6, 126 MHz): **δ** 162.9 (**C**=O), 159.4 (Ar**C**), 153.0 (Phen**C**), 151.1 (α**C**), 150.4 (Phen**C**), 143.3 (Phen**C**), 139.2 (Phen**C**), 139.2 (Phen**C**), 133.4 (Phen**C**), 132.4 (Phen**C**), 129.6 (Ar**C**), 127.2 (Phen**C**), 126.1 (Phen**C**), 125.8 (Phen**C**), 125.1 (Ar**C**), 122.4 (Phen**C**), 122.3 (Phen**C**), 116.3 (Ar**C**), 72.9 (β**C**), 53.6 (-O**C**H_3).

2.3.5A2: $[Cu(3.3a)_3](ClO_4)_2.2H_2O$ (3.5a2):

A 10 mL MeOH solution of $Cu(ClO_4)_2.6H_2O$ (0.064 g, 174 µmol) was added to a stirred heated 40 mL MeOH suspension of **3.3a** (0.200 g, 519 µmol). The resulting clear green solution was refluxed for 2 h. The resulting clear green solution was reduced to 10 mL under vacuum and allowed to stand overnight. The resulting bright green precipitate was filtered, washed with 3 x 5 mL portions of cold MeOH, and dried under vacuum.

Yield: 0.072 g, 29%

CHN (%): Calculated $[Cu(C_{22}H_{15}N_3O_4)_3](ClO_4)_2.2H_2O$:

Carbon, 54.54; Hydrogen, 3.40; Nitrogen, 8.67. Found: Carbon, 54.30; Hydrogen, 3.62; Nitrogen, 8.41

IR (KBr, cm^{-1}): 3392, 1720, 1609, 1515, 1436, 1352, 1263, 1174, 1085, 1038, 813, 731, 624.

μ_{eff} = 2.3 BM

2.3.5A3: [Mn(3.3a)$_3$](ClO$_4$)$_2$.MeOH.2H$_2$O (3.5a3):

A 20 mL MeOH solution of Mn(ClO$_4$)$_2$.6H$_2$O (0.063 g, 173 µmol) was added to a stirred heated 80 mL MeOH suspension of **3.3a** (0.200 g, 519 µmol). The resulting clear yellow solution was refluxed for 2 h. The resulting clear yellow solution was reduced to 10 mL under vacuum and allowed to stand overnight. The resulting bright yellow precipitate was filtered, washed with 3 x 5 mL portions of cold MeOH, and dried under vacuum.

Yield: 0.134 g, 52%

CHN (%): Calculated [Mn(C$_{22}$H$_{15}$N$_3$O$_4$)$_3$](ClO$_4$)$_2$.MeOH.2H$_2$O:

Carbon, 54.45; Hydrogen, 3.61; Nitrogen, 8.53. Found: Carbon, 54.51; Hydrogen, 3.61; Nitrogen, 8.52

IR (KBr, cm^{-1}): 3399, 1719, 1607, 1515, 1438, 1353, 1263, 1174, 1100, 1035, 813, 734, 623.

μ_{eff} = 6.0 BM

2.3.5B: [Cu(3.3b)$_3$](ClO$_4$)$_2$.2H$_2$O (3.5b): A 10 mL MeCN solution of Cu(ClO$_4$)$_2$.6H$_2$O (0.062 g, 0.166 mmol) was added to a stirred heated 40 mL MeCN suspension of **3.3b** (0.207 g, 0.500 mmol). The resulting clear, luminescent green solution was refluxed for 2 h. The solution was reduced to 5 mL under vacuum. The product was precipitated via addition of ~400 mL diethyl ether, filtered, washed with 3 x 50 mL portions of diethyl ether, and dried under vacuum.

Yield: 0.202 g, 80%

CHN (%): Calculated [Cu(C$_{24}$H$_{19}$N$_3$O$_4$)$_3$](ClO$_4$)$_2$.2H$_2$O:

Carbon, 56.20; Hydrogen, 4.00; Nitrogen, 8.19. Found: Carbon, 56.36; Hydrogen, 3.79; Nitrogen, 8.18

IR (KBr, cm^{-1}): 3379, 1713, 1610, 1515, 1438, 1353, 1265, 1174, 1086, 1037, 814, 732, 625.

^{1}H NMR (DMSO-d6, 500 MHz): **δ** 9.80 (bs, 3H, O**H**), 7.23 – 7.15 (m, 9H, 2Ar**H** & β**H**), 6.70 (bs, 6H, Ar**H**), 4.26 – 4.20 (m, 6H, -OC**H$_2$**), 1.65 (bs, 6H, C**H$_2$**), 0.86 (bs, 9H, C**H$_3$**).

^{13}C NMR (DMSO-d6, 126 MHz): **δ** 159.0, 129.4, 124.9, 118.1, 115.9, 67.3, 21.4, 10.1, 1.1.

μ_{eff} = 2.0 BM

2.3.5C: [Cu(3.3c)$_3$](ClO$_4$)$_2$.2H$_2$O (3.5c): 3.3c (0.200 g, 0.439 mmol) was reacted with $Cu(ClO_4)_2.6H_2O$ (0.054 g, 0.146 mmol) following the same method as **2.3.5B**.

Yield: 0.196 g, 81%

CHN (%): Calculated $[Cu(C_{27}H_{25}N_3O_4)_3](ClO_4)_2.2H_2O$:

Carbon, 58.43; Hydrogen, 4.78; Nitrogen, 7.57. Found: Carbon, 57.72; Hydrogen, 4.71; Nitrogen, 7.79

IR (KBr, cm^{-1}): 3390, 2954, 1714, 1610, 1515, 1452, 1438, 1352, 1260, 1174, 1101, 1037, 814, 732, 623.

^{1}H NMR (DMSO-d6, 500 MHz): **δ** 9.78 (bs, 3H, O**H**), 7.21 – 7.13 (m, 9H, 2Ar**H** & β**H**), 6.70 (bs, 6H, Ar**H**), 4.28 – 4.23 (m, 6H, -OC**H$_2$**), 1.61 (bs, 6H, C**H$_2$**), 1.22 (bs, 18H, 3 x C**H$_2$**), 0.83 (bs, 9H, C**H$_3$**).

^{13}C NMR (DMSO-d6, 126 MHz): **δ** 159.0, 129.4, 124.9, 115.8, 65.8, 30.7, 27.8, 24.8, 21.9, 13.7.

μ_{eff} = 2.2 BM

2.3.5D: [Cu(3.3d)$_3$](ClO$_4$)$_2$.CH$_3$CN (3.5d): 3.3d (0.200 g, 0.414 mmol) was reacted with $Cu(ClO_4)_2.6H_2O$ (0.051 g, 0.138 mmol) following the same method as **2.3.5B**.

Yield: 0.176 g, 74%

CHN (%): Calculated $[Cu(C_{29}H_{29}N_3O_4)_3](ClO_4)_2.CH_3CN$:

Carbon, 60.94; Hydrogen, 5.17; Nitrogen, 7.98. Found: Carbon, 60.78; Hydrogen, 5.11; Nitrogen, 8.20

IR (KBr, cm^{-1}): 3400, 2927, 1714, 1610, 1515, 1452, 1437, 1383, 1262, 1173, 1087, 1046, 814, 731, 626.

^{1}H NMR (DMSO-d6, 500 MHz): **δ** 9.80 (bs, 3H, O**H**), 7.223 – 7.16 (m, 9H, 2Ar**H** & β**H**), 6.69 (bs, 6H, Ar**H**), 4.28 – 4.22 (m, 6H, -OC**H$_2$**), 1.61 (bs, 6H, C**H$_2$**), 1.21 (bs, 24H, 4 x C**H$_2$**), 0.82 (bs, 9H, C**H$_3$**).

^{13}C NMR (DMSO-d6, 126 MHz): **δ** 159.1, 129.4, 124.9, 115.8, 65.9, 31.1, 28.53, 28.49, 27.9, 25.2, 22.0, 13.9.

μ_{eff} = 2.1 BM

2.3.5E: [Cu(3.3e)$_3$](ClO$_4$)$_2$. (3.5e1): 3.3e (0.219 g, 0.406 mmol) was reacted with $Cu(ClO_4)_2.6H_2O$ (0.050 g, 0.135 mmol) following the same method as **2.3.5B**.

Yield: 0.180 g, 71%

CHN (%): Calculated $[Cu(C_{33}H_{37}N_3O_4)_3](ClO_4)_2$:

Carbon, 63.20; Hydrogen, 5.95; Nitrogen, 6.70. Found: Carbon, 63.45; Hydrogen, 6.28; Nitrogen, 5.79

IR (KBr, cm^{-1}): 3411, 2924, 2852, 1714, 1610, 1515, 1452, 1438, 1383, 1261, 1173, 1102, 1036, 813, 731, 622.

^{1}H NMR (DMSO-d6, 500 MHz): **δ** 9.77 (bs, 3H, O**H**), 7.21 – 7.15 (m, 9H, 2Ar**H** & β**H**), 6.69 (bs, 6H, Ar**H**), 4.28 – 4.23 (m, 6H, -OC**H$_2$**), 1.61 (bs, 6H, C**H$_2$**), 1.20 (bs, 48H, 9 x C**H$_2$**), 0.79 (bs, 9H, C**H$_3$**).

μ_{eff} = 2.1 BM

2.4: Synthesis of Schiff Base Isoniazid Derivatives of 1,10-phenanthroline and their Metal Complexes.

2.4.1: Synthesis of (*Z*)-*N'*-(6-oxo-1,10-phenanthrolin-5(6*H*)-ylidene)isonicotinohydrazide (4.1, Figure 29):

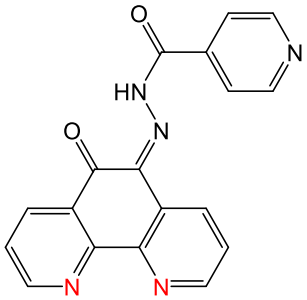

4.1

*Figure 29: structure of (Z)-*N'*-(6-oxo-1,10-phenanthrolin-5(6*H*)-ylidene)isonicotinohydrazide (**4.1**):*

Using an adaption of a reported procedure[218] to synthesise a related compound, **3.1** (0.210 g, 1.00 mmol) was added to a 25 mL EtOH solution of isonicotinic acid hydrazide (0.137 g, 1.00 mmol). *p*-toluenesulfonic acid (0.020 g, 0.116 mmol) was added to the resulting bright yellow solution and the solution was allowed to reflux for 6 hours. The resulting suspension was hot-filtered to remove a minimal amount of undesired 1,10-phenanthroline-5,6-diol (**phendiol**) and the bright orange filtrate was allowed to stand overnight in the absence of light to give yellow needle like crystals of **4.1**. The product was filtered, washed with 3 x 10 mL washings of EtOH, and air dried. The filtrate was allowed to stand in the dark.

Yield: 0.263 g, 79%

mp: 210-211 °C

CHN (%): Calculated ($C_{18}H_{11}N_5O_2$.1/2H_2O):

Carbon, 63.90; Hydrogen, 3.58; Nitrogen, 20.70. Found: Carbon, 63.84; Hydrogen, 3.39; Nitrogen, 20.78

MS: Calculated *m/z* for: $(M+H)^+$ 330.0986; Found: $(M+H)^+$ 330.0997; Difference (ppm): 3.41

IR (KBr, cm^{-1}): 3424, 1723, 1635, 1576, 1557, 1509, 1445, 1407, 1223, 1180, 1064, 1011, 752, 686.

^{1}H NMR (DMSO-d6, 500 MHz): **δ** 15.13 (s, 1H, O--**H**N), 9.11 (dd, *J* = 4.5, 1.7 Hz, 1H, Phen**H**), 8.94 (dd, *J* = 4.4, 1.6 Hz, 2H, Py**H**), 8.90 (dd, *J* = 4.5, 1.7 Hz, 1H, Phen**H**), 8.61 (dd, *J* = 7.9, 1.7 Hz, 1H, Phen**H**), 8.50 (d, *J* = 7.9 Hz, 1H, Phen**H**), 7.88 (dd, *J* = 4.4, 1.6 Hz, 2H, Py**H**), 7.75 (dd, *J* = 7.9, 4.5 Hz, 1H, Phen**H**), 7.67 (dd, *J* = 7.9, 4.5 Hz, 1H, Phen**H**)

^{13}C NMR (DMSO-d6, 126 MHz): **δ** 181.9 (Phen**C**=O), 164.5 (**C**=O), 156.2 (Phen**C**), 152.7 (Phen**C**), 151.6 (Phen**C**), 151.4(Pyr**C**), 147.1 (Phen**C**), 139.4 (Pyr**C**), 136.3 (Phen**C**), 135.1 (Phen**C**-N), 132.2 (Phen**C**), 128.6 (Phen**C**), 127.8 (Phen**C**), 125.6 (Phen**C**), 125.3 (Phen**C**), 122.0 (Pyr**C**).

2.4.2: Metal Complexation of 4.1

2.4.2A1: $[Ag(4.1)_2](ClO_4)$ (4.2a1):

A 20 mL EtOH solution of $Ag(ClO_4)$ (0.104 g, 0.501 mmol) was added to a heated 80 mL EtOH solution of **4.1** (0.329 g, 1.00 mmol). The resulting bright yellow suspension was refluxed in the dark for 3 h. A bright orange suspension was observed and hot-filtered to give a yellow-orange solid. The solid was washed with 3 x 20 mL portions of hot EtOH and 3 x 20 mL portions of DCM.

Yield: 0.353 g, 82%

CHN (%): Calculated $[Ag(C_{18}H_{11}N_5O_2)_2](ClO_4)$:

Carbon, 49.93; Hydrogen, 2.56; Nitrogen, 16.18. Found: Carbon, 50.06; Hydrogen, 2.66; Nitrogen, 16.34

IR (KBr, cm^{-1}): 3408, 1712, 1630, 1578, 1559, 1514, 1456, 1418, 1409, 1329, 1292, 1260, 1221, 1185, 1065, 1017, 820, 750, 679, 624.

^{1}H NMR (DMSO-d6, 500 MHz): **δ** 15.12 (s, 2H, O--**H**N), 9.19 – 9.07 (m, 2H, Phen**H**), 8.96-8.92 (m, 6H, Phen**H** & 2Py**H**), 8.82 (d, *J* = 8.0 Hz, 2H, Phen**H**), 8.70 (d, *J* = 8.0 Hz, 2H, Phen**H**), 7.97 (dd, *J* = 8.0, 4.8 Hz, 2H, Phen**H**), 7.91-7.88 (m, 6H, Phen**H** & 2Py**H**).

^{13}C NMR (DMSO-d6, 126 MHz): **δ** 180.9 (**C**=O), 164.6 (**C**=O), 156.4 (Phen**C**), 152.2 (Phen**C**), 151.5 (Pyr**C**), 149.7 (Phen**C**), 144.2 (Phen**C**), 139.3 (Pyr**C**), 137.9 (Phen**C**), 134.6 (Phen**C**=N), 133.9 (Phen**C**), 130.0 (Phen**C**), 128.8 (Phen**C**), 127.2 (Phen**C**), 126.9 (Phen**C**), 122.0 (Pyr**C**).

2.4.2A2: [Ag(4.1)$_2$](NO$_3$) (4.2a2):

A 20 mL MeCN solution of Ag(NO_3) (0.085 g, 0.500 mmol) was added to a heated 80 mL MeCN solution of **4.1** (0.329 g, 1.00 mmol). The resulting bright orange suspension was refluxed in the dark for 3 h. A bright orange suspension was observed and hot-filtered to give an orange solid. The solid was washed with 3 x 20 mL portions of hot MeCN, 5 x 20 mL portions of hot DCM, and dried under vacuum.

Yield: 0.316 g, 76%

CHN (%): Calculated [Ag($C_{18}H_{11}N_5O_2$)$_2$](NO_3).2H_2O:

Carbon, 50.01; Hydrogen, 3.03; Nitrogen, 17.82. Found: Carbon, 50.44; Hydrogen, 2.79; Nitrogen, 17.91

MS: Calculated *m/z* for [Ag($C_{18}H_{11}N_5O_2$)$_2$]$^+$: $(M)^+$ 765.0876; Found: $(M)^+$ 765.0873; Difference (ppm): -0.39

IR (KBr, cm^{-1}): 3412, 1712, 1631, 1578, 1564, 1510, 1455, 1409, 1340, 1217, 1187, 1068, 1048, 1020, 844, 830, 749, 679, 633.

^{1}H NMR (DMSO-d6, 500 MHz): **δ** 15.15 (s, 2H, O--**H**N), 9.14 (dd, *J* = 4.8, 1.7 Hz, 2H, Phen**H**), 8.97-8.93 (m, 6H, Phen**H** & 2Py**H**), 8.84 (dd, *J* = 8.0, 1.7 Hz, 2H, Phen**H**), 8.73 (d, *J* = 8.0 Hz, 2H, Phen**H**), 7.98 (dd, *J* = 8.0, 4.8 Hz, 2H, Phen**H**), 7.93-7.90 (m, 6H, Phen**H** & 2Py**H**).

^{13}C NMR (DMSO-d6, 126 MHz): **δ** 180.9 (Phen**C**=O), 164.5 (**C**=O), 156.4 (Phen**C**), 152.2 (Phen**C**), 151.5 (Pyr**C**), 149.6 (Phen**C**), 144.1 (Phen**C**), 139.3 (Pyr**C**), 137.9 (Phen**C**),

134.7 (Phen**C**=N), 134.0 (Phen**C**), 130.1 (Phen**C**), 128.9 (Phen**C**), 127.3 (Phen**C**), 126.9 (Phen**C**), 122.1 (Pyr**C**).

2.4.2A3: [Ag(4.1)$_2$](BF$_4$) (4.2a3):

A 20 mL MeCN solution of Ag(BF$_4$) (0.097 g, 0.500 mmol) was added to a heated 80 mL MeCN solution of **4.1** (0.329 g, 1.00 mmol). The resulting bright yellow suspension was refluxed in the dark for 3 h. A bright yellow suspension was observed and hot-filtered to give a bright yellow solid. The solid was washed with 3 x 20 mL portions of hot MeCN, 5 x 20 mL portions of hot DCM, and dried under vacuum.

Yield: 0.305 g, 72%

CHN (%):

Calculated [Ag($C_{18}H_{11}N_5O_2$)$_2$](BF$_4$): Carbon, 50.67; Hydrogen, 2.60; Nitrogen, 16.41

Found: Carbon, 50.02; Hydrogen, 2.24; Nitrogen, 16.06

MS: Calculated *m/z* for [Ag($C_{18}H_{11}N_5O_2$)$_2$]$^+$: (M)$^+$ 765.0876; Found: (M)$^+$ 765.0908; Difference (ppm): 4.2

IR (KBr, cm^{-1}): 3402, 1706, 1629, 1580, 1564, 1521, 1458, 1409, 1290, 1228, 1185, 1080-1030 [s. br *v*(BF$_4$)], 1021, 846, 816, 747, 681, 631.

^{1}H NMR (DMSO-d6, 500 MHz): **δ** 15.14 (s, 2H, O--**H**N), 9.13 (dd, *J* = 4.8, 1.7 Hz, 2H, Phen**H**), 8.95-8.92 (m, 6H, Phen**H** & 2Py**H**), 8.82 (dd, *J* = 8.0, 1.7 Hz, 2H, Phen**H**), 8.70 (d, *J* = 8.0 Hz, 2H, Phen**H**), 7.97 (dd, *J* = 8.0, 4.8 Hz, 2H, Phen**H**), 7.94 – 7.83 (m, 6H, Phen**H** & 2Py**H**).

^{13}C NMR (DMSO-d6, 126 MHz): **δ** 180.5 (Phen**C**=O), 164.5 (**C**=O), 156.0 (Phen**C**), 151.8 (Phen**C**), 151.1 (Pyr**C**), 149.2 (Phen**C**), 143.6 (Phen**C**), 138.8 (Pyr**C**), 137.5 (Phen**C**), 134.2 (Phen**C**=N), 133.5 (Phen**C**), 129.6 (Phen**C**), 128.3 (Phen**C**), 126.9 (Phen**C**), 126.5 (Phen**C**), 121.6 (Pyr**C**).

2.4.2B1: Attempted Synthesis of [$Cu(4.1)_2$](ClO_4)$_2$.$2H_2O$ (4.2b1):

A 5 mL EtOH solution of $Cu(ClO_4)_2.6H_2O$ (0.185 g, 0.500 mmol) was added to a heated 80 mL EtOH solution of **4.1** (0.329 g, 1.00 mmol). The resulting muddy brown suspension was refluxed for 3 h. The resulting brown suspension was hot-filtered to give a dark brown powder. The solid was washed with 3 x 20 mL portions of hot EtOH and dried under vacuum.

Yield: 0.363 g, 72%

CHN (%): Calculated $[Cu(C_{18}H_{11}N_5O_2)_2](ClO_4)_2.2H_2O$: Carbon, 45.18; Hydrogen, 2.74; Nitrogen, 14.63. Found: Carbon, 45.65; Hydrogen, 2.64; Nitrogen, 14.95

IR (KBr, cm^{-1}): 3434, 2128, 1708, 1647, 1577, 1557, 1517, 1461, 1427, 1269, 1226, 1188, 1091, 1024, 817, 754, 730, 685, 623.

μ_{eff} = 1.539 BM

2.4.2B2: Attempted Synthesis of [$Cu(4.1)](BF_4)_2$ (4.2b2):

A 20 mL MeCN solution of $Cu(BF_4)_2.xH_2O$ (0.237 g, 1.00 mmol) was added to a heated 80 mL MeCN solution of **4.1** (0.180 g, 0.550 mmol). The resulting brown solution was stirred for 18 h. The resulting brown suspension was filtered to give a dark brown powder. The solid was washed with 3 x 20 mL portions of cold MeCN and dried under vacuum.

Yield: 0.121 g, 39%

CHN (%): Calculated $[Cu(C_{18}H_{11}N_5O_2)](BF_4)_2$:

Carbon, 38.17; Hydrogen, 1.96; Nitrogen, 12.36. Found: Carbon, 38.32; Hydrogen, 2.29; Nitrogen, 11.80

IR (KBr, cm^{-1}): 3435, 2130, 1706, 1640, 1577, 1517, 1488, 1426, 1305, 1267, 1227, 1184, 1073-1054 [s. br $\nu(BF_4)$], 818, 754, 738, 687.

μ_{eff} = 1.2 BM

2.4.2C1: [Mn(4.1)$_2$](ClO$_4$)$_2$.H$_2$O (4.2c1):

A 10 mL EtOH solution of Mn(ClO$_4$)$_2$.6H$_2$O (0.181 g, 0.500 mmol) was added to a heated 80 mL EtOH solution of **4.1** (0.329 g, 1.00 mmol). The resulting reddish brown suspension was refluxed for 3 h. The resulting red suspension was hot-filtered to give a brick red powder. The solid was washed with 3 x 20 mL portions of hot EtOH and dried under vacuum.

Yield: 0.303 g, 65%

CHN (%): Calculated [Mn(C$_{18}$H$_{11}$N$_5$O$_2$)$_2$](ClO$_4$)$_2$.H$_2$O:

Carbon, 46.47; Hydrogen, 2.60; Nitrogen, 15.05. Found: Carbon, 46.29; Hydrogen, 2.79; Nitrogen, 15.32

IR (KBr, cm^{-1}): 3434, 1705, 1629, 1577, 1557, 1518, 1461, 1422, 1269, 1227, 1183, 1108, 1021, 818, 746, 734, 685, 624.

μ_{eff} = 6.5 BM

2.4.2C2: [Mn(4.1)$_2$](NO$_3$)$_2$.2H$_2$O (4.2c2):

A 20 mL MeCN solution of Mn(NO$_3$)$_2$.4H$_2$O (0.126 g, 0.500 mmol) was added to a heated 80 mL MeCN solution of **4.1** (0.329 g, 1.00 mmol). The resulting bright yellow suspension was refluxed for 3 h. A bright orange suspension was observed and hot-filtered to give an orange solid. The solid was washed with 3 x 20 mL portions of hot MeCN, 5 x 20 mL portions of hot DCM, and dried under vacuum.

Yield: 0.310 g, 70%

CHN (%): Calculated [Mn(C$_{18}$H$_{11}$N$_5$O$_2$)$_2$](NO$_3$)$_2$.2H$_2$O:

Carbon, 49.50; Hydrogen, 3.00; Nitrogen, 19.24. Found: Carbon, 49.67; Hydrogen, 2.45; Nitrogen, 19.02

IR (KBr, cm^{-1}): 3422, 1719, 1642, 1575, 1520, 1443, 1421, 1385, 1303, 1265, 1225, 1186, 1071, 1020, 844, 819, 748, 682, 639.

μ_{eff} = 6.2 BM

2.4.3: Formation of (*E*)-6,6'-(diazene-1,2-diyl)bis(1,10-phenanthrolin-5-ol), (4.3a), and *N'*-isonicotinoylisonicotinohydrazide, (4.3b), From the Filtrate of 2.4.1 (Scheme 1)

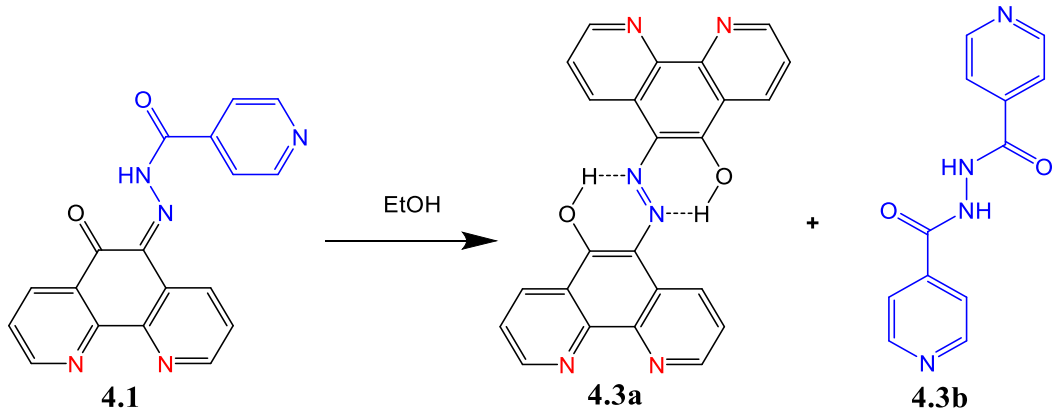

*Scheme 1: Formation of **4.3a** and **4.3b***

The filtrate from reaction **2.4.1** was allowed to stand in the dark for over 4 wks. The bright orange filtrate changed to a dark green suspension. The suspension was heated to reflux and filtered whilst hot to give a clear green filtrate and a dark purple powder. The precipitate was crystallised from $CHCl_3$ to produce X-ray quality crystals. The crystals were filtered and washed with 3 x 20 mL washings of $CHCl_3$ and identified to be **4.3a**. Upon leaving the green filtrate to stand for a further few days, a white solid was observed along the walls of the flask. The contents of the flask were decanted and the white solid was dissolved in hot acetone to give a clear colourless solution. This solution was reduced to dryness on a rotary evaporator to give the white solid identified to be isoniazid diamide, **4.3b**. The characterisation data for **4.3b** was consistent with the literature[219].

Yield (**4.3a**): 0.026 g

CHN (%) (**4.3a**): Calculated ($C_{24}H_{14}N_6O_2$).2$CHCl_3$:

Carbon, 47.52; Hydrogen, 2.45; Nitrogen, 12.79. Found: Carbon, 47.73; Hydrogen, 2.52; Nitrogen, 12.77

IR (KBr, cm^{-1}) (**4.3a**)**:** 3434, 2951, 1626, 1506, 1467, 1418, 1341, 1262, 1106, 1026, 804, 751

^{1}H NMR Protonated (**4.3a**)(CF_3COOD, 500 MHz): **δ** 9.60 (d, *J* = 8.5 Hz, 2H, Phen**H** 9.56 (d, *J* = 8.5 Hz, 2H, Phen**H**), 9.47 (d, *J* = 5.0 Hz, 2H, Phen**H**), 9.37 (d, *J* = 5.0 Hz, 2H, Phen**H**), 8.57 (dd, *J* = 8.5, 5.0 Hz, 2H, Phen**H**), 8.38 (dd, *J* = 8.5, 5.0 Hz, 2H, Phen**H**), 4.12 (s, 2H, O**H**).

Yield: 0.015 g

MS: (**4.3b**): Calculated *m/z* for: $(M+H)^+$ 243.0877; Found: $(M+H)^+$ 243.0882; Difference (ppm): 2.15

IR (KBr, cm^{-1})(**4.3b**): 3435, 3210, 3045, 1682, 1642, 1546, 1489, 1406, 1299, 838, 751.

^{1}H NMR (**4.3b**)(CD_3OD, 500 MHz): **δ** 9.03 – 8.66 (m, 4H, Py**H**), 8.15 – 7.74 (m, 4H, Py**H**).

^{13}C NMR (**4.3b**)(CD_3OD, 126 MHz): **δ** 165.60 (**C**=O), 149.85 (Pyr**C**), 140.52 (Pyr**C**), 121.78 (Pyr**C**).

2.4.3A: Synthesis of 6-nitroso-1,10-phenanthrolin-5-ol (4.3c, Figure 30):

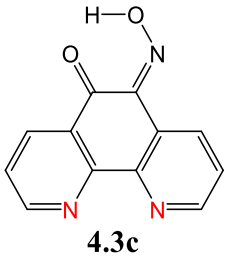

4.3c

*Figure 30: 6-nitroso-1,10-phenanthrolin-5-ol (**4.3c**)*

Following a reported procedure[220], a 4 mL H_2O solution of hydroxylamine hydrochloride (0.350 g, 5.04 mmol) was added dropwise to a refluxing 37 mL EtOH solution of **3.1** (1.050 g, 5.01 mmol). The mixture was allowed to reflux for a further 5 min and allowed to stand overnight. The resulting precipitate was filtered, washed with a large amount of hot EtOH, and dried to give a bright yellow precipitate.

Yield: 0.561 g, 50%

mp: 219-220 °C

MS: Calculated *m/z* for: $(M+H)^+$ 226.0611; Found: $(M+H)^+$ 226.0622; Difference (ppm): 4.95

^{1}H NMR (DMSO-d6, 500 MHz): **δ** 14.75 (s, 1H (major), O--**H**O), 9.53 (d, *J* = 8.3 Hz, 1H (major), Phen**H**), 9.13 (d, *J* = 3.7 Hz, 1H (major), Phen**H**), 8.99 – 8.88 (m, 1H (major) + 1H (minor), Phen**H**), 8.79 (m, 2H (minor), Phen**H**), 8.72 – 8.60 (m, 1H (major) + 1H (minor), Phen**H**), 8.02 – 7.81 (m, 2H (major) + 2H (minor), Phen**H**).

2.4.3B: Synthesis of 6-amino-1,10-phenanthrolin-5-ol (4.3d, Figure 31):

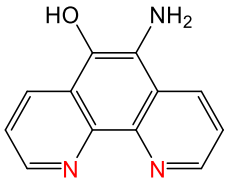

4.3d

*Figure 31: 6-amino-1,10-phenanthrolin-5-ol (**4.3d**)*

To a suspension of **4.3c** (0.225 g, 1.00 mmol) was added 0.1 g of 10% Pd/C in 50 mL EtOH and refluxed for 1 h. The mixture was further refluxed for 6 h following the addition of 4 mL hydrazine hydrate. The mixture was filtered through a celite cake and the filtrate was reduced to dryness on rotary evaporator to yield a red precipitate.

Yield: 0.196 g, 92%

MS: Calculated *m/z* for: $(M+H)^+$ 212.0817; Found: $(M+H)^+$ 212.0818; Difference (ppm): 0.71

IR (KBr, cm^{-1}): 3434, 3344, 3196, 1633, 1569, 1487, 1462, 1437, 1410, 1305, 1227, 1013, 803, 735.

^{1}H NMR (DMSO-d6, 500 MHz): **δ** 8.93 (dd, *J* = 4.2, 1.7 Hz, 1H, Phen**H**), 8.79 (dd, *J* = 4.2, 1.7 Hz, 1H, Phen**H**), 8.64 (dd, *J* = 8.4, 1.7 Hz, 1H, Phen**H**), 8.50 (dd, *J* = 8.4, 1.7 Hz, 1H, Phen**H**), 7.70 (dd, *J* = 8.4, 4.2 Hz, 1H, Phen**H**), 7.64 (dd, *J* = 8.4, 4.2 Hz, 1H, Phen**H**), 7.22 (br. s, 2H, N**H$_2$**).

^{13}C NMR (DMSO-d6, 126 MHz): **δ** 147.21, 145.66, 142.28, 140.65, 130.95, 130.52, 128.95, 127.09, 125.17, 123.10 123.08, 122.62.

2.5: Biological Screening of Compounds 3.3a-e and their Metal Complexes 3.5a-e

2.5.1: Materials and Instruments

All growth media, pipette tips, and falcon vials used for preparation of test solution for biological screening were sterilised in an autoclave (Dixons ST2228) at 120˚C and 124 kPa for 30 minutes. All worktop benches, fume hoods, and analytical equipment were sterilised by washing with 70% (v/v) EtOH/H_2O prioir to use. The loading of 96-well plate were carried out under sterile environment. Deionised water (dH_2O) was used to make all media.

Fungal density was measured using a Neubauer haemocytometer under a light microscope. The bacterial density was measured using Eppendorf BioPhotometer 6131 Spectrophotometer at 600 nm. The growth of microbes in 96-well plate was measured using the Synergy HT Bio-Tek plate reader.

Nutrient broth and PBS were obtained from Sigma Aldrich and prepared according to the manufacturer's instructions. Minimal Growth Media (MM) was made by dissolving glucose (2% w/v), Yeast Nitrogen Base without amino acid (0.17% w/v), and ammonium sulfate (0.5% w/v) in dH_2O. Yeast Extract Peptone Dextrose (YEPD) media composed of glucose (2% w/v), bacteriological peptone (2% w/v), and yeast extract (1% w/v).

Sixt instar larvae of *Galleria mellonella* were obtained from the Mealworm Company, Sheffield, England and stored in the dark at 15˚C.

Myjector U100 insulin syringes used for administration of compound to *G. mellonella* were obtained from Terumo Europe, Leuven, Belgium.

2.5.2: Antimicrobial Susceptibility Testing Methods

2.5.2.1: *in vitro* Antimicrobial Susceptibility Testing Methods

2.5.2.1.1: Preparation of Test Compound Stock Solutions for Susceptibility Testing

Solution of the test compounds were prepared by two methods depending on the solubility of the compound in aqueous media.

Water soluble compounds such as **3.1**, $AgClO_4$, $Mn(ClO_4)_2.6H_2O$, and $Cu(ClO_4)_2.6H_2O$ were dissolved in neat DMSO to yield 4 mM stock solutions. These stock solutions were loaded onto the 96 well plate and doubly-diluted on the plate to give a concentration range of 1 – 0.0039 mM (results were obtained for 0.125 – 0.0039 mM doses which were the solution that contained the DMSO % below 5%).

Water insoluble compounds such as **3.3a-e**, **3.5a-e** and the known antibacterial agents (ampicillin, doxycycline, streptomycin, tetracycline, and vancomycin) were dissolved in neat DMSO to produce 600 µM solutions. These were then doubly-diluted with neat DMSO to produce solutions with concentration range of 600 – 4.69 µM. Each solution was then diluted with growth media (1:5 dilution) to yield stock solutions of concentration range of 120 – 0.94 µM. Each stock solution was then loaded onto the 96-well plate, leading to the final concentration range of 30 – 0.2344 µM being tested against microbial strains. This was 5% DMSO was present in each well that contained compound solutions.

2.5.2.1.2: Determination of Bacterial Cell Minimum Inhibitory Concentrations

Cells (*S. aureus* and *E. coli*) were cultured overnight in an aerated conical flask in an orbital shaker at 37 °C and 200 rpm in nutrient broth. The optical density at 600 nm (OD_{600}) of the bacterial culture was measured and the culture was diluted with nutrient broth to produce a bacterial suspension with OD_{600} of 0.1.

The 96-well plate was loaded with nutrient broth (100 µL) being pipetted into each well. The stock solutions (100 µL) of the test compounds were then loaded onto the 96-well plate. In the case of the water soluble compounds, the 4mM stock solutions were loaded and doubly-diluted on the 96-well plate to give a concentration range of 2 – 0.0078 mM. The bacterial suspension with OD_{600} of 0.1 was loaded (100 µL) onto the appropriate wells of the plate and the bacterial growth was measured at 600 nm after 24 h at 37 °C using a spectrophotometer (BioPhotometer). The final concentration range upon addition of bacterial suspension was 1 – 0.0039 mM (results were obtained for 0.125 – 0.0039 mM ranges as the DMSO % was below 5% for this range).

In the case of the water insoluble compounds, the stock solution prepared in neat DMSO and diluted with media (1:5 dilution) to give a concentration range of 120 – 0.94 µM were loaded onto the 96-well plate (previously loaded with nutrient broth (100 µL). The contents of the wells containing the solution of the test compounds were halved, leading to each well containing 100 µL solutions. The bacterial suspension with OD_{600} of 0.1 was loaded (100 µL) onto the appropriate wells of the plate and the bacterial growth was measured at 600 nm after 24 h at 37 °C using a spectrophotometer (BioPhotometer). The final concentration range of the test compounds upon addition of bacterial suspension was 30 – 0.23 µM.

For all compounds tested, the screening was carried out with a repetition of 2 and in 8 replicates.

2.5.2.1.3: Determination of Minimum Inhibitory Concentrations of 3.3a and its Complexes 3.5a1-3 against Yeast Cells

Cells (*C. albicans*) were cultured overnight in an aerated conical flask in an orbital shaker at 37 °C and 200 rpm in MM. The OD_{600} of the yeast culture was measured and the culture was diluted with MM to produce a yeast suspension with OD_{600} of 0.1.

The 96-well plate was loaded with MM (100 µL) being pipetted into each well. The stock solutions (100 µL) prepared in neat DMSO and diluted with media (1:5 dilution)

to give a concentration range of 120 – 0.94 µM of the test compounds (**3.3a** and **3.5a1-3**) were then loaded onto the 96-well plate. The contents of the wells containing the solution of the test compounds were halved, leading to each well containing 100 µL solutions. The yeast suspension with OD_{600} of 0.1 was loaded (100 µL) onto the appropriate wells of the plate and the yeast growth was measured at 600 nm after 24 h at 37 °C using a spectrophotometer (BioPhotometer). The final concentration range of the test compounds upon addition of yeast suspension was 30 – 0.23 µM.

For all compounds tested, the screening was carried out with a repetition of 2 and in 8 replicates.

2.5.2.2: *in vivo* Antimicrobial Susceptibility Testing Methods

2.5.2.2.1: Inoculation of *Galleria mellonella* Larvae

Sixth instar larvae were used for this testing. The larvae of the same age were weighed and the larvae with weight of 0.22g – 0.27g were used. Five larvae were placed in a clean petri dish and innoculated with 20 µL solution of the appropriate compounds. The dose was administered through the last pro-leg of the insect using a Myjector U100 insulin syringe.

2.5.2.2.2: Survival rate of *Galleria mellonella* Infected with *S. aureus* and then Treated with Compounds 3.3a-e, 3.5a-e

Cells (*S. aureus*) were cultured overnight in an aerated conical flask in an orbital shaker at 37 °C and 200 rpm in nutrient broth. The OD_{600} of the bacterial culture was measured and the culture was diluted with PBS to produce a bacterial suspension with OD_{600} of 0.1 and 0.25.

Larvae were injected with *S. aureus* as described above with *S. aureus* (20 µL) through the last proleg. One hour post infection, the larvae were treated with solutions (20 µL) to test compounds **3.3a-e** and **3.5a-e.** DMSO (10% v/v), dH_2O, PBS, and larvae

innoculated with *S. aureus* were used as controls. The larvae were incubated for 24 h at 37˚C. The survival rate of the insect was monitored at 24, 48 and 72 h.

2.5.3: *in vivo* Toxicity towards *Galleria mellonella*

Compounds **3.3a-e**, **3.5a-e** were dissolved in neat DMSO to produce 600 µM solutions. These were then doubly-diluted with neat DMSO to produce solutions with concentration range of 600 – 30 µM. Each solution was then diluted with dH_2O media (1:10 dilution) to yield stock solutions within the concentration range of 60 – 3 µM being. DMSO (10%) solution was also prepared using dH_2O. The *G. mellonella* larvae were then injected with 20 µL of stock solution, 10% DMSO solution, and dH_2O solution through the last pro-leg as described in **Section 2.5.2.2.1.** The larvae were incubated for 24 h at 37˚C. The survival rate of the insect was monitored at 24, 48 and 72 h.

2.5.4: Cell Leakage Assay

Cells (*S. aureus*) were cultured overnight in an aerated conical flask in an orbital shaker at 37˚C and 200 rpm in nutrient broth. The stationary phase *S. aureus* cells were harvested by centrifugation on a Beckman GS-6 bench centrifuge at 1850g for 5 min. The cell pellet were washed twice with PBS and re-suspended in 5 mL (30 µM made up in 5% DMSO (v/v) solution) solution of **3.5a-c**, $[Cu\mathbf{(3.1)}_3].(ClO_4)_2$, and 5% DMSO (v/v). The cells were incubated at 37˚C and 200 rpm for 1, 4 and 24 h. The cells were harvested as before and the supernatant was collected. The free amine and the protein content of the supernatant was determined using ninhydrin assay and Bradsford assay, respectively.

Chapter 3

Discussion of Synthesis, Chraracterisation and Biological Evaluation of Oxazine-based ligands (3.3a-g) and their Metal Complexes (3.5a-e)

3.1: Introduction

The synthesis, characterisation and biological screening of the oxazine-based **phen** ligands **3.3a-e** and their metal complexes **3.5a-e** will be discussed in this chapter. The synthesis and characterisation of starting materials necessary for the synthesis of these ligands, which include **3.1** and **3.2a-e**, will also be discussed. In addition, the synthesis of further derivatives (**3.3f-g**) of the oxazine-based ligands will also be discussed, alongside their respective starting materials **3.2f-g**, as well as the interesting side products, **3.4a-c**, which are isolated from the reaction of **3.2f-h** with **3.1**.

The work presented in this chapter starts from discussing the synthesis and characterisation of the quinone **3.1** and the amino acid ester based starting materials **3.2a-h**, and then proceeds to the synthesis, reaction conditions optimization and characterization of the oxazine-based ligands **3.3a-e**. The synthesis and characterization of the unexpected pyrido-type products **3.4a-c** as well as the concurrent formation of the oxazine-type products **3.3f-g** is also discussed. The mechanism of formation of these oxazine-based product as well as the pyrido-based products is outlined and discussed. Finally, the synthesis and characterisation of the metal complexes **3.5a-e**, which arise from metal-complexation of **3.3a-e** is discussed. An overview of the chemical reactions and the chemicals used in this project is given in (**Scheme 2**).

The oxazine-based ligands **3.3a-e** and their metal complexes **3.5a-e** are screened for their anti-microbial activity and their results are discussed.

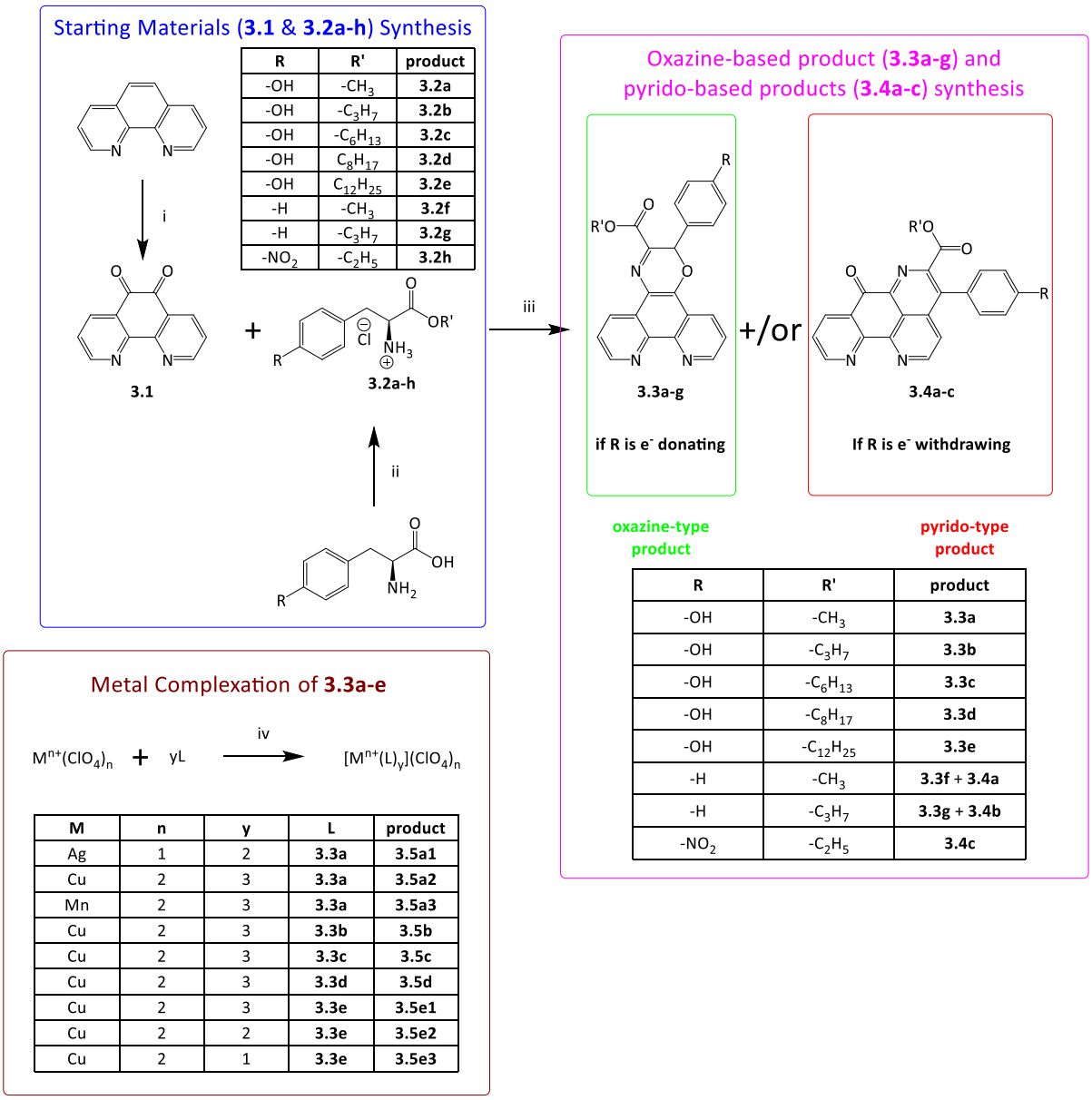

R	R'	product
-OH	$-CH_3$	**3.2a**
-OH	$-C_3H_7$	**3.2b**
-OH	$-C_6H_{13}$	**3.2c**
-OH	C_8H_{17}	**3.2d**
-OH	$C_{12}H_{25}$	**3.2e**
-H	$-CH_3$	**3.2f**
-H	$-C_3H_7$	**3.2g**
$-NO_2$	$-C_2H_5$	**3.2h**

R	R'	product
-OH	$-CH_3$	**3.3a**
-OH	$-C_3H_7$	**3.3b**
-OH	$-C_6H_{13}$	**3.3c**
-OH	$-C_8H_{17}$	**3.3d**
-OH	$-C_{12}H_{25}$	**3.3e**
-H	$-CH_3$	**3.3f + 3.4a**
-H	$-C_3H_7$	**3.3g + 3.4b**
$-NO_2$	$-C_2H_5$	**3.4c**

M	n	y	L	product
Ag	1	2	**3.3a**	**3.5a1**
Cu	2	3	**3.3a**	**3.5a2**
Mn	2	3	**3.3a**	**3.5a3**
Cu	2	3	**3.3b**	**3.5b**
Cu	2	3	**3.3c**	**3.5c**
Cu	2	3	**3.3d**	**3.5d**
Cu	2	3	**3.3e**	**3.5e1**
Cu	2	2	**3.3e**	**3.5e2**
Cu	2	1	**3.3e**	**3.5e3**

Scheme 2: Overveiw of the the synthetic reactions and products. i) $KBrO_3$/60% H_2SO_4; ii)MeCOCl/R'OH; iii) N-methylmorpholine/DMSO; iv) MeOH or MeCN

3.2: Synthesis and Characterisation of Phenanthroline-Based Oxazine and their Metal Complexes

3.2.1: Synthesis and Characterisation of Starting Materials 3.1 and 3.2a-h

1,10-phenanthroline-5,6-dione (**3.1**) was synthesised by following a reported procedure[216] to obtain the product with moderate yields (80%) and sufficient purity. The product was characterised by NMR, IR, and MS and the results matched those reported in the literature.

The synthesis of amino acid esters (**3.2a-h**) was carried out by modification of a reported procedure[217] (**Scheme 3**). By utilising acetyl chloride, HCl can be generated *in situ* to facilitate acid catalysed esterification of the amino acid and to generate the hydrochloride salts of the resulting esters. The ability of the alcohol to act as both as a reactant and solvent allowed for the synthesis of pure, high yielding esters. In the case where the more lipophilic alcohols were used, often the unreacted amino acid could be easily removed via filtration of the cold reaction mixture.

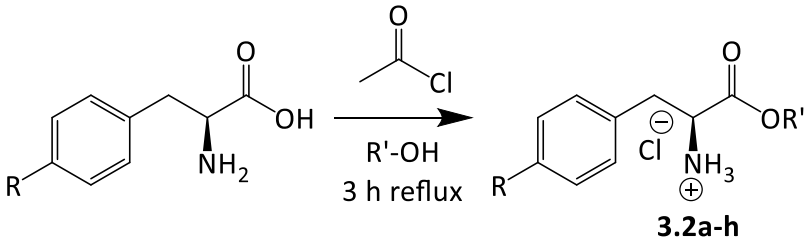

3.2a-h

Stoichiometric Equivalents			**-R**	**-R'**	**product**	**Yield**
Amino acid	Acetyl chloride	R'-OH				
1	5.51	~127	-OH	CH_3	**3.2a**	94%
1	5.51	~127	-OH	C_3H_7	**3.2b**	93%
1	5.51	~57	-OH	C_6H_{13}	**3.2c**	89%
1	5.51	~43	-OH	C_8H_{17}	**3.2d**	85%
1	5.51	~30	-OH	$C_{12}H_{25}$	**3.2e**	80%
1	5.51	~125	-H	CH_3	**3.2f**	94%
1	5.51	~125	-H	C_3H_7	**3.2g**	95%
1	5.51	~125	$-NO_2$	C_2H_5	**3.2h**	93%

*Scheme 3: Esterification of L-phenylalanine, L-tyrosine and their NO_2 substitute analogue to produce **3.2a-h***

After removal of any unreacted amino acid, the precipitation of the amino acid ester was achieved by addition of diethyl ether and/or petroleum ether. In the case of the higher boiling point alcohols such as 1-hexanol, 1-octanol, and 1-dodecanol the stoichiometric equivalents of alcohol used were lowered to allow precipitation of the lipophilic product from these solvents. In addition, the removal of these solvents from the final product required multiple washings of the product with warm diethyl ether. The final products were characterised using NMR, IR and MS analysis. The IR spectra of the final amino acid ester products show the presence of a band at 1740 - 1750 cm^{-1} due to $(C=O)_{ester}$ stretch, which is not present in the amino acid precursor. In addition, the broad band at 2600-3200 cm^{-1} due to $(–OH)_{COOH}$ stretch of the carboxylic acid functionality of the amino acid is no longer present in the IR spectrum of the respective amino acid ester. The HRMS analysis of the products **3.2a-h** detects the presence of the [amino acid ester + H]$^+$ cation. The solubility profile of the products is also different from the starting amino acids which do not readily dissolve in any organic solvent, whereas the products are easily soluble in most polar organic solvents. In addition, the ^{1}H NMR spectrum of the products **3.2a-h** also display the presence of the alkyl peaks associated with the ester group as well as the broad peak arising from $(NH_3)^+$ group which integrates to give a value of 3 H atoms.

3.2.2: Synthesis of Ligands (3.3a-e) and their Characterisation

The synthesis of compounds **3.3a-e** was carried out by reacting the respective amino acid ester (**3.2a-e**) with **3.1** in the presence of a base (N-methylmorpholine). Although the synthesis of the oxazine-based ligand **3.3a** has previously been reported by our group[221], due to the low yields reported and the failure to produce ligands with varying lengths of ester groups by following the reported procedure, the ligands **3.3a-e** (**Scheme 4**) were synthesised by an optimised procedure. Ligands **3.3a-e** were successfully synthesised with moderate yields, purified and characterised using NMR, IR, MS and X-ray crystallography.

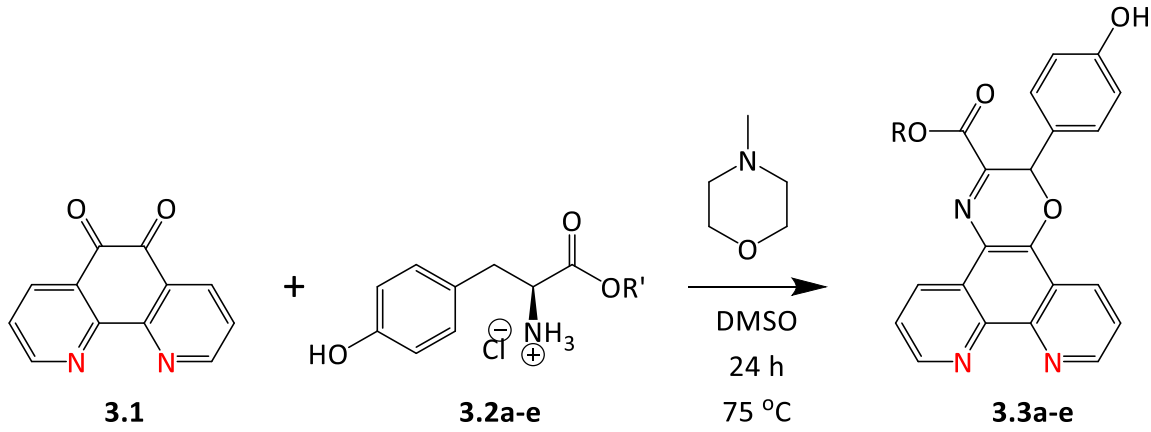

-R	product	Yield
CH_3	**3.3a**	45%
C_3H_7	**3.3b**	41%
C_6H_{13}	**3.3c**	38%
C_8H_{17}	**3.3d**	35%
$C_{12}H_{25}$	**3.3e**	31%

*Scheme 4: Synthesis of oxazine-based ligands **3.3a-e***

The ligands **3.3a-e** were moderately soluble in DMSO and sparingly soluble in organic solvents such as alcohols, DCM, $CHCl_3$, MeCN and acetone. These ligands were completely insoluble in H_2O, EtOAc, ether, toluene and highly hydrophobic solvents. Due to their solubility profile, their NMR characterisation was carried out in DMSO.

The ^{1}H NMR spectrum of the ligands **3.3a-e** shows clear differences from the spectra of the starting materials. For example, the ^{1}H NMR spectrum of **3.3a** possesses 6 peaks within the region of 9.15 – 7.70 ppm which can be attributed to the 6 non-equivalent protons of the **phen** moiety, demonstrating the loss of symmetry within

the **phen** backbone which is present in the starting material. In addition, when compared to the ^{1}H NMR spectrum of the amino acid ester **3.2a**, it is observed that the signal (dd) attributed to the α-H (4.13 ppm) and the pair of signals (dd) attributed to the diastereotopic β-H atoms (3.10 & 2.95 ppm) can no longer be observed due to the formation of the C=N bond at the α-C atom and the C-O bond at the β-C atom. Instead, the appearance of the signal (s) at 6.57 ppm in the ^{1}H NMR spectra of **3.3a** is attributed to the β-H atom (β to carbonyl C) which is a characteristic signal of these 2,3 substituted *2H*-1,4-oxazine derivatives. The ^{13}C NMR spectra of the ligands **3.3a-e** is also in agreement with the structure proposed.

The IR spectra of the ligands **3.3a-e** display characteristic differences to those of the respective amino acid ester starting material. For example, when comparing the spectra of **3.2a** and the corresponding oxazine-based product **3.3a**, the band arising from the $\nu(C=O)_{ester}$ stretch shifts from 1744 cm^{-1} in the spectrum of starting material **3.2a** to 1707 cm^{-1} in that of **3.3a**. This is to be expected due to the formation of C=N bond at the α-C atom, leading to conjugation of the C=O in the ligand. In addition, the broad band at 614 cm^{-1} assigned to the N-H torsional oscillation in the IR spectra of **3.2a-e** is absent from the IR spectra of the final products **3.3a-e.** When the IR spectra of the ligands **3.3a-e** are compared to the spectrum of **3.1**, the two characteristic bands arising from the diketone functionality present in **3.1** are also absent from the spectra of **3.3a-e**.

The structure of the ligands **3.3b,c,e** was also confirmed by X-ray crystallographic analysis (**Figure 32, Figure 33, Figure 34**).

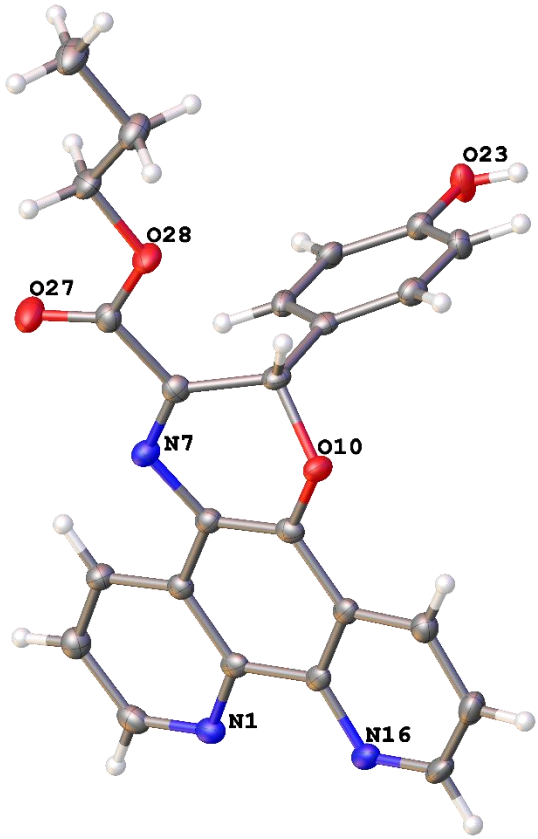

*Figure 32: asymmetric unit of **3.3b** with partial atom labelling for clarity. Atomic displacement shown at 50% probability*

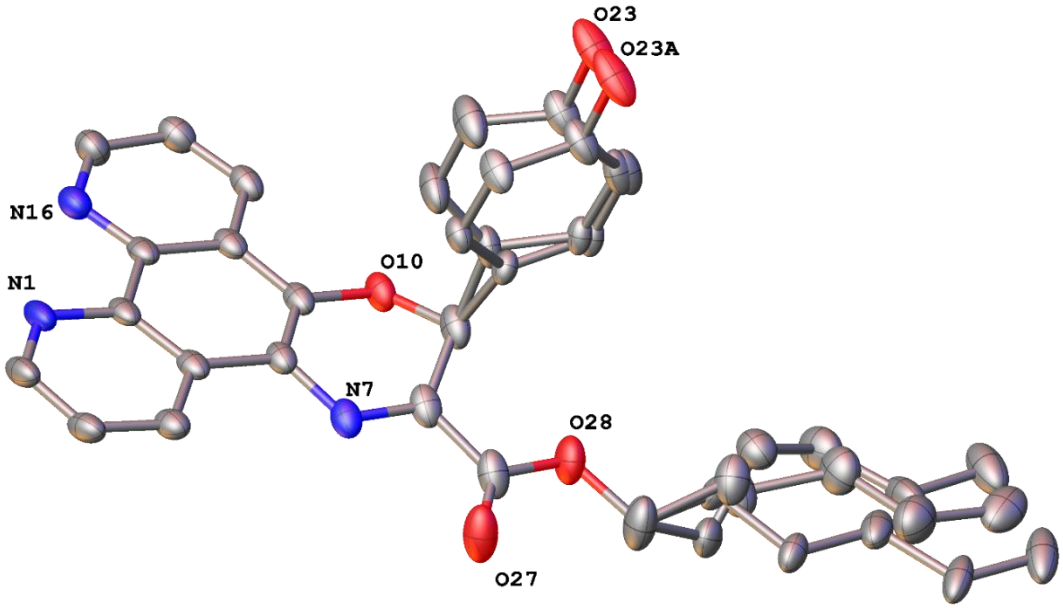

*Figure 33: disordered asymmetric unit of **3.3c** with heteroatom labelling only for clarity. Moiety occupancy 54:46% for phenol ring and 50:25:25% for hexyl aliphatic arm. Atomic displacement shown at 50% probability. Hydrogen atoms omitted for clarity.*

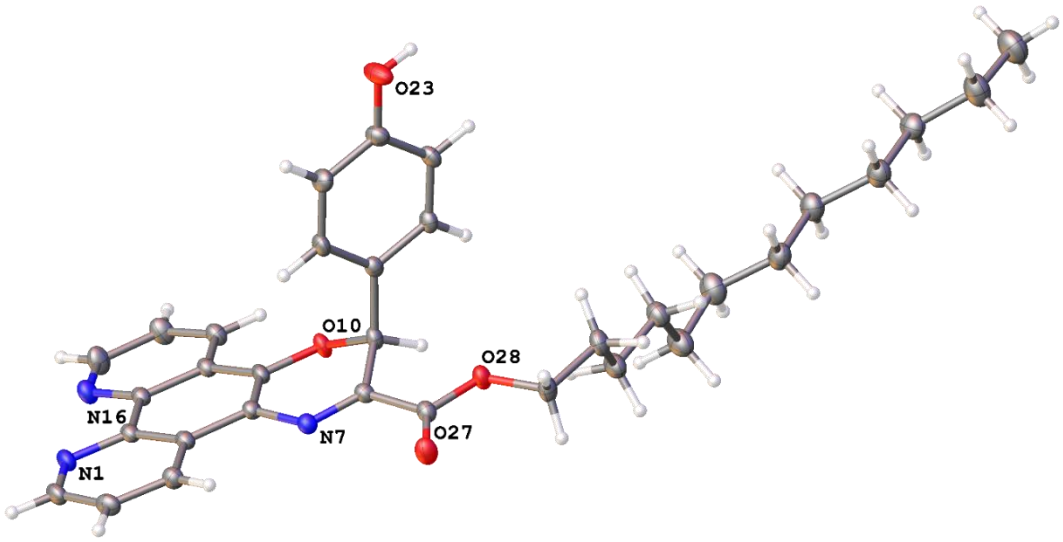

*Figure 34: Molecular structure of **3.3e** with atomic displacement shown at 50% probability. Only heteroatoms labelled for clarity*

3.2.3: Optimisation of Experimental Conditions for the Synthesis of Oxazine-based Products 3.3a-g

The experimental conditions for the synthesis of the oxazine-based products **3.3a-g** (outlined in **Scheme 4**) were optimised by carrying out the synthesis of **3.3a** with minor variations in experimental conditions and monitoring the yields of the product. Below is the presentation and discussion of the experimental conditions reported in the literature[221], the limitation of the synthesis conditions and the modifications of this protocol to optimise the yields of the product **3.3a**, which eventually led to an increase in the yield of **3.3b-g**.

3.2.3.1: Synthetic Protocol for Synthesis of 3.3a in Literature and its Limitations

The experimental conditions reported in the literature for the formation of the ligand **3.3a** involve the reaction of **3.1** with **3.2a** by refluxing in MeOH for 24 h. Although these conditions lead to the crystallisation of the desired product with purity, the yield obtained was low (21%) and the same conditions did not lead to an appreciable yield for the reaction to form the desired products **3.3b-g**. In addition, the formation of a significant amount of **phendiol** leads to the undesirable waste of **3.1**.

The proposed mechanism[221] for the formation of the desired ligand in the literature is given below (**Scheme 5**) and involves the formation of a single-Schiff base product from the reaction of the **3.2a** and **3.1**. Upon the formation of the Schiff base imine, it is proposed that a second **3.1** molecule acts as dehydrogenating agent to lead to concerted ring formation by forming a bond between the O atom of **3.1** and the β-C atom of the amino acid ester to yield 21% of **3.3a**.

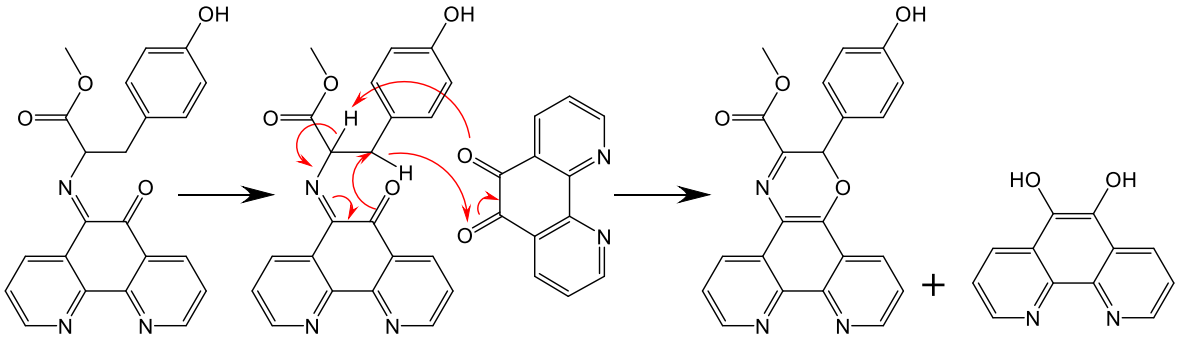

*Scheme 5: reported proposed mechanism for **3.3a** formation*

The ability of **3.1** to act as dehydrogenating agent is to be expected due to the redox behaviour of **3.1** observable through its conversion to the reduced **phendiol** in this reaction. Indeed, even as early as 1983, it was reported that the reduction of **3.1** to **phendiol** was observable when reacted with amines[222]. In 2014, Alison Wendlandt reported the conversion of 1,2,3,4-tetrahydroisoquinoline to 3,4-dihydroisoquinoline (**Scheme 6**) in presence of 5% equivalent of **3.1**, to give 7% of the oxidised amine and the complete conversion of **3.1** to the reduced **phendiol**[152].

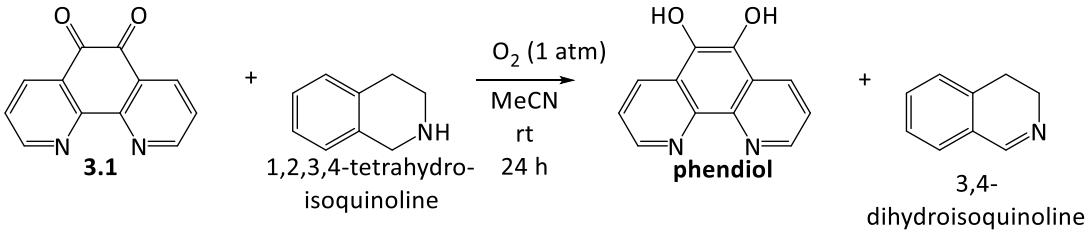

*Scheme 6: conversion of 1,2,3,4-tetrahydroisoquinoline to 3,4-dihydroquinoline by oxidative dehydrogenation caused by **3.1***

The ability of **3.1** to dehydrogenate amines with a negligible catalytic turnover suggests that in the above proposed mechanism (**Scheme 5**), a maximum of 50% yield of **3.3a** is to be expected. A combination of the following factors may be responsible for the low yield (21%) observed for the formation of **3.3a**: 1) the initial Schiff base imine intermediate is not present in a sufficiently high concentration for the

maximum formation of the product **3.3a** through the concerted mechanism proposed above or; 2) the dehydrogenation of the Schiff-base imine may not occur through a concerted mechanism and thus may lead to alternative products. Interestingly, changing the stoichiometric equivalent of **3.1**:**3.2a** from 1:1 to 2:1 does not lead to an increase in the yield of the product, suggesting that the reduction of **3.1** to **phendiol** is not the sole cause for the low yields of the desired product.

3.2.3.2: Optimisation of 3.3a Synthesis via Base Catalysed Schiff Base Formation in MeOH

In an attempt to enhance the Schiff base formation between the amino acid ester **3.2a** and **3.1**, the reaction was carried out with the addition of a 1.1 equivalents of base (triethylamine, TEA). In MeOH this reaction resulted in the precipitation of a yellow solid. Upon carrying out ^{1}H NMR spectroscopy of the precipitate, it was discovered that the desired product **3.3a** co-precipitated with **phendiol** and **3.1**. The desired product along with **3.1** was isolated via soxhlet extraction using $CHCl_3$. The residual **3.1** was removed by washing of the extracted product with hot $CHCl_3$ to yield 29% of the pure **3.3a** and 40% **phendiol**. Although an increase in yield of the desired product was observed along with a reduction in the amount of **phendiol** produced, the yields were still fairly low. The use of higher equivalents of base resulted in the formation of **phendiol** to a greater extent but produced **3.3a** at a much lower yield. Interestingly, the use of lower equivalents of base (0.1 equivalents) did result in the formation of **3.3a** in higher yields, demonstrating that the base is acting as a catalyst. Attempts were also made to carry out the reaction in other common solvents (EtOAc, acetone, MeCN, DCM, $CHCl_3$ and toluene). However, due to solubility issues none of these modifications proved to be more efficient. The use of other mild bases (pyridine and N-methylmorpholine) did not lead to any significant increase in the yield of **3.3a** when using MeOH as a solvent. The results from these modifications are summarised below (**Table 1**).

Product	Base	Base equivs	Reaction Temperature	Reaction Time	Yield (%)
3.3a	TEA	1.1	75˚C	24 h	29%
3.3a	TEA	0.1	75˚C	24 h	27%
3.3a	TEA	3	75˚C	24 h	15%
3.3a	TEA	5	75˚C	24 h	5%
3.3a	Pyridine	1.1	75˚C	24 h	27%
3.3a	N-methylmorpholine	1.1	75˚C	24 h	28%

*Table 1: effect of use of various catalytic base on the yield of **3.3a** in MeOH*

3.2.3.3: Optimisation of 3.3a Synthesis by Variation of Reaction Temperature, Solvent Dilution and Controlled Mixing of Starting Materials in MeOH.

To probe the reaction conditions further, a slow addition of **3.1** to a solution of **3.2a** with 1.1 equivalent of TEA base was attempted. A further change to the reaction conditions was the use of a larger amount of the MeOH. A 250 mL solution of **3.1** (1 mmol, 0.210 g) was added dropwise over a few hours to a 60˚C, 250 mL solution of **3.2a** (1 mmol, 0.237 g) and TEA (1.1 mmol). This method resulted in the formation of a clear bright yellow solution which was reduced to 100 mL on a rotary evaporator and allowed to stand over a fortnight. A bright yellow precipitate formed, which was determined to be pure **3.3a** at a 35% yield. This method not only resulted in a higher yield of the product but also prevented the formation of **phendiol**. This may be attributed to the lower concentration of **3.1** present in the reaction mixture which would lead to a low concentration of **phendiol** being produced as part of the dehydrogenating step. At low concentration, **phendiol** could remain in solution allowing it to be then oxidised *in situ* to reproduce **3.1** by aerobic oxidation.

3.2.3.4: Use of DMSO as Reaction Solvent to Optimise Synthesis of 3.3a

In an attempt to facilitate the oxidation of **phendiol** back to **3.1** *in situ* during the formation of **3.3a**, the reaction was carried out in DMSO. **Phendiol** is more soluble in DMSO over MeOH, making it easier to keep higher concentrations of **phendiol** in solution, and the DMSO can also act as a very mild oxidant to lead to the oxidation of **phendiol** back to **3.1**. The reactants (**3.1** and **3.2a**, 1 mmol) and the TEA (1.1

equivalents) were dissolved in 25 mL DMSO and heated for 24 hours at 75 °C. The resulting clear bright red solution was allowed to cool to room temperature and the desired product **3.3a** can be extracted into the organic layer using a H_2O and DCM solvent mixture. This methodology produced yields of **3.3a** up to 39% and a very minimal formation of **phendiol**.

Probing the reaction conditions further, the temperature of the reaction with DMSO as a solvent was varied. It was discovered that carrying out the reaction below 60 °C led to no observable formation of **phendiol**. However, the yield of the desired **3.3a** was also diminished when compare to carrying out the reaction at 75 °C. In contrast, carrying out the reaction at higher temperatures leads to a greater formation of **phendiol** (up to 50% yield) and other side products, with diminished yield of **3.3a**.

By varying the amount of DMSO used, it was observed that by lowering the volume of DMSO, a lower yield of **3.3a** was obtained with an increased yield of **phendiol**. On the other hand, if the reaction mixture was too dilute, no **phendiol** formation was observed, however a lower quantity of **3.3a** was obtained. This may be due to the loss of the product during the liquid-liquid extraction stage. In addition, pyridine and N-methylmorpholine were also used as bases. Although the difference in yields of the product were minimal, the use of N-methylmorpholine produced the highest yields and it was ultimately chosen as the base for the optimised conditions (**Scheme 4**).

The reaction was also carried out with lower equivalents of base. Interestingly, these reaction conditions produced respectively comparable yields even when the base was used at 0.1 equivalents, demonstrating that the base plays only a catalytic role. When the reaction was carried out in DMSO without any presence of the base, the reaction only produced the ligand at 21% yield. The results from these experiments are given below **(Table 2**).

Product	Solvent	Vol. Solvent (mL)	Base	Base equiv.	Reaction Temperature (˚C)	Yield
3.3a	DMSO	25	TEA	1.1	75	39%
3.3a	DMSO	25	TEA	0.1	75	36%
3.3a	DMSO	25	-	-	75	21%
3.3a	DMSO	50	TEA	1.1	75	30%
3.3a	DMSO	10	TEA	1.1	75	15%
3.3a	DMSO	25	TEA	1.1	60	27%
3.3a	DMSO	25	TEA	1.1	90	19%
3.3a	DMSO	25	pyridine	1.1	75	40%
3.3a	DMSO	25	N-methyl-morpholine	1.1	75	45%

*Table 2: Synthesis Optimisation of **3.3a** in DMSO reaction solvent and reaction time of 24 h.*

3.2.3.5: Synthesis of 3.3b-e, the Lipophilic Derivatives of 3.3a

From the results of these studies the conditions used in **Scheme 4** were applied to form all of the products **3.3a-e**. The products **3.3b-e** were successfully synthesised, purified and characterised. However, the yields of the ligands decreased with the elongation of the ester chain. In addition, it was observed that the formation of the products could be carried out at higher temperatures (up to 90 ˚C) in the case of longer ester chains and often led to an increase in yield.

To measure the lipophilicity of these new derivatives, the experimental determination of log*P* using octanol:water separation method was not possible due to the insolubility of the compounds in the two solvents. As an alternative, reverse phase HPLC analysis of these ligands was carried out using gradient elution of H_2O and MeCN. As expected, the retention time for the ligands **3.3a-e** increased with increasing ester chain. In addition, log*P* values were calculated using ChemDraw Ultra 16.1. The results are given below in **Table 3.**

Compound	Retention time (min)	Calculated Log*P*
3.3a	21.7	2.8
3.3b	22.5	3.6
3.3c	27.8	4.9
3.3d	30.7	5.7
3.3e	35.4	7.4

*Table 3: retention time and theoretical logP values of the ligands **3.3a-e***

3.2.3.6: Synthesis of Pyrido-based Phenanthroline Derivatives 3.4a-c

In an attempt to produce a variety of oxazine-based products, modifications at the aromatic ring of the amino acid ester were made and the synthesis was attempted. Since the –OH of the L-tyrosine acts as an electron donating group (EDG), the natural next derivative to use as a substitute for the oxazine formation was L-phenylalanine, possessing neither an electron donating nor an electron withdrawing group (EWG). For this reaction, L-phenyalanine esters **3.2f-g** were synthesised, purified and fully characterised using NMR, IR and MS analysis. These esters were then reacted with **3.1** under the optimised reaction conditions. Upon completion of the experiment for the reaction of **3.1** with **3.2f**, when the crude product was allowed to stand in MeOH as per general procedure given in **Section 2.3.3,** no product precipitated. An NMR study of the crude product was carried out and the desired oxazine was observed alongside another prominent **phen**-based product as well as other impurities. To the MeOH solution of the crude product EtOAc was added and the solution was allowed to stand in a freezer. Bright yellow crystals were observed and filtered off. The NMR characterisation of these crystals proved that this compound was not the desired oxazine-based product (**Figure 35**) and the structure of this pyrido-based product was solved using X-ray crystallography (**Figure 36)**. A possible mechanism of formation of this product is given in **Section 3.2.4.**

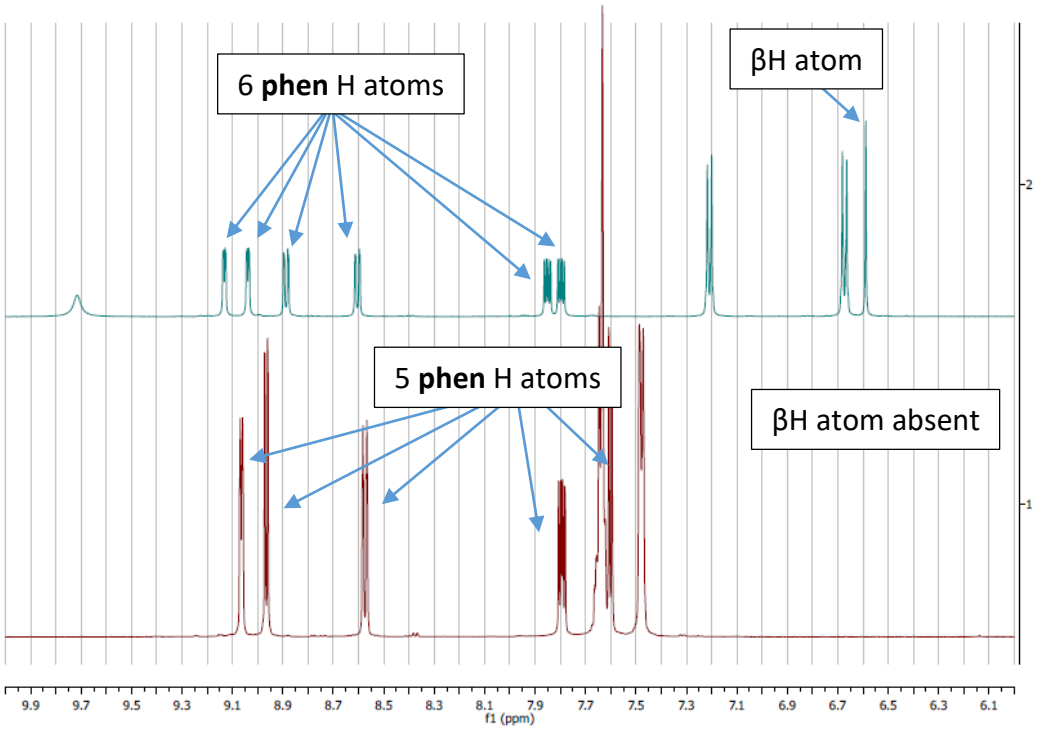

*Figure 35: Aromatic region of the ^{1}H NMR spectrum of **3.3a** (blue trace) and **3.4a** (red trace), demonstrating the absence of signal for both a **phen** H atom and the characteristic β-H atom.*

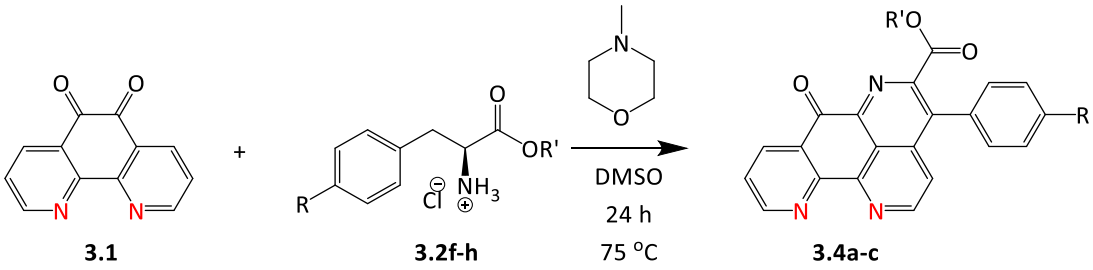

3.1 **3.2f-h** **3.4a-c**

R	R'	product
H	$-CH_3$	**3.4a** and **3.3f**
H	$-C_3H_7$	**3.4b** and **3.3g**
NO_2	$-C_2H_5$	**3.4c**

*Scheme 7: Synthesis of pyrido-based products **3.4a-c***

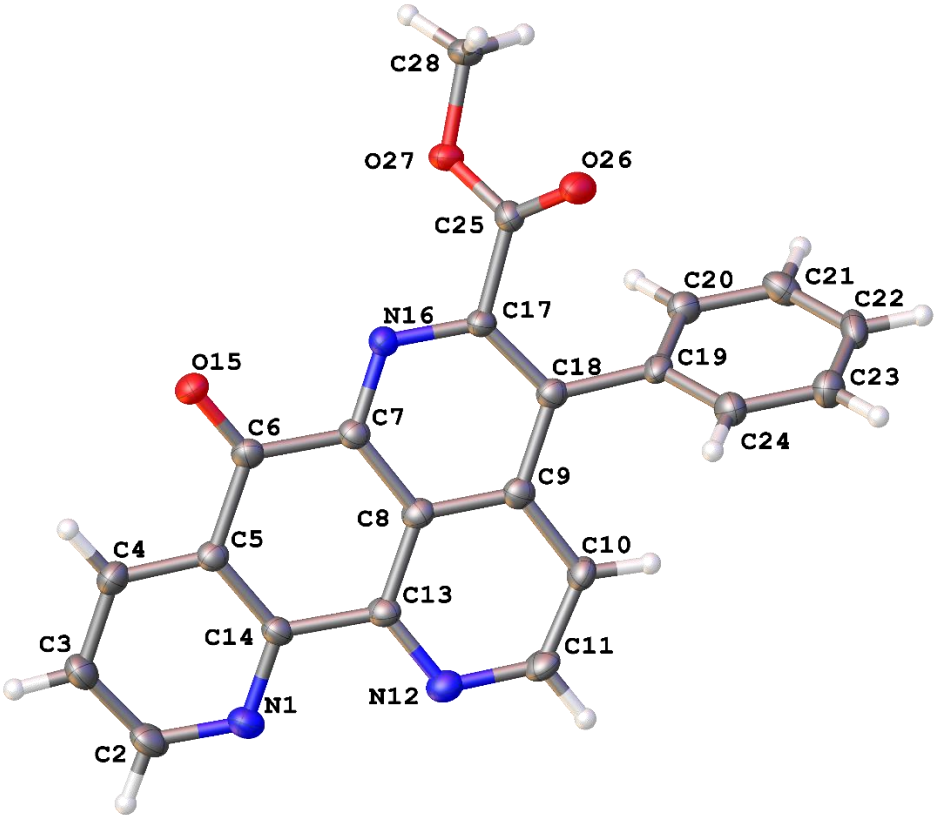

*Figure 36: Asymmetric unit of **3.4a** with atomic displacement shown at 50% probability*

Following the extraction of this novel product, the crude product was again studied through NMR spectroscopy and the characteristic peaks expected from the oxazine-based product, **3.3f**, were the major peaks in the NMR spectrum. The presence of the oxazine-based product was confirmed by HRMS. Many various methods for crystallisation and precipitation were attempted in order to purify the oxazine-based product which all ultimately proved unsuccessful. Fortunately, the lipophilic derivative containing a propyl ester chain, **3.3g**, was easily obtained with purity from a solution of diethyl ether. Upon extraction of **3.4b** from the reaction mixture, the mother liquor was removed under vacuum and the residue was heated in diethyl ether. Slow evaporation of the diethyl ether solution lead to the formation of pure **3.3g**.

To further study the effects of substituents at *para* position of the benzyl ring of the amino acid ester, 4-nitro-L-phenylalanine ethyl ester **3.2h** was used for the above reaction. Interestingly, this reaction yielded exclusively the formation of the pyrido-type product **3.4c** (**Scheme 7**). In addition, the NMR analysis of the crude product of

this reaction revealed no observable formation of the oxazine-based product. This would suggest that the formation of either the oxazine-type or pyrido-type product depends on the electronic nature of the *para*-substituent of the phenyl ring of the amino acid ester. This sheds further light on the mechanism of formation of these products.

3.2.4: Mechanism of Formation of 3.3a-g and 3.4a-c

It is very likely that the first step (**Step 1**) of this reaction is the Schiff base imine formation. However, upon the formation of this imine, the mechanism of formation of the oxazine ring through a concerted ring formation due to dehydrogenation proposed previously (**Scheme 5**), cannot account for the formation of the pyrido-product which was also formed. Due to the formation of the pyrido-type co-product alongside the oxazine-based product from the reaction of **3.2f** and **3.1**, it is very likely that the two types of products derive their formation from a common intermediate. A possible mechanism to account for the formation of both these products is given below (**Scheme 8**).

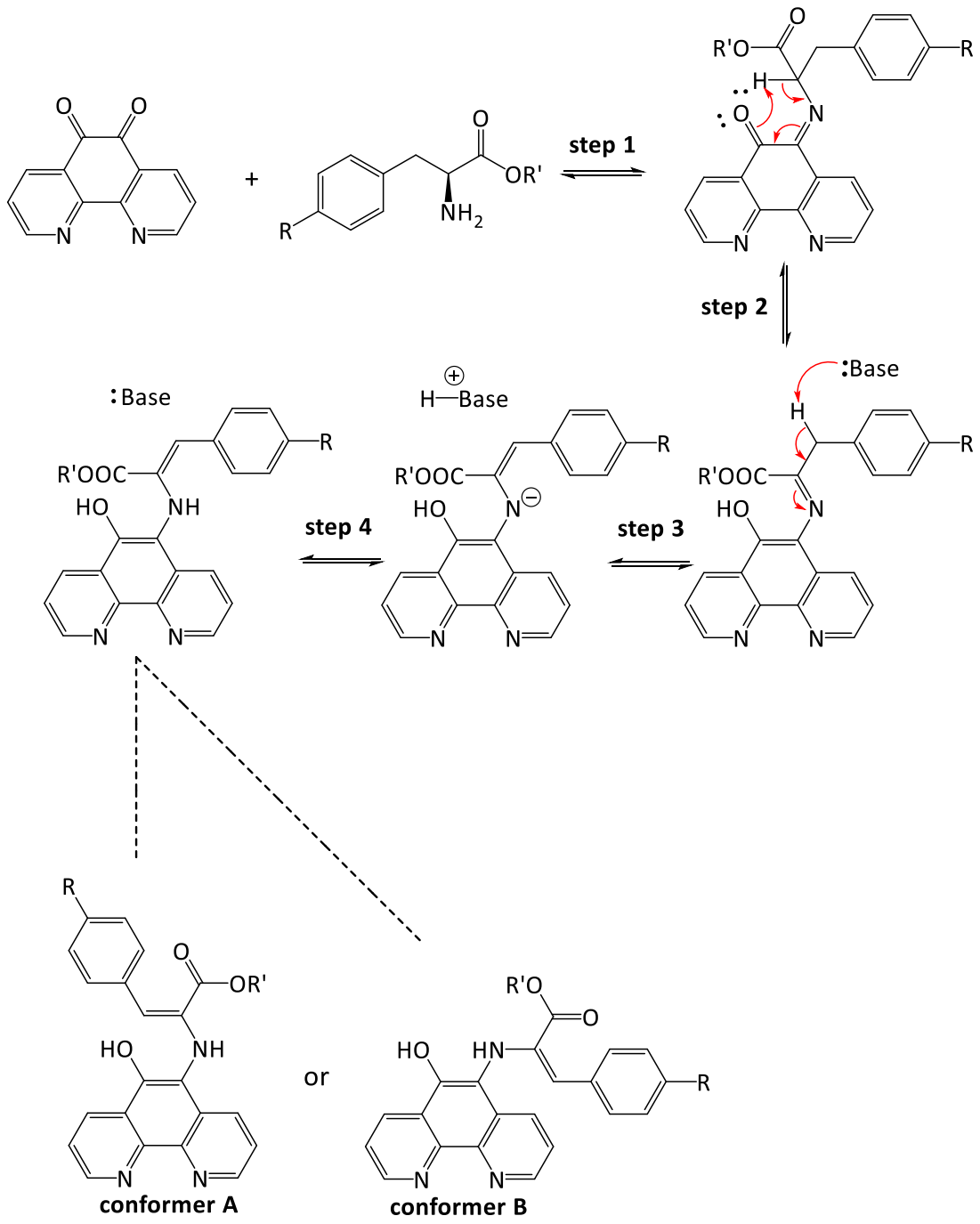
step 1
step 2
step 3
step 4
:Base
H—Base
conformer A
conformer B
or

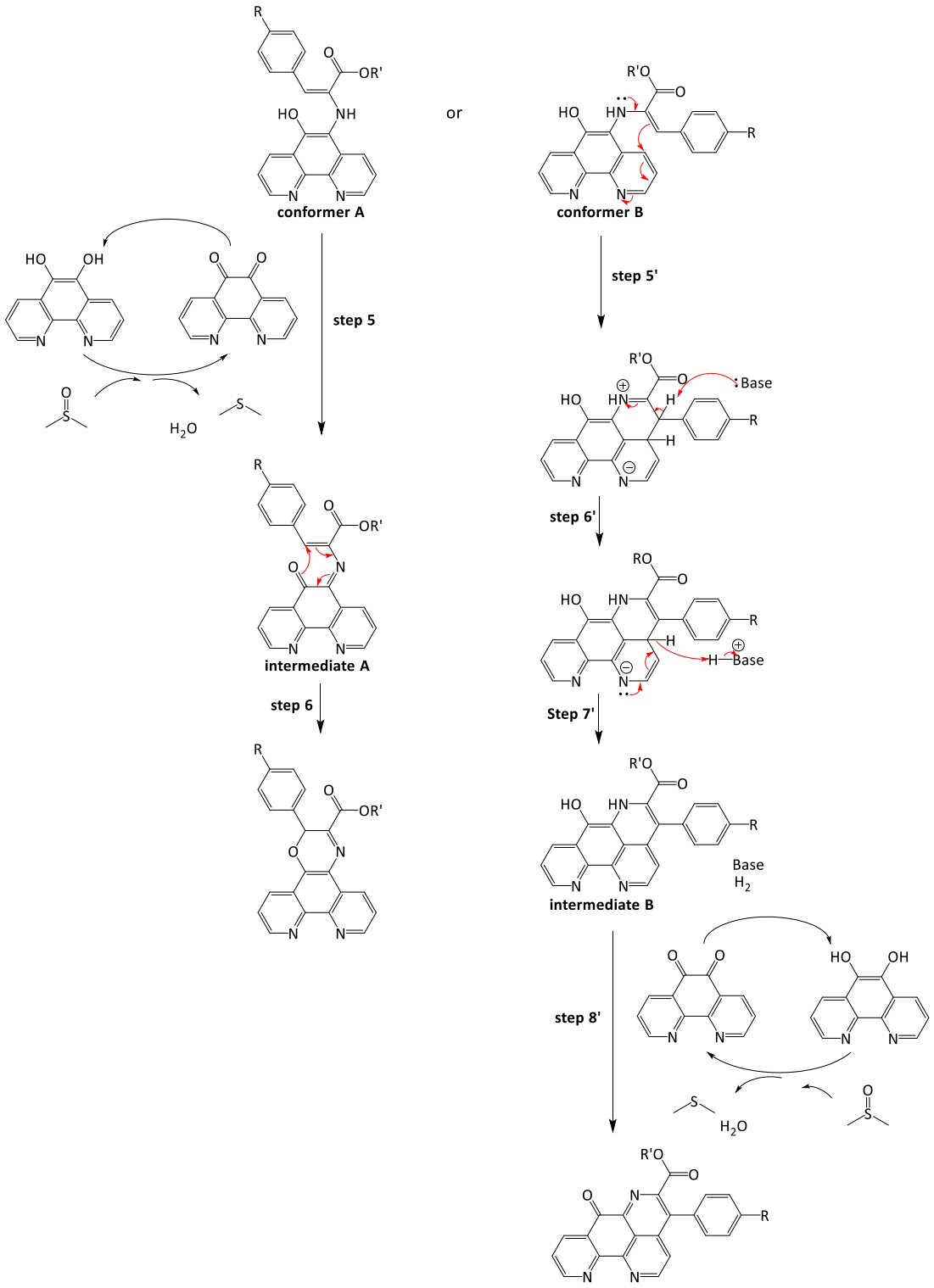

*Scheme 8: Proposed mechanism of formation of **3.3a-g** and **3.4a-c***

Step 1 of the proposed mechanism is the formation of the Schiff-base product. This intermediate then undergoes intramolecular H^+ transfer from the carbon α to the ester group onto the carbonyl group of the **phen** unit (**Step 2**). The acidity of this α-H atom allows for this 1,5-prototropic tautomerisation and has been proposed as the

step for the C-H oxidation of amine[223] catalysed by quinones. In **Step 3** of the mechanism, deprotonation of the H^+ ion from the C atom β to the ester group by base (TEA, N-methylmorpholine, pyridine) leads to the formation of an α,β-unsaturated carbonyl and the subsequent **Step 4** leads to the formation of a secondary amine. This amine intermediate is proposed to exist as two conformers. In the case where R is an EDG (electron donating group), **conformer A** is preferred due to the delocalisation of the electrons donated into the aromatic ring which then further delocalises across the α,β-unsaturated carbonyl. This leads to a net negative charge over the alkene and the potential for a dipole-dipole interaction between the alkene and the H atom of the –OH group of the **phen**, leading to the stabilisation of **conformer A**. On the other hand, if the *para*-substituent is electron withdrawing, the same stabilisation cannot be observed and **conformer B** can be stabilised due to hydrogen bonding interaction between the H atom of the NH group and the O atom of the OH group.

In **Step 5**, oxidation of **conformer A** by **3.1** present in solution leads to the formation of **intermediate A**. It is proposed that this reaction is catalytic and this is supported by the fact that only a small amount of the highly insoluble **phendiol** is separated during the separation stage of the work-up of **3.3(a),(c),(f)** and characterised using NMR[224]. In addition, the reaction mixture for the synthesis of **3.3a** after 24 h reaction was added to an excess of H_2O with the aim of fully precipitating out the **phendiol** and the **3.3a** present in the DMSO solution. Both of these products are extremely insoluble in H_2O and the composition of resulting precipitate was analysed using ^1H NMR. This precipitate contained an excess of **3.3a** compared to **phendiol** with a very rough **phendiol**:**3.3a** ratio being 1:7 (**Figure 37**). In a separate experiment, the oxidation of **phendiol** back to **3.1** in DMSO solution heated for 6 hours at 75 °C was also observed using NMR (**Figure 38**). Following the oxidation of **conformer A**, the resulting **intermediate A** then undergoes ring closure cyclization (**Step 6**). While **conformer A** leads to the formation of the oxazine-based product, **conformer B** undergoes cyclization and aromatization (**step 5',6',7'**) to produce the pyrido-type **intermediate B** and H_2 gas. **Intermediate B** then undergoes a similar oxidation process as shown in **Step 5** to yield the pyrido-type product (**Step 8'**).

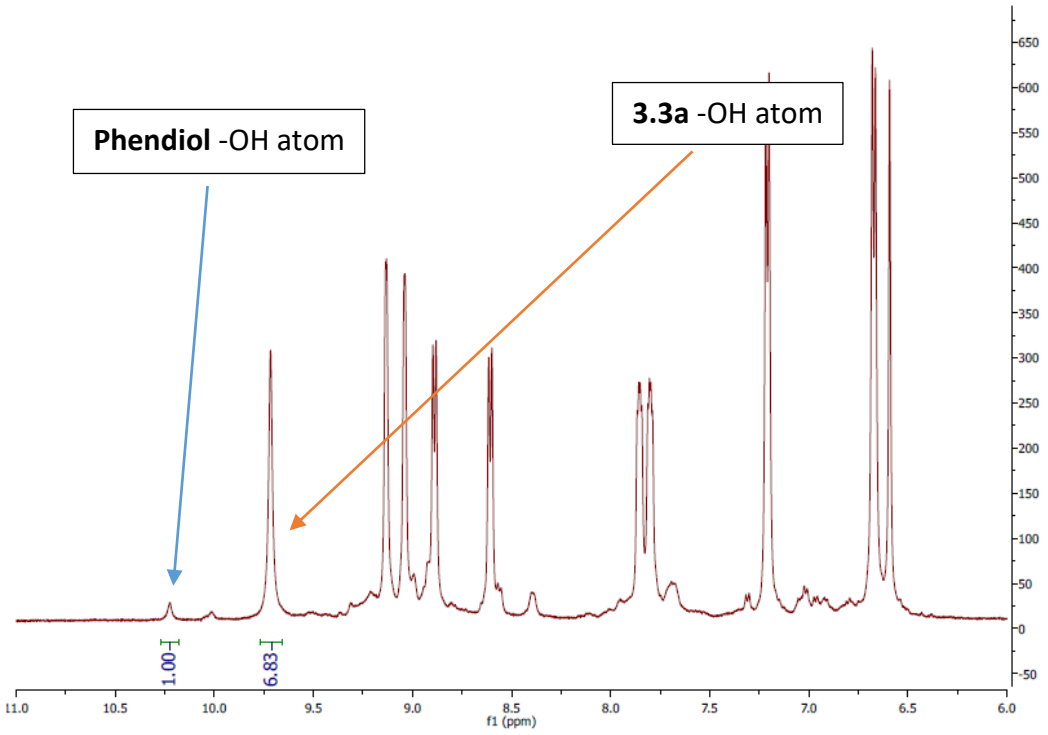

*Figure 37: ^{1}H NMR spectrum of the reaction mixture for the formation of **3.3a** precipitated over H_2O showing **phendiol** present in much lower quantity than the stoichiometric equivalent to **3.3a***

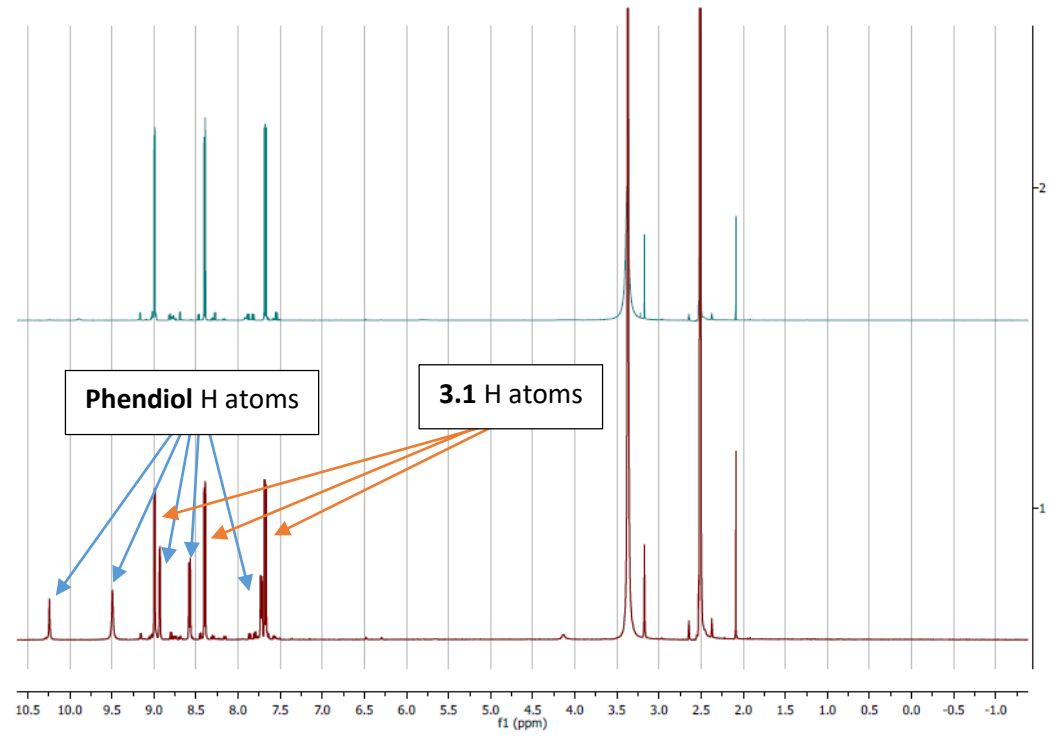

*Figure 38: ^{1}H NMR spectra showing oxidation of **phendiol** (red trace contains peaks for **phendiol** and **3.1**) to **3.1** (blue trace) in d6-DMSO over 6 h at 75°C*

3.2.5: Synthesis and Characterisation of Metal Complexes 3.5a-e

The metal complexes of the **3.3a-e** were synthesised by heating a solution/suspension of the ligand with the appropriate equivalent of the simple metal perchlorate salts. The Ag(I), Cu(II) and Mn(II) complexes of the methyl ester oxazine-based compound **3.3a** were synthesised in MeOH and produced the Ag(I) complex in good yield (70%), the Mn(II) complex in moderate yield (52%), and the Cu(II) complex in low yields (29%). The Ag(I) complexes were characterised using MS, CHN%, IR and NMR spectroscopy. The Cu(II) complexes were characterised using magnetic moments analysis, CHN%, FAAS, IR and NMR spectroscopy. The Mn(II) complexes were characterised using magnetic moment analysis, CHN% and IR spectroscopy. Many crystallisation techniques, such as single-solvent crystallisation, multi-solvent crystallisation, slow solvent evaporation, vapour diffusion, solvent diffusion, were used in an attempt to grow crystals of these complexes which all ultimately proved unsuccessful.

3.2.5.1: Synthesis and Characterisation of $[Ag(3.3a)_2].ClO_4$ (3.5a1) Complex

Silver complexes are predominantly formed by complexation of ligands to the Ag(I) ion, however Ag(II) and Ag(III) complexes have also been reported[225]. Ag(I) is known to form linear complexes with N-donor atoms, for example the stable *bis*-coordinated linear complex $[Ag(NH_3)_2]^+$. The stability of the linear complex can be explained by examining the electronic structure of Ag(I). The energy gap between the $4d_z^2$ and 5s orbital is small; these hybridise to form 2 sd_z hybrids orbitals. The electron density is transferred from the z-axis to produce a ring of high electron density along the xy plane. The donor ligands are repelled from this ring and align themselves along the *z*-axis, where the electron density is reduced[226]. Although linear is a common geometry, other coordination geometries are known. For example, the tri-amine and the tetra-amine geometries of NH_3 complexes of Ag(I)[227].

In the case of **phen** related metal complexes the common geometries found are tetrahedral or distorted tetrahedral. The crystal structure of $[Ag(\mathbf{3.1})_2]ClO_4$ shows the metal complex adopting a pseudo-tetrahedral geometry, with each of the N atoms

of the **phen** forming a bond with the Ag metal centre[228]. In a similar metal complex, where the **phen** ring possess methyl substituents at the 2 and 9 positions, the bulky methyl group force the metal complex to adopt a tetrahedral geometry[229]. When the unsubstituted 1,10-phenanthroline ligand is used, [Ag(**phen**)$_2$](NO_3) produces a distorted tetrahedron[230].

The Ag(I) complex **3.5a1** was precipitated out of the MeOH solution and was easily purified by washing of MeOH and characterized using NMR, IR, HRMS and CHN%.

The ^{1}H NMR spectrum of the metal complex displays small but noticeable shifts in the peaks assigned to the **phen** H atoms. The H atoms *ortho*- to the chelating N atoms of the **phen** do not display a noticeable shift, whereas the H atoms *meta*- and *para*- to the N atoms are deshielded and resonate downfield by a ppm difference of 0.15 ppm when compared to the ^{1}H NMR spectrum of the free ligand. This slight deshielding effect is consistent with values reported in the literature for related complexes and suggests that the **phen** is coordinated to the Ag(I) metal centre[231–233]. It should also be noted that the peaks assigned to the phenolic H atoms and the H atom β to the carbonyl group do not display a shift in ppm value, demonstrating that it is the **phen** N atoms that the metal centre is coordinating to.

The IR spectrum of **3.5a1** also shows characteristic differences compared to the IR spectrum of **3.3a** and are to be expected upon complexation. The band at 741 cm^{-1} in the IR spectrum of **3.3a** is assigned to the out-of-plane bending vibration of the **phen** C-H bonds. Upon coordination with a metal centre, this band is expected to appear at a lower wavenumber, and can be observed at 734 cm^{-1} in the IR spectrum of the Ag(I) complex **3.5a1.** A similar decrease in wavenumber for this band due to complexation has been observed in metal complexes of **phen** with rare-earth metals[234]. The aromatic ring stretching bands which can be observed at 1609, 1586, and 1502 cm^{-1} in the spectrum of the ligand **3.3a** are expected to increase in wavenumbers upon coordination[235]. Very slight shifts can be observed for these vibrations in the spectra of the Ag(I) metal complex with the respective bands being observed at 1611, 1596 and 1509 cm^{-1}. The expected bands to arise from the ClO_4^- ion can be observed at 1098 and 622 cm^{-1}. In addition, no band is observed at 650 cm^{-1}, suggesting that the ClO_4^- ion is not coordinated to the Cu(II) metal centre[236].

Accurate HRMS analysis of the sample **3.5a1** displays a peak that corresponds to the $[Ag(\mathbf{3.3a})_2]^+$ species with the isotopic pattern expected for a Ag(I) species. The CHN% is also in agreement with the proposed complexation of two ligands to one metal centre and suggests the formulation $[Ag(\mathbf{3.3a})_2](ClO_4).2MeOH.H_2O$ for the product obtained.

3.2.5.2: Synthesis and Characterisation of $[Cu(3.3a)_3](ClO_4)_2$ (3.5a2) Complex

Although copper in large excess is toxic to humans, it is considered as an essential trace metal, being the third most abundant transition metal, after zinc and iron. The most common oxidation states of copper are Cu(I) and Cu(II), however, Cu(III) and Cu(IV) complexes have also been reported in the literature[237]. The coordination numbers and geometries associated with copper complexes vary with the oxidation state of the metal centre and can range from linear-two coordination number to octahedral/distorted octahedral-6 coordination number as well as seven- and eight-coordination number complexes[237]. In the case of Cu(I) complexes, which are often colourless except where charge transfer bands occur, the most common geometries are linear, trigonal planar, and tetrahedral with some distortions observed with chelating ligands. In contrast, the d^9 Cu(II) metal centre most commonly displays the distorted octahedral geometry owing to the Jahn-Teller distortion, which leads to the two longer axial bonds with four shorter equatorial bonds and, in some instances, four longer equatorial bonds and two shorter axial bonds. However, tetrahedral, square planar and trigonal bipyramidal complexes are also known for Cu(II) metal centre. Owing to its smaller size and greater charge density, the Cu(II) ion is a harder acid than the Cu(I) ion and can be considered as a borderline hard acid. Therefore, ligands containing O and N donor atoms are the most favourable ligands in Cu(II) coordination chemistry.

In the case of Cu(II) complexes of **phen**, homoleptic *bis* and *tris*-**phen** based metal complexes have been reported in the literature. Heteroleptic complexes containing **phen**-based ligands are also quite common. In the case of the homoleptic **phen** complexes, the *bis*-complexes rarely demonstrate four-coordinate geometry, and often a H_2O, CH_3COO^-, ClO_4^-, or BF_4^- counter ion will occupy a coordination site[238]. An

Example of such systems include the [Cu(**3.1**)$_2$(OH_2)($OClO_3$)](ClO_4) complex, where an extra H_2O molecule and the ClO_4^- molecule coordinate to the Cu(II) metal centre to give rise to a six-coordinated tetragonal bipyramidal complex[239]. In contrast, the structure of very few four-coordinate complexes of Cu(II) containing **phen**-based ligands are known. An example of such was reported by Mark T. Miller[238], where the coordination sphere of the complex is almost square planar, but is described as a flattened tetrahedral. In addition, the complex [Cu(**phen**)$_2$](PF_6)$_2$ is also four-coordinated compressed tetrahedral species with the PF_6^-, not being a part of the coordination sphere[240]. The solid-state structure of *tris*-**phen**-based Cu(II) complexes are generally thought to be of distorted octahedral geometry. In a report by Polyanskaya and co-workers, a crystal structure of a bimetallic [Cu(**phen**)$_3$]$^{2+}${Co[η^5-(3)-1,2-dodecaborate]$_2$}$_2^-$.2CH_3CN was given and in this case the coordination geometry of the Cu(II) ion is that of a distorted octahedral possessing two equal short axial bonds of 2.076 Å length and four equal longer equatorial bonds of 2.147 Å length[241].

The *tris*-**3.3a** Cu(II) complex was prepared by reaction of a MeOH solution of $Cu(ClO_4)_2.6H_2O$ to a suspension of **3.3a** in MeOH. The desired product **3.5a2** was obtained in low yield (<30%) and characterized using IR, CHN% and magnetic moment analysis.

As observed with the complexation of **3.3a** with a Ag(I) metal centre, the band at 741 cm^{-1} associated with the out-of-plane bending vibration of **phen** C-H bonds, is shifted to a lower wavenumber (732 cm^{-1}) upon complexation to the Cu(II) centre. In addition, the bands arising from the aromatic stretching vibrations also slightly shift to higher wavenumbers. The bands associated with the ν(ClO_4^-) counterion can also be observed at 1085 cm^{-1} and 634^{-1}.

The CHN% of the sample is also in agreement with the proposed stoichiometry of 3 ligands to 1 Cu(II) metal centre and suggest the formulation of [Cu(**3.3a**)$_3$](ClO_4)$_2$.2H_2O. HRMS analysis of the sample did not confirm this *tris*-**3.3a** complex. The base peak observed is that of the ligand and it is suggested that the coordination metal complex fragments upon being exposed to ionisation. Further

proof for the proposed stoichiometry of the metal complex is discussed in **Section 3.2.5.3.**

3.2.5.3: Synthesis and Characterization of Cu(II) Complexes 3.5b-e1

The synthesis of the complexes **3.5b-e1** was carried out by refluxing a mixture of $Cu(ClO_4)_2.6H_2O$ with 3 equivalents of the ligands **3.3b-e** in MeCN. The resulting solution was concentrated under vacuum and the complexes were precipitated with the addition of diethyl ether to produce good yields (70-80%). The final products **3.5b-e1** were characterised with the help of CHN%, IR and magnetic moment analysis. Compound **3.5c** and **3.5d** were also analysed by atomic absorption spectroscopy to determine %Cu of the sample.

Compounds **3.5c**, **3.5d** and **3.5e1** were also analysed by IR (KBr), where the samples of these complexes were doped with the respective free ligand and the spectra were recorded at a high resolution in order to determine if any uncoordinated ligand was present in the isolated product. In addition, complexes **3.5c**, **3.5d** and **3.5e1** were studied using NMR. Discussion of the CHN% results of complexes **3.5b-e1**, MS results of **3.5b-e1**, atomic absorption spectroscopic analysis of **3.5c**, IR analysis of **3.5c**, and NMR analysis of **3.5e1** is given below.

For all complexes **3.5b-e1** the elemental analysis is in good agreement with the proposed *tris*-complex and further proof for this was obtained by carrying out FAAS analysis to check the Cu content of sample **3.5c** complex. A solution of **3.5c** was prepared by dissolving 26.485 mg of **3.5c** in 50 mL of 14% w/v HNO_3. If we assume that the molecular formula of the sample to be the *tris*-complex $[Cu(\mathbf{3.3c})_3](ClO_4)_2.2H_2O$, the concentration of Cu present would be 20 ppm. Alternatively, if we assume that the sample is a *bis*- complex and assume the molecular formula to be $[Cu(\mathbf{3.3c})_2](ClO_4)_2.2H_2O$ then the concentration of Cu would be 27.4 ppm. The FAAS analysis reported the concentration of Cu to be 18 ppm. Although this suggests that the Cu(II) % is lower than expected for a *tris*-, it demonstrates that the concentration of Cu(II) is too low for the sample to be either *bis*- or *mono*- complex.

The HRMS analysis of these samples does not produce a conclusive result for the characterisation of these samples. We propose that these metal complexes are not stable when exposed to ESI conditions. The magnetic moment determined for **3.3a-e1** were to be 2.3, 2.0, 2.2, 2.1, and 2.1 BM respectively. These values are comparable to the value calculated using the spin-only formula which is 1.7 BM.

Although the CHN% supports the composition of the samples to be of *tris*-Cu(II) complex in all complexes **3.5b-e1**, it is uncertain whether all of these ligands are coordinated to the Cu(II) metal centre. In an attempt to provide further justification for the proposed molecular formula for samples **3.5b-e1** to those of *tris*-Cu(II) complexes, IR studies were carried out on **3.5c** and **3.5e1**.

The IR spectra of these metal complexes (**3.5b-e1**) are similar to that obtained for **3.5a** except for the increase in intensity of the bands ~2950 cm^{-1} associated with the C-H stretching mode. In addition, high resolution (0.5 cm^{-1} resolution) spectra of sample **3.5c**-**e1** were also carried out in the region 700-760 cm^{-1} and were examined for both the ligands, **3.3c-e**, and their respective metal complexes, **3.5c-e1**. When analysing the spectrum of both **3.5c** and **3.3c**, it can be observed that the band arising from the out-of-plane bending vibration of the **phen** C-H bond moves downward in wavenumber upon complexation. This band comes at 743 cm^{-1} in the spectrum of the ligand **3.3c**, whereas in the metal complex **3.5c** this band arises at 733 cm^{-1}. By carrying out IR analysis at high resolution it was observed that no peak could be observed at 743 cm^{-1} in the IR spectrum of the **3.5c** metal complex (**Figure 39**). However, if a mixture of the metal complex and the ligand were mixed together in the one KBr disc for IR analysis, a peak at 743 cm^{-1} could be visibly observed. This suggests that all of the ligand **3.3c** is complexed to the Cu(II) centre in the sample **3.5c**. Due to this result, it can be proposed that no residual ligand could have co-precipitated with the metal salt to account for the stoichiometry suggested by the CHN%.

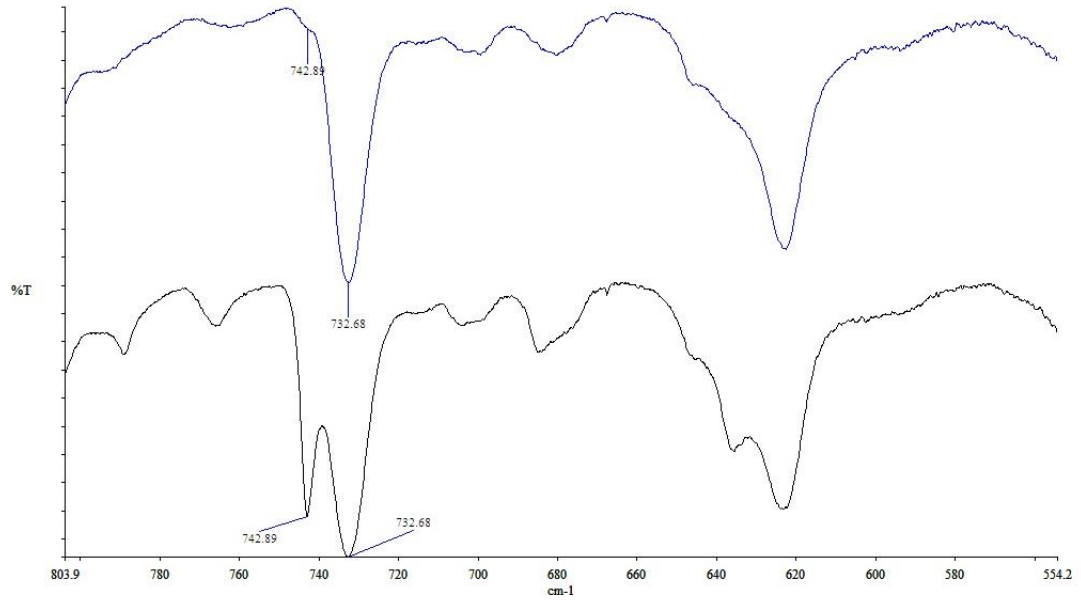

*Figure 39: High resolution IR spectrum of **3.5c*** (upper trace) and ***3.*5c** doped with ***3.*3c** (lower trace) *showing the region of 555-800 cm^{-1}*

The ^{1}H NMR spectrum of both **3.5e1** in d_6-DMSO shows severe broadening and shift in peaks position which should be assigned to the H atoms of the **phen** ring. The ^{1}H NMR spectrum of **3.5e1** is given in **Figure 40** along with the ^{1}H NMR spectrum of **3.3e**. In contrast, although the peaks assigned to the appended L-tyrosine ester are also broadened, leading to the loss of multiplicity, these can be clearly seen and integrated. The *bis*-Cu(II) complex (**3.5e2**) of the ligand **3.3e** and the *mono*-Cu(II) complex (**3.5e3**) of the same ligand were synthesised by reaction of the ligand **3.3e** in 2:1 (ligand:metal) and 1:1 ratio respectively. The CHN% analysis of complex **3.5e2** was in good agreement with the complex being 2:1 (ligand:metal). Unfortunately, CHN% analysis could not be performed on **3.5e3** due to the sample being a sticky solid. The samples **3.5e2** and **3.5e3** were analysed using ^{1}H NMR spectroscopy. For the relatively sharp bands in the spectra, no significant ppm shifts can be observed when comparing the *bis*- and *tris*-ligand complex. Interestingly, a very obvious ppm shift can be observed for the signal arising from the H atom β to the carbonyl group on the *mono*-ligand complex when compared to the *bis*- and *tris*-ligand complex (**Figure 41**). In addition, some very minor peak differences can be observed when examining the spectra of the *mono*-, *bis*- and *tris*- complex in the expanded region of 12-17 ppm (**Figure 42**). I would assign these as being peaks due the H-atoms of the

phen ring which have significantly shifted in position due to being close to the paramagnetic Cu(II) centre.

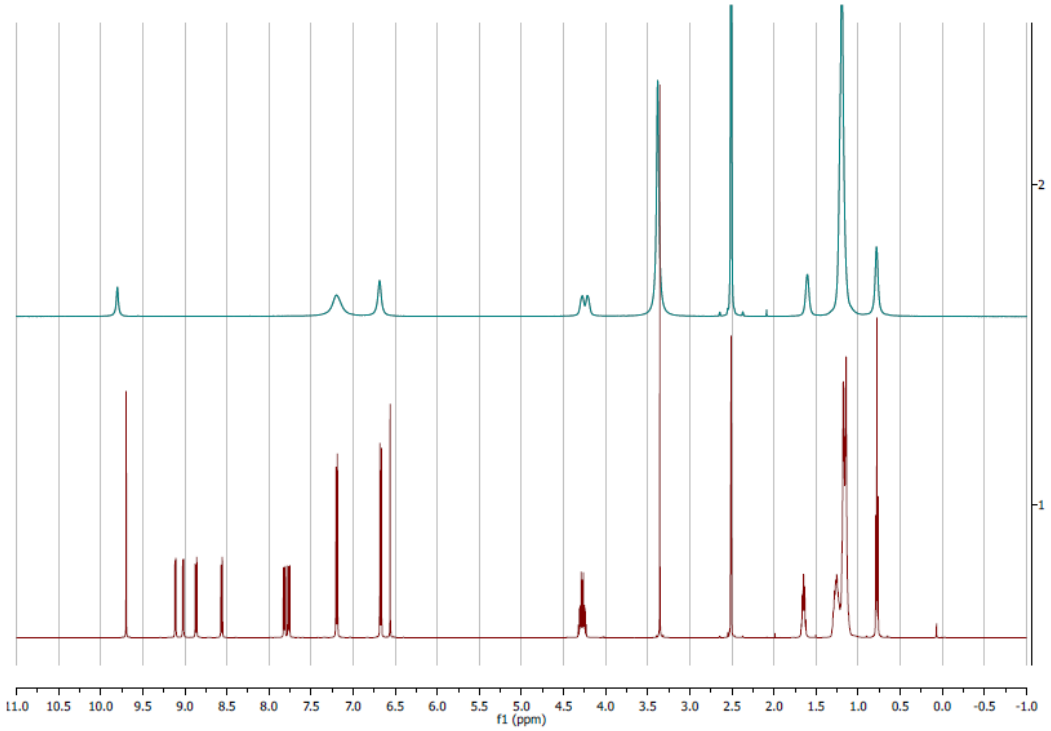

*Figure 40: ^{1}H NMR spectra of **3.5e1** (blue trace) and **3.3e** (red trace)*

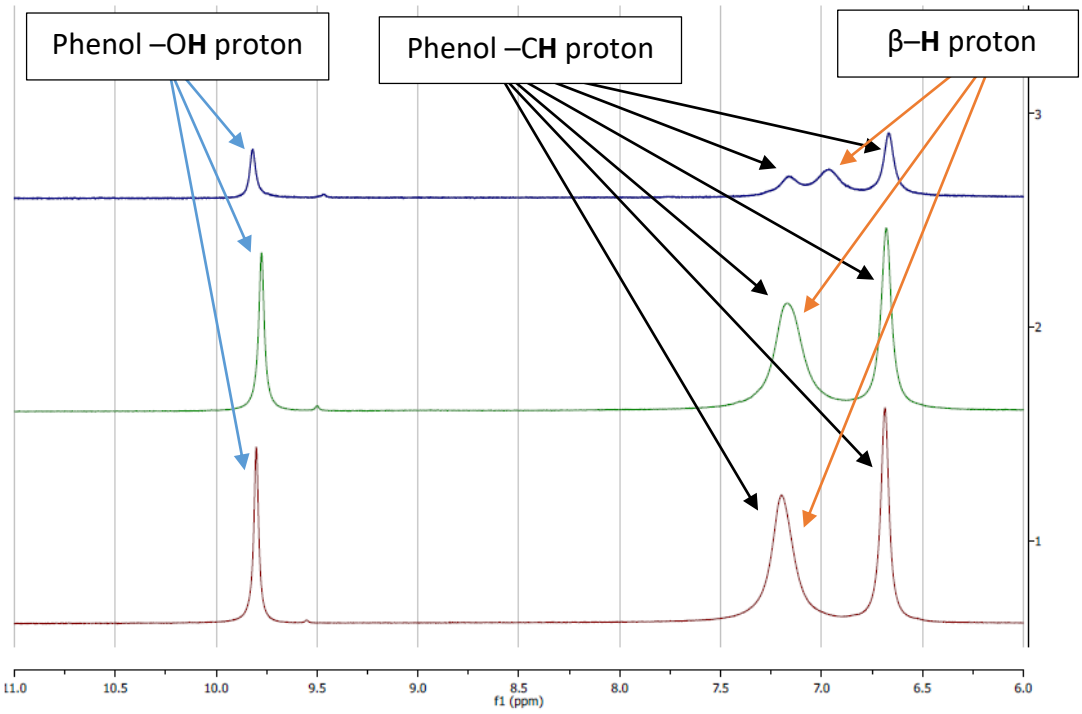

*Figure 41: ^{1}H NMR spectra of **3.5e1** (red trace), **3.5e2** (green trace) and **3.5e3** (blue trace) showing aromatic region region of the spectra*

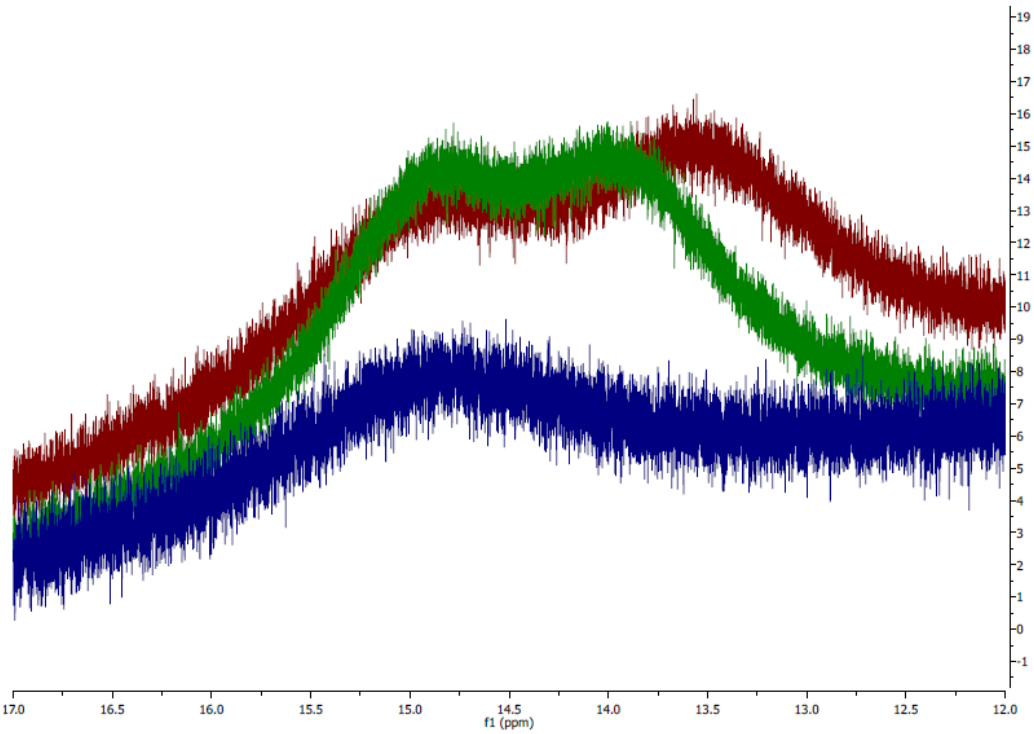

*Figure 42: expanded ^{1}H NMR spectrum of **3.5e1** (red trace), **3.5e2** (green trace) and **3.5e3** (blue trace) showing the 12-17 ppm region of the spectrum*

To probe whether any uncoordinated ligand is present, free ligand was added to the NMR tube of **3.5e1** and it was observed that broad peaks were observed in the region of 7.5-9.5 ppm where the peaks for the uncoordinated **phen** ligand would be expected to appear (**Figure 43**). A similar addition of ligand was made to the solution of *bis*- complex and it was observed that no significant difference could be observed, suggesting that the extra ligand may have become coordinated to the metal centre. However, when further free ligand was added to the same solution, it was observed that the broad peaks in the region of 7.5-9.5 ppm were seen and the ^{1}H NMR spectrum resembled that of the *tris*- complex with additional ligand. In addition, a similar process was carried out with the *mono*-ligand complex (**3.5e3**). When a small amount of free ligand was added to the NMR sample of the *mono*-ligand complex, and a ^{1}H NMR experiment was carried out, the ^{1}H NMR spectrum of the solution produced a spectrum identical to that of the spectrum of **3.5e2**. When further addition of free ligand was made to the same NMR sample and a ^{1}H NMR experiment was carried out the new spectrum was identical to that of **3.5e1** complex (**Figure 44**). Upon further additions of the free ligand into the same sample, the NMR spectrum displayed the growth of broadened peaks in the 7.5-9.5 ppm region. Furthermore, although the addition of ligand into the NMR sample leads to growth of peaks around the aromatic region in the NMR spectrum, the broad peaks observed in the 12-17 ppm region do not display shifts in ppm. This suggest that the additional free ligand which was added to the solution containing the *tris*-complex does not partake in a ligand exchange reaction with the metal complex which is fast on the NMR timescale (**Figure 45**).

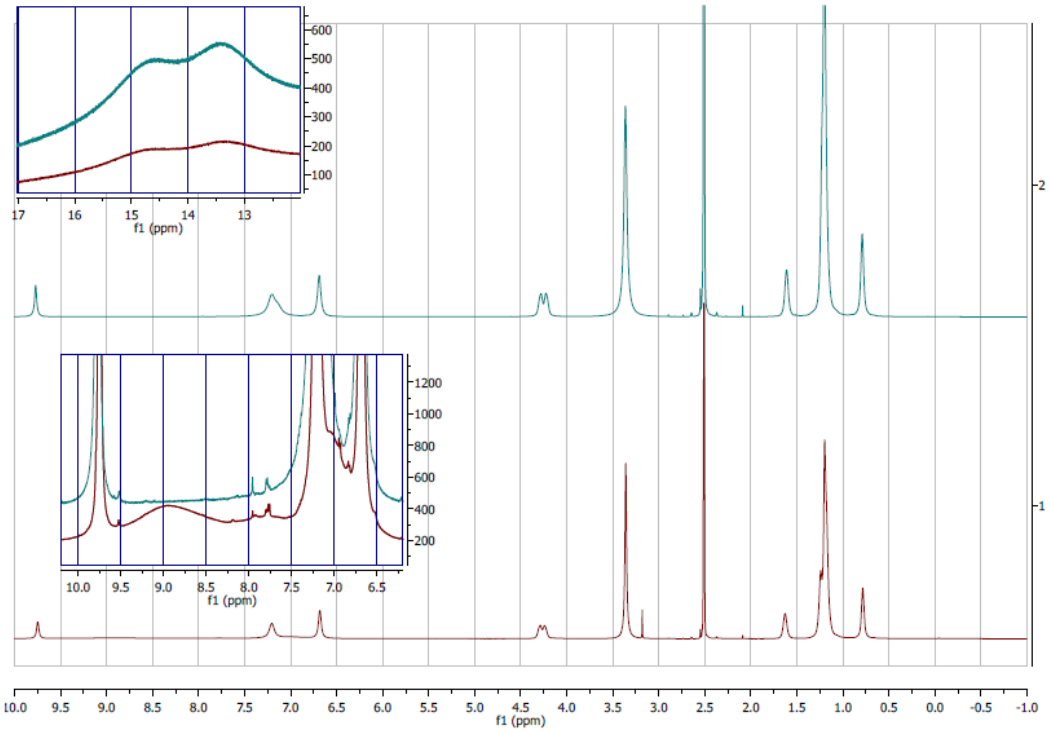

*Figure 43: ^{1}H NMR spectrum of **3.5e1** (blue trace) and spectrum of **3.5e1** with addition of extra uncoordinated ligand **3.3e** (red trace).*

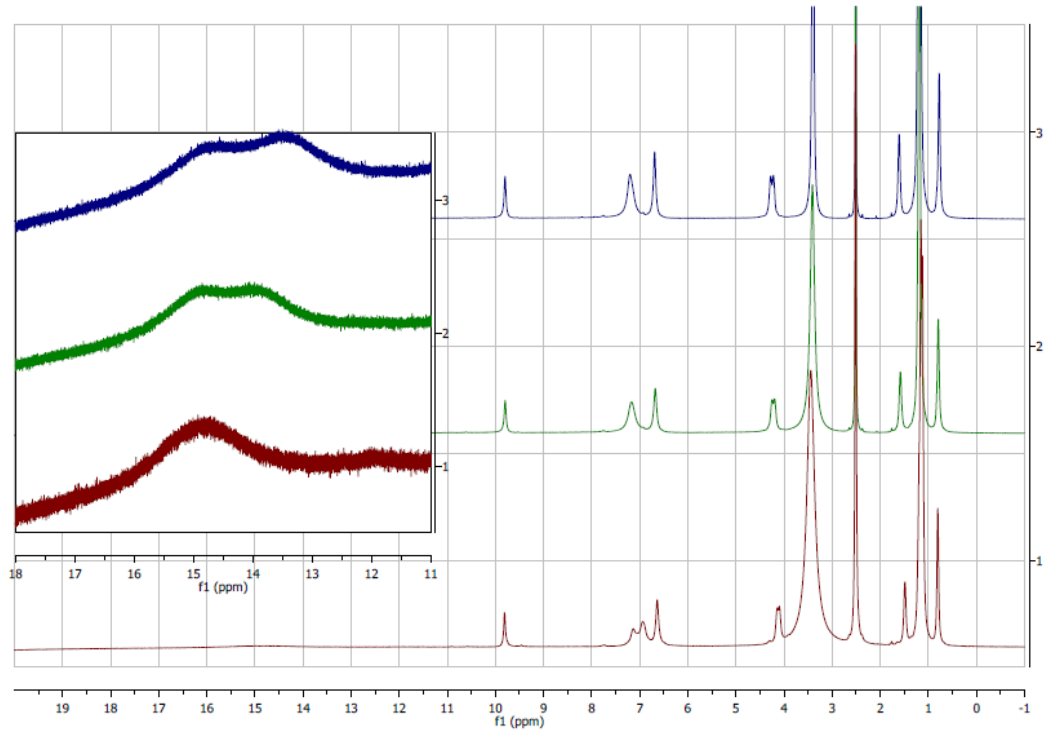

*Figure 44: ^{1}H NMR spectrum of **3.5e3** (red trace) with addition of uncoordinated ligand **3.3e** (green and blue trace)*

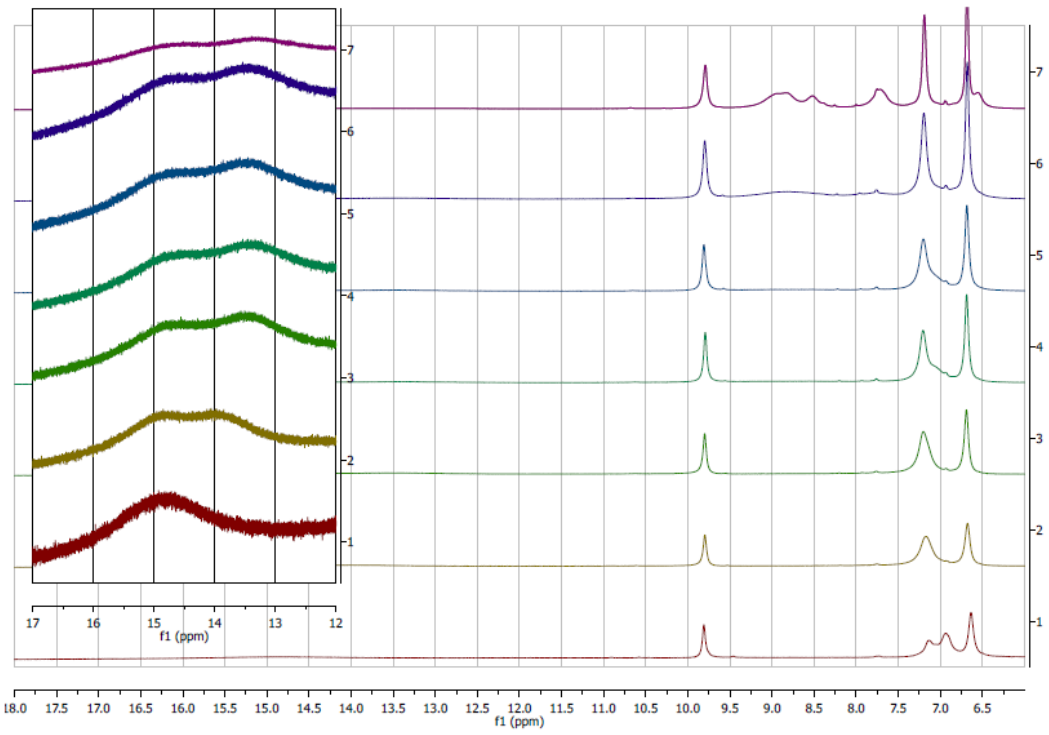

*Figure 45: ^{1}H NMR spectra of **3.5e3** (red trace) with multiple additions of uncoordinated ligand **3.3e** (gold, green, blue and purple trace)*

Similar broadening/disappearance of peaks can be observed in the ^{13}C NMR spectra.

The stability of the metal complexes could also be monitored using ^{1}H NMR spectroscopy. By carrying out the ^{1}H NMR analysis of **3.5e1** over a period of 10 days, it was observed that a growth of extra peaks was observed (**Figure 46**). It is unclear why these drastic changes occur, but the spectrum does not match those of the *bis*- and *mono*- complex. Interestingly, when the same study was carried out with **3.5c** complex, a similar behaviour was not observed and the spectra recorded on day 1 and day 10 were identical. It is currently not understood why the stability of the two complexes differ but it could be established that these complexes do not immediately speciate.

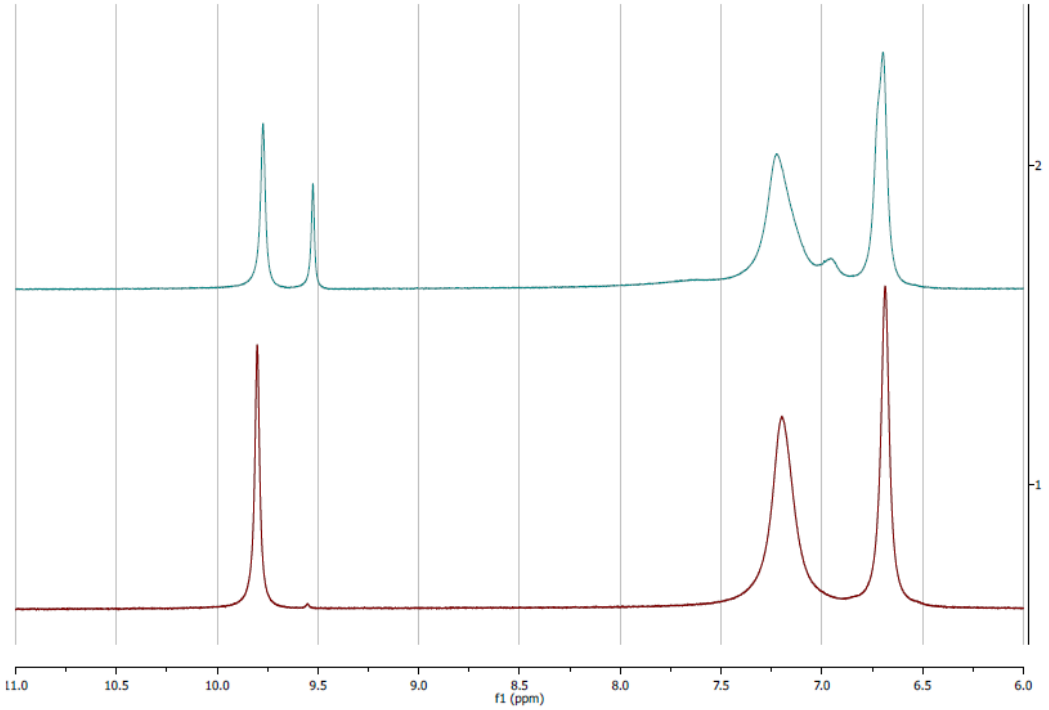

*Figure 46: ^{1}H NMR spectra of **3.5e1** (red trace) and **3.5e1** after 10 days (blue trace) showing the aromatic region of the spectra*

3.2.5.4: Synthesis and Characterisation of $[Mn(3.3a)_3].(ClO_4)_2$ Complex(3.5a3)

Manganese can exhibit many oxidation states ranging from +1 to +7. Of these, the +2 oxidation state is the most stable and common. The most common coordination number across the oxidation states of Mn is six, and as the oxidation state increases four-coordinate complexes are favoured which begins to become favoured at oxidation number of +4.

Complexes of manganese(II) prefer the octahedral geometry, however four-coordinated tetrahedral complexes containing halides have been reported. The use of tridentate ligands can also produce five-coordinated complex and square-planar complexes alongside seven-coordinated and eight-coordinated complexes have also been reported[128,225,242]. Mn(II) complexes of *bis*- and *tris*-**phen**, $[Mn(\textbf{phen})_2(ClO_4)_2]$ and $[Mn(\textbf{phen})_3](ClO_4)_2.2H_2CO_3$, have also be reported and characterised using X-ray crystallography. In the case of the *bis*-**phen** complex, the metal centre is 6-coordinated with 2 ClO_4^{-1} ions being coordinated to the metal centre. However, the geometry is not octahedral and this can be associated to the bite angel of the **phen**

ligand. In the *tris*-complex, the metal centre possesses a distorted octahedral geometry with each of the Mn-N bond length being almost equal[243].

The *tris*-**3.3a** Mn(II) complex was prepared by reaction of a MeOH solution of $Mn(ClO_4)_2.6H_2O$ with a suspension of **3.3a** in MeOH. The desired product was obtained in 52% yield as a bright yellow solid and characterized using IR, CHN% and magnetic moment analysis. The IR spectrum of the metal complex shows the expected downward shift of the frequency associated with the out-of-plane bending vibration of the **phen** C-H bonds from 741 to 734 cm^{-1}. In addition, the peaks assigned to the ClO_4^- stretch can be clearly seen at 1100 and 623 cm^{-1}. The elemental analysis is in agreement with the *tris*-**3.3a** complex.

No peaks corresponding to the $[Mn(\mathbf{3.3a})_3]^{2+}$ ion were observed in the HRMS analysis. We speculate that as with the Cu(II) complexes, this Mn(II) complex is also unstable under ESI conditions. The CHN% suggests the formulation of $[Mn(\mathbf{3.3a})_3](ClO_4)_2.MeOH.2H_2O$.

3.3: Biological Activity of 3.3a, its Derivatives and Ag(I), Mn(II) and Cu(II) Complexes

The antimicrobial activity of compounds **3.3a-e**, and their metal complexes as well as the respective metal salts, known clinical antimicrobial agents (ampicillin, doxycycline, streptomycin, tetracycline, and vancomycin), and **3.1** was studied *in vitro* against *S. aureus*, *E. coli*, and for some compounds, against *C. albicans*. The *in vivo* toxicity of compounds **3.3a-e** and the metal complexes **3.5a-e1** was also studied using *G. mellonella* insect as the model.

The broth microdilution method was used to study the antimicrobial effect of the compounds mentioned above against *S. aureus, E. coli* and *C. albicans*. The compounds (1 mg) were dissolved in 1 mL of sterile DMSO to yield the stock solution. This was loaded onto the 96-well plate loaded with appropriate media (nutrient broth for *S. aureus* and *E. coli*, and minimal media for *C. albicans*) onto 8 rows and doubly-diluted over 9 columns to yield serial dilutions of the test compound loaded

onto the plate. The plates were then loaded with the microbial solution and the inhibitory effects of the test compounds was measured after 24 hours. Although this protocol was appropriate for water soluble compounds (metal salts and **3.1**), the ligands **3.3a-e** and the complexes **3.5a-e1** showed signs of precipitation upon double-dilution of the DMSO concentration.

It was determined that the growth of the microbial strains was not inhibited when treated with 5% DMSO solution. For this reason, all doses of the ligands **3.3a-e** and the metal complexes **3.5a-e1** were administered in 5% v/v DMSO solution. The initial stock solution of these compounds were made up in neat DMSO and double diluted to produce serial solutions of stock solutions. These diluted solutions were then loaded individually onto the 96-well plates in adequate quantities to lead to the final DMSO concentration (after fully loading the plate) to be 5% in each of the wells in the 96 well plate.

The solubility of the ligands **3.3a-e** and the metal complexes **3.5a-e1** limited the antibacterial screening to be carried out at concentrations below 30 µM. It was determined that the ligands and the metal complexes could precipitate out of 5% DMSO solution if the concentration of the sample was >30 µM. The precipitation of these compounds when loaded onto the 96 well plate could lead to irreproducible results as the detection method used for the measure of bacterial growth was light scattering and this will not distinguish between dead microbes and precipitate which will lead to false results. The ability of compounds **3.5a-c** to stay in solution was examined by UV-Vis analysis. UV-Vis spectra of these compounds (solution made up in 5% DMSO in nutrient broth) were compared to the UV-Vis spectra of nutrient broth (5% DMSO). Presence of any precipitate would lead to scattering which would raise the baseline. Through this analysis, it was determined that no solid particulates were suspended in the tested solution. Complexes **3.5d-e1** showed visible precipitation at 30 µM concentration, however complex **3.5d-e1** did not precipitate at lower concentrations. Although these complexes precipitate at the 30 µM dosage, this does not affect their activity measured at lower concentrations. This is because the stock solution for each dose is prepared separately from mixing of 100% DMSO solution of the compound.

3.3.1: Antimicrobial Activity of 3.3a and its Ag(I), Mn(II) and Cu(II) Complexes

The inhibitory effects of **3.3a** and its metal complexes, **3.5a1-3** were examined against *S. aureus, E. coli* and *C. albicans*. The results from these tests are reported in **Figure 47**, **Figure 48**, and **Figure 49**, with the MIC_{80} and MIC_{50} values (**Appendix**) being reported in **Table 4**. For comparison, the antimicrobial effects of the simple metal salts $Ag(ClO_4)$, $Cu(ClO_4)_2.6H_2O$, $Mn(ClO_4)_2.6H_2O$, and **3.1** as well as the antibacterial activity of commercially available drugs ampicillin, doxycycline, streptomycin, tetracycline, and vancomycin is also summarised in **Figure 50**, **Figure 51** and **Table 4.**

Compounds	*S. aureus* MIC(μM)		*E. coli* MIC(μM)		*C. albicans* MIC(μM)	
	MIC_{50}	MIC_{80}	MIC_{50}	MIC_{80}	MIC_{50}	MIC_{80}
3.3a	ND	ND	ND	ND	ND	ND
3.5a1	15	ND	ND	ND	5	6
3.5a2	9	12	24	28	ND	ND
3.5a3	19	28	26	ND	ND	ND
$Ag(ClO_4)$	72	188	83	125	NT	44*
$Cu(ClO_4)_2.6H_2O$	ND	ND	ND	ND	ND	ND
$Mn(ClO_4)_2.6H_2O$	ND	ND	439	ND	358	ND
3.1	ND	ND	5	8	NT	2.9*
Ampicillin	ND	ND	ND	ND	NT	NT
Doxycycline	9	ND	5	ND	NT	NT
Streptomycin	10	ND	1	3	NT	NT
Tetracycline	6	ND	ND	ND	NT	NT
Vancomycin	2	3	20	ND	NT	NT

Table 4: in vitro *inhibitory effects of **3.3a**, **3.5a1-3**, $Ag(ClO_4)$, $Cu(ClO_4)_2.6H_2O$, $Mn(ClO_4)_2.6H_2O$, **3.1**, ampicillin, doxycycline, streptomycin, tetracycline, and vancomycin. NT = Not Tested. ND = Not Determined. MIC_{50} and MIC_{80} values are determined by ploting the data given in **Figure 47**, **Figure 48**, **Figure 49**, **Figure 50**, and **Figure 51** and fitting it to a curve. *values taken from publication by McCann et al*[228].

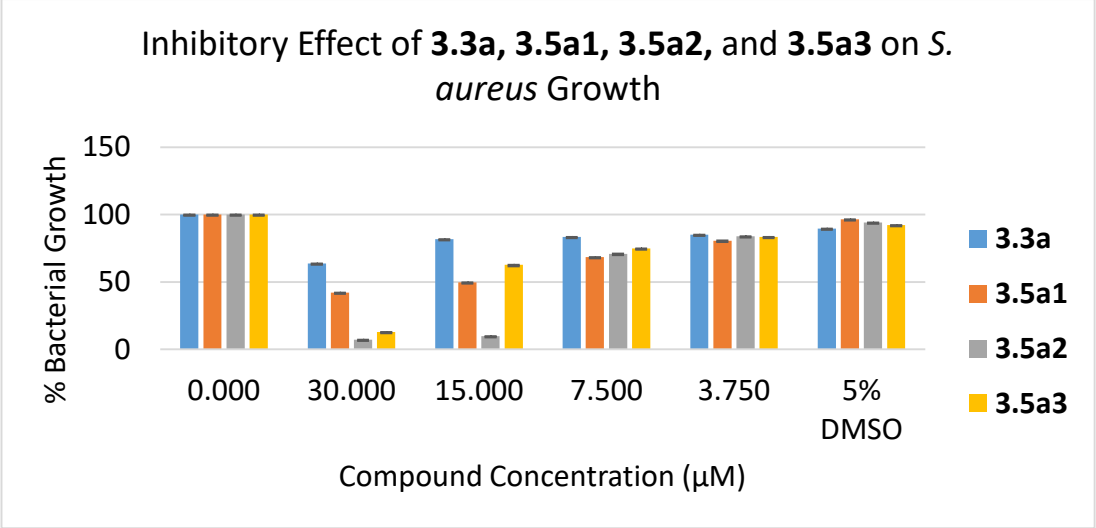

*Figure 47: inhibitory effects of **3.3a** and its metal complexes **3.5a1-3** against S. aureus. n=2 (8 replicates)*

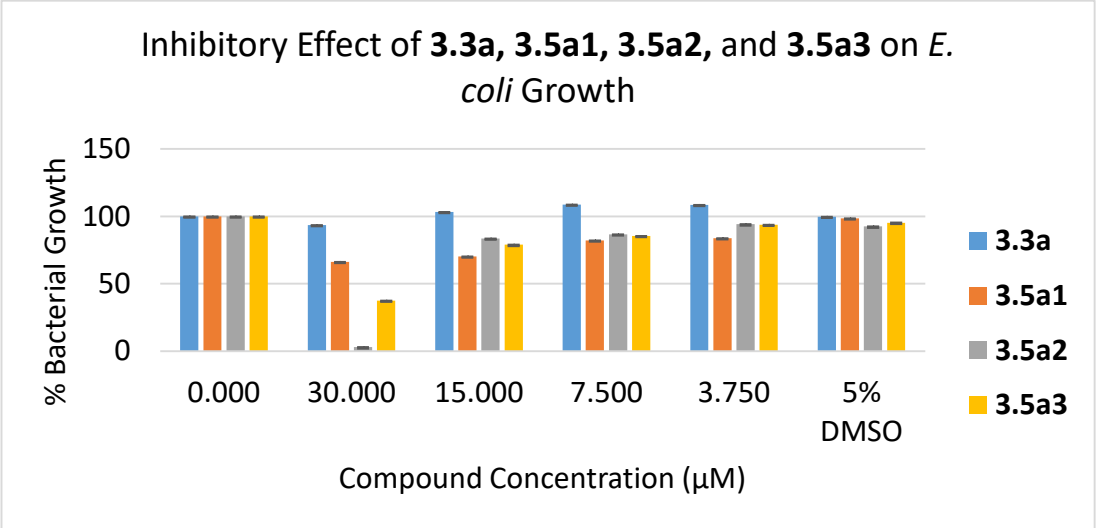

*Figure 48: inhibitory effects of **3.3a** and its metal complexes **3.5a1-3** against E. coli. n=2 (8 replicates)*

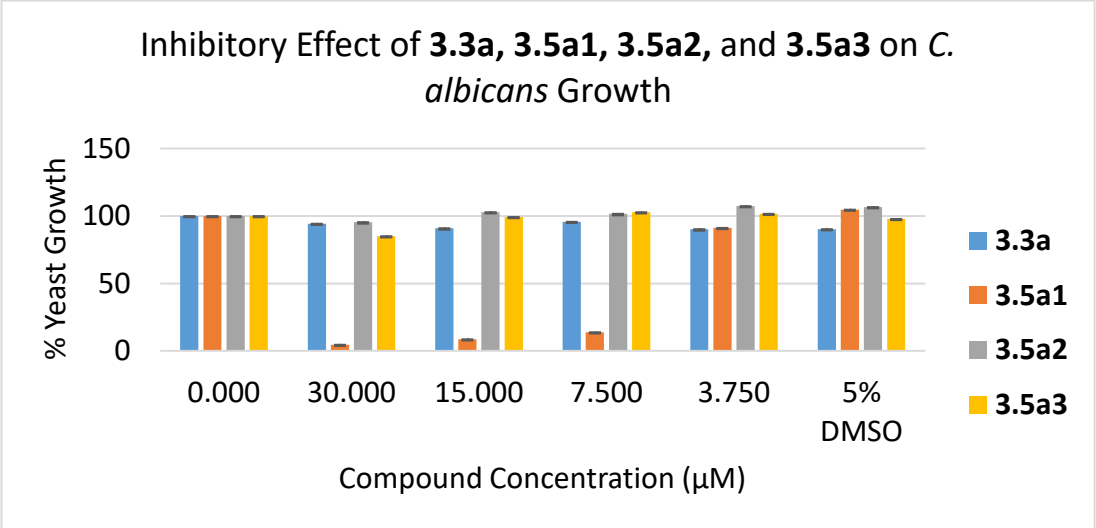

*Figure 49: inhibitory effects of **3.3a** and its metal complexes **3.5a1-3** against C. albicans. n=2 (8 replicates)*

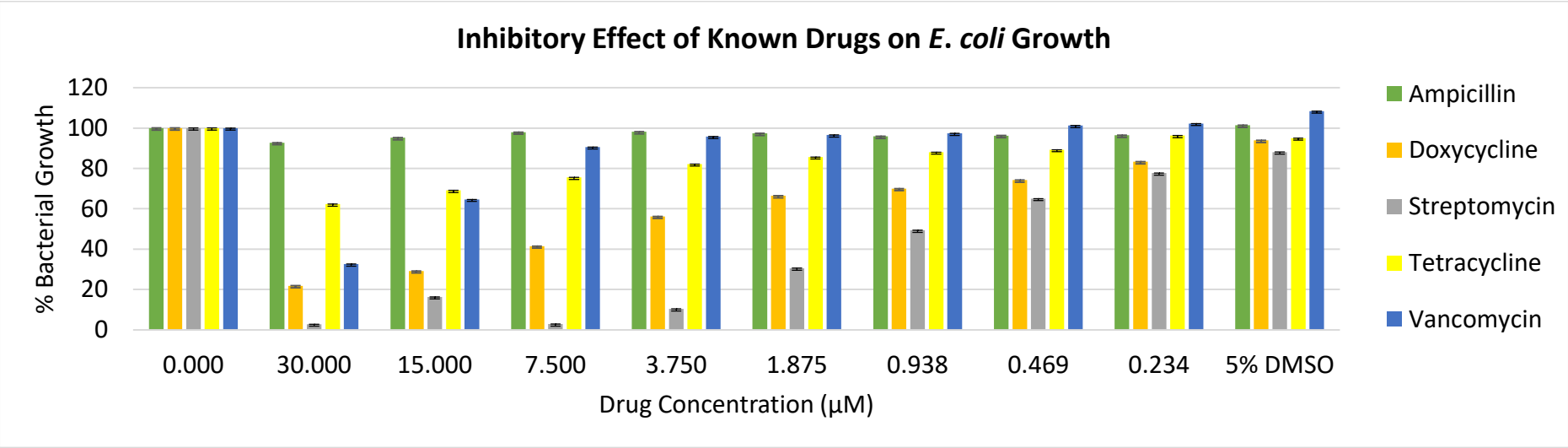

Figure 50: inhibitory effects of known clinical drugs ampicillin, doxycycline, streptomycin, tetracycline, vancomycin against E. coli. n = 2 (8 replicate)

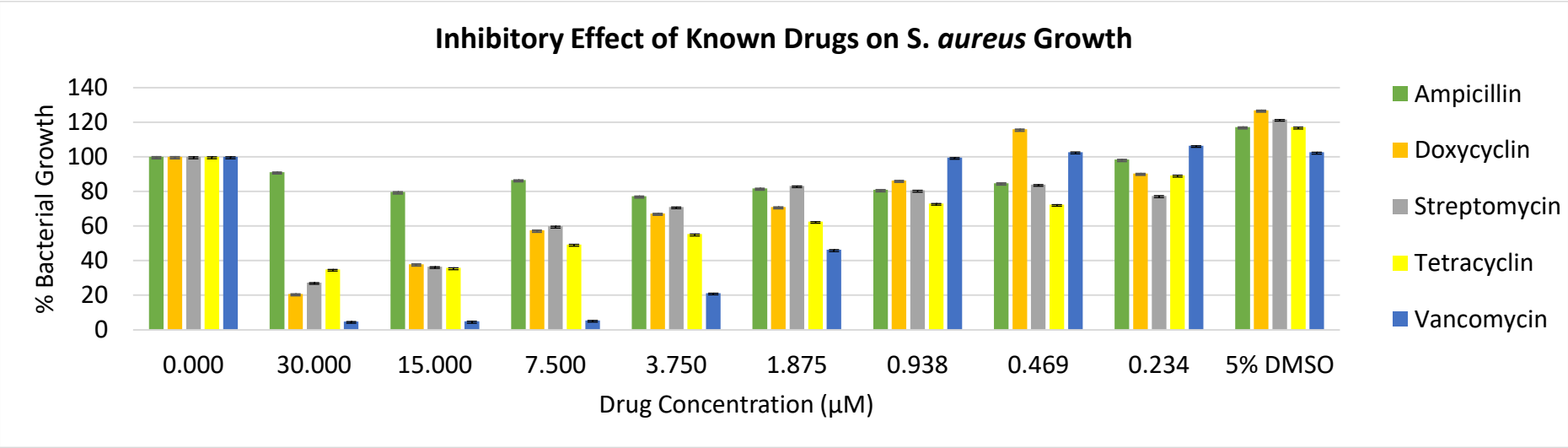

Figure 51: inhibitory effects of known clinical drugs ampicillin, doxycycline, streptomycin, tetracycline, vancomycin against S. aureus. n = 2 (8 replicate)

3.3.1.1: Inhibitory Effect against *S. aureus* Growth

The screening of **3.3a** and its Ag(I), Cu(II), Mn(II) complexes against *S. aureus* revealed that all three metal complexes show promising inhibitory effects towards *S. aureus* growth at 30 μM dose. Out of the three metal complexes, the Cu(II) complex exhibits the greatest activity, with excellent inhibitory effects towards *S. aureus* growth being observed at the 15 μM dose. The Mn(II) complex also shows excellent inhibitory effects towards bacterial growth, but at the higher dose of 30 μM. At the 15 μM dose, the Mn(II) complex only shows moderate inhibitory effects. The Ag(I) complex only exhibits moderate antibacterial effects at 30 and 15 μM doses. In comparison, the ligand **3.3a** only exhibits very low antibacterial activity towards *S. aureus* at 30 μM. Although the activity of the ligand is poor, it does lead to ~35% reduction in bacterial growth at 30 μM dose, suggesting that the ligand itself could potentially lead to promising antibacterial effects at higher concentrations.

The Cu(II) complex displays a MIC_{80} value at 12 μM dose and the MIC_{50} value of 9 μM. In comparison the MIC_{80} and the MIC_{50} values of the Mn(II) complex are determined to be 28 μM and 19 μM respectively. Although the Ag(I) complex does not display a MIC_{80} within the 30 μM range, its MIC_{50} values is determined to be 15 μM. It is noteworthy that when compared to the activity of just the respective metal cation, these complexes display superior antibacterial activity against *S. aureus.* Whereas the $AgClO_4$ metal salt has a MIC_{80} value of 188 μM, and a MIC_{50} value of 72 μM, which is almost twice as much as the MIC value exhibited by Ag(I) metal complex of **3.3a**. In addition, the Cu(II) and Mn(II) simple ClO_4^- salts display no noticeable inhibitory activity at <500 μM range, whereas the metal complexes incorporating these metal cations show promising activity.

For comparison, the antibacterial screening of clinically used antibiotics was also examined following our protocol. It was discovered that out of the five antibiotics studied, namely ampicillin, doxycycline, streptomycin, tetracycline, and vancomycin, the greatest inhibitory effect towards *S. aureus* was exhibited by vancomycin. The MIC_{80} value exhibited by vancomycin was determined to be 3 μM and the MIC_{50} value was determined to be 2 μM. The MIC_{50} value of the remaining antibiotics, ampicillin, doxycycline, streptomycin, and tetracycline were determined to be ND, 9, 10, and 6

μM respectively, with none of these antibiotics exhibiting MIC_{80} values below a concentration of 30 μM. The activity displayed by **3.3a** and its metal complexes compares competitively with the activity displayed by these clinical drugs and demonstrates that these complexes are promising agents to target *S. aureus*.

3.3.1.2: Inhibitory Effect against *E. coli* Growth

A similar trend of activity is observed against *E. coli* by the metal complexes when compared to *S. aureus*. The Cu(II) complex again is the most active complex, and the Ag(I) complex being the least active. However, in contrast to the activity against *S. aureus*, these metal complexes are less active towards *E. coli.* Whereas the Cu(II) complex exhibited MIC_{80} value at 12 μM and MIC_{50} value of 9 μM against *S. aureus*, against *E. coli* the MIC_{80} value is reduced to 28 μM and the MIC_{50} value to 24 μM. Although the decrease in anti-bacterial activity against *E. coli* is not as significant for the Mn(II) and Ag(I) complex, the activity of these complexes are also reduced. *E. coli* belongs to the Gram-negative category of bacteria and the intrinsic resistance of these bacteria towards harmful agents has been outlined in **Section 1.1.2.3.** The outer membrane of the Gram-negative bacteria acts as an additional permeability barrier which further prevents the uptake of harmful substances. Another major factor which confers protection upon Gram-negative cells from harmful substances is the presence of efflux pumps, which can pump harmful agents from the periplasm and the cytoplasm across the cell envelope and into the extracellular environment.

It is interesting to note that although the metal complexes **3.5a1-3** demonstrate inhibitory effects towards *E. coli* growth at doses below 30 μM, the respective starting metal salts for these complexes do not display the same characteristic. Out of the metal complexes tested, it was the Cu(II) complexes which showed the greatest activity towards *E. coli* displaying MIC_{80} value at 28 μM and the MIC_{50} value at 24 μM. In comparison, the simple $Cu(ClO_4)_2.6H_2O$ metal salt displays no inhibitory effect towards *E. coli* at the tested concentration range of <1200 μM. The $Mn(ClO_4)_2.6H_2O$ metal salt also displays poor antibacterial activity, possessing an MIC_{50} value at 439 μM, whereas in comparison the metal complex **3.5a3** possess a MIC_{50} value at 26 μM. These results suggest that the complexation of the metal

centre with the ligand **3.3a** is essential for the antibacterial activity of these complexes. In addition, the ligand **3.3a** itself does not display any promising inhibitory effects towards *E. coli* at the 30 µM dose. A possible explanation of why complexation can either enhance the activity of the metal centre or that of the ligand is given in **Section 1.2**. In summary, the metal centre may reduce the lipophilic nature of the ligand upon complexation, and in return, the ligand can mask the cationic nature of the metal centre, and therefore prevent the complexation of the metal centre to the anionic species present in the cell envelope of the bacteria. In this way, both the ligand and the metal centre can be taken up by the cell in larger quantities, leading to an increase in antibacterial effects of the metal centre as well as that of the ligand.

In the case of the $AgClO_4$ metal salt, the MIC_{80} and MIC_{50} values were determined to be 105 and 69 µM respectively. Unfortunately, due to solubility issues which limited the range of doses tested for the Ag(II) metal complex (**3.5a1**) we were unable to determine MIC_{80} and MIC_{50} values. Although these values could not be determined, the complex **3.5a1** does indeed inhibit ~35% bacterial growth at 30 µM dose, suggesting that the metal complex does possess some antibacterial effects.

The same antibiotics that were tested against *S. aureus* were also tested against *E. coli*. Whereas vancomycin was the most effective antibiotic tested against *S. aureus*, it was streptomycin which possessed the lowest MIC values. In this case, tetracycline also displayed excellent inhibitory effect against *S. aureus* displaying MIC_{50} value of 5.8 µM, but against *E. coli* its MIC values could not be determined below the 30 µM dose.

3.3.1.3: Inhibitory Effect against *C. albicans*

The activity of Ag(I) ion and its metal complexes against *C. albicans* is well known[150,244,245]**.** As expected, out of the Cu(II), Mn(II) and Ag(I) metal complexes tested, it was the Ag(I) complex (**3.5a1**) which presented the highest activity. In addition, the Cu(II) and the Mn(II) complexes exhibited no inhibitory effects within the 30 – 3.75 µM concentration range. The free ligand itself (**3.3a**) was ineffective

also below a 30 µM concentration, suggesting that the ligand acts as a carrier of the Ag(I) metal ion into the candida cell. The reported MIC_{80} for $AgClO_4.H_2O$ metal salt is 44 µM[228]. In comparison, the MIC_{80} value for the Ag(I) complex is determined to be 6.4 µM and the MIC_{50} value is 4.6 µM.

Although the incorporation of the ligand with the Ag(I) metal centre confers enhanced anti-*Candida* activity upon the metal cation, it is noteworthy that the activity exhibited by this metal complex is far lower than that of the Ag(I) complex of **3.1.** The reported activity of the $[Ag(\mathbf{3.1})_2](ClO_4)$ metal complex is 0.5 µM doses for MIC_{80} effect[228]. In addition, the reported activity of $[Ag(\mathbf{phen})_2](ClO_4)$ complex is 8.8 µM for a MIC_{80} effect which is quite similar to that of the Ag(I) complex **3.5a1**, suggesting that both **phen** and **3.3a** are acting as carrier ligands. A further support for this can be observed from the differences in activity of the ligand **3.3a** and **3.1** as well as the Cu(II) complexes of these two ligands. The anti-*Candida* activity of **3.1** and $[Cu(\mathbf{3.1})_3](ClO_4)_2.4H_2O$ exhibit MIC_{80} effects at 2.9 and 1.3 µM doses respectively, whereas the ligand **3.3a** and its Cu(II) complex exhibit no anti-*Candida* activity. The better activity observed for **3.1** and its Cu(II) complex may be due to the presence of the redox-active carbonyl groups on the back-bone, suggesting that appropriate chemical modifications to the ligand can lead to a significant increase in its potency as an antimicrobial agent.

3.3.1.4: *In vivo* Toxicity Studies of 3.3a and its Ag(I), Mn(II) and Cu(II) Complexes in *Galleria Mellonella*

The *in vivo* toxicity of the Ag(I), Mn(II) and Cu(II) complexes of the ligand **3.3a** as well as that of the free ligand were studied in the wax moth larvae of *G. mellonella*.

G. mellonella is a greater wax moth insect which belong to the order of Lepidoptera and it has been utilised in various biological screening studies such as testing for virulence, pathogenicity and antimicrobial efficacy[246]. The use of *G. mellonella* as an *in vivo* model can provide a great deal of useful information about the pharmacokinetic and pharmacodynamics associated with the administered agent. In

addition, the immune system found within this insect resembles very closely the innate immune system of mammals[247].

The toxicity of the agent of interest can be studied by injecting a solution of the agent into the last left pro-leg of the insect which directly leads to the haemocoel (body cavity). Upon squeezing the insect gently from the sides, the pro-leg alongside the cavity can be exposed and easily accessed. The solution can be injected at this stage and upon removal of the pressure, the cavity will close without leading to scaring or damaging of the exterior of the insect. The insect can then be monitored at 37˚C. The immune response towards injected agent can be easily monitored by visually observing the formation of melanisation on the exterior of the insect[248]. In addition, the LD_{50} (lethal dosage) can be deduced by carrying out a dose dependant study.

The use of *G. mellonella* as an *in vivo* model offers many practical advantages[249]. Alongside being a cheaper alternative to mammalian (mice, hamster, rabbits and dogs) models, the use of this insect requires minimal training. The defence of the insect cells against pathogens is carried out through the haemocytes, which act similarly to macrophages and neutrophils. These larvae can be easily maintained in a laboratory at ambient temperature, easily procured, do not require complicated pre-treatment operations and offer quick administration of agents and therefore lead to a faster screening of a large number of compounds. In addition, the ethical approval required for the use of mammalian models is not necessary for the use of these insects.

Solutions of the free ligand **3.3a** and its Ag(I), Cu(II) and Mn(II) complexes **3.5a1-3** were made up with a 5% DMSO solution in PBS to yield 30, 15 and 7.5 µM solutions. These solutions were injected into a batch of 5 larvae each which were then monitored every 24 hours over a period of 72 hours. Positive controls were set up using PBS 5% v/v DMSO solution. The results from this experiment are tabulated in **Table 5.**

Compound		Survival rate (%)		
		24 h	48 h	72 h
3.3a	30 µM	100%	100%	100%
	15 µM	100%	100%	100%
	7.5 µM	100%	100%	100%
3.5a1	30 µM	100%	100%	100%
	15 µM	100%	100%	100%
	7.5 µM	100%	100%	100%
3.5a2	30 µM	100%	100%	100%
	15 µM	100%	100%	100%
	7.5 µM	100%	100%	100%
3.5a3	30 µM	100%	100%	100%
	15 µM	100%	100%	100%
	7.5 µM	100%	100%	100%

*Table 5: Survival rate of G. mellonella administered with 30, 15, 7.5 µM doses of **3.3a** and its metal complexes **3.5a1-3***

It was discovered that all of the larvae survived the treatment of each of the injected solution. All of the larvae exhibited movements similar to that of the healthy larvae and in addition, none of the larvae exhibited any signs of melanisation over the period of 72 hours, indicating that the injected solutions do not lead to an immune response within the larvae. Upon leaving the treated larvae at 37 °C for a further 2 weeks, it was observed that the larvae had entered the pupal stage, forming pupae which then proceeded to the development of the adult moths. These results indicate that the injected solution also do not lead to long-term disruption of the life cycle of *G. mellonella*. The results indicate that these compounds are well tolerated *in vivo* by *G. mellonella* and therefore have potential to be tolerated by mammalian models also. In addition, the effect of these compounds as antimicrobial agents can also be monitored *in vivo* at these doses.

3.3.2: Antibacterial Activity of Lipophilic Derivatives of 3.3a and their Cu(II) Complexes

Following the promising results displayed by the Cu(II) complex of **3.3a** against *S. aureus* and *E. coli*, it was decided that the ligand will be further modified with the

aim of potentially increasing antibacterial activity. A straightforward approach to enhance the antibacterial effect of an agent is to increase the uptake of the anti-bacterial compound. As mentioned in **Section 1.1.2.2**, the bacterial cell envelope of Gram-positive bacteria consists of the peptidoglycan layer and TAs entrapped within the peptidoglycan layer. It is therefore postulated that by increasing the lipophilicity of the anti-bacterial agent, its uptake by Gram-positive bacteria will also be increased and thus this will lead to an increase in its antibacterial effect. In a report by Kumar *et al* modifications were made to the pyridyl-based ligands via elongation of the alkyl chain on the N-atom of the triazole moiety (**Figure 52**) to lead to the formation of lipophilic ligands[250]. It was discovered that the elongation of the alkyl chain lead to an enhancement of the activity of the Ru(II) based metal complexes against *S. aureus* and its resistant strain MRSA.

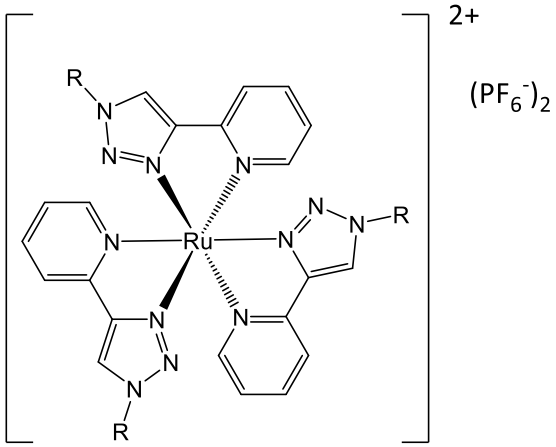

Figure 52: tris-homoleptic Ruthenium(II) 2-pyridyl-1,2,3-triazole complexes

The ester chain of the ligand **3.3a** was modified to yield propyl, hexyl, octyl and dodecyl ester derivatives (**3.3b-e**). These ligands were fully characterized and purified, and their *tris*-Cu(II) (**3.5b-e**) complexes were formed. The free ligands along with their Cu(II) complexes were tested for their inhibitory effects with doses below 30 µM against *S. aureus* and *E. coli* in an *in vitro* screening. The ligands and their metal complexes were dissolved in neat DMSO and doubly diluted with DMSO to yield a series of stock solutions. These were then loaded onto the 96 well plate for antibacterial screening using appropriate dilutions to keep the final DMSO concentration to be 5% when the plates were fully loaded. The results obtained from

these studies are displayed in **Figure 53**, **Figure 54**, **Figure 55**, and **Figure 56** and the MIC values obtained for the ligand as well as the metal complexes are presented in **Table 6**.

Compounds			*S. aureus* MIC(μM)		*E. coli* MIC(μM)	
	Retention time (min)	Calculated log*P*	MIC_{50}	MIC_{80}	MIC_{50}	MIC_{80}
3.3a	21.7	2.8	ND	ND	ND	ND
3.3b	22.5	3.6	8	9	ND	ND
3.3c	27.8	4.9	2	4	ND	ND
3.3d	30.7	5.7	2	3	ND	ND
3.3e	35.4	7.4	ND	ND	ND	ND
3.5a2	ND	ND	9	12	24	28
3.5b	ND	ND	4	4	22	28
3.5c	ND	ND	1	2	ND	ND
3.5d	ND	ND	1	2	ND	ND
3.5e1	ND	ND	ND	ND	ND	ND

*Table 6: minimum inhibitory concentration (MIC) of ligands **3.3a-e** and their tris-Cu(II) complexes and the retention times and theoretical logP values of the ligands. ND = Not Determined. MIC_{50} and MIC_{80} values are determined by ploting the data given in **Figure 53**, **Figure 54**, **Figure 55**, and **Figure 56** and fitting it to a curve.*

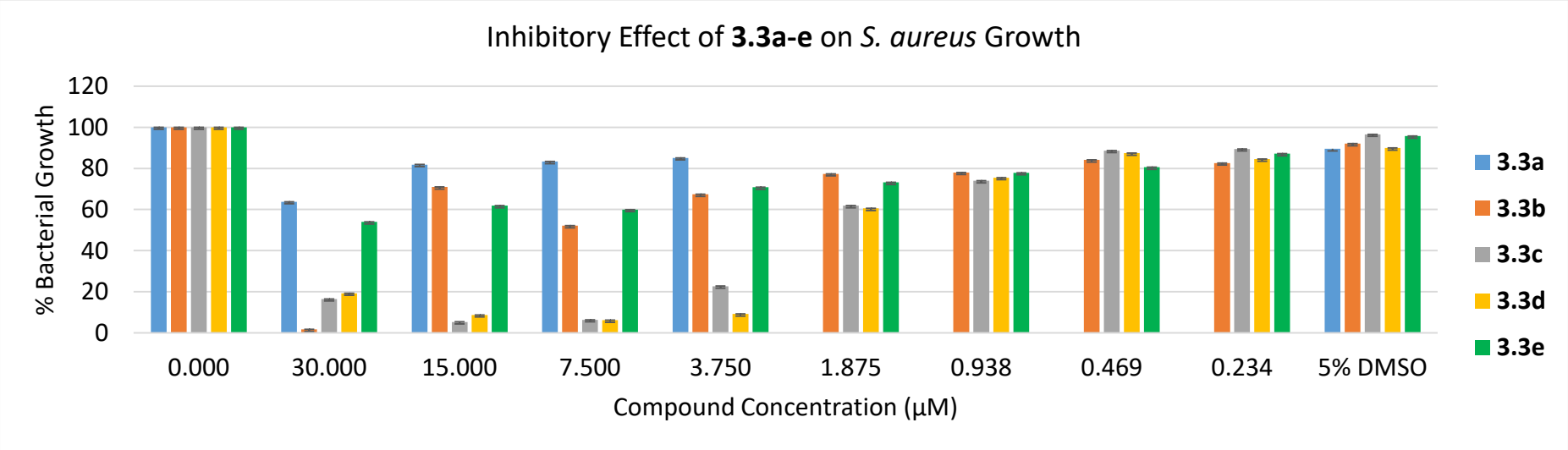

*Figure 53: inhibitory effects of ligands **3.3a-e** against S. aureus. n = 2 (8 replicate)*

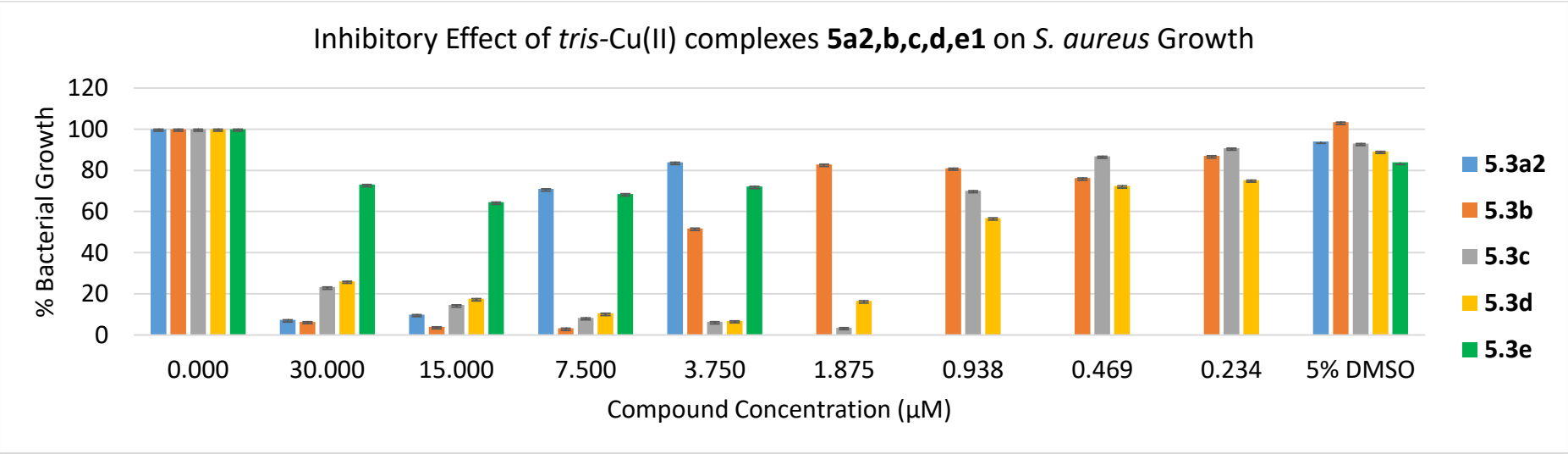

*Figure 54: inhibitory effects of tris-Cu(II) complexes of ligands **3.3a-e** against S. aureus. n = 2 (8 replicate)*

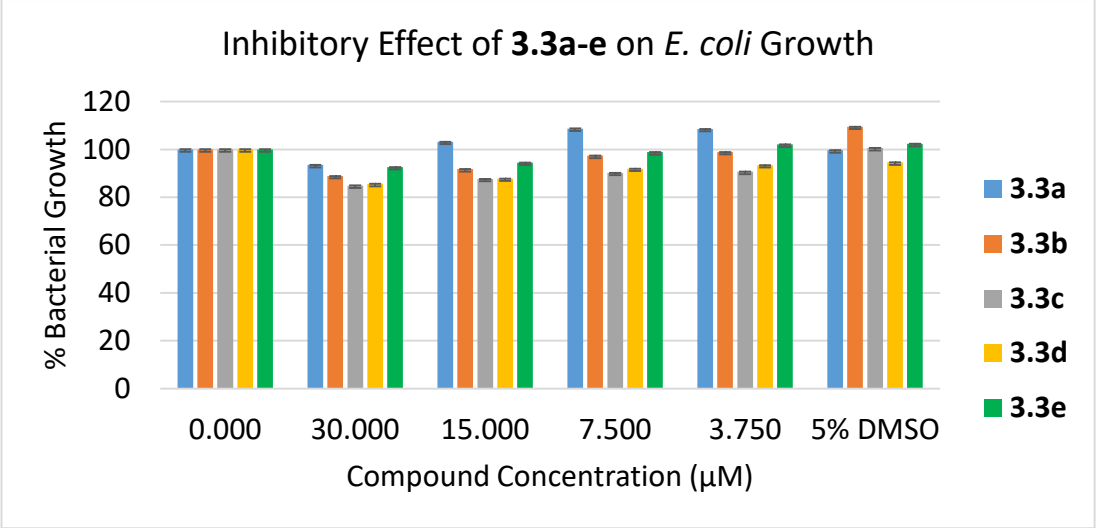

*Figure 55: inhibitory effects of ligands **3.3a-e** against E. coli. n = 2 (8 replicate)*

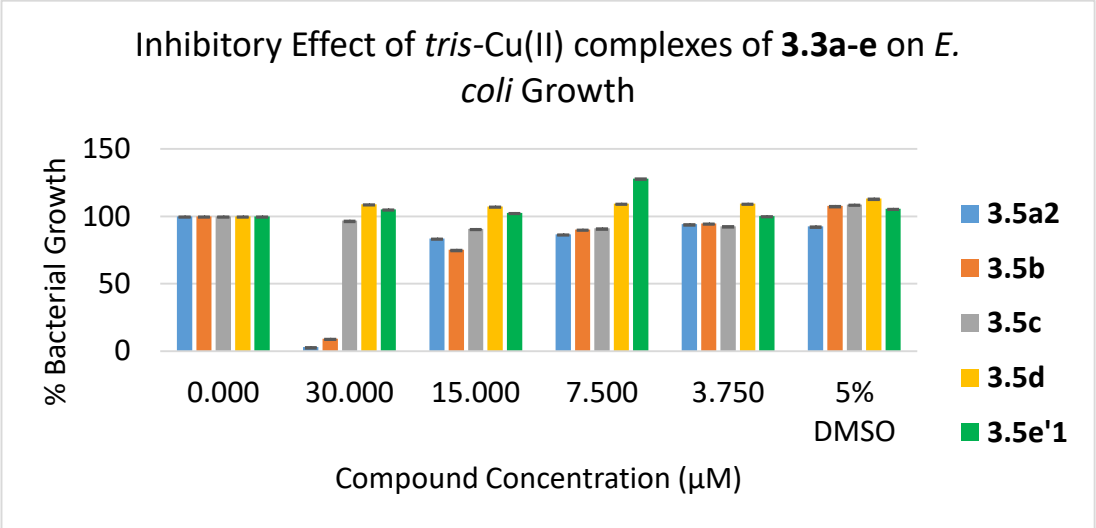

*Figure 56: inhibitory effects of tris-Cu(II) complexes of ligands **3.3a-e** against E. coli. n = 2 (8 replicate)*

3.3.2.1: Inhibitory Effect against *S. aureus*

As expected, the activity of the ligand and their respective metal complexes increases with an increase in lipophilicity. Out of the free ligands tested the hexyl ester and octyl ester derivatives (**3.3c** and **3.3d**) were the most active as these two derivative demonstrate excellent inhibitory effects towards *S. aureus* growth at the 3.75 µM dose. The next most active derivative is the propyl ester derivative (**3.3b**) which displayed excellent inhibitory effects at the 30 µM dose. Interestingly, the most lipophilic derivative tested, the dodecyl ester derivative (**3.3e**), only showed poor activity against bacterial growth, with similar growth inhibition to that caused by

3.3a. A similar trend is observed when the *tris*-homoleptic Cu(II) complexes of these ligands are screened against *S. aureus*. The Cu(II) complexes of the octyl ester derivative (**3.5d**) and the hexyl ester derivative (**3.5c**) were also the most active out of the five metal complexes, exhibiting excellent antibacterial activity towards *S. aureus* at 1.875 μM dose. The next most active complex is that of the propyl ester derivative (**3.5b**), displaying excellent antibacterial activity at 7.5 μM dose. Unlike the trend observed in the series of the ligand, the Cu(II) complex of the dodecyl ester ligand (**3.5e1**) did not exhibit the same activity as that of the Cu(II) complex of the methyl ester ligand. Whereas the Cu(II) complex of the methyl ester ligand (**3.5a2**) displays excellent activity at the 15 μM dose, the Cu(II) complex **3.5e1** does not display any promising activity at concentrations lower than 30 μM.

It is evident that the increase in lipophilicity of the ligand **3.3a** leads to a significant increase its antibacterial activity since even a slight increase in lipophilicty by the formation of the propyl ester ligand **3.3b**, also leads to a significant increase in activity. The MIC_{80} and MIC_{50} for **3.3b** being determined to be 19 and 8 μM whereas the MIC values of the original ligand **3.3a** cannot be determined under 30 μM doses. The activity of the octyl ester ligand (**3.3d**) and the hexyl ester ligand (**3.3c**) is extremely similar with the MIC_{80} and MIC_{50} values for **3.3d** being determined to be 3 and 2 μM, respectively, while the MIC_{80} and MIC_{50} values for **3.3c** are determined to be 4 and 2 μM. Interestingly, the increase in lipophilicity to yield the dodecyl ester leads to a severe decrease in the antibacterial activity with the MIC_{80} and MIC_{50} values both not being observed at doses below 30 μM. In addition, the Cu(II) complex of this ligand also does not demonstrate any antibacterial activity within this range. A similar trend with a 'sweet spot' in lipophilicity leading to good activity was observed in the study reported by Kumar *et al*[250]. This trend of increase in lipophilicty leading to increase in antibacterial activity demonstrates that the ligand itself possess antibacterial activity and requires further modification to increase its bioavailability which is accomplished by increasing the lipophilicty of the ligand.

As observed with the ligand **3.3a**, metal complexation of these ligands also leads to a significant increase in their inhibitory effect towards *S. aureus* growth. Whereas the MIC_{80} (MIC_{50}) value of the ligands **3.3c** and **3.3d** are 4 (2) and 3 (2) μM respectively,

the respective Cu(II) complexes of these ligands display MIC_{80} (MIC_{50}) values determined to be 2 (1) and 2 (1) µM respectively. A similar twofold decrease is observed in the MIC values of the propyl ester ligand (**3.3b**) upon complexation with Cu(II) metal centre. Whereas the MIC_{80} (MIC_{50}) values of the ligand **3.3b** are 19 (8) µM, its Cu(II) metal complex **3.5b** displays MIC_{80} (MIC_{50}) values at 4 (4) µM.

In comparison to the results obtained from clinically relevant antibiotics reported in **Section 3.3.1,** these modifications to the ligand **3.3a** have significantly increased the antibacterial activity against *S. aureus*, making the newly synthesised ligands and complexes even more active than most of the antibiotics tested. The most active of the antibiotic was found to be vancomycin, exhibiting MIC_{80} and MIC_{50} values of 3 and 2 µM respectively. In comparison, the free ligand **3.3d** performed equally to vancomycin. Additionally, the metal complexes of the ligands **3.3b-d** all perform equally if not better when compared to vancomycin.

3.3.2.2: Inhibitory Effect towards *E. coli* Growth

Although increasing the alkyl chain led to an increase in activity towards *S. aureus*, the same was not observed in the case of *E. coli*. Apart from the Cu(II) complexes of methyl ester (**3.5a2**) and the propyl ester ligand (**3.5b**), none of the ligand or their metal complexes were active towards *E. coli*. In the case of the Cu(II) complex **3.5b**, the MIC_{80} value was 28 µM and the MIC_{50} value was 22 µM. Although the cell envelope of the Gram-negative bacterial cell also consists of lipophilic components, the multi-layered envelope of the bacterial cell possesses various inherent defensive mechanisms as well as the multi-component efflux pumps which are responsible for protecting the bacterial cell from lipophilic substances.

3.3.2.3: *In vivo* Biological Profile of Lipophilic Derivatives of 3.3a

The *in vivo* biological profile of the lipophilic derivatives of **3.3a** and their Cu(II) complexes was studied using *G. mellonella*.

Just as the original free ligand **3.3a** and its metal complexes were non-toxic towards *G. mellonella,* the lipophilic derivatives of the free ligands **3.3b**-**e** and their Cu(II) complexes **3.5b-e** were also non-toxic towards the larvae. The larvae not only survived the treatment with these compounds at 30, 15, 3 µM doses (in 5% v/v DMSO PBS solution) but also proceeded to form pupae and form the adult moth without any disruption to their normal life-cycle. In addition, 60 and 120 µM solution were also made for the free ligands in 10% DMSO solution in PBS. The larvae also tolerated these solutions without showing any signs of toxicity.

Having established the non-toxic nature of these ligands and their metal complexes, their ability to inhibit *S. aureus in vivo* was studied according to the procedure outline in **Section 2.5.2.2.2**. The larvae were injected with various doses of *S. aureus.* The culture of *S. aureus* was cultivated according to the procedure in **Section 2.5.2.1.2**. From this culture, a sample was taken and diluted with PBS or dH_2O to produce cultures of OD_{600} 1.00, 0.50, 0.25 and 0.10. Healthy larvae were inoculated with 20 µL solution of these cultures and allowed to rest at 37 °C for 72 hours. It was discovered that the larvae injected with culture of OD_{600} 1 displayed no survivors after 1 hour, and the larvae injected with OD_{600} 0.10 did not display any toxicity or immune response towards treatment with *S. aureus*. The larvae infected with *S. aureus* culture with OD_{600} 0.50 showed 60% survival rate after 24 hours and 0% survival rate after 48 hours, and those infected with OD_{600} 0.25 showed 80% survival rated after 24 hours, 60% survival rate after 48 hours and 40% survival rate after 72 hours. For this reason, the culture of OD_{600} 0.50 and 0.25 were used to study *in vivo* antibacterial activity of the free ligands and their metal complexes.

The results obtained from these studies are reported in **Table 7.** Unfortunately, none of the ligands and their Cu(II) complexes led to an inhibition of *S. aureus* infection *in vivo*, however, there are certain factors which could have led to this lack of activity. One major factor to consider is the concentration of the administered compound in the *in vivo* system. Although the administered dose of the free ligands and their Cu(II) complexes were 30, 15 and 3 µM, all doses which present antibacterial activity *in vitro*, upon being administered into the insect, these concentrations are expected to be lowered by a factor of approximately 5. In addition, the OD_{600} of the bacterial dose

administered *in vivo* is higher than that of the OD_{600} used for the *in vitro* testing. Therefore, it can be speculated that a higher concentration dose of the ligand and the metal complexes needs to be administered to lead to observable *in vivo* antibacterial activity. This issue cannot be resolved without increasing the solubility of the ligands and the metal complexes. One further study which could be performed to check the *in vivo* activity of the free ligands and their Cu(II) complexes is to first administer the compound solution to the larvae and then inoculate the larvae with the *S. aureus* isolate cultivated in nutrient broth. Although the current results obtained do not demonstrate promising *in vivo* activity for the free ligands and their metal complexes, further tests and modifications need to be carried out to fully rule out these compounds as effective antibacterial agents.

Compounds	Strains						*In vivo* toxicity (% survival)			*In vivo* activity at 30 µM	
	S. aureus MIC (µM)		*E. coli* MIC (µM)		*C. albicans* MIC (µM)		30 µM	60 µM	120 µM	*S .aureus* (OD)	
	MIC_{50}	MIC_{80}	MIC_{50}	MIC_{80}	MIC_{50}	MIC_{80}				0.5 OD	0.25 OD
3.3a	ND	ND	ND	ND	ND	ND	100	100	100	No	No
3.5a1	15	ND	ND	ND	5	6	100	NT	NT	NT	NT
3.5a2	9	12	24	28	ND	ND	100	NT	NT	No	No
3.5a3	19	28	26	ND	ND	ND	100	NT	NT	NT	NT
3.3b	8	19	ND	ND	NT	NT	100	100	100	No	No
3.3c	2	4	ND	ND	NT	NT	100	100	100	No	No
3.3d	2	3	ND	ND	NT	NT	100	100	100	No	No
3.3e	ND	ND	ND	ND	NT	NT	100	100	100	No	No
3.5b	4	4	22	28	NT	NT	100	NT	NT	No	No
3.5c	1	2	ND	ND	NT	NT	100	NT	NT	No	No
3.5d	1	2	ND	ND	NT	NT	100	NT	NT	No	No
3.5e1	ND	ND	ND	ND	NT	NT	100	NT	NT	No	No
$Ag(ClO_4)$	72	188	83	125	NT	44*	NT	NT	NT	NT	NT
$Cu(ClO_4)_2.6H_2O$	ND	ND	ND	ND	ND	ND	NT	NT	NT	NT	NT
$Mn(ClO_4)_2.6H_2O$	ND	ND	439	ND	358	ND	NT	NT	NT	NT	NT
3.1	NT	NT	5	8	NT	2.9*	NT	NT	NT	NT	NT
Ampicillin	ND	ND	ND	ND	NT	NT	NT	NT	NT	NT	NT
Doxycycline	9	ND	5	ND	NT	NT	NT	NT	NT	NT	NT
Streptomycin	10	ND	1	3	NT	NT	NT	NT	NT	NT	NT
Tetracycline	6	ND	ND	ND	NT	NT	NT	NT	NT	NT	NT
Vancomycin	2	3	20	ND	NT	NT	NT	NT	NT	NT	NT

*Table 7: overview of results from biological screening of the oxazine-based ligands and their metal complexes NT = Not Tested. ND = Not Determined. *values taken from publication by McCann et al[228].*

3.3.3: Cell Leakage Assay

Phen-based metal complexes can exhibit antibacterial activity through various modes of actions such as:

- DNA binding and/or DNA damage
- Cell wall damage
- Generation of reactive oxygen species
- Enzyme inhibition

The various complexes which have exhibited antibacterial activity reported in the literature by the above mechanisms have been discussed in **Section 1.2.2.3.** For the *bis*-Cu(II) and *bis*-Ag(I) complexes of the ligand **3.3a** it has been reported that these complexes along with the ligand possess DNA binding capabilities. Although the ligand itself does not bind very strongly to DNA, the metal complexes have been reported to have a higher-binding capacity than known groove binding drugs netropsin and pentamidine[221]. Although the DNA binding capabilities of the ligand and its metal may be a factor conferring antibacterial activity upon these compounds, it is often the case that these compounds can have multiple modes of actions. A potential mode of action of an active complex is to cause cell wall damage which eventually leads to cell wall leakage. The cell wall permeabilisation capabilities of the complexes of **3.3a**, **3.3b** and **3.3c** were tested.

A culture of *S. aureus* was grown according to procedure in **Section 2.5.2.1.2**. The culture was harvested at ~1850 rpm for 5 min to form a pellet of the bacterial cell. The nutrient broth was decanted and the pellet was washed with PBS. The bacterial cells were then suspended in 5 ml solution (5% DMSO in PBS/dH_2O) of compound tested at 30 μM solution and incubated at 37 °C at 200 rpm. Aliquots were taken from this solution at 1 hour, 4 hours and 24 hours time points and checked for their amine (including α amino acids) contents via the ninhydrin test[251], and protein content using the Bradford protein assay[252]. An increase in absorbance at λ = 600 nm indicated the presence of amine functional groups in the supernatant. The results from these tests are reported in **Figure 57** and **Figure 58**.

It can be observed from the results from the Bradford protein assay that the level of proteins released from the cell overtime does in fact increases, yet the protein leakage caused by the metal complexes **3.5a2**, **3.5b** and **3.5c** is not significantly different from that caused by the control 5% DMSO solution. A similar observation is made when the amine leakage is measured by mixing the supernatant mention

above with ninhydrin solution. From these results it can be deduced that cell wall damage is not a significant mode of antibacterial action utilised by these compounds.

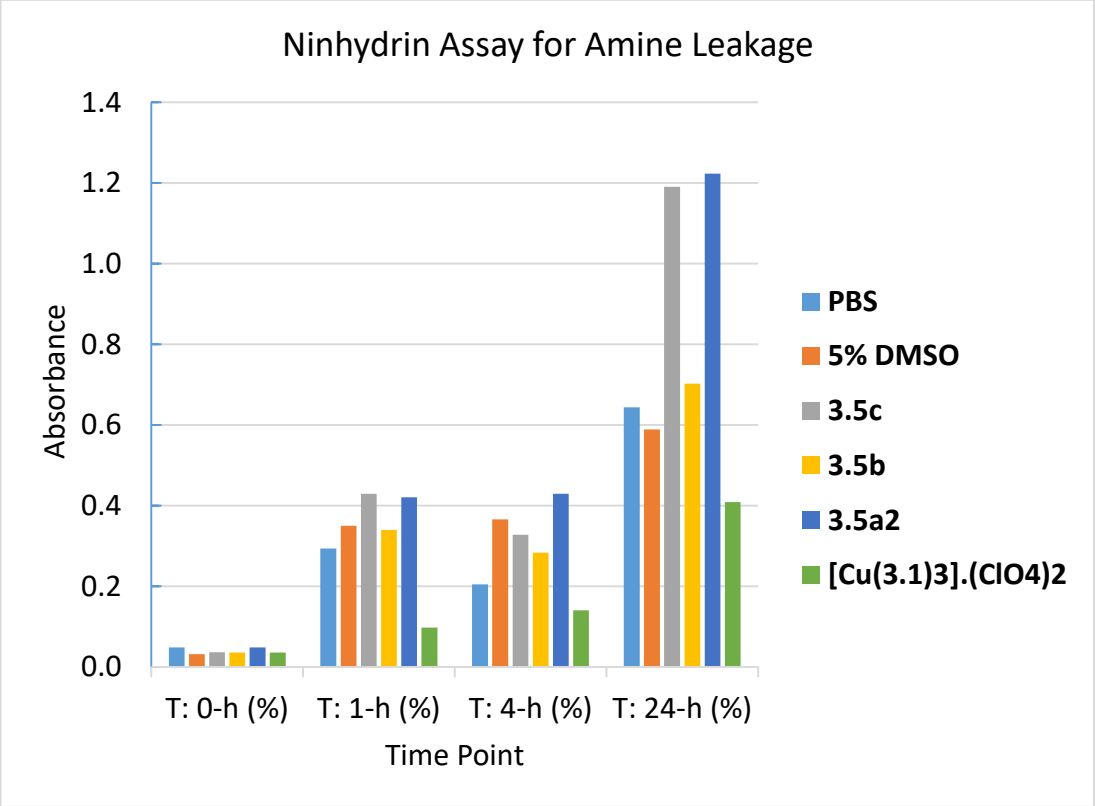

Figure 57: amine leakage from S. aureus measured by ninhydrin assay.

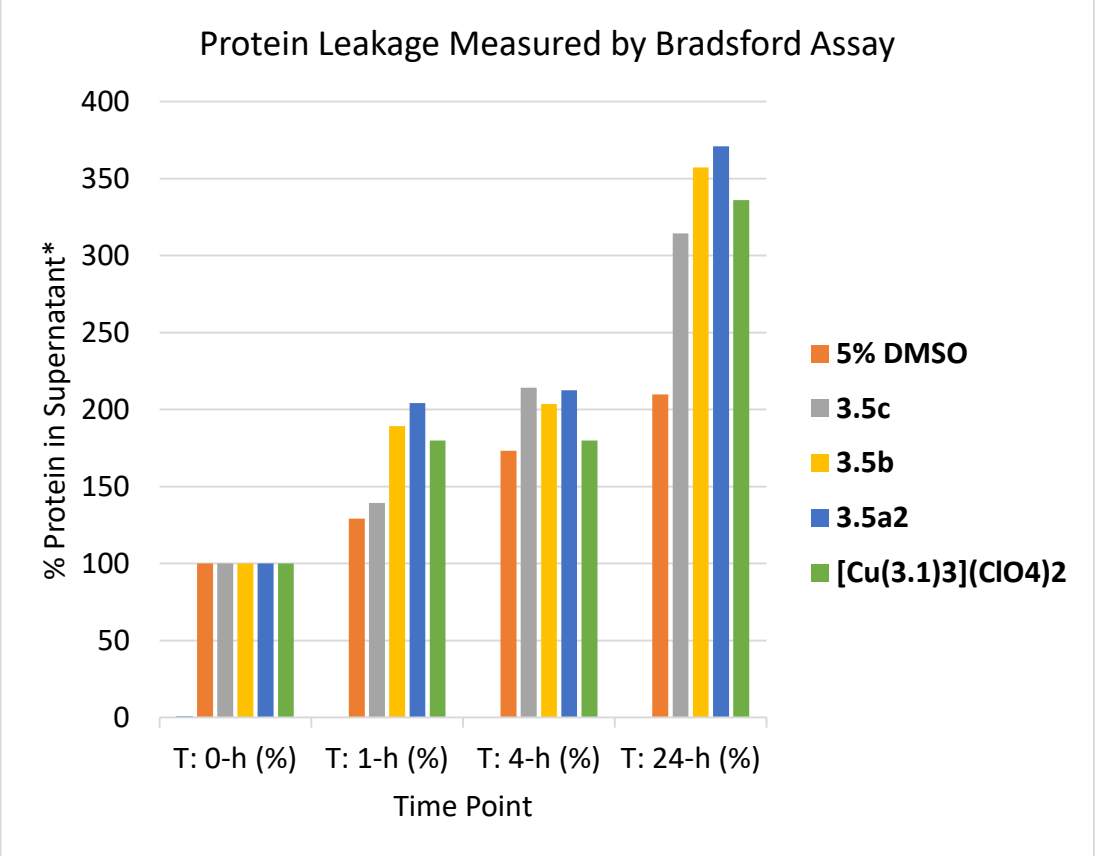

*Figure 58: Respective protein leakage measured by Bradsford assay. *protein content at T = 0 h is taken to be 100%*

3.4: Conclusion

From the results discussed in this chapter, it can be concluded that **3.1** reacts with ester derivatives (**3.2a-g**) of L-tyrosine and L-phenylalanine to give oxazine-based derivatives **3.3a-g**. It is thought that these unusual products form through a multistep mechanism and the first step is a Schiff-base condensation and the resulting imine product then undergoes H-transfer to yield a secondary amine. This intermediate then undergoes oxidation to yield an α,β-unsaturated intermediate which undergoes an intramolecular ring formation reaction to yield the final oxazine-based product. The formation **3.4a-c** also shows that the initial Schiff base product formed from the reaction of **3.1** and amine acid ester derivatives can also follow an alternative path depending on the electron withdrawing nature of the *para*-substitiuent on the aromatic ring of the amino acid.

The oxazine-based derivative **3.3a** was used to form Ag(I), Cu(II) and Mn(II) complexes which were characterised. The screening of these complexes against *S. aureus*, *E. coli*, and *C. albicans* revealed that the Cu(II) complex **3.5a2** is the most active against *S. aureus* and *E. coli*, displaying inhibitory action below a 30 µM concentration, and the Ag(I) comple **3.5a1** is the most active against *C. albicans*, displaying inhibitory effects below a 5 µM concentration.

The Cu(II) complexes of the lipophilic derivatives of **3.3a** were also screened against *S. aureus* and *E. coli*. Against *S. aureus* these ligands and their complexes displayed excellent inhibitory effects which increased with increasing lipophilicity. However, the inhibitory action of these ligands and their metal complexes plateaued at the octyl ester derivative and next more lipophilic derivative studied, the dodecyl ester derivative, displayed negligible inhibitory effects. The ligands **3.3b-d** and their Cu(II) complexes displayed inhibitory effects below 10 µM concentrations, with the Cu(II) complexes of the **3.3c** and **3.3d** displaying MIC_{60} below 2 µM concentrations. Against *E. coli,* increasing lipophilicity of the ligand led to a severe decrease in the inhibitory effects of the ligands.

These ligands and their metal complexes were also tested for their toxicity toward *G. mellonella* and the complexes did not display any toxic effects towards the larvae at 30 µM doses administered and the ligands were well tolerated even at 120 µM doses. The cell permeabilisation ability of the Cu(II) complexes **3.3a2**, **3.3b** and **3.3c** was studied and it was observed that cell wall damage is not the major mode of action toward bacteria possessed by these complexes. These results suggest that these ligands and their metal possess excellent antibacterial propterties and are well tolerated by *G. mellonella.*

Chapter 4

Discussion of Synthesis, Characterisation and Biological Evaluation of 4.1 and its Metal Complexes (4.2a-c)

4.1: Introduction

The work presented in this chapter consists of the results and discussion of the synthesis, characterisation and biological screening of a hydrazone based ligand, **4.1**, and its Ag(I), Cu(II) and Mn(II) metal complexes **4.2a-c**. An outline of the chemicals used as well as the synthetic protocols utilised for the synthesis of **4.1** and metal complexation to yield **4.2a-c** is given below (**Scheme 9**).

The synthesis of **4.1** involves reaction of **3.1** with **INH** through Schiff-base condensation. The stability of **4.1** towards hydrolysis is discussed. The formation of an azo-type product, **4.3a**, and the diamide **4.3b**, indicates the possible degradation of **4.1** through a radical reaction when left in MeOH/EtOH solution over 4 weeks. The synthesis of **4.3a** through conventional azo-coupling protocol was also attempted and is discussed here.

The products of metal complexation of the ligand **4.1** to Ag(I), Cu(II) and Mn(II) metal ions and the stability of the Ag(I) complexes are also discussed. Finally, the results from biological screening of the ligand **4.1** and some of its metal complexes against Gram-positive, Gram-negative, fungal, various *M. tb* cell lines, and a human lung cancer cell line (A549), are presented and discussed.

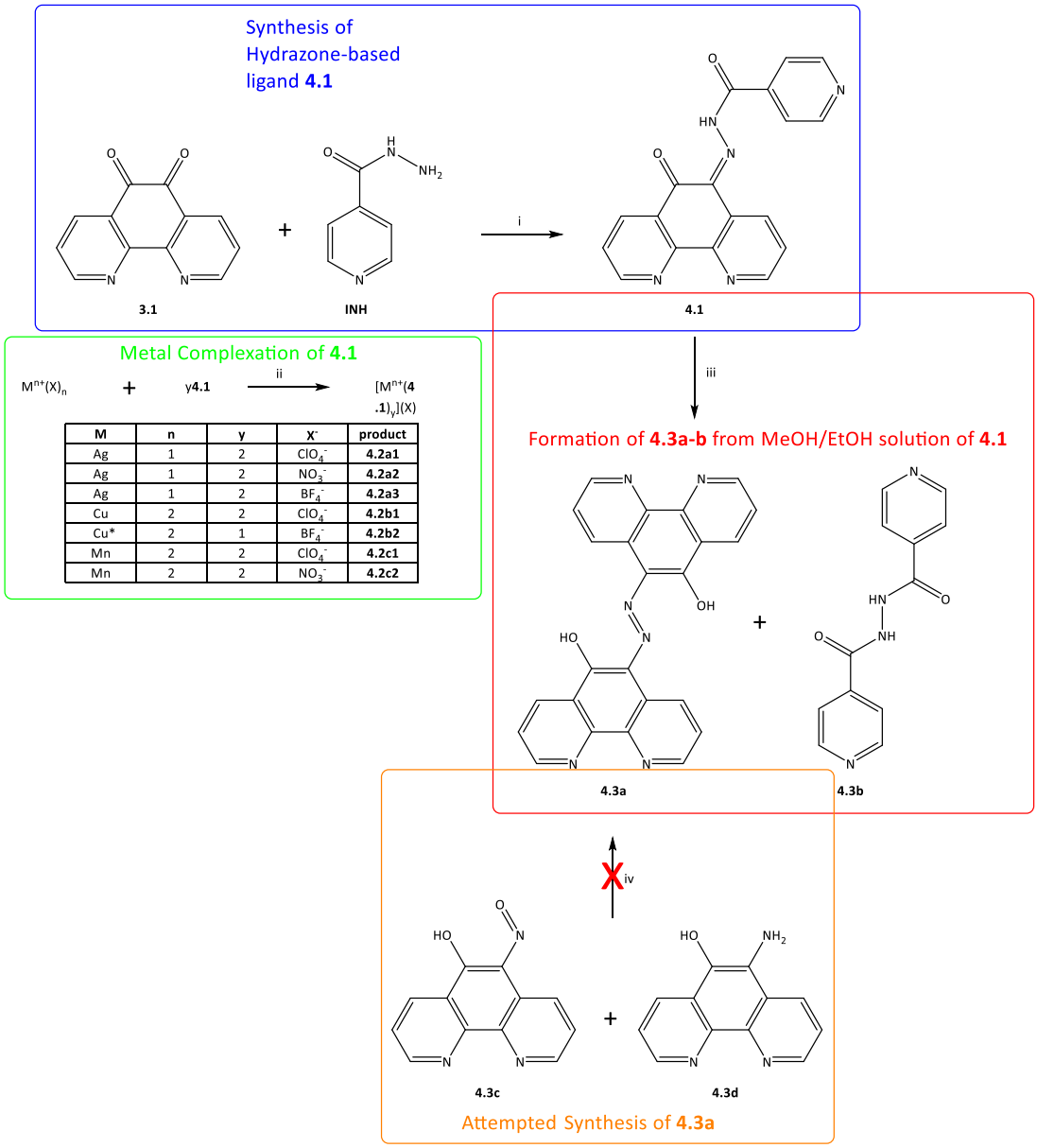

*Scheme 9: Overview of synthesis of **4.1**, its metal complexes **4.2a-c** and attempted synthsis of **4.3a**. i)EtOH/6h/10% p-TSA; ii) EtOh (for X = ClO_4^-) or MeCN (for X = BF_4^- and NO_3^-); iii) MeOH or EtOH; iv) KOH/DMF/150˚C[253] or NaOH/EtOH/80˚C[254] or acetic acid/rt[255]. *Cu(II) stoichiometry not fully determined from the characterisation data.*

4.2: Synthesis and Characterisation of 4.1 and its Metal Complexes (4.2a-c)

4.2.1: Synthesis and Characterisation of 4.1

The synthesis of **4.1** was carried out by adopting a reported procedure[218]. The desired product was isolated with purity and high yield (80%) and fully characterised using IR, NMR, CHN%, and HRMS analysis.

Our intention was to produce the di-imine product of the Schiff-base condensation reaction between **3.1** and **INH**. Although the reaction of **3.1** with **INH** was carried out with much higher equivalents of **INH** (up to 1:4 equivalents for **3.1:INH**) the double Schiff-base product was not observed. We propose that the inability of the second carbonyl to undergo Schiff-base condensation is due to the keto-enol tautomerisation that has been reported to take place for structurally similar hydrazones[256]. Although the presence of this keto-enol tautomerisation cannot be observed using NMR spectroscopy in d6-DMSO, d3-MeCN and $CDCl_3$, it can however be observed that there are two sets of peaks in the ^{1}H NMR spectrum of **4.1** in d4-MeOD solution indicating that tautomerisation is taking place. Further support for the possibility of keto-enol tautomerisation of **4.1** can be seen in the ^{1}H NMR spectra of **4.1** in DMSO, MeCN and $CDCl_3$ solutions. The uncharacteristic downfield resonance of the amide H atom at 15.13 ppm suggests that intramolecular H-bonding is taking place between this H atom and the O atom of the carbonyl group of the **phen** moiety, leading to severe deshielding of the H atom. Due to this H-bonding interaction and keto-enol tautomerisation of **4.1**, it is proposed that the carbonyl C atom of the **phen** moiety is no longer a strong enough electrophile to lead to a second nucleophilic attack from the **INH**. Interestingly, the band arising from the v(C=O) stretch of the C=O functional group on the **phen** moiety, comes at 1723 cm^{-1} in the IR spectrum. In comparison, the v(C=O) in the starting material **3.1**, comes at 1686 cm^{-1}. The increase of ~35 cm^{-1} for the band arising from C=O stretch from the **phen** moiety going from **3.1** to **4.1** suggests that C=O from the **phen** moiety of **4.1** is no longer conjugated. Generally H-bonding causes a downward shift of the v(C=O) stretch[257] , but in this

case the loss of conjugation predominates and lead to an upward shift of the v(C=O) stretching band.

4.2.2: Stability Studies of 4.1

4.2.2.1: Stability of 4.1 towards Hydrolysis

The chemical stability of hydrazone has been known to be compromised by hydrolysis reaction to yield the starting materials when in the presence of H_2O[258,259]. Interestingly, the synthesis of **4.1** was not carried out under anhydrous conditions suggesting that the product is not susceptible to immediate hydrolysis. In addition, the stability of **4.1** towards hydrolysis was also monitored using NMR analysis over 1 week at ambient temperature in a DMSO solution with the addition of a few drops of D_2O. No additional peaks suggesting the hydrolysis of **4.1** were observed.

4.2.2.2: Decomposition of 4.1 in MeOH/EtOH over 4 weeks

Although the hydrazone product **4.1** is stable to hydrolysis, a methanolic/ethanolic solution of **4.1** does not remain stable over a period of 4 weeks. The fresh alcohol solution of **4.1** is clear yellow in appearance. However, over a period of 4 weeks, the bright clear yellow solution changes to a dark green suspension. This behaviour was observed in both the presence, and absence of light. The green suspension was heated to reflux and filtered hot to yield a green filtrate and a dark precipitate. The dark precipitate was dissolved in $CHCl_3$ to produce a dark purple solution, which yielded needle like crystals of the azo compound **4.3a** in very small quantities. This product was then further characterised using IR and CHN% analysis. Furthermore, the diamide **4.3b** was also obtained from the green filtrate and characterised by IR, HRMS and NMR analysis.

Although the mechanism of formation of **4.3a** is currently unknown, **INH**, a prodrug, has been reported to produce the activated isonictinic radical species in the presence of KatG enzyme within *M. tb* (**Section 1.3.1.2** (**Figure 19**)). In addition, the

decomposition of **INH** under various conditions such as exposure to light, heat, mild oxidation and hydrolysis has been studied[219,260] and the results reported suggest that **INH** is susceptible to decomposition to produce a range of products such as isonicotinic acid, isonicotinamide, isonicatinaldehyde and the diamide **4.3b** as well as other products.

4.2.2.2.a: Attempted Synthesis of 4.3a

To probe the mechanism of formation of **4.3a** and increase the yield of this highly conjugated product, various experiments were attempted.

The ability of **INH** to form radical species is well reported and we suspected that the formation of **4.3a** possibly occurs through a radical mechanism. To facilitate this process, a solution of **4.1** in MeOH was treated with the radical initiators azobiisobutyronitrile and 2,2'-azobis(2-amidinopropane). The solution of **4.1** and the radical initiators did not produce the desired purple product **4.3a**.

The linker between the two **phen** rings in the **4.3a** is an azo linker. There are numerous methodologies which involve coupling between an aromatic primary amine and an aromatic nitroso derivative to produce the corresponding azo compound. I synthesised the nitroso derivative **4.3c** and the amino derivative **4.3d** and attempted to produce **4.3a**[253,254]. Three reactions were attempted using reaction conditions reported in the literature to couple **4.3c** and **4.3d** to produce **4.3a** and these are summarised in **Scheme 9.** Unfortunately, none of these coupling reactions produced the desired product **4.3a**.

4.2.2.2.b: Structural analysis of 4.3a

The characterisation of **4.3a** was carried out using CHN%, IR and X-ray crystallography. The X-ray crystal structure of **4.3a** is shown in **Figure 59.** The compound **4.3a** is a fully conjugated *bis*-phenanthroline molecule containing an azo linker connecting the two phenanathroline moieties. **4.3** crystallises with two molecules of $CHCl_3$ molecules per diazo-diphenanthroline. There are hydrogen bonds

between the OH groups and the diazo linker. The CHN% is in good agreement with the proposed composition of the sample containing **4.3a** with two $CHCl_3$ molecules being present. The sharp band in the IR spectrum arising at 1418 cm^{-1} is assigned to the v(N=N) stretch. Carrying out HRMS analysis on the sample did not provide useful information as under typical ESI conditions it appears that **4.3a** is not stable.

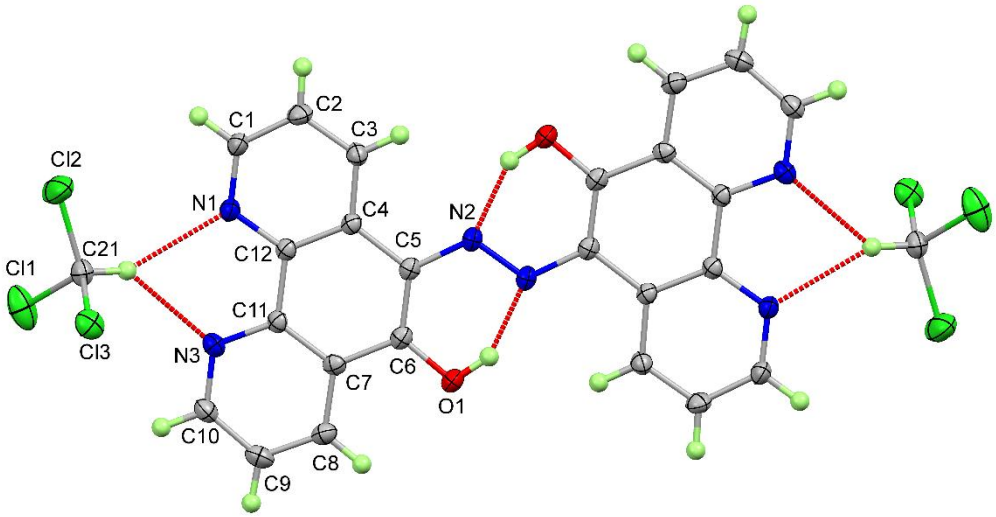

*Figure 59: Perspective view of **4.3a**.2$CHCl_3$ showing the labelling scheme for the asymmetric unit with displacement ellipsoids drawn at the 50% probability level. Hydrogen atoms are shown as spheres of arbitrary radius and hydrogen bonds are indicated by dashed red lines.*

Further characterisation of **4.3a** was limited by its lack of solubility in common organic solvents. Although the **4.3a** presents a clear purple/blue solution in $CDCl_3$/MeOD, only a very poorly resolved ^{1}H NMR spectrum was obtained. To form a more concentrated solution of **4.3a** for NMR analysis, the sample was dissolved in CF_3COOD to produce a red solution. Six signals were observed in the ^{1}H NMR spectrum in the aromatic region which can be attributed to the 6 H-atoms of the **phen** ring. We deduce that **4.3a** dissolves in this solvent with ease due to protonation of the compound at one or more N atoms.

The sample **4.3a** was also dissolved in various organic solvents at lower concentrations. It was observed that **4.3a** displayed solvatochromism. UV-Vis analysis of **4.3a** dissolved in $CHCl_3$, $CHCl_2$, MeOH and EtOH was carried out and the spectra are shown in **Figure 60**. The solutions of **4.3a** in $CHCl_3$ and $CHCl_2$ gives rise to a broad band with λ_{max} at 543 nm. However, in an alcoholic solution, this band

undergoes a bathochromic shift and separates into two bands with λ_{max} at 643 nm and 600 nm. As the compound **4.3a** is very sparingly soluble in the organic solvents, no accurate measurements of the extinction coefficient could be made.

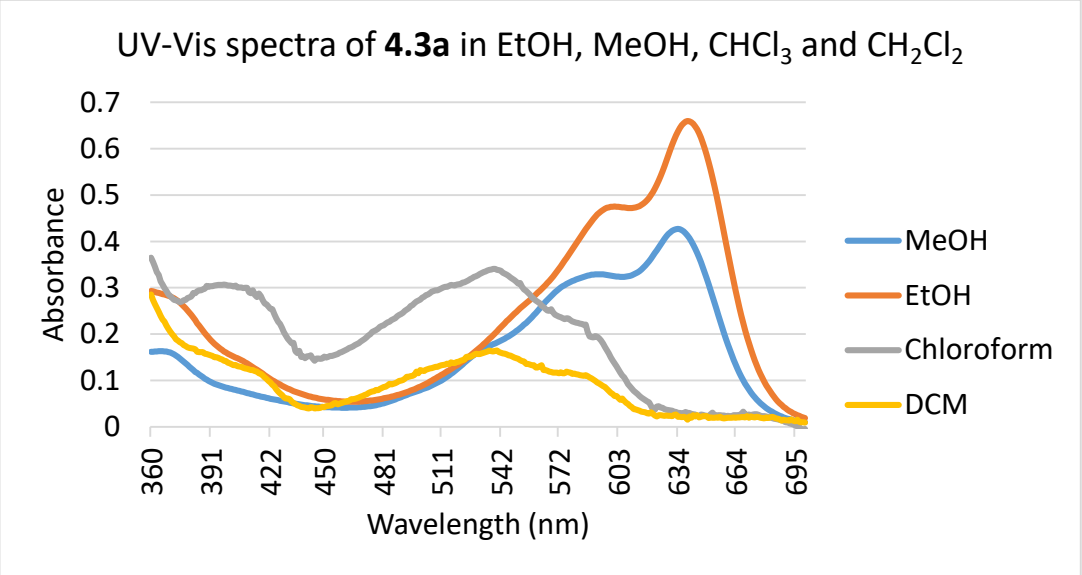

*Figure 60: UV/vis spectra of **4.3** in (grey) $CHCl_3$, (orange) ethanol, (yellow) CH_2Cl_2, and (blue) methanol. The absorbance axis is x10 for the $CHCl_3$ and CH_2Cl_2 solutions.*

4.2.3: Metal Complexation of 4.1

Metal complexes of **4.1** were formed by reacting **4.1** in appropriate stoichiometric amounts with various Ag(I), Cu(II) and Mn(II) metal salts. The complexation of **4.1** with NO_3^- and BF_4^- metal salts was carried out in MeCN whereas the complexation with ClO_4^- salts was carried out in EtOH. With the exception of the metal complexation with $(CuBF_4)_2.xH_2O$, these reactions generally gave good yield (70-80%). The complexation with $(CuBF_4)_2.xH_2O$ only yielded a metal complex in relatively low yields (39%) and we propose it has the composition of [Cu(**4.1**)]$(BF_4)_2$. The Ag(I) metal complexes were characterised with the help of CHN%, HRMS, IR, and NMR analysis. The Cu(II) and Mn(II) complexes were characterised with CHN%, IR and magnetic moments analysis.

4.2.3.1: Synthesis and Characterisation of Ag(I) Complexes of 4.1 (4.2a1-3)

The Ag(I) complexes of **4.1** were prepared by refluxing a EtOH/MeCN solution of **4.1** and Ag(I) metal salts (NO_3^-, BF_4^-, ClO_4^-) in a 2:1 stoichiometric ratio of **4.1**:Ag(I) salts.

The HRMS analysis of the Ag(I) complexes **4.2a2** and **4.2a3** shows the presence of a peak that corresponds to the $[Ag(\mathbf{4.1})_2]^+$ species with the isotopic pattern expected for a Ag(I) species. The CHN% analysis is also in good agreement of complexation of 2 ligands to 1 metal centre.

The IR spectra of the Ag(I) complexes reveals slight shifts in various bands. As expected upon complexation, the band arising from the out-of-plane bending of the **phen** C-H bonds shifts to lower wavenumber. The presence of the counter ions was also confirmed by IR with the $\nu(NO_3^-)$ band appearing at 1340 cm^{-1}, the $\nu(ClO_4^-)$ band appearing at 1100-1065 and 624 cm^{-1}, and the $\nu(BF_4^-)$ band coming at 1080-1030 cm^{-1}. The IR band for ν(C=O) stretch of the ketone group shifts to a lower wavenumber going from 1723 cm^{-1} for the ligand to 1712, 1712, and 1706 cm^{-1} for the NO_3^-, ClO_4^-, and BF_4^- complexes respectively. This indicates that in both the free ligand and the Ag(I) metal complexes, the keto form dominates in the solid state and that the C=O bond is localised.

The ^1H NMR spectra of the Ag(I) complexes also revealed slight shifts in ppm of the peaks arising from the ligand **4.1**. When analysing the ^1H NMR spectra, for the **phen** H-atoms, the H atoms *ortho*- to the ring N atoms do not show any significant shifts. Similarly, the peaks assigned to H-atoms of the pyridine ring only shift by <0.1 ppm. Significant shifts of 0.3 ppm can be seen in signals for the *meta*- and *para*- H atom of the **phen** ring. These shifts indicate that the ligand binds to the metal centre predominantly through the **phen** N atoms. Similar shifts can be observed in the ^{13}C spectra of the ligand when compared to the Ag(I) complexes **4.2a1-3**.

The stability of the metal complexes **4.2a1-3** was studied using ^1H NMR. Solutions of the metal complexes were prepared in d6-DMSO and analysed using ^1H NMR over 3 days at 24 hour intervals. Although the Ag(I) complexes containing BF_4^- and ClO_4^- counter ions did not display any changes in their ^1H NMR spectrum, the Ag(I) complex containing the NO_3^- counterion displayed the growth of a series of small peaks in its

^{1}H NMR spectrum. The growth of these peaks could be observed from the 12 hour time point and the intensitiy of these peaks increased as the experiment carried on. The same stability analysis was carried out in the dark and it was observed that the same behaviour was exhibited by the metal complexes. We are uncertain why the [Ag(**4.1**)$_2$](NO$_3$) complex is unstable whereas the other two complexes do not show any signs of decomposition over the 3 days. Interestingly, when a DMSO solution of [Ag(**4.1**)$_2$](NO$_3$) was allowed to stand over a prolonged period of time for crystallisation under DCM vapour diffusion into the solution, X-ray crystallography quality crystals were produced and these show the formation of a polymeric chain with Ag(I):**4.1** present in a 1:1 ratio with the NO_3^- ion taking up a coordination site around the Ag(I) metal centre (**Figure 61** and **Figure 62**).

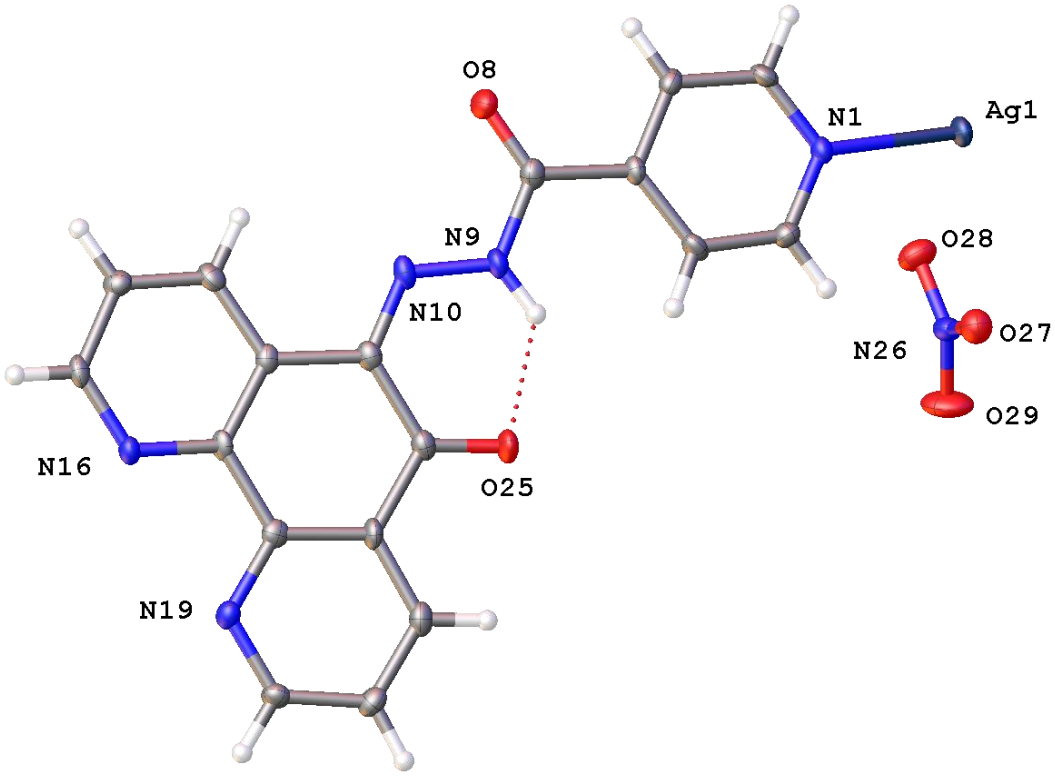

*Figure 61: Asymmetric unit of {[Ag(**4.1**)(NO$_3$)]}n with selected atom numbering. Atomic displacement shown at 50% probability. Intramolecular hydrogen bonding shown as a dotted line.*

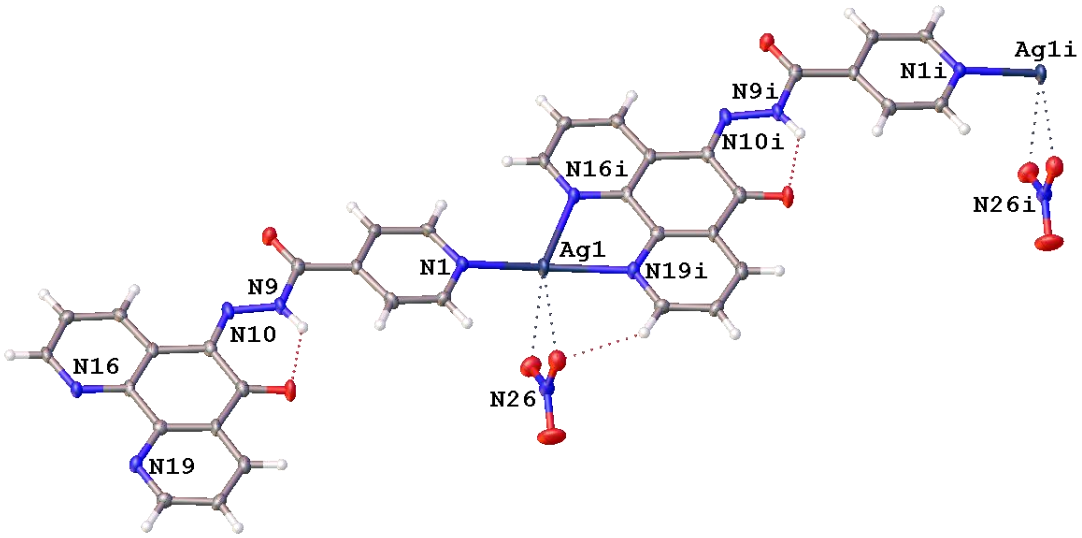

*Figure 62: Symmetry generated (symmetry code used to generate equivalent atoms i = x-1, y+1, z-1) chain for {[Ag(**4.1**)(NO_3)]}n with intramolecular hydrogen bonding showing the Ag(I) coordination by the nitrate anion.*

4.2.3.2: Synthesis and Characterisation of Cu(II) Complexes of 4.1 (4.2b1-2)

The Cu(II) complex **4.2b1** was formed by reaction of $Cu(ClO_4)_2.6H_2O$ with **4.1** in a 1:2 ratio in an EtOH solution. The resulting brown precipitate was characterised using CHN%, IR and magnetic moments analysis. The CHN% analysis indicates the composition to be $[Cu(\mathbf{4.1})_2](ClO_4)_2.2H_2O$. The IR spectrum shows the shifting of the v(C=O) stretch from 1723 cm^{-1}, found in IR spectrum of **4.1**, to 1708 cm^{-1}. The presence of the ClO_4^- counterion was determined by the presence of a bands arising at 1091 and 623 cm^{-1}. Interestingly, the magnetic moment determined for this sample was 1.5 BM which is much lower than the 1.7 BM value calculated by using the spin-only formula. Although HRMS analysis of the sample was attempted, we were unable to determine the accurate mass value for the sample. We propose this is due to the complex being unstable under ESI conditions.

The Cu(II) complex **4.2b2** was also prepared by stirring a solution of $Cu(BF_4)_2.xH_2O$ (in excess, an exact stoichiometry cannot be defined as the salt is hydrated) with a solution of **4.1** in MeCN. The resulting suspension was filtered to produce a brown solid which was characterised using CHN%, IR and magnetic moment analysis. The CHN% analysis is in good agreement with the formation of a 1:1 complex of metal:ligand. The IR spectrum shows a decrease in wavenumbers of the band arising

from the v(C=O) stretch going from 1723 cm^{-1} in the IR spectrum of the ligand **4.2** to 1706 cm^{-1} in the spectrum of **4.3b2**. The presence of the counterion was determined by the presence of a broad band ranging from 1073-1054 cm^{-1} arising from the v(BF_4^-) stretch. The magnetic moment determined for the sample was 1.2 BM and like the sample **4.2b1** it is well below the calculated value of 1.7 BM. Although the elemental analysis suggest the composition to be [Cu(**4.1**)]$(BF_4)_2$ the characterisation of this complex is not complete. Due to this we are unsure of the composition of this product the complete characterisation of this sample will require further work.

4.2.3.3: Synthesis and Characterisation of Mn(II) Complexes of 4.1 (4.2c1-2)

Two Mn(II) complexes were prepared by reacting the ligand **4.1** in a 2:1 ratio (**4.1**:Mn(II) salt) with $Mn(ClO_4)_2.6H_2O$ and $Mn(NO_3)_2.4H_2O$. The *bis*-complexes were obtained in high yields with the [Mn(**4.1**)$_2$]$(ClO_4)_2.H_2O$ (**4.2c1**) being isolated at 65% yield and the [Mn(**4.1**)$_2$]$(NO_3)_2.2H_2O$ (**4.2c2**) being obtained in 70% yield. These complexes were characterised using CHN%, IR and magnetic moment analysis.

The CHN% analysis displays the formation of a *bis*-homoleptic Mn(II) complexes with one H_2O molecule being present in **4.2c1** and two H_2O molecules being present in **4.2c2**. The IR spectrum of the two metal complexes display shifts in the band arising from out-of-plane C-H bend going from 752 cm^{-1} in the IR spectrum of the ligand to 746 and 748 cm^{-1} for **4.2c1** and **4.2c2** respectively. The presence of the counterion was determined by the presence of broad bands arising from v(ClO_4^-) stretch at 1108 and 624 cm^{-1}, and the sharp band arising from the v(NO_3^-) stretch at 1385 cm^{-1}. The magnetic moment determined for **4.2c1** and **4.2c2** are 6.5 BM and 6.22 BM respectively and the expected value calculated value (by spin only formula) is 5.9 BM.

4.3: Biological Screening of 4.1 and its Metal Complexes 4.2a-c

The ligand **4.1** and its metal complexes (**4.2a1**, **4.2a1**, **4.2b2** and **4.2c2**) were screened for their antimicrobial activity towards *M. tb* (four strains)*, S. aureus, P. aeruginosa*

and *C. albicans*. These compounds were also screened for their toxicity towards mammalian cells by measuring their CC_{50} against A549 cell line. For comparison, the simple metal salts ($AgBF_4$, $Cu(BF_4)_2.H_2O$, $Mn(NO_3)_2.4H_2O$), **phen**, **INH**, and known clinical drugs (ciprofloxacin, ceftazidime, amphotericin B) were also screened for their antimicrobial activity. The results from this screening are summarised below in **Table 8.** These studies were carried out by the groups of Professor Maria Cristina Lourenço (Fundação Oswaldo Cruz) and Professor André Luis Souza dos Santos (Federal University of Rio de Janeiro) in Rio de Janeiro, Brazil.

Compound	A549 CC_{50} (µM)	*M.tuberculosis* $H_{37}RV$ ATCC 27294[a]	*M.tuberculosis* 665/0514[b]	*M.tuberculosis* SR Cult 84/17[c]	*M.tuberculosis* SR 2571/0215[d]	*S. aureus*	*P. aeruginosa*	*C. albicans*
4.1	157.3	15.18 (10.4)	<9.5 (>16.6)	<9.5 (>16.6)	<9.5 (>16.6)	48.6 (3.2)	388.7 (0.4)	12.2 (12.9)
4.2a2	50.6	3.02 (16.8)	<3.8 (>13.3)	<3.8 (>13.3)	<3.8 (>13.3)	19.3 (2.6)	9.7 (5.2)	2.4 (21.1)
4.2a3	44.1	2.93 (15.0)	<3.7 (>11.0)	<3.7 (>11.0)	<3.7 (>11.0)	9.4 (4.7)	9.4 (4.7)	2.3 (19.2)
4.2b2*	109.8	17.65 (6.3)	<5.5 (>19.9)	<5.5 (>19.9)	<5.5 (>19.9)	56.5 (1.9)	451.9 (0.2)	14.1 (7.8)
4.2c2	56.6	2.99 (18.9)	<3.7 (>15.3)	<3.7 (>15.3)	<3.7 (>15.3)	19.1 (2.9)	611.3 (0.1)	19.1 (2.9)
$AgBF_4$	95.5	51.36 (1.9)	32.1 (2.9)	32.1 (2.9)	32.1 (2.9)	20.5 (4.7)	10.3 (9.3)	<5.1 (>18.7)
$Cu(BF_4)_2.H_2O$	458.8	52.71 (8.7)	26.4 (17.4)	26.4 (17.4)	26.4 (17.4)	>2158.8 (<0.2)	>2158.8 (<0.2)	269.9 (1.7)
$Mn(NO_3)_2.4H_2O$	ND	>558.82	>558.8	>558.8	>558.8	>2861.1	>2861.1	>2861.1
Phen	2422.7	13.87 (174.7)	<17.3 (>140.0)	<17.3 (>140.0)	<17.3 (>140.0)	355.1 (6.8)	355.1 (6.8)	<5.6 (>432.6)
INH	3500.1	11.38 (307.6)	>729.0 (<4.8)	>729.0 (<4.8)	>729.0 (<4.8)	ND	ND	ND
Ciprofloxacin	ND	ND	ND	ND	ND	12.1	12.1	ND
Ceftazidime	ND	ND	ND	ND	ND	29.3	7.3	ND
Amphotericin B	ND	ND	ND	ND	ND	ND	ND	0.07

*Table 8: In vitro anti-A549 (CC_{50}) and antimicrobial activity (MIC) values (µM). SI value in parenthesis. (a) Rifampicin and **INH** sensitive strain. (b) Rifampicin and **INH** resistant strain (*katG*). (c) Rifampicin and **INH** resistant strain. (d) Rifampicin and **INH** resistant strain (*katG *and* inhA*). *concentration based on the proposed $[Cu(\mathbf{4.1})](BF_4)_2$ formulation.*

4.3.1: Inhibitory Effect against *M. tuberculosis* Growth

The antimycobacterial activity the ligand **4.1** and its metal complexes (**4.2a2**, **4.2a3**, **4.2b2** and **4.2c2**) was studied against four *M. tb* strains: *M. tb* H_{37}RV ATCC 27294 (**INH** and rifampicin sensitive); *M. tb* 665/0514 (**INH** and rifampicin resistant); *M. tb* SR Cult 84/17 (**INH** and rifampicin resistant); *M. tb* SR 2571/0215 (**INH** and rifampicin resistant). The general results from these studies suggest that the Ag(I) and Mn(II) based complexes were the most active, displaying almost equal inhibitory effects, followed by the Cu(II) complex which is the least active of the metal complexes tested. Interestingly, the ligand itself, which was less active than most of the metal complexes, displayed activity similar to that of the clinical drug **INH**.

4.3.1.1: Inhibitory Effect against Drug Sensitive *M. tuberculosis* Growth

Against the **INH** and rifampicin sensitive strain, *M. tb* H_{37}RV ATCC 27294, the Ag(I) metal complexes **4.2a2** and **4.2a3** were extremely active, displaying MIC values at 3.02 and 2.93 µM respectively. It is interesting to note that both of the individual starting materials for the complex **4.2a3** are also active, with **4.1** displaying an MIC value of 15.18 µM and the simple metal salt $AgBF_4$ displaying an MIC value of 52.71 µM. Although these two starting materials are active, their activity can be clearly seen to be enhanced upon complexation to each other with the metal complex **4.2a3** displaying inhibitor effects at a fifth and a sixteenth times lower concentration towards *M. tb* when compared to **4.1** and $AgBF_4$ respectively. Not only is the metal complex **4.2a3** more active toward inhibition of *M. tb* when compared to the ligand and the metal salt, it is also less toxic towards the mammalian cell line A549, displaying SI value of 15.0 which slightly higher than the SI value of **4.1** (SI = 10.4) and significantly higher than the SI value of $AgBF_4$ (SI = 1.9). A similar effect can be observed with the biological screening of the Ag(I) complex **4.2a2** which presents an SI value of 16.8. The reported CC_{50} value of $AgNO_3$ is <30 µM[261], making its SI value <1.5. To the best of our knowledge the most active Ag(I) complexes towards *M. tb* exhibit MIC at >10 µM dosage and possess very low SI values <7[191]. In comparison,

the Ag(I) complexes tested (**4.2a2** and **4.2a3**) exhibit greater inhibitory effects towards *M. tb* as well as less toxicity towards mammalian cells.

Although the excellent activity of Ag(I) complexes can be expected due to the activity of the Ag(I) metal salt, the excellent activity exhibited by the Mn(II) complex **4.2c2** is quite surprising. Whereas the simple Mn(II) salts, $Mn(NO_3)_2.4H_2O$, does not exhibit any noticeable inhibitory effects at doses below 558.8 µM the metal complex **4.2c2** displays MIC value of 2.99 µM. In addition, out of all of the complexes tested, this complex presented the highest SI value of 18.9. In comparison, the Cu(II) complex does not exhibit a similar activity profile. The complexation of Cu(II) to **4.1** to produce **4.2b2**, not only leads to an increase in the MIC value of the complex when compared to the ligand, it also leads to the complex being more toxic towards the mammalian cells. The MIC value towards *M. tb* exhibited by **4.2b2** is 17.65 µM with an SI value of 6.3. Although the MIC value of this complex is lower than that of the simple metal salt $Cu(BF_4)_2.H_2O$ (MIC = 52.71), the SI value of the complex is lower than that of the simple metal salt (SI = 8.7) indicating that the complexation of the ligand does not allow the metal complex to be more selective towards *M. tb* cells.

With the exception of the Cu(II) complex, all of the complexes generated were more active than the ligand **4.1** as well as their respective metal salts. In addition, these complexes also exhibit competitive MIC values when compared to the clinical drug **INH** and a known anti-TB agent **phen**. The biological screening found the MIC value for **phen** and **INH** to be 13.87 and 11.87 µM respectively. The reported MIC value for **INH** is 0.2 - 0.02 µg/mL[191]. The results from this study suggest that the metal complexes possess lower MIC values than those of **phen** and **INH**. Although our complexes are more active, they are not as selective towards *M. tb* over mammalian cells as **phen** and **INH**. Whereas the highest SI value observed from the metal complexes studied in this study is that of **4.2c2**, displaying SI of 18.9, the SI values possessed by **phen** and **INH** are 174.7 and 307.6 respectively.

4.3.1.2: Inhibitory Effect against Drug Resistant *M. tuberculosis* Growth

The inhibitory effects of **4.1** and its complexes, **4.2a2**, **4.2a3**, **4.2b2** and **4.2c2**, were also studied against **INH** and rifampicin resistant strains. The three strains used for this screening were *M. tb* 665/0514; *M. tb* SR Cult 84/17; *M. tb* SR 2571/0215. Unfortunately, the MIC values were not observed within the results displayed in **Table 8.** The results from these screenings show that the clinical drug, **INH**, possesses no antimycobacterial activity towards these strains at doses below 729.0 µM. On the other hand, similar to the activity observed towards the drug sensitive strain, the simple metal salts tested display good activity in the case of $AgBF_4$ and $Cu(BF_4)_2.H_2O$ (MIC = 32.1 and 26.4 µM respectively), or non-existant activity in the case of $Mn(NO_3)_2.4H_2O$ (MIC >558.8 µM). Although the **INH** was inactive towards these strains, the metal complexes display excellent activity with the Ag(I) and Mn(II) complexes being extremely active, and the Cu(II) complex also displaying activity. Against all of the strains, all of the metal complexes possess inhibitory effects at doses lower than 10 µM with the Ag(I) and Mn(II) complexes possessing activity at <4 µM doses. Additionally, the ligand itself also possesses inhibitory effects at <9.5 µM doses. Although **INH** possesses no activity towards these strains, the **INH**-**phen** hybrid retains it activity towards the *M. tb*. This suggests that the ligand **4.1** possesses an alternative mode of action to inhibit *M. tb* growth. Additionally, these compounds are not only active towards these resistant strains of *M. tb* they also maintain their selectivity toward the mycobacterial cells over mammalian cells. All of the new compounds tested display SI values >10 indicating that they classify as potential therapeutics for further development in the pharmaceutical industry[262].

4.3.2: Inhibitory Effect against *S. aureus* Growth

The broad spectrum antimicrobial activity of the ligand **4.1** and its metal complexes, **4.2a2**, **4.2a3**, **4.2b2** and **4.2c2,** were tested against a Gram-positive and negative strain of bacteria as well as a yeast strain. For the Gram-positive strain, *S. aureus* was the bacterial strain used for screening the inhibitory activity of the ligand and its complexes.

The ligand **4.1** exhibited MIC at 48.6 µM dosage and possessed an SI value of 3.2. Out of the metal complexes tested, the Ag(I) complexes were the most active, followed by the Mn(II) complex and then finally the Cu(II) complex. The Ag(I) complexes **4.2b2** and **4.2b3** display MIC values at 19.3 and 9.4 µM respectively. Although these MIC values are very competitive with the MIC value determined for the clinically used drugs, Ciprofloxacin (MIC = 12.1 µM) and Ceftazidime (MIC = 29.3 µM), these complexes displayed very low SI values (2.6 and 4.7 for **4.2b2** and **4.2b3** respectively). Interestingly, the activity of the Ag(I) complex is only very slightly better than the Ag(I) salt $AgBF_4$. The simple Ag(I) salt displays MIC value at 20.5 µM dosage and possesses an SI value of 4.7. These values are extremely similar to the metal complexes, suggesting that complexation of the ligand on the Ag(I) metal salt does not change its activity profile towards *S. aureus* cells.

The next most active metal complex was the Mn(II) complex, **4.2c2**, which displayed MIC at 19.1 µM and a SI value of 2.9. This complex, too, inhibits the growth of *S. aureus* at a competitive dose with the known clinical drugs Ciprofloxacin and Ceftazidime. Additionally, when compared to the simple metal salt, $Mn(NO_3)_2.4H_2O$, the activity of the metal complex is far superior as the simple metal salt does not exhibit any inhibitory effects at doses below 2861.1 µM. Finally, the Cu(II) complex **4.2b2** exhibits a MIC value of 56.6 µM and possesses a SI of 1.9. Although this is an enhancement of inhibitory effects when compared to the simple metal salt $Cu(BF_4)_2.H_2O$ (MIC >2159 µM), this complex possesses a higher MIC value than the free ligand **4.1** and possesses a lower SI value than the ligand also.

4.3.3: Inhibitory Effect against *P. aeruginosa* Growth

To measure the inhibitory effects of the ligand **4.1** and its metal complexes towards Gram-negative bacteria, these compounds were screened against the Gram-negative Bacterium *P. aeruginosa*. Similar to the Gram-positive bacterium, the growth of *P. aeruginosa* was inhibited most by the Ag(I) complexes **4.2b2** and **4.2b3** which displayed MIC values 9.7 and 9.4 µM respectively. These values are competitive with the clinically used drugs tested, Ciprofloxacin (MIC = 12.1 µM) and Ceftazidime (MIC

= 7.3 μM). Although the Ag(I) complexes are active, their SI values are very low being 5.2 and 4.7 for **4.2b2** and **4.2b3** respectively. For the simple metal salt $AgBF_4$, the MIC values are similar to the complexes as the MIC value possessed by the simple metal salt is 10.3 μM. Although the inhibitory effects of the Ag(I) complexes and the simple salt are similar towards *P. aeruginosa*, the SI of the metal salt is roughly twice (9.3) that of the metal complexes, demonstrating that the complexation of the Ag(I) metal with the ligand has increased the toxicity of the metal complex towards mammalian cells. Surprisingly, the Cu(II) and the Mn(II) complexes, **4.2b2** and **4.2c2**, display no significant inhibitory effects, possessing MIC values of 451.9 and 611.3 μM respectively. The free ligand **4.1** itself also does not display a promising inhibitory effects and possesses a MIC value of 389 μM.

4.3.4: Inhibitory Effect against *C. albicans* Growth

The ligand **4.1** and its Ag(I), Cu(II) and Mn(II) complexes display promising activity towards *C. albicans*. The two Ag(I) complexes, **4.2a2** and **4.2a3**, were the most active and exhibited MIC values of 2.4 and 2.3 μM respectively and possessed SI of 21.1 and 19.2 respectively. These values display an improvement upon the potency of the free ligand **4.1** which possesses MIC value of 12.2 μM and SI of 12.9. Although these values are promising, they are to be expected as Ag(I) metal centre is extremely active towards *C. albicans* and the $AgBF_4$ metal salt possesses MIC value <5.1 and SI greater than 18.7. The Cu(II) and Mn(II) complexes also show promising inhibitory effects and possess MIC values of 14.1 and 19.1 μM respectively. Although these complexes show good anti-candida effects, their SI values are low, with the Cu(I) complex possessing SI of 7.8 and the Mn(II) complexes possessing SI of 2.9. Although the ligand **4.1** and its complexes displayed promising effect against *C. albicans*, they were much less effective than the clinical drug Amphotericin B (MIC = 0.07 μM).

4.4: Conclusion

Although Schiff-base condensation products are normally unstable and readily hydrolyse back to the starting materials, the novel **phen**-**INH** hydrazone hybrid **4.1** was easily synthesised and it displayed excellent stability towards hydrolysis. The formation of the highly conjugated azo derivative **4.3a** and the isonictinic diamide **4.3b** from methanolic/ethanolic solution of **4.1** suggests that the hybrid can potentially produce radicals *in situ* which lead to the formation of **4.3a** and **4.3b**. In addition, this radical formation could offer **INH** a self-activating mechanism to produce radicals that can have anti-TB effects. The chemical structure of **4.1**, **4.3a**, and **4.3b** was characterised using HRMS, NMR and IR spectroscopy and **4.3a** was also characterised using X-ray crystallography.

In addition, 7 novel metal complexes of **4.1** were produced using Ag(I), Cu(II) and Mn(II) metal salts with ClO_4^-, NO_3^-, and BF_4^- counter ions. The compositions of these metal complexes was derived using elemental analysis and IR spectroscopy, and in the case of the Ag(I) complexes NMR and HRMS spectroscopy was also used. The stability of the Ag(I) complexes **4.2a-c** was also studied using ^{1}H NMR and it was determined that while **4.2a** and **4.2c** were stable in a DMSO solution over 72 hr, **4.2b** ([Ag(**4.1**)$_2$]NO_3) was unstable in a DMSO solution. This also confirmed through the X-ray crystallography analysis of the crystals formed from a DMSO solution of **4.2b** which possessed the chemical composition [Ag(**4.1**)(NO_3)].

Four of the metal complexes prepared as well as the ligand were screened against drug sensitive and resistant *M. tb* strains. The metal complexes tested (**4.2a2**, **4.2a3**, **4b2** and **4.2c2**) along with free ligand displayed excellent anti-tuberculosis activity regardless of the sensitivity of these strains towards clinically used drugs. The complexes possessed MIC values <10 µM, with the Ag(I) complexes possessing MIC values <4 µM. In addition, the free ligand itself also displayed MIC values at 15 µM concentration. All of the novel compounds tested displayed SI values >10. The Ag(I) complexes also displayed good broad-spectrum antimicrobial activity when tested against *S. aureus, P. aeruginosa* and *C. albicans.*

Future Work

As mentioned in the outline of the thesis, the research presented in this thesis can be divided into two parts. The first part of the work presented in this thesis focuses on the synthesis, characterisation and biological screening oxazine-based **phen** derivatives and their metal complexes. The least liphophilic derivative out of the ligands, **3.3a**, and its Ag(I), Mn(II) and Cu(II) complexes were screened against a Gram-positive, Gram-negative and a fungal strain. From these results it was observed that the Cu(II) complex was the most active against the Gram-positive and Gram-negative bacterial strains and the Ag(I) complex was the most active against the fungal strain. To enhance the activity of the Cu(II) complex against the Gram-positive bacterial strain, *S. aureus*, the lipophilicity of the ligand was increased which in turn increased the lipophilicity of the Cu(II) complex of these ligands. Unsurprisingly, the activity of the ligands as well as the Cu(II) complexs increase with an increase in liphophilicty. As shown in a recent study[263,264], specific increase in lipophilicity leads to an increase in inhibitory activity towards specific bacterial and fungal strains. Therefore, an interesting study which could be carried out is screening of these ligands, and their metal complexes (Cu(II), Mn(II) and Ag(I)) against various bacterial strains. As seen by the results from the biological screening of the Ag(I) complex, **3.5a1**, against *C. albicans*, it is a logical next step to screen the inhibitory effects of the more lipophilic derivatives and their Ag(I) complexes against *C. albicans*. In addition, a more threatening strain of *S. aureus* is the Methicillin Resistant *Staphylococcus aureus* (MRSA). As seen in a recent study, lipophilic derivatives of Ru(II) complexes of a 2-pyridyl-1,2,3-triazole based ligands were shown to possess excellent inhibitory effects towards MRSA[250]. Therefore, a further study could be to measure the inhibitory effects of the ligands and the Cu(II) complexes presented in this work towards MRSA.

The ligand **3.3a** was published by the McCann group and the work carried out by these researchers showed that the *bis*-Ag(I) and *bis*-Cu(II) complexes of this ligand possessed DNA binding capabilities stronger than those of the known groove-binding agents pentamidine and netropsin. Interestingly, these complexes did not display any DNA nuclease mimetic activity, even though the DNA nuclease activity of

(Cu(**phen**)$_2$)$^{2+}$ in the presence of an oxidant and/or reductant is well known. Although the complexes reported by the McCann group does not possess DNA nuclease activity, their DNA binding activity makes them potential therapeutics for anticancer studies. Therefore, the ligands and the Cu(II) complexes presented in this work could also be promising candidates for anti-cancer studies.

The formation of the co-products **3.4a-c** forms products with a scaffold of pyridoacridin. The derivatives of pyridoacridine are difficult to synthesize and often require multiple steps with expensive starting materials. Fortunately, the derivatives of this natural product possess anti-tumour activity at low µM ranges. The formation of the products **3.4a-c**, through the simple reaction of amino acid ester derivatives (**3.2f-h**) with **3.1**, offers a simple and desirable route to the synthesis of pyridoacridine derivatives. It is also suspected that metal complexation of these ligands could produce highly active therapeutics.

The second part of the work presented in this thesis focuses on the formation of a **phen**-**INH** hybrid and its metal complexes and studying the anti-mycobacterial activity of these compounds. As seen in **Chapter 4**, these compounds possessed excellent inhibitory effects towards *M. tB*. Additionally, their inhibitory effect did not decrease when tested against **INH** and rifampicin resistant strains of *M. tb*. Further biological studies can be carried out to examine the *in vivo* activity of these compounds towards *M. tb*. In addition, the mechanism of action of these compounds is clearly not reliant of the presence of KatG enzyme. Therefore, further studies on the mechanism of action of these compounds for causing anti-mycobacterial activity could offer beneficial insight into development of further therapeutic compounds. A problem displayed by using **INH** as treatment for TB is the hepacytoxicity, mutagenicity and carcinogenicity caused as a side-effect[205]. Therefore, the hepacytotoxic, mutagenic and carcinogenic nature of the ligand **4.1** and its complexes should be studied to determine the potential of developing these compounds further as anti-TB agents.

Bibliography

(1) WHO. No Title https://www.who.int/en/news-room/fact-sheets/detail/the-top-10-causes-of-death (accessed Jan 18, **2019**).

(2) Butler, H. M.; Hurse, A.; Thursky, E.; Shulman, A. Bactericidal Action of Selected Phenanthroline Chelates and Related Compounds. *Aust J Exp Biol Med* **1969**, *47* (5), 541–552. https://doi.org/10.1038/icb.1969.148.

(3) Urry, L. A.; Cain, M. L.; Wasserman, S. A.; Minorsky, P. V; Reece, J. B. *Campbell Biology, 11th Ed*; Biology for Student; Pearson, **2017**.

(4) Mader, S. *Essentials of Biology*; **2014**.

(5) Merroun, M. L.; Selenska-Pobell, S. Bacterial Interactions with Uranium: An Environmental Perspective. *J. Contam. Hydrol.* **2008**, *102* (3–4), 285–295. https://doi.org/10.1016/j.jconhyd.2008.09.019.

(6) Young, K. D. Bacterial Morphology: Why Have Different Shapes? *Curr. Opin. Microbiol.* **2007**, *10* (6), 596–600. https://doi.org/10.1016/j.mib.2007.09.009.

(7) Mader, S. *Mader, Biology {\copyright} 2010, 10e, Student Edition (Reinforced Binding)*; AP BIOLOGY MADER; McGraw-Hill Education, **2009**.

(8) Doyle, M. P.; Steenson, L. R.; Meng, J. Bacteria in Food and Beverage Production. In *The Prokaryotes: Applied Bacteriology and Biotechnology*; Rosenberg, E., DeLong, E. F., Lory, S., Stackebrandt, E., Thompson, F., Eds.; Springer Berlin Heidelberg: Berlin, Heidelberg, **2013**; pp 241–256. https://doi.org/10.1007/978-3-642-31331-8_27.

(9) Rogers, K.; Kadner, R. No Title www.britannica.com/science/bacteria (accessed May 18, **2018**).

(10) Wagner, M.; Loy, A. Bacterial Community Composition and Function in Sewage Treatment Systems. *Curr. Opin. Biotechnol.* **2002**, *13* (3), 218–227. https://doi.org/10.1016/S0958-1669(02)00315-4.

(11) Rossi, F.; Motta, O.; Matrella, S.; Proto, A.; Vigliotta, G. Nitrate Removal from Wastewater through Biological Denitrification with OGA 24 in a Batch Reactor. *Water (Switzerland)* **2015**, *7* (1), 51–62. https://doi.org/10.3390/w7010051.

(12) Dellagnezze, B. M.; de Sousa, G. V.; Martins, L. L.; Domingos, D. F.; Limache, E. E. G.; de Vasconcellos, S. P.; da Cruz, G. F.; de Oliveira, V. M. Bioremediation Potential of Microorganisms Derived from Petroleum Reservoirs. *Mar. Pollut. Bull.* **2014**, *89* (1–2), 191–200. https://doi.org/10.1016/j.marpolbul.2014.10.003.

(13) Pollmann, K.; Raff, J.; Merroun, M.; Fahmy, K.; Selenska-Pobell, S. Metal Binding by Bacteria from Uranium Mining Waste Piles and Its Technological Applications. *Biotechnol. Adv.* **2006**, *24* (1), 58–68. https://doi.org/10.1016/j.biotechadv.2005.06.002.

(14) Jain, A.; Bhatia, P.; Chugh, A. Microbial Synthetic Biology for Human Therapeutics. *Syst. Synth. Biol.* **2012**, *6* (1–2), 9–22. https://doi.org/10.1007/s11693-012-9092-0.

(15) Encyclopedia.com. Human Commensal and Mutual Organisms https://www.encyclopedia.com/science/news-wires-white-papers-and-books/human-commensal-and-mutual-organisms (accessed May 19, **2018**).

(16) Nikaido, H. Multidrug Resistance in Bacteria. *Annu. Rev. Biochem.* **2009**, *78*, 119–146. https://doi.org/10.1146/annurev.biochem.78.082907.145923.

(17) Cockayne, A. Bacterial Cell Walls. In *Encyclopedia of Immunology (Second Edition)*; Delves, P. J., Ed.; Elsevier: Oxford, **1998**; pp 320–323.

https://doi.org/https://doi.org/10.1006/rwei.1999.0082.
(18) Vollmer, W.; Blanot, D.; De Pedro, M. A. Peptidoglycan Structure and Architecture. *FEMS Microbiol. Rev.* **2008**, *32* (2), 149–167. https://doi.org/10.1111/j.1574-6976.2007.00094.x.
(19) Beveridge, T. J. Use of the Gram Stain in Microbiology. *Biotech. Histochem.* **2001**, *76* (3), 111–118. https://doi.org/10.1080/bih.76.3.111.118.
(20) Thomas, J. S.; Daniel, K.; Suzanne, W. The Bacterial Cell Envelope. *Cold Spring Harb. Perspect. Biol.* **2010**, *2* (5), 1–16. https://doi.org/10.1101/cshperspect.a000414.
(21) Wientjes, F. B.; Woldringh, C. L.; Nanninga, N. Amount of Peptidoglycan in Cell Walls of Gram-Negative Bacteria Sacculu . Frceichal Dtoerminoatio Do. **1991**, *173* (23), 7684–7691.
(22) Xia, G.; Kohler, T.; Peschel, A. The Wall Teichoic Acid and Lipoteichoic Acid Polymers of Staphylococcus Aureus. *Int. J. Med. Microbiol.* **2010**, *300* (2–3), 148–154. https://doi.org/10.1016/j.ijmm.2009.10.001.
(23) Marquis, R. E.; Mayzel, K.; Carstensen, E. L. Cation Exchange in Cell Walls of Gram-Positive Bacteria. *Can. J. Microbiol.* **1976**, *22* (7), 975–982. https://doi.org/10.1139/m76-142.
(24) Mason, A. J.; Marquette, A.; Bechinger, B. Zwitterionic Phospholipids and Sterols Modulate Antimicrobial Peptide-Induced Membrane Destabilization. *Biophys. J.* **2007**, *93* (12), 4289–4299. https://doi.org/10.1529/biophysj.107.116681.
(25) Li, F.; Collins, J. G.; Keene, F. R. Ruthenium Complexes as Antimicrobial Agents. *Chem. Soc. Rev.* **2015**, *44* (8), 2529–2542. https://doi.org/10.1039/c4cs00343h.
(26) Peschel, A.; Vuong, C.; Otto, M.; Gotz, F. The D-Alanine Residues of Staphylococcus Aureus Teichoic Acids Alter the Susceptibility to Vancomycin and the Activity of Autolytic Enzymes. *Antimicrob. Agents Chemother.* **2000**, *44* (10), 2845–2847. https://doi.org/10.1128/AAC.44.10.2845-2847.2000.
(27) Kohler, T.; Weidenmaier, C.; Peschel, A. Wall Teichoic Acid Protects Staphylococcus Aureus against Antimicrobial Fatty Acids from Human Skin. *J. Bacteriol.* **2009**, *191* (13), 4482–4484. https://doi.org/10.1128/JB.00221-09.
(28) Kluytmans J., van Belkum A et Verbrugh H. Nasal Carriage of Staphylococcus Aureus: Epidemiology, Underlying Mechanisms, and Associated Risks. Clinical Microbiology Reviews, 10 (3), 505-520. **1997**, *10* (3), 505–520.
(29) Tong, S. Y. C.; Davis, J. S.; Eichenberger, E.; Holland, T. L.; Fowler, V. G. Staphylococcus Aureus Infections: Epidemiology, Pathophysiology, Clinical Manifestations, and Management. *Clin. Microbiol. Rev.* **2015**, *28* (3), 603–661. https://doi.org/10.1128/CMR.00134-14.
(30) Harris, L. G.; Foster, S. J.; Richards, R. G.; Lambert, P.; Stickler, D.; Eley, A. An Introduction to Staphylococcus Aureus, and Techniques for Identifyingand Quantifying S. Aureus Adhesins in Relation to Adhesion to Biomaterials:Review. *Eur. Cells Mater.* **2002**, *4*, 39–60. https://doi.org/10.22203/eCM.v004a04.
(31) ELEK, S. D. Experimental Staphylococcal Infections in the Skin of Man. *Ann. N. Y. Acad. Sci.* **1956**, *65* (3), 85–90.
(32) A., B.; K., I.; E., R.; T., T. Strategies to Prevent the Occurrence of Resistance against Antibiotics by Using Advanced Materials. *Appl. Microbiol. Biotechnol.* **2018**, *102* (5), 2075–2089. https://doi.org/10.1007/s00253-018-8776-0.
(33) Bush, L. M.; C E, S. Staphylococcus aureus Infections

https://www.msdmanuals.com/home/infections/bacterial-infections-gram-positive-bacteria/staphylococcus-aureus-infections (accessed May 21, 2018).
(34) Mishra, A. K.; Yadav, P.; Mishra, A. A Systemic Review on Staphylococcal Scalded Skin Syndrome (SSSS): A Rare and Critical Disease of Neonates. *Open Microbiol. J.* **2016**, *10* (1), 150–159. https://doi.org/10.2174/1874285801610010150.
(35) Mandal, S.; Berendt, A. R.; Peacock, S. J. Staphylococcus Aureus Bone and Joint Infection. *J. Infect.* **2002**, *44* (3), 143–151. https://doi.org/10.1053/jinf.2001.0952.
(36) Wertheim, H. F. L.; Vos, M. C.; Ott, A.; Van Belkum, A.; Voss, A.; Kluytmans, J. A. J. W.; Van Keulen, P. H. J.; Vandenbroucke-Grauls, C. M. J. E.; Meester, M. H. M.; Verbrugh, H. A. Risk and Outcome of Nosocomial Staphylococcus Aureus Bacteraemia in Nasal Carriers versus Non-Carriers. *Lancet* **2004**, *364* (9435), 703–705. https://doi.org/10.1016/S0140-6736(04)16897-9.
(37) Chang, B.; Frendl, G. Nosocomial Infections. *Essent. Clin. Anesth. Rev. Keywords, Quest. Answers Boards* **2015**, *5* (1), 494–498. https://doi.org/10.1017/CBO9781139584005.161.
(38) Hiramatsu, K. Molecular Evolution of MRSA. *Microbiol. Immunol.* **1995**, *39* (8), 531–543. https://doi.org/10.1111/j.1348-0421.1995.tb02239.x.
(39) Loomba, P. S.; Taneja, J.; Mishra, B. Methicillin and Vancomycin Resistant S. Aureus in Hospitalized Patients. *J. Glob. Infect. Dis.* **2010**, *2* (3), 275–283. https://doi.org/10.4103/0974-777X.68535.
(40) Morris, A.; Kellner, J. D.; Low, D. E. The Superbugs: Evolution, Dissemination and Fitness. *Curr. Opin. Microbiol.* **1998**, *1* (5), 524–529. https://doi.org/10.1016/S1369-5274(98)80084-2.
(41) Nash, J. A.; Ballard, T. N. S.; Weaver, T. E.; Akinbi, H. T. The Peptidoglycan-Degrading Property of Lysozyme Is Not Required for Bactericidal Activity In Vivo. *J. Immunol.* **2006**, *177* (1), 519–526. https://doi.org/10.4049/jimmunol.177.1.519.
(42) Delcour, A. H. Outer Membrane Permeability and Antibiotic Resistance. *Biochim. Biophys. Acta* **2009**, *1794* (5), 808–816. https://doi.org/10.1016/j.bbapap.2008.11.005.
(43) Manuscript, A.; Endotoxins, L. NIH Public Access. *October* **2008**, *71*, 1–57. https://doi.org/10.1146/annurev.biochem.71.110601.135414.Lipopolysaccharide.
(44) Hancock, R. E. Alterations in Outer Membrane Permeability. *Annu. Rev. Microbiol.* **1984**, *38*, 237–264. https://doi.org/10.1146/annurev.mi.38.100184.001321.
(45) LEIVE, L. ACTINOMYCIN SENSITIVITY IN ESCHERICHIA COLI PRODUCED BY EDTA. *Biochem. Biophys. Res. Commun.* **1965**, *18*, 13–17.
(46) Nikaido, H. Molecular Basis of Bacterial Outer Membrane Permeability Revisited. *Microbiol. Mol. Biol. Rev.* **2003**, *67* (4), 593–656.
(47) Fernández, L.; Hancock, R. E. W. Adaptive and Mutational Resistance: Role of Porins and Efflux Pumps in Drug Resistance. *Clin. Microbiol. Rev.* **2012**, *25* (4), 661–681. https://doi.org/10.1128/CMR.00043-12.
(48) Cascales, E.; Bernadac, A.; Gavioli, M.; Lazzaroni, J.; Lloubes, R. Pal Lipoprotein Of. *Society* **2002**, *184* (3), 754–759. https://doi.org/10.1128/JB.184.3.754.
(49) Miller, S. I.; Salama, N. R. The Gram-Negative Bacterial Periplasm: Size Matters. *PLoS Biol.* **2018**, *16* (1), 1–7.

https://doi.org/10.1371/journal.pbio.2004935.
(50) Nikaido, H. Outer Membrane Barrier as a Mechanism of Antimicrobial Resistance. *Antimicrob. Agents Chemother.* **1989**, *33* (11), 1831–1836.
(51) H, N. Multidrug Efflux Pumps of Gram-Negative Bacteria. *J. Bacteriol.* **1996**, *178* (20), 5853–5859.
(52) Levy, S. B. Active Efflux Mechanisms for Antimicrobial Resistance. *Antimicrob. Agents Chemother.* **1992**, *36* (4), 695–703.
(53) Sun, J.; Deng, Z.; Yan, A. Bacterial Multidrug Efflux Pumps: Mechanisms, Physiology and Pharmacological Exploitations. *Biochem. Biophys. Res. Commun.* **2014**, *453* (2), 254–267. https://doi.org/10.1016/j.bbrc.2014.05.090.
(54) NIKAIDO, H. Structure and Mechanism of Rnd-Type Multidrug Efflux Pumps. *Adv. Enzymol. Relat. Areas Mol. Biol.* **2011**, *77* (3), 1–60. https://doi.org/10.1111/j.1365-2958.2011.07544.x.Chlorinated.
(55) Blanco, P.; Hernando-Amado, S.; Reales-Calderon, J.; Corona, F.; Lira, F.; Alcalde-Rico, M.; Bernardini, A.; Sanchez, M.; Martinez, J. Bacterial Multidrug Efflux Pumps: Much More Than Antibiotic Resistance Determinants. *Microorganisms* **2016**, *4* (1), 14. https://doi.org/10.3390/microorganisms4010014.
(56) Vila, J.; Sáez-López, E.; Johnson, J. R.; Römling, U.; Dobrindt, U.; Cantón, R.; Giske, C. G.; Naas, T.; Carattoli, A.; Martínez-Medina, M.; et al. Escherichia Coli: An Old Friend with New Tidings. *FEMS Microbiol. Rev.* **2016**, *40* (4), 437–463. https://doi.org/10.1093/femsre/fuw005.
(57) Kaper, J. B.; Nataro, J. P.; Mobley, H. L. Pathogenic Escherichia Coli. *Nat. Rev. Microbiol.* **2004**, *2* (2), 123–140. https://doi.org/10.1038/nrmicro818.
(58) Melton-Celsa, A. R. Shiga Toxin (Stx) Classification, Structure, and Function. *Microbiol. Spectr.* **2014**, *2* (4), 1–21. https://doi.org/10.1128/microbiolspec.EHEC-0024-2013.
(59) Coleman, J. P.; Smith, C. J. Structure and Composition of Microbes. *xPharm Compr. Pharmacol. Ref.* **2011**, 1–7. https://doi.org/10.1016/B978-008055232-3.60224-7.
(60) Hoffmann, C.; Leis, A.; Niederweis, M.; Plitzko, J. M.; Engelhardt, H. Disclosure of the Mycobacterial Outer Membrane: Cryo-Electron Tomography and Vitreous Sections Reveal the Lipid Bilayer Structure. *Proc. Natl. Acad. Sci.* **2008**, *105* (10), 3963–3967. https://doi.org/10.1073/pnas.0709530105.
(61) Hooper, D. C. Mechanisms of Action of Antimicrobials: Focus on Fluoroquinolones. *Clin. Infect. Dis.* **2001**, *32* (Supplement 1), S9–S15. https://doi.org/10.1086/319370.
(62) Schlecht, B. H. P.; Medicine, A. Overview of Antibiotics. **2018**, 1–6.
(63) Mingeot-Leclercq, M.-P.; Glupczynski, Y.; Tulkens, P. M. Aminoglycosides: Activity and Resistance. *Antimicrob. Agents Chemother.* **1999**, *43* (4), 727–737. https://doi.org/10.1128/AAC.43.4.727.
(64) Papp-Wallace, K. M.; Endimiani, A.; Taracila, M. A.; Bonomo, R. A. Carbapenems: Past, Present, and Future. *Antimicrob. Agents Chemother.* **2011**, *55* (11), 4943–4960. https://doi.org/10.1128/AAC.00296-11.
(65) Allen, N. E.; Nicas, T. I. Mechanism of Action of Oritavancin and Related Glycopeptide Antibiotics. *FEMS Microbiol. Rev.* **2003**, *26* (5), 511–532. https://doi.org/10.1016/S0168-6445(02)00144-4.
(66) Gaynor, M.; Mankin, A. Macrolide Antibiotics: Binding Site, Mechanism of Action, Resistance. *Curr. Top. Med. Chem.* **2003**, *3* (9), 949–960. https://doi.org/10.2174/1568026033452159.

(67) Zhanel, G. G.; Shroeder, C.; Vercaigne, L.; Gin, A. S.; Embil, J.; Hoban, D. J. A Critical Review of Oxazolidinones: An Alternative or Replacement for Glycopeptides and Streptogramins? *Can. J. Infect. Dis.* **2001**, *12* (6), 379–390.
(68) Hancock, R. E. W.; Chapple, D. S. MINIREVIEW Peptide Antibiotics. *Antimicrob. Agents Chemother.* **1999**, *43* (6), 1317–1323. https://doi.org/10.1016/S0140-6736(97)80051-7.
(69) Floss, H. G.; Yu, T.-W. Rifamycin-Mode of Action, Resistance, and Biosynthesis. *Chem. Rev.* **2005**, *105* (2), 621–632. https://doi.org/10.1021/cr030112j.
(70) Connor, E. E. Sulfonamide Antibiotics. *Prim. Care Update Ob. Gyns.* **1998**, *5* (1), 32–35. https://doi.org/https://doi.org/10.1016/S1068-607X(97)00121-2.
(71) Chopra, I.; Roberts, M. Tetracycline Antibiotics: Mode of Action, Applications, Molecular Biology, and Epidemiology of Bacterial Resistance. *Microbiol. Mol. Biol. Rev.* **2001**, *65* (2), 232–60 ; second page, table of contents. https://doi.org/10.1128/MMBR.65.2.232-260.2001.
(72) Rammelkamp, C. H.; Maxon, T. Resistance of Staphylococcus Aureus to the Action of Penicillin. *Proc. Soc. Exp. Biol. Med.* **1942**, *51* (3), 386–389. https://doi.org/10.3181/00379727-51-13986.
(73) Ventola, C. L. The Antibiotic Resistance Crisis: Part 1: Causes and Threats. *Pharmacy and Therapeutics Journal*. **2015**, pp 277–283. https://doi.org/Article.
(74) Alanis, A. J. Resistance to Antibiotics: Are We in the Post-Antibiotic Era? *Arch. Med. Res.* **2005**, *36* (6), 697–705. https://doi.org/10.1016/j.arcmed.2005.06.009.
(75) Levy, S. B.; Bonnie, M. Antibacterial Resistance Worldwide: Causes, Challenges and Responses. *Nat. Med.* **2004**, *10* (12S), S122–S129. https://doi.org/10.1038/nm1145.
(76) Blair, J. M. A.; Webber, M. A.; Baylay, A. J.; Ogbolu, D. O.; Piddock, L. J. V. Molecular Mechanisms of Antibiotic Resistance. *Nat. Rev. Microbiol.* **2015**, *13* (1), 42–51. https://doi.org/10.1038/nrmicro3380.
(77) Miller, S. I. Antibiotic Resistance and Regulation of the Gram-Negative Bacterial Outer Membrane Barrier by Host Innate Immune Molecules. *MBio* **2016**, *7* (5), 5–7. https://doi.org/10.1128/mBio.01541-16.
(78) Munita, J. M.; Arias, C. A. Mechanisms of Antibiotic Resistance. *Microbiol. Spectr.* **2016**, *4* (2), 10.1128/microbiolspec.VMBF-0016-2015. https://doi.org/10.1128/microbiolspec.VMBF-0016-2015.
(79) Tomlinson, J. H.; Thompson, G. S.; Kalverda, A. P.; Zhuravleva, A.; O'Neill, A. J. A Target-Protection Mechanism of Antibiotic Resistance at Atomic Resolution: Insights into FusB-Type Fusidic Acid Resistance. *Sci. Rep.* **2016**, *6* (October 2015), 1–12. https://doi.org/10.1038/srep19524.
(80) Lambert, P. A. Bacterial Resistance to Antibiotics: Modified Target Sites. *Adv. Drug Deliv. Rev.* **2005**, *57* (10), 1471–1485. https://doi.org/10.1016/j.addr.2005.04.003.
(81) Satpathy, S.; Sen, S. K.; Pattanaik, S.; Raut, S. Review on Bacterial Biofilm: An Universal Cause of Contamination. *Biocatal. Agric. Biotechnol.* **2016**, *7*, 56–66. https://doi.org/10.1016/j.bcab.2016.05.002.
(82) Jamal, M.; Ahmad, W.; Andleeb, S.; Jalil, F.; Imran, M.; Nawaz, M. A.; Hussain, T.; Ali, M.; Rafiq, M.; Kamil, M. A. Bacterial Biofilm and Associated Infections. *J. Chinese Med. Assoc.* **2018**, *81* (1), 7–11. https://doi.org/10.1016/j.jcma.2017.07.012.
(83) Kumar, A.; Alam, A.; Rani, M.; Ehtesham, N. Z.; Hasnain, S. E. Biofilms:

Survival and Defense Strategy for Pathogens. *Int. J. Med. Microbiol.* **2017**, *307* (8), 481–489. https://doi.org/10.1016/j.ijmm.2017.09.016.

(84) Vasudevan, R. Biofilms: Microbial Cities of Scientific Significance. *J. Microbiol. Exp.* **2014**, *1* (3), 1–16. https://doi.org/10.15406/jmen.2014.01.00014.

(85) Høiby, N.; Bjarnsholt, T.; Givskov, M.; Molin, S.; Ciofu, O. Antibiotic Resistance of Bacterial Biofilms. *Int. J. Antimicrob. Agents* **2010**, *35* (4), 322–332. https://doi.org/10.1016/j.ijantimicag.2009.12.011.

(86) Orvig, C.; Abrams, M. J. Medicinal Inorganic Chemistry: Introduction. *Chem. Rev.* **1999**, *99* (9), 2201–2204. https://doi.org/10.1021/cr980419w.

(87) Mjos, K. D.; Orvig, C. Metallodrugs in Medicinal Inorganic Chemistry. *Chem. Rev.* **2014**, *114* (8), 4540–4563. https://doi.org/10.1021/cr400460s.

(88) Guo, Z.; Sadler, P. J. Metals in Medicine. *Angew. Chemie Int. Ed.* **1999**, *38* (11), 1512–1531. https://doi.org/10.1002/(SICI)1521-3773(19990601)38:11<1512::AID-ANIE1512>3.0.CO;2-Y.

(89) Zhang, C. X.; Lippard, S. J. New Metal Complexes as Potential Therapeutics. *Curr. Opin. Chem. Biol.* **2003**, *7* (4), 481–489. https://doi.org/10.1016/S1367-5931(03)00081-4.

(90) Rizzotto, M. Metal Complexes as Antimicrobial Agents. In *A Search for Antibacterial Agents*; Bobbarala, V., Ed.; IntechOpen: Rijeka, **2012**. https://doi.org/10.5772/45651.

(91) Infect, J.; Epidemiol, D.; Borthagaray, G.; Mondelli, M.; Torre, M. H. Review Article : Open Access Essential Transition Metal Ion Complexation as a Strategy to Improve the Antimicrobial Activity of Organic Drugs ClinMed. **2016**, *2* (2).

(92) Szymański, P.; Fraczek, T.; Markowicz, M.; Mikiciuk-Olasik, E. Development of Copper Based Drugs, Radiopharmaceuticals and Medical Materials. *BioMetals* **2012**, *25* (6), 1089–1112. https://doi.org/10.1007/s10534-012-9578-y.

(93) Jopp, M.; Becker, J.; Becker, S.; Miska, A.; Gandin, V.; Marzano, C.; Schindler, S. Anticancer Activity of a Series of Copper(II) Complexes with Tripodal Ligands. *Eur. J. Med. Chem.* **2017**, *132*, 274–281. https://doi.org/https://doi.org/10.1016/j.ejmech.2017.03.019.

(94) Arnaud, C.; Beseme, F.; Sabbagh, I.; Gallet, J. P. [Anti-inflammatory activity of 5 copper complexes]. *C. R. Acad. Sci. III.* **1986**, *302* (7), 239–242.

(95) Liu, H.; Yang, W.; Zhou, W.; Xu, Y.; Xie, J.; Li, M. Crystal Structures and Antimicrobial Activities of Copper(II) Complexes of Fluorine-Containing Thioureido Ligands. *Inorganica Chim. Acta* **2013**, *405*, 387–394. https://doi.org/https://doi.org/10.1016/j.ica.2013.06.029.

(96) Annaraj, J.; Srinivasan, S.; Ponvel, K. M.; Athappan, P. R. Mixed Ligand Copper(II) Complexes of Phenanthroline/Bipyridyl and Curcumin Diketimines as DNA Intercalators and Their Electrochemical Behavior under Nafion® and Clay Modified Electrodes. *J. Inorg. Biochem.* **2005**, *99* (3), 669–676. https://doi.org/https://doi.org/10.1016/j.jinorgbio.2004.11.018.

(97) Sigman, D. S. Nuclease Activity of 1,10-Phenanthroline-Copper Ion. *Acc. Chem. Res.* **1986**, *19* (6), 180–186. https://doi.org/10.1021/ar00126a004.

(98) O'Connor, M.; Kellett, A.; McCann, M.; Rosair, G.; McNamara, M.; Howe, O.; Creaven, B. S.; McClean, S.; Foltyn-Arfa Kia, A.; O'Shea, D.; et al. Copper(II) Complexes of Salicylic Acid Combining Superoxide Dismutase Mimetic Properties with DNA Binding and Cleaving Capabilities Display Promising

Chemotherapeutic Potential with Fast Acting in Vitro Cytotoxicity against Cisplatin Sensitive and Resista. *J. Med. Chem.* **2012**, *55* (5), 1957–1968. https://doi.org/10.1021/jm201041d.

(99) Joseph, J.; Nagashri, K.; Rani, G. A. B. Synthesis, Characterization and Antimicrobial Activities of Copper Complexes Derived from 4-Aminoantipyrine Derivatives. *J. Saudi Chem. Soc.* **2013**, *17* (3), 285–294. https://doi.org/10.1016/j.jscs.2011.04.007.

(100) Iakovidis, I.; Delimaris, I.; Piperakis, S. M. Copper and Its Complexes in Medicine: A Biochemical Approach. *Mol. Biol. Int.* **2011**, *2011*, 1–13. https://doi.org/10.4061/2011/594529.

(101) Haeili, M.; Moore, C.; Davis, C. J. C.; Cochran, J. B.; Shah, S.; Shrestha, T. B.; Zhang, Y.; Bossmann, S. H.; Benjamin, W. H.; Kutsch, O.; et al. Copper Complexation Screen Reveals Compounds with Potent Antibiotic Properties against Methicillin-Resistant Staphylococcus Aureus. *Antimicrob. Agents Chemother.* **2014**, *58* (7), 3727–3736. https://doi.org/10.1128/AAC.02316-13.

(102) Bencini, A.; Lippolis, V. 1,10-Phenanthroline: A Versatile Building Block for the Construction of Ligands for Various Purposes. *Coord. Chem. Rev.* **2010**, *254* (17), 2096–2180. https://doi.org/https://doi.org/10.1016/j.ccr.2010.04.008.

(103) Tsuneo ISHIDA, S. Bacteriolyses of Bacterial Cell Walls by Cu(II) and Zn(II) Ions Based on Antibacterial Results of Dilution Medium Method and Halo Antibacterial Test. **2017**, No. Ii.

(104) Karlsson, H. L.; Cronholm, P.; Hedberg, Y.; Tornberg, M.; De Battice, L.; Svedhem, S.; Wallinder, I. O. Cell Membrane Damage and Protein Interaction Induced by Copper Containing Nanoparticles-Importance of the Metal Release Process. *Toxicology* **2013**, *313* (1), 59–69. https://doi.org/10.1016/j.tox.2013.07.012.

(105) Manning, T.; Mikula, R.; Lee, H.; Calvin, A.; Darrah, J.; Wylie, G.; Phillips, D.; Bythell, B. J. The Copper (II) Ion as a Carrier for the Antibiotic Capreomycin against Mycobacterium Tuberculosis. *Bioorganic Med. Chem. Lett.* **2014**, *24* (3), 976–982. https://doi.org/10.1016/j.bmcl.2013.12.053.

(106) German, N.; Doyscher, D.; Rensing, C. Bacterial Killing in Macrophages and Amoeba: Do They All Use a Brass Dagger? *Future Microbiol.* **2013**, *8* (10), 1257–1264. https://doi.org/10.2217/fmb.13.100.

(107) Baker, J.; Sitthisak, S.; Sengupta, M.; Johnson, M.; Jayaswal, R. K.; Morrissey, J. A. Copper Stress Induces a Global Stress Response in Staphylococcus Aureus and Represses Sae and Agr Expression and Biofilm Formations. *Appl. Environ. Microbiol.* **2010**, *76* (1), 150–160. https://doi.org/10.1128/AEM.02268-09.

(108) Bondarczuk, K.; Piotrowska-Seget, Z. Molecular Basis of Active Copper Resistance Mechanisms in Gram-Negative Bacteria. *Cell Biol. Toxicol.* **2013**, *29* (6), 397–405. https://doi.org/10.1007/s10565-013-9262-1.

(109) Hindo, S. S.; Frezza, M.; Tomco, D.; Heeg, M. J.; Hryhorczuk, L.; McGarvey, B. R.; Dou, Q. P.; Verani, C. N. Metals in Anticancer Therapy: Copper(II) Complexes as Inhibitors of the 20S Proteasome. *Eur. J. Med. Chem.* **2009**, *44* (11), 4353–4361. https://doi.org/10.1016/j.ejmech.2009.05.019.

(110) Kremer, E.; Facchin, G.; Estévez, E.; Alborés, P.; Baran, E. J.; Ellena, J.; Torre, M. H. Copper Complexes with Heterocyclic Sulfonamides: Synthesis, Spectroscopic Characterization, Microbiological and SOD-like Activities: Crystal Structure of [Cu(Sulfisoxazole)2(H2O)4] · 2H2O. *J. Inorg. Biochem.* **2006**, *100* (7), 1167–1175. https://doi.org/10.1016/j.jinorgbio.2006.01.042.

(111) Viganor, L.; Howe, O.; McCarron, P.; McCann, M.; Devereux, M. The

Antibacterial Activity of Metal Complexes Containing 1,10- Phenanthroline: Potential as Alternative Therapeutics in the Era of Antibiotic Resistance. *Curr. Top. Med. Chem.* **2017**, *17* (11), 1280–1302. https://doi.org/10.2174/1568026616666161003143333.

(112) Al-Awqati, Q. One Hundred Years of Membrane Permeability: Does Overton Still Rule? *Nat. Cell Biol.* **1999**, *1* (8), E201–E202. https://doi.org/10.1038/70230.

(113) Clement, J. L.; Jarrett, P. S. Antibacterial Silver. *Met. Based. Drugs* **1994**, *1* (5–6), 467–482. https://doi.org/10.1155/MBD.1994.467.

(114) Lansdown, A. B. G. Silver in Health Care: Antimicrobial Effects and Safety in Use. *Curr. Probl. Dermatol.* **2006**, *33*, 17–34. https://doi.org/10.1159/000093928.

(115) Gupta, A.; Maynes, M.; Silver, S. Effects of Halides on Plasmid-Mediated Silver Resistance in Escherichia Coli. *Appl. Environ. Microbiol.* **1998**, *64* (12), 5042–5045.

(116) Chernousova, S.; Epple, M. Silver as Antibacterial Agent: Ion, Nanoparticle, and Metal. *Angew. Chemie Int. Ed.* **2013**, *52* (6), 1636–1653. https://doi.org/10.1002/anie.201205923.

(117) Lansdown, A. B. G. Silver I: Its Antibacterial Properties and Mechanism of Action. *J. Wound Care* **2002**, *11* (4), 125–130. https://doi.org/10.12968/jowc.2002.11.4.26389.

(118) Chopra, I. The Increasing Use of Silver-Based Products as Antimicrobial Agents: A Useful Development or a Cause for Concern? *J. Antimicrob. Chemother.* **2007**, *59* (4), 587–590. https://doi.org/10.1093/jac/dkm006.

(119) Melaiye, A.; Youngs, W. J. Silver and Its Application as an Antimicrobial Agent. *Expert Opin. Ther. Pat.* **2005**, *15* (2), 125–130. https://doi.org/10.1517/13543776.15.2.125.

(120) Smith, A.; McCann, M.; Kavanagh, K. Proteomic Analysis of the Proteins Released from Staphylococcus Aureus Following Exposure to Ag(I). *Toxicol. Vitr.* **2013**, *27* (6), 1644–1648. https://doi.org/10.1016/j.tiv.2013.04.007.

(121) Lansdown, A. B. A Review of the Use of Silver in Wound Care: Facts and Fallacies. *Br. J. Nurs.* **2004**, *13* (Sup1), S6–S19. https://doi.org/10.12968/bjon.2004.13.Sup1.12535.

(122) Nomiya, K.; Yokoyama, H. Syntheses, Crystal Structures and Antimicrobial Activities of Polymeric Silver(i) Complexes with Three Amino-Acids [Aspartic Acid (H2asp), Glycine (Hgly) and Asparagine (Hasn)]Note: For Ease of Reference during Discussion of Their Anions, H2asp, Hgly And . *J. Chem. Soc. Dalt. Trans.* **2002**, No. 12, 2483–2490. https://doi.org/10.1039/b200684g.

(123) Nomiya, K.; Takahashi, S.; Noguchi, R.; Nemoto, S.; Takayama, T.; Oda, M. Synthesis and Characterization of Water-Soluble Silver(I) Complexes with L-Histidine (H2his) and (S)-(-)-2-Pyrrolidone-5-Carboxylic Acid (H2pyrrld) Showing a Wide Spectrum of Effective Antibacterial and Antifungal Activities. Crystal Structures of Chiral . *Inorg. Chem.* **2000**, *39* (15), 3301–3311. https://doi.org/10.1021/ic990526o.

(124) Salomon, E.; Keren, N.; Kanteev, M.; Adir, N. Manganese in Biological Systems: Transport and Function. *PATAI'S Chem. Funct. Groups* **2011**, 1–16. https://doi.org/10.1002/9780470682531.pat0540.

(125) Kaim, W.; Schwederski, B. *BIOINORGANIC CHEMISTRY : INORGANIC ELEMENTS*.

(126) Gupta, K. C.; Sutar, A. K. Catalytic Activities of Schiff Base Transition Metal

Complexes. *Coord. Chem. Rev.* **2008**, *252* (12–14), 1420–1450. https://doi.org/10.1016/j.ccr.2007.09.005.
(127) Feng, C.; Zhang, Y.; Liang, D.; Liu, S.; Chi, Z.; Xu, J. Flame Retardancy and Thermal Degradation Behaviors of Polypropylene Composites with Novel Intumescent Flame Retardant and Manganese Dioxide. *J. Anal. Appl. Pyrolysis* **2013**, *104*, 59–67. https://doi.org/10.1016/j.jaap.2013.09.009.
(128) Ali, B.; Iqbal, M. A. Coordination Complexes of Manganese and Their Biomedical Applications. *ChemistrySelect* **2017**, *2* (4), 1586–1604. https://doi.org/10.1002/slct.201601909.
(129) Pan, D.; Schmieder, A. H.; Wickline, S. A.; Lanza, G. M. Manganese-Based MRI Contrast Agents: Past, Present and Future. *Tetrahedron* **2011**, *67* (44), 8431–8444. https://doi.org/10.1016/j.tet.2011.07.076.
(130) Coassin, M.; Ursini, F.; Bindoli, A. Antioxidant Effect of Manganese. *Arch. Biochem. Biophys.* **1992**, *299* (2), 330–333. https://doi.org/10.1016/0003-9861(92)90282-2.
(131) Rosu, T.; Pahontu, E.; Maxim, C.; Georgescu, R.; Stanica, N.; Almajan, G. L.; Gulea, A. Synthesis, Characterization and Antibacterial Activity of Some New Complexes of Cu(II), Ni(II), VO(II), Mn(II) with Schiff Base Derived from 4-Amino-2,3-Dimethyl-1-Phenyl-3-Pyrazolin-5-One. *Polyhedron* **2010**, *29* (2), 757–766. https://doi.org/10.1016/j.poly.2009.10.017.
(132) Nithya, P.; Simpson, J.; Govindarajan, S. Template Synthesis, Structural Variation, Thermal Behavior and Antimicrobial Screening of Mn(II), Co(II) and Ni(II) Complexes of Schiff Base Ligands Derived from Benzyl Carbazate and Three Isomers of Acetylpyridine. *Inorganica Chim. Acta* **2017**, *467*, 180–193. https://doi.org/10.1016/j.ica.2017.07.059.
(133) Patel, N. H.; Parekh, H. M.; Patel, M. N. Synthesis, Characterization and Biological Evaluation of Manganese(II), Cobalt(II), Nickel(II), Copper(II), and Cadmium(II) Complexes with Monobasic (NO) and Neutral (NN) Schiff Bases. *Transit. Met. Chem.* **2005**, *30* (1), 13–17. https://doi.org/10.1007/s11243-004-3226-5.
(134) Sharma, S.; Meena, R.; Satyawana, Y.; Fahmi, N. Manganese(II) Complexes of Biological Relevance: Synthesis and Spectroscopic Characterization of Novel Manganese(II) Complexes with Monobasic Bidentate Ligands Derived from Halo-Substituted 1H-Indole-2,3-Diones. *Russ. J. Gen. Chem.* **2016**, *86* (12), 2807–2816. https://doi.org/10.1134/S1070363216120446.
(135) Singh, R. K.; Rai, D.; Yadav, D.; Bhargava, A.; Balzarini, J.; De Clercq, E. Synthesis, Antibacterial and Antiviral Properties of Curcumin Bioconjugates Bearing Dipeptide, Fatty Acids and Folic Acid. *Eur. J. Med. Chem.* **2010**, *45* (3), 1078–1086. https://doi.org/10.1016/j.ejmech.2009.12.002.
(136) Barrett, S.; Delaney, S.; Kavanagh, K.; Montagner, D. Evaluation of in Vitro and in Vivo Antibacterial Activity of Novel Cu(II)-Steroid Complexes. *Inorganica Chim. Acta* **2018**, *479*, 261–265. https://doi.org/10.1016/j.ica.2018.04.054.
(137) Ren, R.; Yang, P.; Zheng, W.; Hua, Z. A Simple Copper(II)-L-Histidine System for Efficient Hydrolytic Cleavage of DNA. *Inorg. Chem.* **2000**, *39* (24), 5454–5463. https://doi.org/10.1021/ic0000146.
(138) Stănilă, A.; Braicu, C.; Stănilă, S.; Pop, R. M. Antibacterial Activity of Copper and Cobalt Amino Acids Complexes. **2011**, *39* (2), 124–129.
(139) Patra, A. K.; Roy, S.; Chakravarty, A. R. Synthesis, Crystal Structures, DNA Binding and Cleavage Activity of l-Glutamine Copper(II) Complexes of

Heterocyclic Bases. *Inorganica Chim. Acta* **2009**, *362* (5), 1591–1599. https://doi.org/10.1016/j.ica.2008.08.003.

(140) Zhang, S.; Zhu, Y.; Tu, C.; Wei, H.; Yang, Z.; Lin, L.; Ding, J.; Zhang, J.; Guo, Z. A Novel Cytotoxic Ternary Copper(II) Complex of 1,10-Phenanthroline and l-Threonine with DNA Nuclease Activity. *J. Inorg. Biochem.* **2004**, *98* (12), 2099–2106. https://doi.org/10.1016/j.jinorgbio.2004.09.014.

(141) Kumar, R. S.; Arunachalam, S. DNA Binding and Antimicrobial Studies of Polymer-Copper(II) Complexes Containing 1,10-Phenanthroline and l-Phenylalanine Ligands. *Eur. J. Med. Chem.* **2009**, *44* (5), 1878–1883. https://doi.org/10.1016/j.ejmech.2008.11.001.

(142) Mahon, K. P.; Ortiz-Meoz, R. F.; Prestwich, E. G.; Kelley, S. O. Photosensitized DNA Cleavage Promoted by Amino Acids. *Chem. Commun. (Camb).* **2003**, *18* (15), 1956–1957.

(143) Goswami, T. K.; Gadadhar, S.; Karande, A. A.; Chakravarty, A. R. Photocytotoxic Ferrocene-Appended (l-Tyrosine)Copper(II) Complexes of Phenanthroline Bases. *Polyhedron* **2013**, *52*, 1287–1298. https://doi.org/https://doi.org/10.1016/j.poly.2012.06.018.

(144) Wang, H.; Yuan, H.; Li, S.; Li, Z.; Jiang, M. Synthesis, Antimicrobial Activity of Schiff Base Compounds of Cinnamaldehyde and Amino Acids. *Bioorganic Med. Chem. Lett.* **2016**, *26* (3), 809–813. https://doi.org/10.1016/j.bmcl.2015.12.089.

(145) Chohan, Z. H.; Arif, M.; Sarfraz, M. Metal-Based Antibacterial and Antifungal Amino Acid Derived Schiff Bases: Their Synthesis, Characterization and in Vitro Biological Activity. *Appl. Organomet. Chem.* **2007**, *21* (4), 294–302. https://doi.org/10.1002/aoc.1200.

(146) Chohan, Z. H.; Praveen, M.; Ghaffar, A. Structural and Biological Behaviour of Co(II), Cu(II) and Ni(II) Metal Complexes of Some Amino Acid Derived Schiff-Bases. *Met. Based. Drugs* **1997**, *4* (5), 267–272. https://doi.org/10.1155/MBD.1997.267.

(147) Sakiyan, I.; Loğoğlu, E.; Arslan, S.; Sari, N.; Şakiyan, N. Antimicrobial Activities of N-(2-Hydroxy-1-Naphthalidene)-Amino Acid(Glycine, Alanine, Phenylalanine, Histidine, Tryptophane) Schiff Bases and Their Manganese(III) Complexes. *BioMetals* **2004**, *17* (2), 115–120. https://doi.org/10.1023/B:BIOM.0000018380.34793.df.

(148) Roy, S.; Hagen, K. D.; Maheswari, P. U.; Lutz, M.; Spek, A. L.; Reedijk, J.; Van Wezel, G. P. Phenanthroline Derivatives with Improved Selectivity as DNA-Targeting Anticancer or Antimicrobial Drugs. *ChemMedChem* **2008**, *3* (9), 1427–1434. https://doi.org/10.1002/cmdc.200800097.

(149) Shulman, A.; White, D. O. Virostatic Activity of 1,10-Phenanthroline Transition Metal Chelates: A Structure-Activity Analysis. *Chem. Biol. Interact.* **1973**, *6* (6), 407–413. https://doi.org/https://doi.org/10.1016/0009-2797(73)90060-4.

(150) Coyle, B.; McCann, M.; Kavanagh, K.; Devereux, M.; McKee, V.; Kayal, N.; Egan, D.; Deegan, C.; Finn, G. J. Synthesis, X-Ray Crystal Structure, Anti-Fungal and Anti-Cancer Activity of [Ag2(NH3)2(SalH)2] (SalH2=salicylic Acid). *J. Inorg. Biochem.* **2004**, *98* (8), 1361–1366. https://doi.org/10.1016/j.jinorgbio.2004.04.016.

(151) McCann, M.; Kellett, A.; Kavanagh, K.; Devereux, M.; L.S. Santos, A. Deciphering the Antimicrobial Activity of Phenanthroline Chelators. *Curr. Med. Chem.* **2012**, *19* (17), 2703–2714.

https://doi.org/10.2174/092986712800609733.
(152) Wendlandt, A. E.; Stahl, S. S. Bioinspired Aerobic Oxidation of Secondary Amines and Nitrogen Heterocycles with a Bifunctional Quinone Catalyst. *J. Am. Chem. Soc.* **2014**, *136* (1), 506–512. https://doi.org/10.1021/ja411692v.
(153) Dolan, N.; McGinley, J.; Stephens, J. C.; Kavanagh, K.; Hurley, D.; Maher, N. J. Synthesis, Characterisation and Antimicrobial Studies of Organotin(IV) Complexes with 1,10-Phenanthroline Derivatives. *Inorganica Chim. Acta* **2014**, *409* (PART B), 276–284. https://doi.org/10.1016/j.ica.2013.09.038.
(154) Liu, X.; Sun, B.; Kell, R. E. M.; Southam, H. M.; Butler, J. A.; Li, X.; Poole, R. K.; Keene, F. R.; Collins, J. G. The Antimicrobial Activity of Mononuclear Ruthenium(II) Complexes Containing the Dppz Ligand. *Chempluschem* **2018**, *83* (7), 643–650. https://doi.org/10.1002/cplu.201800042.
(155) Sun, B.; Southam, H. M.; Butler, J. A.; Poole, R. K.; Burgun, A.; Tarzia, A.; Keene, F. R.; Collins, J. G. Synthesis, Isomerisation and Biological Properties of Mononuclear Ruthenium Complexes Containing the Bis[4(4′-Methyl-2,2′-Bipyridyl)]-1,7-Heptane Ligand. *Dalt. Trans.* **2018**, *47* (7), 2422–2434. https://doi.org/10.1039/c7dt04595f.
(156) GARATTINI, S.; LEONARDI, A. [Tuberculostatic action of chelating substances; preliminary note]. *G. Ital. Chemioter.* **1955**, *2* (1–2), 18–22.
(157) Dwyer, F. P.; Reid, I. K.; Shulman, A.; Laycock, G. M.; Dixson, S. The Biological Actions of 1,10-Phenanthroline and 2,2'-Bipyridine Hydrochlorides, Quaternary Salts and Metal Chelates and Related Compounds. 1. Bacteriostatic Action on Selected Gram-Positive, Gram-Negative and Acid-Fast Bacteria. *Aust. J. Exp. Biol. Med. Sci.* **1969**, *47* (2), 203–218.
(158) McCann, M.; Santos, A. L. S.; Da Silva, B. A.; Romanos, M. T. V; Pyrrho, A. S.; Devereux, M.; Kavanagh, K.; Fichtner, I.; Kellett, A. In Vitro and in Vivo Studies into the Biological Activities of 1,10-Phenanthroline, 1,10-Phenanthroline-5,6-Dione and Its Copper(Ii) and Silver(i) Complexes. *Toxicol. Res. (Camb).* **2012**, *1* (1), 47–54. https://doi.org/10.1039/c2tx00010e.
(159) Li, F.; Mulyana, Y.; Feterl, M.; Warner, J. M.; Collins, J. G.; Keene, F. R. The Antimicrobial Activity of Inert Oligonuclear Polypyridylruthenium(Ii) Complexes against Pathogenic Bacteria, Including MRSA. *Dalt. Trans.* **2011**, *40* (18), 5032–5038. https://doi.org/10.1039/c1dt10250h.
(160) Barbosa, M. I. F.; Corrêa, R. S.; De Oliveira, K. M.; Rodrigues, C.; Ellena, J.; Nascimento, O. R.; Rocha, V. P. C.; Nonato, F. R.; Macedo, T. S.; Barbosa-Filho, J. M.; et al. Antiparasitic Activities of Novel Ruthenium/Lapachol Complexes. *J. Inorg. Biochem.* **2014**, *136* (July), 33–39. https://doi.org/10.1016/j.jinorgbio.2014.03.009.
(161) Creaven, B. S.; Devereux, M.; Karcz, D.; Kellett, A.; McCann, M.; Noble, A.; Walsh, M. Copper(II) Complexes of Coumarin-Derived Schiff Bases and Their Anti-Candida Activity. *J. Inorg. Biochem.* **2009**, *103* (9), 1196–1203. https://doi.org/10.1016/j.jinorgbio.2009.05.017.
(162) Li, F.; Feterl, M.; Warner, J. M.; Keene, F. R.; Collins, J. G. Dinuclear Polypyridylruthenium(II) Complexes: Flow Cytometry Studies of Their Accumulation in Bacteria and the Effect on the Bacterial Membrane. *J. Antimicrob. Chemother.* **2013**, *68* (12), 2825–2833. https://doi.org/10.1093/jac/dkt279.
(163) Morais Cabral, J. H.; Jackson, A. P.; Smith, C. V; Shikotra, N.; Maxwell, A.; Liddington, R. C. Crystal Structure of the Breakage-Reunion Domain of DNA Gyrase. *Nature* **1997**, *388* (6645), 903–906. https://doi.org/10.1038/42294.

(164) Psomas, G.; Kessissoglou, D. P. Quinolones and Non-Steroidal Anti-Inflammatory Drugs Interacting with Copper(II), Nickel(II), Cobalt(II) and Zinc(II): Structural Features, Biological Evaluation and Perspectives. *Dalton Trans.* **2013**, *42* (18), 6252–6276. https://doi.org/10.1039/c3dt50268f.
(165) Fernandes, P.; Sousa, I.; Cunha-Silva, L.; Ferreira, M.; de Castro, B.; Pereira, E. F.; Feio, M. J.; Gameiro, P. Synthesis, Characterization and Antibacterial Studies of a Copper(II) Lomefloxacin Ternary Complex. *J. Inorg. Biochem.* **2014**, *131*, 21–29. https://doi.org/10.1016/j.jinorgbio.2013.10.013.
(166) Saraiva, R.; Lopes, S.; Ferreira, M.; Novais, F.; Pereira, E.; Feio, M. J.; Gameiro, P. Solution and Biological Behaviour of Enrofloxacin Metalloantibiotics: A Route to Counteract Bacterial Resistance? *J. Inorg. Biochem.* **2010**, *104* (8), 843–850. https://doi.org/10.1016/j.jinorgbio.2010.03.017.
(167) Gameiro, P.; Rodrigues, C.; Baptista, T.; Sousa, I.; de Castro, B. Solution Studies on Binary and Ternary Complexes of Copper(II) with Some Fluoroquinolones and 1,10-Phenanthroline: Antimicrobial Activity of Ternary Metalloantibiotics. *Int. J. Pharm.* **2007**, *334* (1–2), 129–136. https://doi.org/10.1016/j.ijpharm.2006.10.035.
(168) Sun, D.; Zhang, W.; Yang, E.; Li, N.; Liu, H.; Wang, W. Investigation of Antibacterial Activity and Related Mechanism of a Ruthenium(II) Polypyridyl Complex. *Inorg. Chem. Commun.* **2015**, *56*, 17–21. https://doi.org/https://doi.org/10.1016/j.inoche.2015.03.044.
(169) Ng, N. S.; Leverett, P.; Hibbs, D. E.; Yang, Q.; Bulanadi, J. C.; Jie Wu, M.; Aldrich-Wright, J. R. The Antimicrobial Properties of Some Copper(Ii) and Platinum(Ii) 1,10-Phenanthroline Complexes. *Dalt. Trans.* **2013**, *42* (9), 3196–3209. https://doi.org/10.1039/c2dt32392c.
(170) Cai, X.; Pan, N.; Zou, G. Copper-1,10-Phenanthroline-Induced Apoptosis in Liver Carcinoma Bel-7402 Cells Associates with Copper Overload, Reactive Oxygen Species Production, Glutathione Depletion and Oxidative DNA Damage. *BioMetals* **2007**, *20* (1), 1–11. https://doi.org/10.1007/s10534-006-9008-0.
(171) Paez, P. L.; Bazan, C. M.; Bongiovanni, M. E.; Toneatto, J.; Albesa, I.; Becerra, M. C.; Arguello, G. A. Oxidative Stress and Antimicrobial Activity of Chromium(III) and Ruthenium(II) Complexes on Staphylococcus Aureus and Escherichia Coli. *Biomed Res. Int.* **2013**, *2013*, 906912. https://doi.org/10.1155/2013/906912.
(172) Urquiza, N. M.; Islas, M. S.; Dittler, M. L.; Moyano, M. A.; Manca, S. G.; Lezama, L.; Rojo, T.; Medina, J. J. M.; Diez, M.; Tévez, L. L.; et al. Inhibition Behavior on Alkaline Phosphatase Activity, Antibacterial and Antioxidant Activities of Ternary Methimazole–phenanthroline–copper(II) Complex. *Inorganica Chim. Acta* **2013**, *405*, 243–251. https://doi.org/https://doi.org/10.1016/j.ica.2013.05.022.
(173) Medina, J. J. M.; Islas, M. S.; Tévez, L. L. L.; Ferrer, E. G.; Okulik, N. B.; Williams, P. A. M. Copper(II) Complexes with Cyanoguanidine and o-Phenanthroline: Theoretical Studies, in Vitro Antimicrobial Activity and Alkaline Phosphatase Inhibitory Effect. *J. Mol. Struct.* **2014**, *1058*, 298–307. https://doi.org/https://doi.org/10.1016/j.molstruc.2013.11.014.
(174) Smit, H.; van der Goot, H.; Nauta, W. T.; Timmerman, H.; de Bolster, M. W.; Stouthamer, A. H.; Vis, R. D. Mechanism of Action of the Copper(I) Complex of 2,9-Dimethyl-1,10-Phenanthroline on Mycoplasma Gallisepticum.

Antimicrob. Agents Chemother. **1982**, *21* (6), 881–886. https://doi.org/10.1128/AAC.21.6.881.
(175) Barberis, I.; Bragazzi, N. L.; Galluzzo, L.; Martini, M. The History of Tuberculosis: From the First Historical Records to the Isolation of Koch's Bacillus. *J. Prev. Med. Hyg.* **2017**, *58* (1), E9–E12. https://doi.org/10.15167/2421-4248/jpmh2017.58.1.728.
(176) Hayman, J. Mycobacterium Ulcerans: An Infection from Jurassic Time? *Lancet (London, England)* **1984**, *2* (8410), 1015–1016.
(177) Daniel, T. M. The History of Tuberculosis. *Respir. Med.* **2006**, *100* (11), 1862–1870. https://doi.org/10.1016/j.rmed.2006.08.006.
(178) noberlprize.org. Robert Koch - Nobel Lecture https://www.nobelprize.org/prizes/medicine/1905/koch/lecture/ (accessed Mar 15, 2018).
(179) Organization, W. H. No TitleTuberculosis http://www.who.int/en/news-room/fact-sheets/detail/tuberculosis (accessed Jan 21, **2019**).
(180) Janin, Y. L. Antituberculosis Drugs: Ten Years of Research. *Bioorganic Med. Chem.* **2007**, *15* (7), 2479–2513. https://doi.org/10.1016/j.bmc.2007.01.030.
(181) Centers for Disease Control and Prevention. Tuberculosis (TB) https://www.cdc.gov/tb/topic/treatment/tbdisease.html (accessed Jul 17, 2018).
(182) Forget, E. J.; Menzies, D. Adverse Reactions to First-Line Antituberculosis Drugs. *Expert Opin. Drug Saf.* **2006**, *5* (2), 231–249. https://doi.org/10.1517/14740338.5.2.231.
(183) Scholar, E. M.; Scholar, E. M.; Pratt, W. B. *The Antimicrobial Drugs*; The Antimicrobial Drugs; Oxford University Press, 2000.
(184) Mathuria, J. P.; Samaria, J. K.; Srivastava, G. N.; Mathuria, B. L.; Ojha, S. K.; Anupurba, S. Primary and Acquired Drug Resistance Patterns of Mycobacterium Tuberculosis Isolates in India: A Multicenter Study. *J. Infect. Public Health* **2013**, *6* (6), 456–464. https://doi.org/10.1016/j.jiph.2013.03.003.
(185) Zhang, Y.; Heym, B.; Allen, B.; Young, D.; Cole, S. The Catalase-Peroxidase Gene and Isoniazid Resistance of Mycobacterium Tuberculosis. *Nature* **1992**, *358* (6387), 591–593. https://doi.org/10.1038/358591a0.
(186) Timmins, G. S.; Deretic, V. Mechanisms of Action of Isoniazid. *Mol. Microbiol.* **2006**, *62* (5), 1220–1227. https://doi.org/10.1111/j.1365-2958.2006.05467.x.
(187) Argyrou, A.; Vetting, M. W.; Aladegbami, B.; Blanchard, J. S. Mycobacterium Tuberculosis Dihydrofolate Reductase Is a Target for Isoniazid. *Nat. Struct. Mol. Biol.* **2006**, *13* (5), 408–413. https://doi.org/10.1038/nsmb1089.
(188) Bernardes-Génisson, V.; Deraeve, C.; Chollet, A.; Bernadou, J.; Pratviel, G. Isoniazid: An Update on the Multiple Mechanisms for a Singular Action. *Curr. Med. Chem.* **2013**, *20* (35), 4370–4385. https://doi.org/10.2174/15672050113109990203.
(189) Lavender, C.; Globan, M.; Sievers, A.; Billman-Jacobe, H.; Fyfe, J. Molecular Characterization of Isoniazid-Resistant Mycobacterium Tuberculosis Isolates Collected in Australia. *Antimicrob. Agents Chemother.* **2005**, *49* (10), 4068–4074. https://doi.org/10.1128/AAC.49.10.4068-4074.2005.
(190) Unissa, A. N.; Subbian, S.; Hanna, L. E.; Selvakumar, N. Overview on Mechanisms of Isoniazid Action and Resistance in Mycobacterium Tuberculosis. *Infect. Genet. Evol.* **2016**, *45* (1), 474–492. https://doi.org/10.1016/j.meegid.2016.09.004.
(191) Viganor, L.; Skerry, C.; McCann, M.; Devereux, M. Tuberculosis: An

Inorganic Medicinal Chemistry Perspective. *Curr. Med. Chem.* **2015**, *22* (18), 2199–2224. https://doi.org/10.2174/0929867322666150408112357.

(192) Wang, P.; Pradhan, K.; Zhong, X. bo; Ma, X. Isoniazid Metabolism and Hepatotoxicity. *Acta Pharm. Sin. B* **2016**, *6* (5), 384–392. https://doi.org/10.1016/j.apsb.2016.07.014.

(193) Vosátka, R.; Krátký, M.; Švarcová, M.; Janoušek, J.; Stolaříková, J.; Madacki, J.; Huszár, S.; Mikušová, K.; Korduláková, J.; Trejtnar, F.; et al. New Lipophilic Isoniazid Derivatives and Their 1,3,4-Oxadiazole Analogues: Synthesis, Antimycobacterial Activity and Investigation of Their Mechanism of Action. *Eur. J. Med. Chem.* **2018**, *151*, 824–835. https://doi.org/10.1016/j.ejmech.2018.04.017.

(194) Hu, Y. Q.; Zhang, S.; Zhao, F.; Gao, C.; Feng, L. S.; Lv, Z. S.; Xu, Z.; Wu, X. Isoniazid Derivatives and Their Anti-Tubercular Activity. *Eur. J. Med. Chem.* **2017**, *133*, 255–267. https://doi.org/10.1016/j.ejmech.2017.04.002.

(195) Oliveira, J. S.; Sousa, E. H. S.; Basso, L. A.; Palaci, M.; Dietze, R.; Santos, D. S.; Moreira, I. S. An Inorganic Iron Complex That Inhibits Wild-Type and an Isoniazid-Resistant Mutant 2-Trans-Enoyl-ACP (CoA) Reductase from Mycobacterium Tuberculosis. *Chem. Commun. (Camb).* **2004**, No. 3, 312–313. https://doi.org/10.1039/b313592f.

(196) Wiseman, B.; Carpena, X.; Feliz, M.; Donald, L. J.; Pons, M.; Fita, I.; Loewen, P. C. Isonicotinic Acid Hydrazide Conversion to Isonicotinyl-NAD by Catalase-Peroxidases. *J. Biol. Chem.* **2010**, *285* (34), 26662–26673. https://doi.org/10.1074/jbc.M110.139428.

(197) Sousa, E. H. S.; Basso, L. A.; Santos, D. S.; Diógenes, I. C. N.; Longhinotti, E.; De França Lopes, L. G.; De Sousa Moreira, Í. Isoniazid Metal Complex Reactivity and Insights for a Novel Anti-Tuberculosis Drug Design. *J. Biol. Inorg. Chem.* **2012**, *17* (2), 275–283. https://doi.org/10.1007/s00775-011-0848-x.

(198) Pavan, F. R.; Sato, D. N.; Leite, C. Q. F. An Approach to the Search for New Drugs Against Tuberculosis. In *Understanding Tuberculosis*; Cardona, P.-J., Ed.; IntechOpen: Rijeka, **2012**. https://doi.org/10.5772/31618.

(199) Rodrigues-Junior, V. S.; Machado, P.; Calixto, J. B.; Siqueira, J. M.; Andrade, E.; Bento, A.; Campos, M. M.; Basso, L. A.; Santos, D. S. Preclinical Safety Evaluation of IQG-607 in Rats: Acute and Repeated Dose Toxicity Studies. *Regul. Toxicol. Pharmacol.* **2017**, *86* (April), 11–17. https://doi.org/10.1016/j.yrtph.2017.02.016.

(200) Abbadi, B. L.; Villela, A. D.; Rodrigues-Junior, V. S.; Subtil, F. T.; Dalberto, P. F.; Pinheiro, A. P. S.; Santos, D. S.; Machado, P.; Basso, L. A.; Bizarro, C. V. Revisiting Activation of and Mechanism of Resistance to Compound IQG-607 in Mycobacterium Tuberculosis. *Antimicrob. Agents Chemother.* **2018**, *62* (2). https://doi.org/10.1128/AAC.02222-17.

(201) Abbadi, B. L.; Rodrigues-Junior, V. da S.; Dadda, A. da S.; Pissinate, K.; Villela, A. D.; Campos, M. M.; Lopes, L. G. de F.; Bizarro, C. V; Machado, P.; Sousa, E. H. S.; et al. Is IQG-607 a Potential Metallodrug or Metallopro-Drug With a Defined Molecular Target in Mycobacterium Tuberculosis? *Front. Microbiol.* **2018**, *9*, 880. https://doi.org/10.3389/fmicb.2018.00880.

(202) Rodrigues-Junior, V. S.; Dos Santos Junior, A. A.; Villela, A. D.; Belardinelli, J. M.; Morbidoni, H. R.; Basso, L. A.; Campos, M. M.; Santos, D. S. IQG-607 Abrogates the Synthesis of Mycolic Acids and Displays Intracellular Activity against Mycobacterium Tuberculosis in Infected Macrophages. *Int. J.*

Antimicrob. Agents **2014**, *43* (1), 82–85. https://doi.org/10.1016/j.ijantimicag.2013.08.021.

(203) Poggi, M.; Barroso, R.; Costa-Filho, A. J.; De Barros, H. B.; Pavan, F.; Leite, C. Q.; Gambino, D.; Torre, M. H. New Isoniazid Complexes, Promising Agents against Mycobacterium Tuberculosis. *J. Mex. Chem. Soc.* **2013**, *57* (3), 198–204.

(204) Hearn, M. J.; Cynamon, M. H.; Chen, M. F.; Coppins, R.; Davis, J.; Joo-On Kang, H.; Noble, A.; Tu-Sekine, B.; Terrot, M. S.; Trombino, D.; et al. Preparation and Antitubercular Activities in Vitro and in Vivo of Novel Schiff Bases of Isoniazid. *Eur. J. Med. Chem.* **2009**, *44* (10), 4169–4178. https://doi.org/10.1016/j.ejmech.2009.05.009.

(205) Castelo-Branco, F. S.; de Lima, E. C.; Domingos, J. L. de O.; Pinto, A. C.; Lourenço, M. C. S.; Gomes, K. M.; Costa-Lima, M. M.; Araujo-Lima, C. F.; Aiub, C. A. F.; Felzenszwalb, I.; et al. New Hydrazides Derivatives of Isoniazid against Mycobacterium Tuberculosis: Higher Potency and Lower Hepatocytotoxicity. *European Journal of Medicinal Chemistry*. **2018**, pp 529–540. https://doi.org/10.1016/j.ejmech.2018.01.071.

(206) Hearn, M. J.; Cynamon, M. H. Design and Synthesis of Antituberculars: Preparation and Evaluation against Mycobacterium Tuberculosis of an Isoniazid Schiff Base. *J. Antimicrob. Chemother.* **2004**, *53* (2), 185–191. https://doi.org/10.1093/jac/dkh041.

(207) Sah, B. P. P. T.; Peoplest, S. A. JOURNAL OF THE AMERICAN PHARMACEUTICAL ASSOCIATION Isonicotinyl Hydrazones as Antitubercular Agents and Derivatives for Identification of Aldehydes. **1952**.

(208) Mathew, B.; Suresh, J.; Ahsan, M.; Mathew, G.; Usman, D.; Subramanyan, P.; Safna, K.; Maddela, S. Hydrazones as a Privileged Structural Linker in Antitubercular Agents: A Review. *Infect. Disord. - Drug Targets* **2015**, *15* (2), 76–88. https://doi.org/10.2174/1871526515666150724104411.

(209) Rollas, S.; Kucukguzel, S. G. Biological Activities of Hydrazone Derivatives. *Molecules* **2007**, *12* (8), 1910–1939.

(210) Bijev, a. New Heterocyclic Hydrazones in the Search for Antitubercular Agents: Synthesis and In Vitro Evaluations. *Lett. Drug Des. Discov.* **2006**, *3* (7), 506–512. https://doi.org/10.2174/157018006778194790.

(211) McCarron, P.; McCann, M.; Devereux, M.; Kavanagh, K.; Skerry, C.; Karakousis, P. C.; Aor, A. C.; Mello, T. P.; Santos, A. L. S.; Campos, D. L.; et al. Unprecedented in Vitro Antitubercular Activitiy of Manganese(II) Complexes Containing 1,10-Phenanthroline and Dicarboxylate Ligands: Increased Activity, Superior Selectivity, and Lower Toxicity in Comparison to Their Copper(II) Analogs. *Front. Microbiol.* **2018**, *9* (JUL), 1–10. https://doi.org/10.3389/fmicb.2018.01432.

(212) Hoffman, A. E.; DeStefano, M.; Shoen, C.; Gopinath, K.; Warner, D. F.; Cynamon, M.; Doyle, R. P. Co(II) and Cu(II) Pyrophosphate Complexes Have Selectivity and Potency against Mycobacteria Including Mycobacteriumtuberculosis. *Eur. J. Med. Chem.* **2013**, *70*, 589–593. https://doi.org/10.1016/j.ejmech.2013.10.044.

(213) Segura, D. F.; Netto, A. V. G.; Frem, R. C. G.; Mauro, A. E.; Da Silva, P. B.; Fernandes, J. A.; Paz, F. A. A.; Dias, A. L. T.; Silva, N. C.; De Almeida, E. T.; et al. Synthesis and Biological Evaluation of Ternary Silver Compounds Bearing N,N-Chelating Ligands and Thiourea: X-Ray Structure of [{Ag(Bpy)(μ-Tu)} 2](NO3)2 (Bpy = 2,2′-Bipyridine; Tu = Thiourea).

Polyhedron **2014**, *79*, 197–206. https://doi.org/10.1016/j.poly.2014.05.004.
(214) Kidwai, S.; Park, C. Y.; Mawatwal, S.; Tiwari, P.; Jung, M. G.; Gosain, T. P.; Kumar, P.; Alland, D.; Kumar, S.; Bajaj, A.; et al. Dual Mechanism of Action of 5-Nitro-1,10-Phenanthroline against Mycobacterium Tuberculosis. *Antimicrob. Agents Chemother.* **2017**, *61* (11). https://doi.org/10.1128/AAC.00969-17.
(215) Glick, D.; Barth, S.; Macleod, K. F. AutophagGlick, D., Barth, S., & Macleod, K. F. (2010). Autophagy : Cellular and Molecular Mechanisms. Journal of Pathology The, 221, 3–12. Http://Doi.Org/10.1002/Path.2697.Autophagyy : Cellular and Molecular Mechanisms. *J. Pathol.* **2010**, *221* (1), 3–12. https://doi.org/10.1002/path.2697.Autophagy.
(216) Zheng, R. H.; Guo, H. C.; Jiang, H. J.; Xu, K. H.; Liu, B. B.; Sun, W. L.; Shen, Z. Q. A New and Convenient Synthesis of Phendiones Oxidated by KBrO3/H2SO4at Room Temperature. *Chinese Chem. Lett.* **2010**, *21* (11), 1270–1272. https://doi.org/10.1016/j.cclet.2010.05.030.
(217) Stein, G.; Nudelman, A.; Rephaeli, A.; Gil-Ad, I.; Weizman, A. Conjugates for Treating Neurodegenerative Diseases and Disorders., June 26, **2012**.
(218) Barbazán, P.; Hagenbach, A.; Oehlke, E.; Abram, U.; Carballo, R.; Rodríguez-Hermida, S.; Vázquez-López, E. M. Tricarbonyl Rhenium(I) and Technetium(I) Complexes with Hydrazones Derived from 4,5-Diazafluoren-9-One and 1,10-Phenanthroline-5,6-Dione. *Eur. J. Inorg. Chem.* **2010**, No. 29, 4622–4630. https://doi.org/10.1002/ejic.201000522.
(219) Bhutani, H.; Singh, S.; Vir, S.; Bhutani, K. K.; Kumar, R.; Chakraborti, A. K.; Jindal, K. C. LC and LC-MS Study of Stress Decomposition Behaviour of Isoniazid and Establishment of Validated Stability-Indicating Assay Method. *J. Pharm. Biomed. Anal.* **2007**, *43* (4), 1213–1220. https://doi.org/10.1016/j.jpba.2006.10.013.
(220) Terent'ev, P. B.; Strankevicius, A. Mass-Spectrometric Behavior of 9-Hydroxy-10-Nitrosophenanthrene and Its Diaza Analogs. *Khimiya Geterotsiklicheskikh Soedin.* **1988**, No. 11, 1518–1521.
(221) McCann, M.; McGinley, J.; Ni, K.; O'Connor, M.; Kavanagh, K.; McKee, V.; Colleran, J.; Devereux, M.; Gathergood, N.; Barron, N.; et al. A New Phenanthroline-Oxazine Ligand: Synthesis, Coordination Chemistry and Atypical DNA Binding Interaction. *Chem. Commun.* **2013**, *49* (23), 2341–2343. https://doi.org/10.1039/c3cc38710k.
(222) Eckert, T. S.; Bruice, T. C. Chemical Properties of Phenanthrolinequinones and the Mechanism of Amine Oxidation by O-Quinones of Medium Redox Potentials. *J. Am. Chem. Soc.* **1983**, *105* (13), 4431–4441. https://doi.org/10.1021/ja00351a049.
(223) Qin, Y.; Zhang, L.; Lv, J.; Luo, S.; Cheng, J. P. Bioinspired Organocatalytic Aerobic C-H Oxidation of Amines with an Ortho -Quinone Catalyst. *Org. Lett.* **2015**, *17* (6), 1469–1472. https://doi.org/10.1021/acs.orglett.5b00351.
(224) Ettedgui, J.; Neumann, R. Phenanthroline Decorated by a Crown Ether as a Module for Metallorganic-Polyoxometalate Hybrid Catalysts: The Wacker Type Oxidation of Alkenes with Nitrous Oxide as Terminal Oxidant. *J. Am. Chem. Soc.* **2009**, *131* (1), 4–5. https://doi.org/10.1021/ja808523n.
(225) Cotton, A.; Wilkinson, G. Cotton-Wilkinson-Advanced-Inorganic-Chemistry. **1999**. https://doi.org/10.1088/1364-7830/3/4/309.
(226) Orgel, L. E. Orgel: Stereochemistry of Metals of 843. Stereochemistry. *J. Chem. Soc.* **1958**, *0* (4186), 4186–4190. https://doi.org/10.1039/jr9580004186.

(227) Fox, B. S.; Beyer, M. K.; Bondybey, V. E. Coordination Chemistry of Silver Cations. *J. Am. Chem. Soc.* **2002**, *124* (45), 13613–13623. https://doi.org/10.1021/ja0176604.
(228) McCann, M.; Coyle, B.; McKay, S.; McCormack, P.; Kavanagh, K.; Devereux, M.; McKee, V.; Kinsella, P.; O'Connor, R.; Clynes, M. Synthesis and X-Ray Crystal Structure of [Ag(Phendio)2]ClO4(Phendio = 1,10-Phenanthroline-5,6-Dione) and Its Effects on Fungal and Mammalian Cells. *BioMetals* **2004**, *17* (6), 635–645. https://doi.org/10.1007/s10534-004-1229-5.
(229) J. Pallenberg, A.; M. Marschner, T.; M. Barnhart, D. Phenanthroline Complexes of the D10 Metals Nickel(0), Zinc(II) and Silver(I)—comparison to Copper(I) Species. *Polyhedron* **1997**, *16*, 2711–2719. https://doi.org/10.1016/S0277-5387(97)00051-X.
(230) Li, P.-G.; Wang, Q.-L.; Li, D.-S.; Fu, F.; Qi, G.-C. Crystal Structure of Bis(1,10-Phenanthroline-N,N′)Silver(I) Mononitrate, [Ag(C12H8N2)2][NO3]. *Zeitschrift für Krist. - New Cryst. Struct.* **2006**, *221* (3), 391–392. https://doi.org/10.1524/ncrs.2006.0123.
(231) Smolenski, P.; Jaros, S. W.; Pettinari, C.; Lupidi, G.; Quassinti, L.; Bramucci, M.; Vitali, L. A.; Petrelli, D.; Kochel, A.; Kirillov, A. M. New Water-Soluble Polypyridine Silver(I) Derivatives of 1,3,5-Triaza-7-Phosphaadamantane (PTA) with Significant Antimicrobial and Antiproliferative Activities. *Dalton Trans.* **2013**, *42* (18), 6572–6581. https://doi.org/10.1039/c3dt33026e.
(232) Mujahid, M.; Trendafilova, N.; Arfa-Kia, A. F.; Rosair, G.; Kavanagh, K.; Devereux, M.; Walsh, M.; McClean, S.; Creaven, B. S.; Georgieva, I. Novel Silver(I) Complexes of Coumarin Oxyacetate Ligands and Their Phenanthroline Adducts: Biological Activity, Structural and Spectroscopic Characterisation. *J. Inorg. Biochem.* **2016**, *163*, 53–67. https://doi.org/10.1016/j.jinorgbio.2016.07.010.
(233) Wen, M.; Kejia, E.; Munakata, M.; Suenaga, Y.; Kuroda-Sowa, T.; Maekawa, M.; Yan, S. G. Silver(I) Coordination Complexes of 1,10-Phenanthroline-5,6-Dione with 1D Chain and 2D Network Structure. *Mol. Cryst. Liq. Cryst.* **2006**, *457* (1), 203–213. https://doi.org/10.1080/15421400600598768.
(234) Krishnamurthy, S. S.; Soundararajan, S. O-Phenanthroline Complexes of Rare-Earth Perchlorates. *Zeitschrift für Anorg. und Allg. Chemie* **1966**, *348* (5-6), 309–312. https://doi.org/10.1002/zaac.19663480512.
(235) Schilt, A. A.; Taylor, R. C. Infra-Red Spectra of 1:10-Phenanthroline Metal Complexes in the Rock Salt Region below 2000 Cm-1. *J. Inorg. Nucl. Chem.* **1959**, *9* (3–4), 211–221. https://doi.org/10.1016/0022-1902(59)80224-4.
(236) Lewis, D. L.; Estes, E. D.; Hodgson, D. J. The Infrared Spectra of Coordinated Perchlorates. *J. Cryst. Mol. Struct.* **1975**, *5* (1), 67–74. https://doi.org/10.1007/BF01202553.
(237) Conry, R. R. Copper: Inorganic & Coordination ChemistryBased in Part on the Article Copper: Inorganic & Coordination Chemistry by Rebecca R. Conry & Kenneth D. Karlin Which Appeared in the *Encyclopedia of Inorganic Chemistry, First Edition* . *Encycl. Inorg. Bioinorg. Chem.* **2011**. https://doi.org/10.1002/9781119951438.eibc0050.
(238) Miller, M. T.; Gantzel, P. K.; Karpishin, T. B. Structures of the Copper(I) and Copper(II) Complexes of 2,9-Diphenyl-1,10-Phenanthroline: Implications for Excited-State Structural Distortion. *Inorg. Chem.* **1998**, *37* (9), 2285–2290.
(239) Pivetta, T.; Trudu, F.; Valletta, E.; Isaia, F.; Castellano, C.; Demartin, F.; Tuveri, R.; Vascellari, S.; Pani, A. Novel Copper(II) Complexes as New

Promising Antitumour Agents. A Crystal Structure of [Cu(1,10-Phenanthroline-5,6-Dione)2(OH2)(OClO3)](ClO4). *J. Inorg. Biochem.* **2014**, *141*, 103–113. https://doi.org/10.1016/j.jinorgbio.2014.08.011.

(240) Amournjarusiri, K.; J. Hathaway, B. Structure of Bis(1,10-Phenanthroline)Copper(II) Bis(Hexafluorophosphate). *Acta Crystallogr. Sect. C-crystal Struct. Commun. - ACTA CRYSTALLOGR C-CRYST STR* **1991**, *47*, 1383–1385. https://doi.org/10.1107/S0108270190013993.

(241) Polyanskaya, T. M.; Volkov, V. V; Drozdova, M. K. Crystal Structure of [Tris(1,10-Phenanthroline)Copper(II)(2+) Bis3,3{\textasciiacutex}-Commo-Bis-[$η$5-1,2-Dicarba-(3)-Cobalt(III)-Closo-Dodecaborate](1-)-Diacetonitrile, [CuII(1,10-C12H8N2)3] 2+{CoIII[$η$5-(3)-1,2-C2B9H11]2}2-·2CH3CN. *J. Struct. Chem.* **2003**, *44* (4), 632–641. https://doi.org/10.1023/B:JORY.0000017939.50919.77.

(242) Rodríguez-Martín, Y.; Ruiz-Pérez, C.; González-Platas, J.; Sanchiz, J.; Lloret, F.; Julve, M. A New Eight-Coordinate Complex of Manganese(II): Synthesis, Crystal Structure, Spectroscopy and Magnetic Properties of [Mn(Hoxam)2(H2O)4] (H2oxam=oxamic Acid). *Inorganica Chim. Acta* **2001**, *315* (1), 120–125. https://doi.org/https://doi.org/10.1016/S0020-1693(01)00296-1.

(243) KANI, I.; ATLIER, Ö.; GÜVEN, K. Mn(II) Complexes with Bipyridine, Phenanthroline and Benzoic Acid: Biological and Catalase-like Activity. *J. Chem. Sci.* **2016**, *128* (4), 523–536. https://doi.org/10.1007/s12039-016-1050-z.

(244) Curran, R. J.; McCann, D. M. Silver(I) Complexes as Antimicrobial and Anticancer Drugs. *Dep. Chem.* **2009**, *Ph.D.* (October), 386.

(245) Rowan, R.; McCann, M.; Kavanagh, K. Analysis of the Response of Candida Albicans Cells to Silver(I). *Med. Mycol.* **2010**, *48* (3), 498–505. https://doi.org/10.3109/13693780903222513.

(246) Cook, S. M.; McArthur, J. D. Developing Galleria Mellonella as a Model Host for Human Pathogens. *Virulence*. United States July **2013**, pp 350–353. https://doi.org/10.4161/viru.25240.

(247) Browne, N.; Heelan, M.; Kavanagh, K. An Analysis of the Structural and Functional Similarities of Insect Hemocytes and Mammalian Phagocytes. *Virulence* **2013**, *4* (7), 597–603. https://doi.org/10.4161/viru.25906.

(248) Pereira, M. F.; Rossi, C. C.; de Queiroz, M. V.; Martins, G. F.; Isaac, C.; Bosse, J. T.; Li, Y.; Wren, B. W.; Terra, V. S.; Cuccui, J.; et al. Galleria Mellonella Is an Effective Model to Study Actinobacillus Pleuropneumoniae Infection. *Microbiology* **2015**, *161* (Pt 2), 387–400. https://doi.org/10.1099/mic.0.083923-0.

(249) Yang, H.-F.; Pan, A.-J.; Hu, L.-F.; Liu, Y.-Y.; Cheng, J.; Ye, Y.; Li, J.-B. Galleria Mellonella as an in Vivo Model for Assessing the Efficacy of Antimicrobial Agents against Enterobacter Cloacae Infection. *J. Microbiol. Immunol. Infect.* **2017**, *50* (1), 55–61. https://doi.org/10.1016/j.jmii.2014.11.011.

(250) Kumar, S. V; Scottwell, S. O.; Waugh, E.; McAdam, C. J.; Hanton, L. R.; Brooks, H. J. L.; Crowley, J. D. Antimicrobial Properties of Tris(Homoleptic) Ruthenium(II) 2-Pyridyl-1,2,3-Triazole "Click" Complexes against Pathogenic Bacteria, Including Methicillin-Resistant Staphylococcus Aureus (MRSA). *Inorg. Chem.* **2016**, *55* (19), 9767–9777. https://doi.org/10.1021/acs.inorgchem.6b01574.

(251) Friedman, M. Applications of the Ninhydrin Reaction for Analysis of Amino Acids, Peptides, and Proteins to Agricultural and Biomedical Sciences. *J. Agric. Food Chem.* **2004**, *52* (3), 385–406. https://doi.org/10.1021/jf030490p.
(252) Kruger, N. J. The Bradford Method for Protein Quantitation. In *The Protein Protocols Handbook*; Walker, J. M., Ed.; Humana Press: Totowa, NJ, **2002**; pp 15–21. https://doi.org/10.1385/1-59259-169-8:15.
(253) Zhao, R.; Tan, C.; Xie, Y.; Gao, C.; Liu, H.; Jiang, Y. One Step Synthesis of Azo Compounds from Nitroaromatics and Anilines. *Tetrahedron Lett.* **2011**, *52* (29), 3805–3809. https://doi.org/10.1016/j.tetlet.2011.05.054.
(254) Gund, S. H.; Shelkar, R. S.; Nagarkar, J. M. An Efficient Catalyst-Free and Chemoselective Synthesis of Azobenzenes from Nitrobenzenes. *RSC Adv.* **2014**, *4* (81), 42947–42951. https://doi.org/10.1039/c4ra06027j.
(255) Li, J.; Zhou, H.; Zhang, J.; Yang, H.; Jiang, G. AgNO3 as Nitrogen Source for Rhodium(Iii)-Catalyzed Synthesis of 2-Aryl-2H-Benzotriazoles from Azobenzenes. *Chem. Commun.* **2016**, *52* (61), 9589–9592. https://doi.org/10.1039/C6CC04341K.
(256) Cheon, K. S.; Park, Y. S.; Kazmaier, P. M.; Buncel, E. Studies of Azo-Hydrazone Tautomerism and H-Bonding in Azo-Functionalized Dendrimers and Model Compounds. *Dye. Pigment.* **2002**, *53* (1), 3–14. https://doi.org/10.1016/S0143-7208(01)00096-1.
(257) Ramos, J.; Arufe, S.; O'Flaherty, R.; Rooney, D.; Moreira, R.; Velasco-Torrijos, T. Selective Aliphatic/Aromatic Organogelation Controlled by the Side Chain of Serine Amphiphiles. *RSC Adv.* **2016**, *6* (109), 108093–108104. https://doi.org/10.1039/C6RA21391J.
(258) Yildiz, I. A DFT Approach to the Mechanistic Study of Hydrozone Hydrolysis. *J. Phys. Chem. A* **2016**, *120* (20), 3683–3692. https://doi.org/10.1021/acs.jpca.6b02882.
(259) Buss, J. L.; Ponka, P. Hydrolysis of Pyridoxal Isonicotinoyl Hydrazone and Its Analogs. *Biochim. Biophys. Acta* **2003**, *1619* (2), 177–186.
(260) Chiang, H.; Lin, L. Photolysis of Isoniazid. *J. Chinese Chem. Soc.* **1978**, *25*. https://doi.org/10.1002/jccs.197800022.
(261) Wan, G.; Ruan, L.; Yin, Y.; Yang, T.; Ge, M.; Cheng, X. Effects of Silver Nanoparticles in Combination with Antibiotics on the Resistant Bacteria Acinetobacter Baumannii. *Int. J. Nanomedicine* **2016**, *11*, 3789–3800. https://doi.org/10.2147/IJN.S104166.
(262) Nguta, J. M.; Appiah-Opong, R.; Nyarko, A. K.; Yeboah-Manu, D.; Addo, P. G. A. Current Perspectives in Drug Discovery against Tuberculosis from Natural Products. *Int. J. mycobacteriology* **2015**, *4* (3), 165–183. https://doi.org/10.1016/j.ijmyco.2015.05.004.
(263) Shibata, H.; Kondo, K.; Katsuyama, R.; Kawazoe, K.; Sato, Y.; Murakami, K.; Takaishi, Y.; Arakaki, N.; Higuti, T. Alkyl Gallates, Intensifiers of β-Lactam Susceptibility in Methicillin-Resistant Staphylococcus Aureus. *Antimicrob. Agents Chemother.* **2005**, *49* (2), 549–555. https://doi.org/10.1128/AAC.49.2.549-555.2005.
(264) Chew, Y. L.; Mahadi, A. M.; Wong, K. M.; Goh, J. K. Anti-Methicillin-Resistance Staphylococcus Aureus (MRSA) Compounds from Bauhinia Kockiana Korth . And Their Mechanism of Antibacterial Activity. **2018**, 1–9.

Appendix

Biology MIC determination graphs

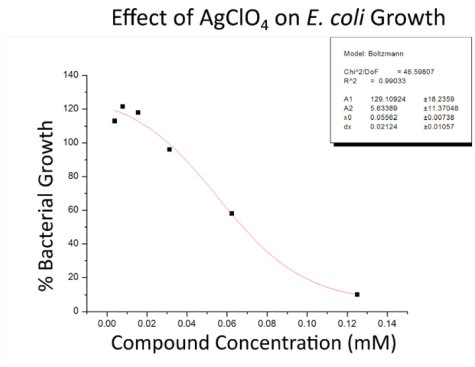

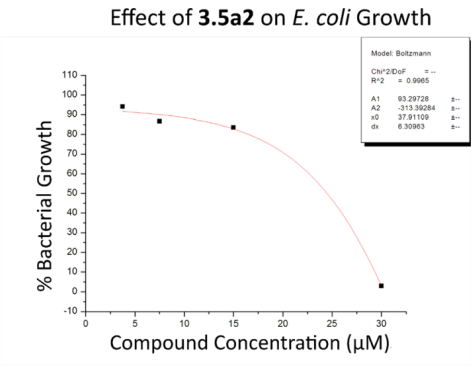

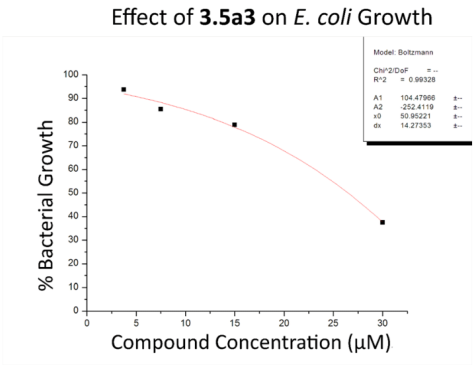

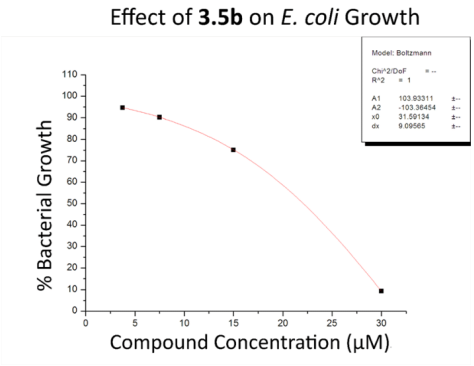

Effect of Doxycycline on *E. coli* Growth

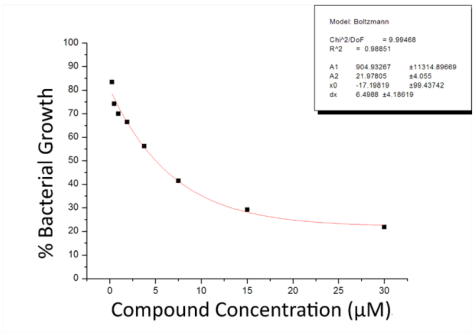

Effect of Streptomycin on *E. coli* Growt

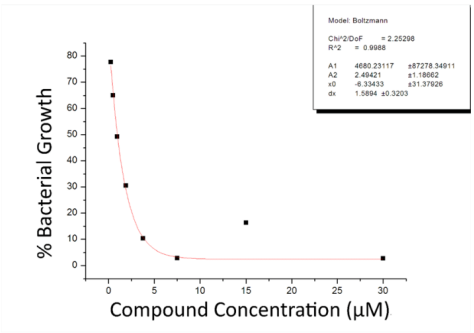

Effect of Vancomycin on *E. coli* Growth

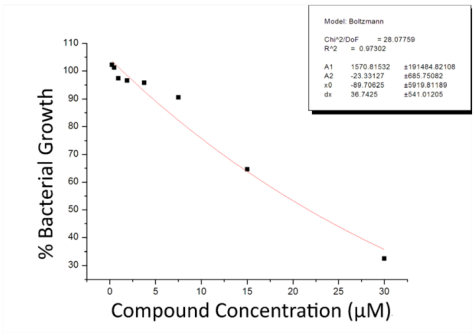

Effect of **3.5a1** on *S. aureus* Growth

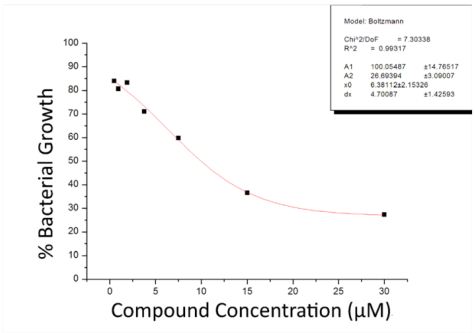

Effect of **3.5a2** on *S. aureus* Growth

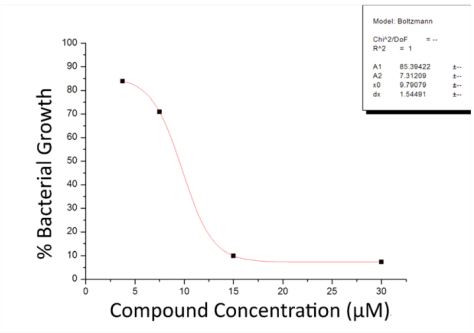

Effect of **3.5a3** on *S. aureus* Growth

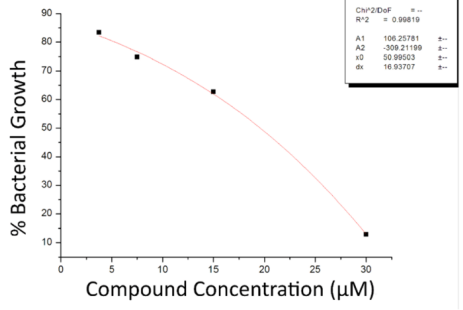

Effect of **3.3b** on *S. aureus* Growth

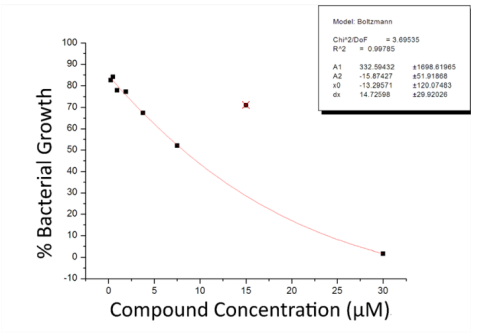

Effect of **3.3c** on *S. aureus* Growth

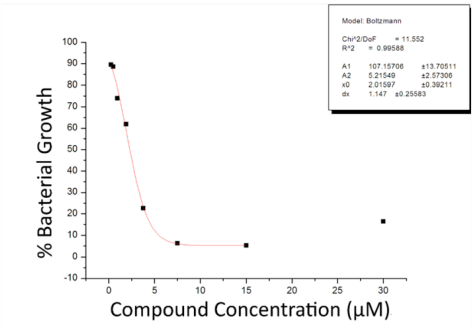

Effect of **3.3c** on *S. aureus* Growth

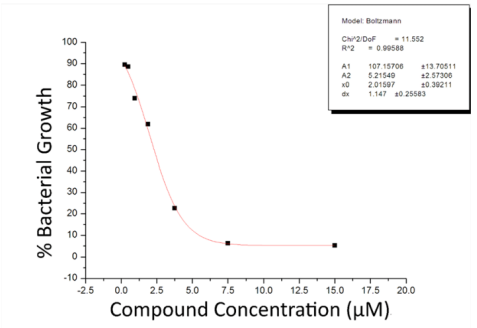

Effect of **3.3d** on *S. aureus* Growth

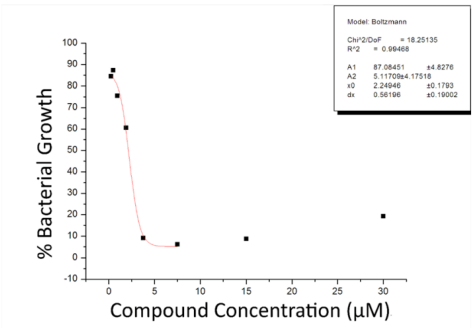

Effect of **3.3d** on *S. aureus* Growth

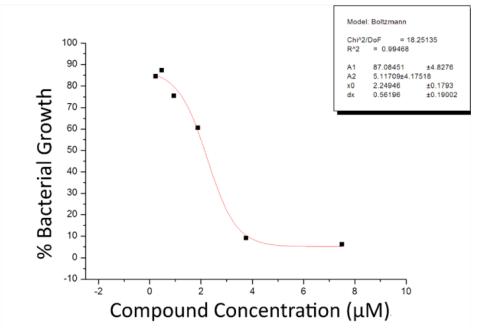

Effect of **3.5b** on *S. aureus* Growth

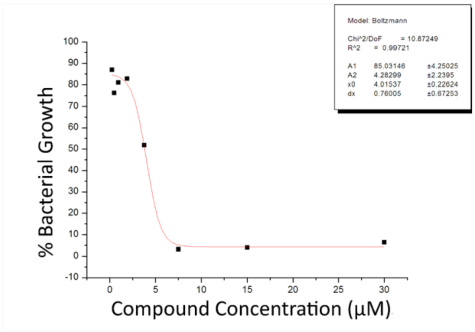

Effect of **3.5c** on *S. aureus* Growth

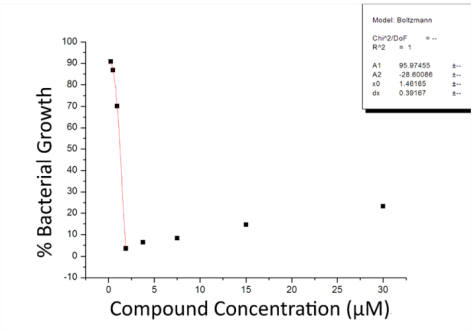

Effect of **3.5c** on *S. aureus* Growth

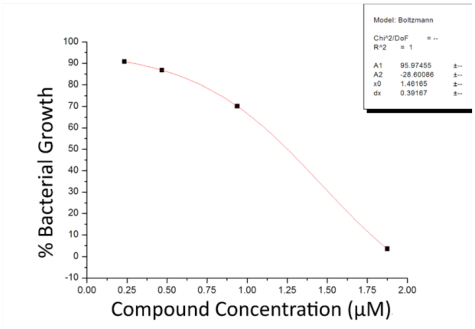

Effect of **3.5d** on *S. aureus* Growth

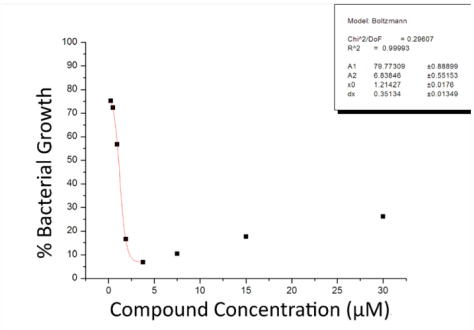

Effect of **3.5d** on *S. aureus* Growth

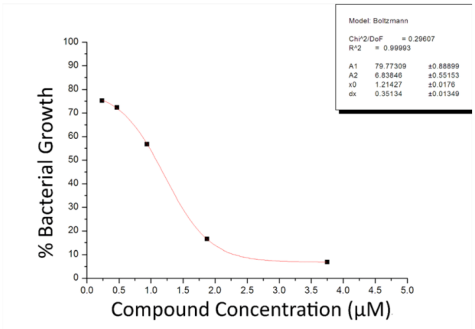

Effect of Doxycycline on *S. aureus* Growth

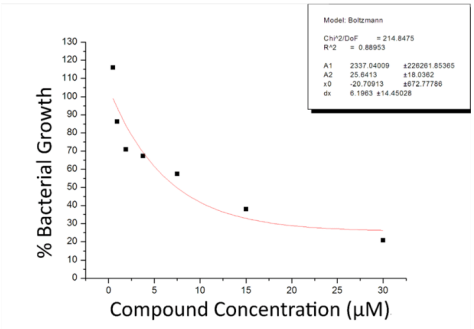

Effect of Streptomycin on *S. aureus* Growt

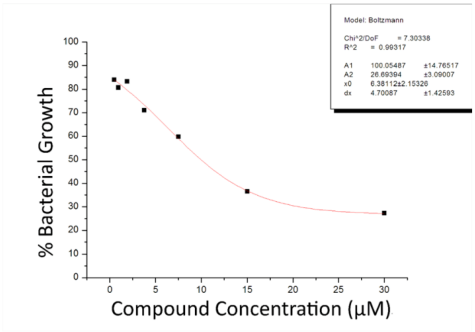

Effect of Tetracycline on *S. aureus* Growth

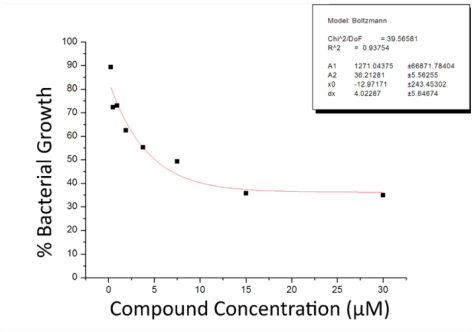

Effect of Vancomycin on *S. aureus* Growth

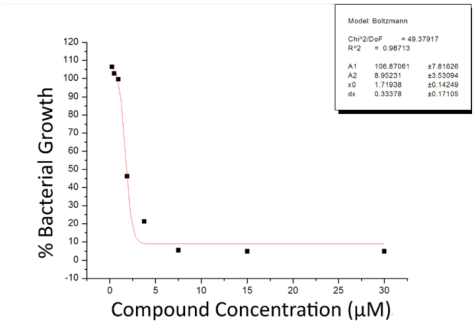

Crystallographic Data

A clear yellow fragment-like specimen of $C_{24}H_{19}N_3O_4$, approximate dimensions 0.110 mm x 0.120 mm x 0.160 mm, was used for the X-ray crystallographic analysis. The X-ray intensity data were measured at 100(2)K on a Bruker D8 Quest ECO with an Oxford Cryosystems low temperature device using a MiTeGen micromount. See Table 1 for collection parameters and exposure time. Bruker APEX software was used to correct for Lorentz and polarization effects.

A total of 936 frames were collected. The total exposure time was 7.80 hours. The frames were integrated with the Bruker SAINT software package using a narrow-frame algorithm. The integration of the data using a monoclinic unit cell yielded a total of 27938 reflections to a maximum θ angle of 26.50° (0.80 Å resolution), of which 4010 were independent (average redundancy 6.967, completeness = 99.9%, R_{int} = 7.02%, R_{sig} = 4.95%) and 2840 (70.82%) were greater than $2\sigma(F^2)$. The final cell constants of a = 5.9471(2) Å, b = 16.7869(4) Å, c = 19.4373(6) Å, β = 96.2126(16)°, volume = 1929.10(10) $Å^3$, are based upon the refinement of the XYZ-centroids of 7671 reflections above 20 σ(I) with 6.430° < 2θ < 59.61°. Data were corrected for absorption effects using the Multi-Scan method (SADABS). The ratio of minimum to maximum apparent transmission was 0.945. The calculated minimum and maximum transmission coefficients (based on crystal size) are 0.7051 and 0.7462.

The structure was solved with the XT structure solution program using Intrinsic Phasing and refined with the XL refinement package using Least Squares minimisation with Olex2, using the space group $P2_1/n$, with Z = 4 for the formula unit, $C_{24}H_{19}N_3O_4$. The final anisotropic full-matrix least-squares refinement on F^2 with 282 variables converged at R1 = 5.26%, for the observed data and wR2 = 11.85% for all data. The goodness-of-fit was 1.060. The largest peak in the final difference electron density synthesis was 0.290 $e^-/Å^3$ and the largest hole was -0.210 $e^-/Å^3$ with an RMS deviation of 0.052 $e^-/Å^3$. On the basis of the final model, the calculated density was 1.423 g/cm^3 and F(000), 864 e^-.

Crystal Data for $C_{24}H_{19}N_3O_4$ (*M* =413.42 g/mol): monoclinic, space group $P2_1/n$ (no. 14), *a* = 5.9471(2) Å, *b* = 16.7869(4) Å, *c* = 19.4373(6) Å, *β* = 96.2126(16)°, *V* = 1929.10(10) Å^3, *Z* = 4, *T* = 100(2) K, μ(MoKα) = 0.099 mm^{-1}, *Dcalc* = 1.423 g/cm^3, 27938 reflections measured (4.854° ≤ 2Θ ≤ 52.998°), 4010 unique (R_{int} = 0.0702, R_{sigma} = 0.0495) which were used in all calculations. The final R_1 was 0.0526 (I > 2σ(I)) and wR_2 was 0.1185 (all data).

Crystal data and structure refinement for **3.3b**.

Empirical formula	$C_{24}H_{19}N_3O_4$	
Formula weight	413.42	
Temperature	100(2) K	
Wavelength	0.71073 Å	
Crystal system	Monoclinic	
Space group	$P2_1/n$	
Unit cell dimensions	a = 5.9471(2) Å	α= 90°.
	b = 16.7869(4) Å	β= 96.2126(16)°.
	c = 19.4373(6) Å	ɣ = 90°.
Volume	1929.10(10) Å^3	
Z	4	
Density (calculated)	1.423 Mg/m^3	
Absorption coefficient	0.099 mm^{-1}	
F(000)	864	
Crystal size	0.16 x 0.12 x 0.11 mm^3	
Theta range for data collection	2.427 to 26.499°.	
Index ranges	-7≤h≤7, -20≤k≤21, -24≤l≤22	
Reflections collected	27938	

Independent reflections	4010 [R(int) = 0.0702]
Completeness to theta = 25.242°	99.9 %
Absorption correction	Semi-empirical from equivalents
Max. and min. transmission	0.7462 and 0.7051
Refinement method	Full-matrix least-squares on F^2
Data / restraints / parameters	4010 / 0 / 282
Goodness-of-fit on F^2	1.060
Final R indices [I>2σ(I)]	R1 = 0.0526, wR2 = 0.1066
R indices (all data)	R1 = 0.0875, wR2 = 0.1185
Largest diff. peak and hole	0.290 and -0.210 e.$Å^{-3}$

Atomic coordinates (x 10^4) and equivalent isotropic displacement parameters ($Å^2$x 10^3) for **3.3b**. U(eq) is defined as one third of the trace of the orthogonalized U^{ij} tensor.

	x	y	z	U(eq)
N(1)	10362(3)	7579(1)	4950(1)	19(1)
C(2)	11840(4)	7028(1)	5187(1)	22(1)
C(3)	11545(4)	6210(1)	5064(1)	22(1)
C(4)	9603(4)	5964(1)	4682(1)	20(1)
C(5)	7980(4)	6525(1)	4430(1)	17(1)
C(6)	5890(4)	6299(1)	4041(1)	17(1)
N(7)	5280(3)	5490(1)	4019(1)	18(1)
C(8)	3567(4)	5297(1)	3601(1)	18(1)
C(9)	2436(4)	5872(1)	3081(1)	18(1)
O(10)	2425(2)	6667(1)	3401(1)	19(1)
C(11)	4399(4)	6869(1)	3772(1)	17(1)
C(12)	4761(4)	7704(1)	3924(1)	18(1)
C(13)	3153(4)	8292(1)	3718(1)	22(1)
C(14)	3605(4)	9069(1)	3910(1)	26(1)

C(15)	5663(4)	9242(1)	4297(1)	24(1)
N(16)	7230(3)	8704(1)	4500(1)	22(1)
C(17)	6773(4)	7935(1)	4324(1)	18(1)
C(18)	8432(4)	7336(1)	4572(1)	17(1)
C(19)	3577(4)	5889(1)	2424(1)	17(1)
C(20)	5675(4)	5535(1)	2370(1)	18(1)
C(21)	6698(4)	5575(1)	1766(1)	19(1)
C(22)	5645(4)	5979(1)	1192(1)	20(1)
O(23)	6746(3)	6026(1)	624(1)	27(1)
C(24)	3524(4)	6320(1)	1236(1)	20(1)
C(25)	2520(4)	6270(1)	1841(1)	20(1)
C(26)	2855(4)	4434(1)	3594(1)	20(1)
O(27)	3898(3)	3916(1)	3919(1)	31(1)
O(28)	975(3)	4318(1)	3171(1)	24(1)
C(29)	252(4)	3488(1)	3105(1)	24(1)
C(30)	-2024(4)	3468(1)	2705(1)	28(1)
C(31)	-2888(4)	2615(1)	2656(1)	32(1)

Bond lengths [Å] and angles [°] for **3.3b**.

N(1)-C(2)	1.325(3)	C(22)-O(23)	1.345(3)
N(1)-C(18)	1.357(3)	C(22)-C(24)	1.396(3)
C(2)-H(2)	0.9500	O(23)-H(23)	0.8400
C(2)-C(3)	1.401(3)	C(24)-H(24)	0.9500
C(3)-H(3)	0.9500	C(24)-C(25)	1.378(3)
C(3)-C(4)	1.368(3)	C(25)-H(25)	0.9500
C(4)-H(4)	0.9500	C(26)-O(27)	1.206(3)
C(4)-C(5)	1.399(3)	C(26)-O(28)	1.329(3)
C(5)-C(6)	1.434(3)	O(28)-C(29)	1.459(2)
C(5)-C(18)	1.408(3)	C(29)-H(29A)	0.9900
C(6)-N(7)	1.404(3)	C(29)-H(29B)	0.9900
C(6)-C(11)	1.369(3)	C(29)-C(30)	1.487(3)
N(7)-C(8)	1.276(3)	C(30)-H(30A)	0.9900
C(8)-C(9)	1.502(3)	C(30)-H(30B)	0.9900
C(8)-C(26)	1.509(3)	C(30)-C(31)	1.522(3)
C(9)-H(9)	1.0000	C(31)-H(31A)	0.9800
C(9)-O(10)	1.473(2)	C(31)-H(31B)	0.9800
C(9)-C(19)	1.510(3)	C(31)-H(31C)	0.9800
O(10)-C(11)	1.353(3)		
C(11)-C(12)	1.443(3)	C(2)-N(1)-C(18)	117.94(18)
C(12)-C(13)	1.402(3)	N(1)-C(2)-H(2)	118.0
C(12)-C(17)	1.409(3)	N(1)-C(2)-C(3)	124.0(2)
C(13)-H(13)	0.9500	C(3)-C(2)-H(2)	118.0
C(13)-C(14)	1.376(3)	C(2)-C(3)-H(3)	120.9
C(14)-H(14)	0.9500	C(4)-C(3)-C(2)	118.2(2)
C(14)-C(15)	1.396(3)	C(4)-C(3)-H(3)	120.9
C(15)-H(15)	0.9500	C(3)-C(4)-H(4)	120.1
C(15)-N(16)	1.327(3)	C(3)-C(4)-C(5)	119.7(2)
N(16)-C(17)	1.355(3)	C(5)-C(4)-H(4)	120.1
C(17)-C(18)	1.454(3)	C(4)-C(5)-C(6)	122.09(18)
C(19)-C(20)	1.396(3)	C(4)-C(5)-C(18)	118.2(2)
C(19)-C(25)	1.392(3)	C(18)-C(5)-C(6)	119.72(19)
C(20)-H(20)	0.9500	N(7)-C(6)-C(5)	118.59(18)
C(20)-C(21)	1.382(3)	C(11)-C(6)-C(5)	120.24(18)
C(21)-H(21)	0.9500	C(11)-C(6)-N(7)	120.65(19)
C(21)-C(22)	1.396(3)	C(8)-N(7)-C(6)	116.83(18)

N(7)-C(8)-C(9)	122.23(18)	C(20)-C(21)-H(21)	119.9
N(7)-C(8)-C(26)	116.99(18)	C(20)-C(21)-C(22)	120.2(2)
C(9)-C(8)-C(26)	120.48(18)	C(22)-C(21)-H(21)	119.9
C(8)-C(9)-H(9)	108.3	O(23)-C(22)-C(21)	117.96(19)
C(8)-C(9)-C(19)	111.75(18)	O(23)-C(22)-C(24)	123.30(19)
O(10)-C(9)-C(8)	108.75(16)	C(24)-C(22)-C(21)	118.7(2)
O(10)-C(9)-H(9)	108.3	C(22)-O(23)-H(23)	109.5
O(10)-C(9)-C(19)	111.29(16)	C(22)-C(24)-H(24)	119.8
C(19)-C(9)-H(9)	108.3	C(25)-C(24)-C(22)	120.3(2)
C(11)-O(10)-C(9)	114.12(16)	C(25)-C(24)-H(24)	119.8
C(6)-C(11)-C(12)	121.7(2)	C(19)-C(25)-H(25)	119.2
O(10)-C(11)-C(6)	121.14(18)	C(24)-C(25)-C(19)	121.6(2)
O(10)-C(11)-C(12)	116.96(18)	C(24)-C(25)-H(25)	119.2
C(13)-C(12)-C(11)	122.9(2)	O(27)-C(26)-C(8)	124.1(2)
C(13)-C(12)-C(17)	118.40(19)	O(27)-C(26)-O(28)	124.7(2)
C(17)-C(12)-C(11)	118.60(19)	O(28)-C(26)-C(8)	111.22(17)
C(12)-C(13)-H(13)	120.5	C(26)-O(28)-C(29)	114.48(16)
C(14)-C(13)-C(12)	119.0(2)	O(28)-C(29)-H(29A)	110.1
C(14)-C(13)-H(13)	120.5	O(28)-C(29)-H(29B)	110.1
C(13)-C(14)-H(14)	120.8	O(28)-C(29)-C(30)	108.10(17)
C(13)-C(14)-C(15)	118.5(2)	H(29A)-C(29)-H(29B)	108.4
C(15)-C(14)-H(14)	120.8	C(30)-C(29)-H(29A)	110.1
C(14)-C(15)-H(15)	117.8	C(30)-C(29)-H(29B)	110.1
N(16)-C(15)-C(14)	124.4(2)	C(29)-C(30)-H(30A)	109.7
N(16)-C(15)-H(15)	117.8	C(29)-C(30)-H(30B)	109.7
C(15)-N(16)-C(17)	117.3(2)	C(29)-C(30)-C(31)	109.61(19)
C(12)-C(17)-C(18)	119.87(18)	H(30A)-C(30)-H(30B)	108.2
N(16)-C(17)-C(12)	122.43(19)	C(31)-C(30)-H(30A)	109.7
N(16)-C(17)-C(18)	117.70(19)	C(31)-C(30)-H(30B)	109.7
N(1)-C(18)-C(5)	121.96(19)	C(30)-C(31)-H(31A)	109.5
N(1)-C(18)-C(17)	118.37(18)	C(30)-C(31)-H(31B)	109.5
C(5)-C(18)-C(17)	119.65(19)	C(30)-C(31)-H(31C)	109.5
C(20)-C(19)-C(9)	122.88(19)	H(31A)-C(31)-H(31B)	109.5
C(25)-C(19)-C(9)	119.54(19)	H(31A)-C(31)-H(31C)	109.5
C(25)-C(19)-C(20)	117.6(2)	H(31B)-C(31)-H(31C)	109.5
C(19)-C(20)-H(20)	119.2		
C(21)-C(20)-C(19)	121.5(2)		
C(21)-C(20)-H(20)	119.2		

Anisotropic displacement parameters ($Å^2 x\ 10^3$) for **3.3b**. The anisotropic displacement factor exponent takes the form: $-2\pi^2[\ h^2\ a^{*2} U^{11} + ...\ + 2\ h\ k\ a^*\ b^*\ U^{12}\ ]$

	U^{11}	U^{22}	U^{33}	U^{23}	U^{13}	U^{12}
N(1)	22(1)	19(1)	17(1)	-2(1)	3(1)	-4(1)
C(2)	22(1)	28(1)	15(1)	-1(1)	3(1)	-5(1)
C(3)	22(1)	23(1)	22(1)	1(1)	3(1)	2(1)
C(4)	23(1)	17(1)	20(1)	-1(1)	1(1)	-1(1)
C(5)	20(1)	17(1)	13(1)	0(1)	4(1)	-1(1)
C(6)	21(1)	16(1)	15(1)	-1(1)	4(1)	-1(1)
N(7)	19(1)	15(1)	21(1)	-1(1)	3(1)	-1(1)
C(8)	17(1)	19(1)	18(1)	-1(1)	4(1)	1(1)
C(9)	18(1)	15(1)	20(1)	-3(1)	0(1)	-3(1)
O(10)	20(1)	15(1)	22(1)	-3(1)	0(1)	1(1)
C(11)	19(1)	19(1)	13(1)	-1(1)	4(1)	-3(1)
C(12)	25(1)	16(1)	13(1)	1(1)	6(1)	-1(1)
C(13)	27(1)	20(1)	19(1)	2(1)	3(1)	1(1)
C(14)	36(1)	17(1)	25(1)	4(1)	6(1)	5(1)
C(15)	40(2)	12(1)	22(1)	-1(1)	8(1)	-2(1)
N(16)	33(1)	16(1)	17(1)	-1(1)	5(1)	-3(1)
C(17)	26(1)	15(1)	13(1)	1(1)	8(1)	-2(1)
C(18)	23(1)	18(1)	13(1)	-1(1)	7(1)	-4(1)
C(19)	17(1)	14(1)	19(1)	-3(1)	0(1)	-3(1)
C(20)	19(1)	14(1)	20(1)	1(1)	-4(1)	0(1)
C(21)	22(1)	14(1)	22(1)	-2(1)	4(1)	2(1)
C(22)	24(1)	16(1)	19(1)	0(1)	4(1)	1(1)
O(23)	32(1)	28(1)	20(1)	8(1)	7(1)	13(1)
C(24)	23(1)	19(1)	18(1)	3(1)	-1(1)	4(1)
C(25)	19(1)	17(1)	24(1)	-2(1)	0(1)	2(1)
C(26)	23(1)	19(1)	17(1)	2(1)	4(1)	0(1)
O(27)	33(1)	20(1)	37(1)	5(1)	-9(1)	-5(1)
O(28)	25(1)	17(1)	28(1)	2(1)	-4(1)	-6(1)
C(29)	32(1)	16(1)	26(1)	2(1)	3(1)	-5(1)
C(30)	26(1)	19(1)	38(2)	4(1)	0(1)	-2(1)
C(31)	28(1)	22(1)	43(2)	3(1)	-6(1)	-5(1)

Hydrogen coordinates (x 10^4) and isotropic displacement parameters ($Å^2$x 10^3) for **3.3b**.

	x	y	z	U(eq)
H(2)	13183	7197	5457	26
H(3)	12663	5837	5241	27
H(4)	9357	5413	4588	24
H(9)	833	5699	2962	22
H(13)	1774	8155	3451	26
H(14)	2540	9479	3782	31
H(15)	5963	9781	4423	29
H(20)	6416	5261	2758	22
H(21)	8123	5327	1742	23
H(23)	6009	6316	327	40
H(24)	2769	6588	846	24
H(25)	1070	6501	1860	24
H(29A)	184	3252	3569	29
H(29B)	1340	3177	2863	29
H(30A)	-1934	3683	2234	33
H(30B)	-3085	3805	2936	33
H(31A)	-1846	2286	2420	47
H(31B)	-4391	2603	2394	47
H(31C)	-2982	2405	3123	47

Torsion angles [°] for **3.3b**.

N(1)-C(2)-C(3)-C(4)	-0.7(3)	O(10)-C(9)-C(19)-C(25)	-70.3(2)
C(2)-N(1)-C(18)-C(5)	0.0(3)	O(10)-C(11)-C(12)-C(13)	1.5(3)
C(2)-N(1)-C(18)-C(17)	178.50(19)	O(10)-C(11)-C(12)-C(17)	178.46(18)
C(2)-C(3)-C(4)-C(5)	-0.2(3)	C(11)-C(6)-N(7)-C(8)	16.8(3)
C(3)-C(4)-C(5)-C(6)	-178.4(2)	C(11)-C(12)-C(13)-C(14)	177.4(2)
C(3)-C(4)-C(5)-C(18)	1.0(3)	C(11)-C(12)-C(17)-N(16)	-178.88(19)
C(4)-C(5)-C(6)-N(7)	11.6(3)	C(11)-C(12)-C(17)-C(18)	0.2(3)
C(4)-C(5)-C(6)-C(11)	-176.5(2)	C(12)-C(13)-C(14)-C(15)	0.6(3)
C(4)-C(5)-C(18)-N(1)	-0.9(3)	C(12)-C(17)-C(18)-N(1)	179.33(19)
C(4)-C(5)-C(18)-C(17)	-179.38(19)	C(12)-C(17)-C(18)-C(5)	-2.1(3)
C(5)-C(6)-N(7)-C(8)	-171.34(19)	C(13)-C(12)-C(17)-N(16)	-1.8(3)
C(5)-C(6)-C(11)-O(10)	179.62(18)	C(13)-C(12)-C(17)-C(18)	177.27(19)
C(5)-C(6)-C(11)-C(12)	-6.1(3)	C(13)-C(14)-C(15)-N(16)	-0.4(4)
C(6)-C(5)-C(18)-N(1)	178.55(19)	C(14)-C(15)-N(16)-C(17)	-0.8(3)
C(6)-C(5)-C(18)-C(17)	0.1(3)	C(15)-N(16)-C(17)-C(12)	2.0(3)
C(6)-N(7)-C(8)-C(9)	8.4(3)	C(15)-N(16)-C(17)-C(18)	-177.13(19)
C(6)-N(7)-C(8)-C(26)	-177.86(18)	N(16)-C(17)-C(18)-N(1)	-1.5(3)
C(6)-C(11)-C(12)-C(13)	-173.0(2)	N(16)-C(17)-C(18)-C(5)	177.02(19)
C(6)-C(11)-C(12)-C(17)	4.0(3)	C(17)-C(12)-C(13)-C(14)	0.5(3)
N(7)-C(6)-C(11)-O(10)	-8.7(3)	C(18)-N(1)-C(2)-C(3)	0.8(3)
N(7)-C(6)-C(11)-C(12)	165.59(19)	C(18)-C(5)-C(6)-N(7)	-167.82(19)
N(7)-C(8)-C(9)-O(10)	-37.9(3)	C(18)-C(5)-C(6)-C(11)	4.0(3)
N(7)-C(8)-C(9)-C(19)	85.4(2)	C(19)-C(9)-O(10)-C(11)	-80.2(2)
N(7)-C(8)-C(26)-O(27)	-5.7(3)	C(19)-C(20)-C(21)-C(22)	0.4(3)
N(7)-C(8)-C(26)-O(28)	176.00(19)	C(20)-C(19)-C(25)-C(24)	-1.9(3)
C(8)-C(9)-O(10)-C(11)	43.4(2)	C(20)-C(21)-C(22)-O(23)	177.62(19)
C(8)-C(9)-C(19)-C(20)	-12.0(3)	C(20)-C(21)-C(22)-C(24)	-1.7(3)
C(8)-C(9)-C(19)-C(25)	167.95(18)	C(21)-C(22)-C(24)-C(25)	1.3(3)
C(8)-C(26)-O(28)-C(29)	176.54(18)	C(22)-C(24)-C(25)-C(19)	0.6(3)
C(9)-C(8)-C(26)-O(27)	168.1(2)	O(23)-C(22)-C(24)-C(25)	-178.0(2)
C(9)-C(8)-C(26)-O(28)	-10.2(3)	C(25)-C(19)-C(20)-C(21)	1.4(3)
C(9)-O(10)-C(11)-C(6)	-23.5(3)	C(26)-C(8)-C(9)-O(10)	148.60(18)
C(9)-O(10)-C(11)-C(12)	161.97(17)	C(26)-C(8)-C(9)-C(19)	-88.1(2)
C(9)-C(19)-C(20)-C(21)	-178.59(19)	C(26)-O(28)-C(29)-C(30)	171.71(19)
C(9)-C(19)-C(25)-C(24)	178.12(19)	O(27)-C(26)-O(28)-C(29)	-1.7(3)
O(10)-C(9)-C(19)-C(20)	109.8(2)	O(28)-C(29)-C(30)-C(31)	-177.2(2)

Hydrogen bonds for **3.3b** [Å and °].

D-H...A	d(D-H)	d(H...A)	d(D...A)	<(DHA)
C(3)-H(3)...O(27)#1	0.95	2.51	3.184(3)	128
C(15)-H(15)...O(23)#2	0.95	2.50	3.365(3)	151
O(23)-H(23)...N(1)#3	0.84	2.02	2.763(2)	148
O(23)-H(23)...N(16)#3	0.84	2.62	3.305(3)	140

Symmetry transformations used to generate equivalent atoms:
#1 -x+2,-y+1,-z+1 #2 -x+3/2,y+1/2,-z+1/2 #3 x-1/2,-y+3/2,z-1/2

3.3c

A clear yellow block-like specimen of $C_{27}H_{25}N_3O_4$, approximate dimensions 0.100 mm x 0.120 mm x 0.270 mm, was used for the X-ray crystallographic analysis. The X-ray intensity data were measured at 100(2)K with an Oxford Cryosystems low temperature device using a MiTeGen micromount. See Table 1 for collection parameters and exposure time. Bruker APEX software was used to correct for Lorentz and polarization effects.

A total of 1532 frames were collected. The total exposure time was 18.28 hours. The frames were integrated with the Bruker SAINT software package using a narrow-frame algorithm. The integration of the data using a monoclinic unit cell yielded a total of 31792 reflections to a maximum θ angle of 26.09° (0.81 Å resolution), of which 4522 were independent (average redundancy 7.031, completeness = 99.5%, R_{int} = 3.56%, R_{sig} = 2.53%) and 3412 (75.45%) were greater than $2\sigma(F^2)$. The final cell constants of a = 26.313(5) Å, b = 9.7065(19) Å, c = 21.789(4) Å, β = 124.545(4)°, volume = 4583.8(15) $Å^3$, are based upon the refinement of the XYZ-centroids of 9710 reflections above 20 σ(I) with 6.21° < 2θ < 52.09°. Data were corrected for absorption effects using the Multi-Scan method (SADABS). The ratio of minimum to maximum apparent transmission was 0.953. The calculated minimum and maximum transmission coefficients (based on crystal size) are 0.7103 and 0.7453.

The structure was solved with the XT structure solution program using Intrinsic Phasing and refined with the XL refinement package using Least Squares minimisation with Olex2, using the space group C2/c, with Z = 8 for the formula unit, $C_{27}H_{25}N_3O_4$.The final anisotropic full-matrix least-squares refinement on F^2 with 449 variables converged at R1 = 5.01%, for the observed data and wR2 = 13.42% for all data. The goodness-of-fit was 1.047. The largest peak in the final difference electron density synthesis was 0.462 $e^-/Å^3$ and the largest hole was -0.241 $e^-/Å^3$ with an RMS deviation of 0.073 $e^-/Å^3$. On the basis of the final model, the calculated density was 1.320 g/cm^3 and F(000), 1920 e^-.

Refinement Note: Phenol ring disordered and modelled in two positions (56:44% occupancy) with restraints (SIMU) and constraints (EADP). Aliphatic hexyl chain was also disordered and modelled in 3 positions (50:25:25%) with restraints (SADI, SIMU).

Crystal Data for $C_{27}H_{25}N_3O_4$ (*M* =455.50 g/mol): monoclinic, space group C2/c (no. 15), *a* = 26.313(5) Å, *b* = 9.7065(19) Å, *c* = 21.789(4) Å, *β* = 124.545(4)°, *V* = 4583.8(15) $Å^3$, *Z* = 8, *T* = 100(2) K, μ(MoKα) = 0.090 mm^{-1}, *Dcalc* = 1.320 g/cm^3, 31792 reflections measured (5.58° ≤ 2Θ ≤ 52.178°), 4522 unique (R_{int} = 0.0356, R_{sigma} = 0.0253) which were used in all calculations. The final R_1 was 0.0501 (I > 2σ(I)) and wR_2 was 0.1342 (all data).

Crystal data and structure refinement for **3.3c**.

Empirical formula	$C_{27}H_{25}N_3O_4$	
Formula weight	455.50	
Temperature	100(2) K	
Wavelength	0.71073 Å	
Crystal system	Monoclinic	
Space group	C2/c	
Unit cell dimensions	a = 26.313(5) Å	α= 90°.

	b = 9.7065(19) Å β= 124.545(4)°.
	c = 21.789(4) Å ɣ = 90°.
Volume	4583.8(15) $Å^3$
Z	8
Density (calculated)	1.320 Mg/m^3
Absorption coefficient	0.090 mm^{-1}
F(000)	1920
Crystal size	0.27 x 0.12 x 0.1 mm^3
Theta range for data collection	2.790 to 26.089°.
Index ranges	-32≤h≤31, -11≤k≤11, -26≤l≤26
Reflections collected	31792
Independent reflections	4522 [R(int) = 0.0356]
Completeness to theta = 25.242°	99.9 %
Absorption correction	Semi-empirical from equivalents
Max. and min. transmission	0.7453 and 0.7103
Refinement method	Full-matrix least-squares on F^2
Data / restraints / parameters	4522 / 176 / 449
Goodness-of-fit on F^2	1.047
Final R indices [I>2σ(I)]	R1 = 0.0501, wR2 = 0.1198
R indices (all data)	R1 = 0.0708, wR2 = 0.1342
Extinction coefficient	0.0014(2)
Largest diff. peak and hole	0.462 and -0.241 $e.Å^{-3}$

Atomic coordinates (x 10^4) and equivalent isotropic displacement parameters ($Å^2$x 10^3) for **3.3c**. U(eq) is defined as one third of the trace of the orthogonalized

U^{ij} tensor.

	x	y	z	U(eq)
O(10)	6111(1)	7308(1)	3754(1)	31(1)
O(23)	7651(3)	6495(6)	7227(3)	50(1)
O(23A)	7725(4)	5875(7)	7239(5)	50(1)
O(27)	6264(1)	2386(2)	3636(1)	50(1)
O(28)	7061(1)	3824(1)	4020(1)	40(1)
N(1)	3650(1)	6925(2)	2754(1)	32(1)
N(7)	5571(1)	4678(2)	3483(1)	30(1)
N(16)	4177(1)	9436(2)	2936(1)	32(1)
C(2)	3391(1)	5701(2)	2650(1)	34(1)
C(3)	3705(1)	4460(2)	2779(1)	34(1)
C(4)	4317(1)	4494(2)	3032(1)	32(1)
C(5)	4609(1)	5775(2)	3154(1)	28(1)
C(6)	5250(1)	5888(2)	3413(1)	27(1)
C(8)	6152(1)	4798(2)	3775(1)	31(1)
C(9)	6516(1)	6115(2)	4109(1)	33(1)
C(11)	5514(1)	7154(2)	3529(1)	28(1)
C(12)	5170(1)	8402(2)	3379(1)	27(1)
C(13)	5430(1)	9715(2)	3483(1)	31(1)
C(14)	5062(1)	10850(2)	3308(1)	33(1)
C(15)	4439(1)	10652(2)	3031(1)	34(1)
C(17)	4537(1)	8311(2)	3106(1)	27(1)
C(18)	4256(1)	6970(2)	3003(1)	27(1)
C(19)	6804(4)	6328(8)	4939(6)	28(2)
C(19A)	6875(6)	5917(9)	4949(7)	22(2)
C(20)	7428(7)	6040(20)	5426(12)	24(2)
C(20A)	7516(10)	6090(30)	5419(15)	24(2)
C(21)	7730(11)	6070(30)	6181(17)	32(2)
C(21A)	7796(14)	6090(40)	6190(20)	32(2)
C(22)	7391(3)	6424(6)	6485(4)	36(1)
C(22A)	7466(4)	5883(8)	6479(5)	34(2)
C(24)	6766(2)	6768(6)	6002(2)	49(1)
C(24A)	6835(2)	5700(6)	6021(2)	32(1)
C(25)	6481(2)	6706(6)	5243(2)	44(1)
C(25A)	6541(2)	5687(5)	5262(2)	25(1)

C(26)	6485(1)	3522(2)	3799(1)	36(1)
C(29)	7427(1)	2668(2)	4054(1)	50(1)
C(30)	8039(2)	3340(6)	4287(4)	30(1)
C(30A)	8136(4)	3064(13)	4584(6)	42(3)
C(30B)	7935(3)	3048(9)	3922(5)	34(2)
C(31)	8452(2)	2145(4)	4385(2)	33(1)
C(31A)	8247(4)	3969(11)	4072(5)	48(2)
C(31B)	8406(4)	3966(9)	4578(5)	41(2)
C(32)	9098(2)	2615(7)	4649(3)	41(1)
C(32A)	8988(4)	3973(12)	4575(8)	50(3)
C(32B)	8916(5)	4565(12)	4495(8)	50(3)
C(33)	9540(2)	1378(5)	4885(2)	46(1)
C(33A)	9369(5)	2591(15)	4868(8)	55(3)
C(33B)	9387(4)	3383(12)	4755(5)	46(2)
C(34)	10186(2)	1808(7)	5172(2)	60(2)
C(34A)	10036(5)	2911(13)	5074(5)	53(2)
C(34B)	10030(4)	3934(14)	5008(6)	63(3)

Bond lengths [Å] and angles [°] for **3.3c**.

O(10)-C(9)	1.463(2)	C(3)-H(3)	0.9500
O(10)-C(11)	1.3642(19)	C(3)-C(4)	1.376(2)
O(23)-H(23)	0.8400	C(4)-H(4)	0.9500
O(23)-C(22)	1.353(10)	C(4)-C(5)	1.405(3)
O(23A)-H(23A)	0.8400	C(5)-C(6)	1.447(2)
O(23A)-C(22A)	1.388(13)	C(5)-C(18)	1.403(3)
O(27)-C(26)	1.202(2)	C(6)-C(11)	1.363(2)
O(28)-C(26)	1.338(2)	C(8)-C(9)	1.513(3)
O(28)-C(29)	1.452(2)	C(8)-C(26)	1.500(3)
N(1)-C(2)	1.323(2)	C(9)-H(9B)	1.0000
N(1)-C(18)	1.363(2)	C(9)-H(9A)	1.0000
N(7)-C(6)	1.405(2)	C(9)-C(19)	1.528(11)
N(7)-C(8)	1.285(2)	C(9)-C(19A)	1.523(13)
N(16)-C(15)	1.323(2)	C(11)-C(12)	1.435(3)
N(16)-C(17)	1.351(2)	C(12)-C(13)	1.403(3)
C(2)-H(2)	0.9500	C(12)-C(17)	1.419(2)
C(2)-C(3)	1.395(3)	C(13)-H(13)	0.9500

C(13)-C(14)	1.370(3)	C(30A)-H(30D)	0.9900
C(14)-H(14)	0.9500	C(30A)-C(31A)	1.572(8)
C(14)-C(15)	1.403(2)	C(30B)-H(30E)	0.9900
C(15)-H(15)	0.9500	C(30B)-H(30F)	0.9900
C(17)-C(18)	1.450(2)	C(30B)-C(31B)	1.537(8)
C(19)-C(20)	1.386(18)	C(31)-H(31A)	0.9900
C(19)-C(25)	1.390(12)	C(31)-H(31B)	0.9900
C(19A)-C(20A)	1.40(2)	C(31)-C(32)	1.525(6)
C(19A)-C(25A)	1.404(15)	C(31A)-H(31C)	0.9900
C(20)-H(20)	0.9500	C(31A)-H(31D)	0.9900
C(20)-C(21)	1.36(4)	C(31A)-C(32A)	1.606(8)
C(20A)-H(20A)	0.9500	C(31B)-H(31E)	0.9900
C(20A)-C(21A)	1.41(5)	C(31B)-H(31F)	0.9900
C(21)-H(21)	0.9500	C(31B)-C(32B)	1.562(8)
C(21)-C(22)	1.42(4)	C(32)-H(32A)	0.9900
C(21A)-H(21A)	0.9500	C(32)-H(32B)	0.9900
C(21A)-C(22A)	1.34(5)	C(32)-C(33)	1.542(7)
C(22)-C(24)	1.399(8)	C(32A)-H(32C)	0.9900
C(22A)-C(24A)	1.381(10)	C(32A)-H(32D)	0.9900
C(24)-H(24)	0.9500	C(32A)-C(33A)	1.578(9)
C(24)-C(25)	1.376(5)	C(32B)-H(32E)	0.9900
C(24A)-H(24A)	0.9500	C(32B)-H(32F)	0.9900
C(24A)-C(25A)	1.372(6)	C(32B)-C(33B)	1.542(8)
C(25)-H(25)	0.9500	C(33)-H(33A)	0.9900
C(25A)-H(25A)	0.9500	C(33)-H(33B)	0.9900
C(29)-H(29C)	0.9900	C(33)-C(34)	1.501(6)
C(29)-H(29D)	0.9900	C(33A)-H(33C)	0.9900
C(29)-H(29E)	0.9900	C(33A)-H(33D)	0.9900
C(29)-H(29F)	0.9900	C(33A)-C(34A)	1.575(9)
C(29)-H(29A)	0.9900	C(33B)-H(33E)	0.9900
C(29)-H(29B)	0.9900	C(33B)-H(33F)	0.9900
C(29)-C(30)	1.533(6)	C(33B)-C(34B)	1.548(8)
C(29)-C(30A)	1.587(8)	C(34)-H(34A)	0.9800
C(29)-C(30B)	1.565(7)	C(34)-H(34B)	0.9800
C(30)-H(30A)	0.9900	C(34)-H(34C)	0.9800
C(30)-H(30B)	0.9900	C(34A)-H(34D)	0.9800
C(30)-C(31)	1.520(6)	C(34A)-H(34E)	0.9800
C(30A)-H(30C)	0.9900	C(34A)-H(34F)	0.9800

C(34B)-H(34G)	0.9800	C(19)-C(9)-H(9A)	108.9
C(34B)-H(34H)	0.9800	C(19A)-C(9)-H(9B)	106.8
C(34B)-H(34I)	0.9800	O(10)-C(11)-C(12)	115.99(15)
		C(6)-C(11)-O(10)	121.92(16)
C(11)-O(10)-C(9)	116.62(13)	C(6)-C(11)-C(12)	121.98(15)
C(22)-O(23)-H(23)	109.5	C(13)-C(12)-C(11)	122.93(15)
C(22A)-O(23A)-H(23A)	109.5	C(13)-C(12)-C(17)	118.29(16)
C(26)-O(28)-C(29)	115.56(16)	C(17)-C(12)-C(11)	118.78(16)
C(2)-N(1)-C(18)	117.98(16)	C(12)-C(13)-H(13)	120.6
C(8)-N(7)-C(6)	116.89(16)	C(14)-C(13)-C(12)	118.86(15)
C(15)-N(16)-C(17)	117.23(14)	C(14)-C(13)-H(13)	120.6
N(1)-C(2)-H(2)	118.2	C(13)-C(14)-H(14)	120.7
N(1)-C(2)-C(3)	123.54(15)	C(13)-C(14)-C(15)	118.58(17)
C(3)-C(2)-H(2)	118.2	C(15)-C(14)-H(14)	120.7
C(2)-C(3)-H(3)	120.5	N(16)-C(15)-C(14)	124.53(18)
C(4)-C(3)-C(2)	118.94(17)	N(16)-C(15)-H(15)	117.7
C(4)-C(3)-H(3)	120.5	C(14)-C(15)-H(15)	117.7
C(3)-C(4)-H(4)	120.4	N(16)-C(17)-C(12)	122.49(16)
C(3)-C(4)-C(5)	119.15(18)	N(16)-C(17)-C(18)	117.82(14)
C(5)-C(4)-H(4)	120.4	C(12)-C(17)-C(18)	119.69(16)
C(4)-C(5)-C(6)	122.13(16)	N(1)-C(18)-C(5)	122.41(16)
C(18)-C(5)-C(4)	117.98(15)	N(1)-C(18)-C(17)	117.96(16)
C(18)-C(5)-C(6)	119.88(16)	C(5)-C(18)-C(17)	119.62(14)
N(7)-C(6)-C(5)	118.45(15)	C(20)-C(19)-C(9)	117.1(12)
C(11)-C(6)-N(7)	121.36(14)	C(20)-C(19)-C(25)	117.8(12)
C(11)-C(6)-C(5)	119.99(16)	C(25)-C(19)-C(9)	125.0(7)
N(7)-C(8)-C(9)	124.45(17)	C(20A)-C(19A)-C(9)	122.2(15)
N(7)-C(8)-C(26)	116.66(17)	C(20A)-C(19A)-C(25A)	119.3(15)
C(26)-C(8)-C(9)	118.87(14)	C(25A)-C(19A)-C(9)	118.2(9)
O(10)-C(9)-C(8)	109.98(13)	C(19)-C(20)-H(20)	118.4
O(10)-C(9)-H(9B)	106.8	C(21)-C(20)-C(19)	123.2(19)
O(10)-C(9)-H(9A)	108.9	C(21)-C(20)-H(20)	118.4
O(10)-C(9)-C(19)	104.0(3)	C(19A)-C(20A)-H(20A)	120.9
O(10)-C(9)-C(19A)	120.3(4)	C(19A)-C(20A)-C(21A)	118(2)
C(8)-C(9)-H(9B)	106.8	C(21A)-C(20A)-H(20A)	120.9
C(8)-C(9)-H(9A)	108.9	C(20)-C(21)-H(21)	120.8
C(8)-C(9)-C(19)	115.9(4)	C(20)-C(21)-C(22)	118.4(18)
C(8)-C(9)-C(19A)	105.3(4)	C(22)-C(21)-H(21)	120.8

C(20A)-C(21A)-H(21A)	119.4	C(30A)-C(29)-H(29E)	109.9
C(22A)-C(21A)-C(20A)	121(2)	C(30A)-C(29)-H(29F)	109.9
C(22A)-C(21A)-H(21A)	119.4	C(30B)-C(29)-H(29A)	108.6
O(23)-C(22)-C(21)	122.9(12)	C(30B)-C(29)-H(29B)	108.6
O(23)-C(22)-C(24)	118.0(6)	C(29)-C(30)-H(30A)	110.8
C(24)-C(22)-C(21)	119.1(12)	C(29)-C(30)-H(30B)	110.8
C(21A)-C(22A)-O(23A)	123.0(16)	H(30A)-C(30)-H(30B)	108.9
C(21A)-C(22A)-C(24A)	121.1(16)	C(31)-C(30)-C(29)	104.8(4)
C(24A)-C(22A)-O(23A)	115.9(8)	C(31)-C(30)-H(30A)	110.8
C(22)-C(24)-H(24)	120.0	C(31)-C(30)-H(30B)	110.8
C(25)-C(24)-C(22)	120.1(5)	C(29)-C(30A)-H(30C)	111.0
C(25)-C(24)-H(24)	120.0	C(29)-C(30A)-H(30D)	111.0
C(22A)-C(24A)-H(24A)	120.1	H(30C)-C(30A)-H(30D)	109.0
C(25A)-C(24A)-C(22A)	119.8(5)	C(31A)-C(30A)-C(29)	103.6(7)
C(25A)-C(24A)-H(24A)	120.1	C(31A)-C(30A)-H(30C)	111.0
C(19)-C(25)-H(25)	119.3	C(31A)-C(30A)-H(30D)	111.0
C(24)-C(25)-C(19)	121.3(5)	C(29)-C(30B)-H(30E)	110.4
C(24)-C(25)-H(25)	119.3	C(29)-C(30B)-H(30F)	110.4
C(19A)-C(25A)-H(25A)	119.9	H(30E)-C(30B)-H(30F)	108.6
C(24A)-C(25A)-C(19A)	120.3(6)	C(31B)-C(30B)-C(29)	106.7(7)
C(24A)-C(25A)-H(25A)	119.9	C(31B)-C(30B)-H(30E)	110.4
O(27)-C(26)-O(28)	124.54(19)	C(31B)-C(30B)-H(30F)	110.4
O(27)-C(26)-C(8)	124.89(16)	C(30)-C(31)-H(31A)	109.1
O(28)-C(26)-C(8)	110.57(17)	C(30)-C(31)-H(31B)	109.1
O(28)-C(29)-H(29C)	111.1	C(30)-C(31)-C(32)	112.4(4)
O(28)-C(29)-H(29D)	111.1	H(31A)-C(31)-H(31B)	107.9
O(28)-C(29)-H(29E)	109.9	C(32)-C(31)-H(31A)	109.1
O(28)-C(29)-H(29F)	109.9	C(32)-C(31)-H(31B)	109.1
O(28)-C(29)-H(29A)	108.6	C(30A)-C(31A)-H(31C)	111.9
O(28)-C(29)-H(29B)	108.6	C(30A)-C(31A)-H(31D)	111.9
O(28)-C(29)-C(30)	103.2(3)	C(30A)-C(31A)-C(32A)	99.2(8)
O(28)-C(29)-C(30A)	108.7(6)	H(31C)-C(31A)-H(31D)	109.6
O(28)-C(29)-C(30B)	114.8(4)	C(32A)-C(31A)-H(31C)	111.9
H(29C)-C(29)-H(29D)	109.1	C(32A)-C(31A)-H(31D)	111.9
H(29E)-C(29)-H(29F)	108.3	C(30B)-C(31B)-H(31E)	108.8
H(29A)-C(29)-H(29B)	107.6	C(30B)-C(31B)-H(31F)	108.8
C(30)-C(29)-H(29C)	111.1	C(30B)-C(31B)-C(32B)	113.6(8)
C(30)-C(29)-H(29D)	111.1	H(31E)-C(31B)-H(31F)	107.7

C(32B)-C(31B)-H(31E)	108.8	C(33)-C(34)-H(34A)	109.5
C(32B)-C(31B)-H(31F)	108.8	C(33)-C(34)-H(34B)	109.5
C(31)-C(32)-H(32A)	109.4	C(33)-C(34)-H(34C)	109.5
C(31)-C(32)-H(32B)	109.4	H(34A)-C(34)-H(34B)	109.5
C(31)-C(32)-C(33)	111.1(5)	H(34A)-C(34)-H(34C)	109.5
H(32A)-C(32)-H(32B)	108.0	H(34B)-C(34)-H(34C)	109.5
C(33)-C(32)-H(32A)	109.4	C(33A)-C(34A)-H(34D)	109.5
C(33)-C(32)-H(32B)	109.4	C(33A)-C(34A)-H(34E)	109.5
C(31A)-C(32A)-H(32C)	107.0	C(33A)-C(34A)-H(34F)	109.5
C(31A)-C(32A)-H(32D)	107.0	H(34D)-C(34A)-H(34E)	109.5
H(32C)-C(32A)-H(32D)	106.7	H(34D)-C(34A)-H(34F)	109.5
C(33A)-C(32A)-C(31A)	121.4(9)	H(34E)-C(34A)-H(34F)	109.5
C(33A)-C(32A)-H(32C)	107.0	C(33B)-C(34B)-H(34G)	109.5
C(33A)-C(32A)-H(32D)	107.0	C(33B)-C(34B)-H(34H)	109.5
C(31B)-C(32B)-H(32E)	110.9	C(33B)-C(34B)-H(34I)	109.5
C(31B)-C(32B)-H(32F)	110.9	H(34G)-C(34B)-H(34H)	109.5
H(32E)-C(32B)-H(32F)	108.9	H(34G)-C(34B)-H(34I)	109.5
C(33B)-C(32B)-C(31B)	104.2(8)	H(34H)-C(34B)-H(34I)	109.5
C(33B)-C(32B)-H(32E)	110.9		
C(33B)-C(32B)-H(32F)	110.9		
C(32)-C(33)-H(33A)	109.1		
C(32)-C(33)-H(33B)	109.1		
H(33A)-C(33)-H(33B)	107.8		
C(34)-C(33)-C(32)	112.6(5)		
C(34)-C(33)-H(33A)	109.1		
C(34)-C(33)-H(33B)	109.1		
C(32A)-C(33A)-H(33C)	110.2		
C(32A)-C(33A)-H(33D)	110.2		
H(33C)-C(33A)-H(33D)	108.5		
C(34A)-C(33A)-C(32A)	107.3(11)		
C(34A)-C(33A)-H(33C)	110.2		
C(34A)-C(33A)-H(33D)	110.2		
C(32B)-C(33B)-H(33E)	109.4		
C(32B)-C(33B)-H(33F)	109.4		
C(32B)-C(33B)-C(34B)	111.3(9)		
H(33E)-C(33B)-H(33F)	108.0		
C(34B)-C(33B)-H(33E)	109.4		
C(34B)-C(33B)-H(33F)	109.4		

Anisotropic displacement parameters ($Å^2 x\ 10^3$) for **3.3c**. The anisotropic displacement factor exponent takes the form: $-2\pi^2[\ h^2\ a^{*2} U^{11} + ...\ + 2\ h\ k\ a^*\ b^*\ U^{12}\ ]$

	U^{11}	U^{22}	U^{33}	U^{23}	U^{13}	U^{12}
O(10)	20(1)	47(1)	28(1)	-1(1)	15(1)	-6(1)
O(23)	32(2)	83(4)	24(1)	17(3)	10(1)	-19(3)
O(23A)	32(2)	83(4)	24(1)	17(3)	10(1)	-19(3)
O(27)	31(1)	44(1)	71(1)	20(1)	27(1)	2(1)
O(28)	24(1)	48(1)	50(1)	10(1)	22(1)	2(1)
N(1)	21(1)	50(1)	26(1)	-16(1)	14(1)	-10(1)
N(7)	23(1)	46(1)	23(1)	4(1)	15(1)	-2(1)
N(16)	24(1)	43(1)	27(1)	-9(1)	14(1)	-7(1)
C(2)	23(1)	51(1)	32(1)	-20(1)	18(1)	-14(1)
C(3)	29(1)	46(1)	34(1)	-18(1)	21(1)	-15(1)
C(4)	28(1)	43(1)	28(1)	-11(1)	19(1)	-8(1)
C(5)	23(1)	44(1)	19(1)	-10(1)	14(1)	-8(1)
C(6)	21(1)	42(1)	19(1)	-4(1)	13(1)	-4(1)
C(8)	23(1)	49(1)	23(1)	10(1)	14(1)	-1(1)
C(9)	20(1)	54(1)	28(1)	7(1)	15(1)	-3(1)
C(11)	21(1)	46(1)	19(1)	-6(1)	13(1)	-7(1)
C(12)	23(1)	43(1)	18(1)	-8(1)	13(1)	-8(1)
C(13)	23(1)	48(1)	21(1)	-5(1)	13(1)	-9(1)
C(14)	30(1)	40(1)	27(1)	-3(1)	16(1)	-9(1)
C(15)	27(1)	42(1)	31(1)	-6(1)	14(1)	-6(1)
C(17)	23(1)	42(1)	18(1)	-10(1)	13(1)	-7(1)
C(18)	21(1)	45(1)	18(1)	-12(1)	12(1)	-8(1)
C(19)	17(3)	37(4)	28(2)	10(3)	10(2)	0(3)
C(19A)	19(3)	28(4)	25(3)	6(3)	16(2)	4(3)
C(20)	17(4)	23(2)	33(1)	9(1)	16(3)	1(3)
C(20A)	17(4)	23(2)	33(1)	9(1)	16(3)	1(3)
C(21)	21(4)	34(1)	32(1)	13(1)	9(3)	-1(2)
C(21A)	21(4)	34(1)	32(1)	13(1)	9(3)	-1(2)
C(22)	28(2)	49(3)	27(2)	10(3)	13(2)	-8(3)
C(22A)	25(3)	49(4)	23(2)	10(3)	10(2)	-9(3)

C(24)	24(2)	93(4)	32(2)	5(2)	18(1)	-5(2)
C(24A)	23(2)	54(3)	26(2)	6(2)	17(2)	-8(2)
C(25)	20(2)	81(4)	29(2)	8(2)	12(1)	2(2)
C(25A)	16(2)	35(3)	22(2)	4(2)	10(1)	-3(2)
C(26)	24(1)	51(1)	33(1)	16(1)	16(1)	1(1)
C(29)	32(1)	48(1)	74(2)	12(1)	32(1)	5(1)
C(30)	29(3)	29(3)	38(4)	1(3)	22(3)	8(2)
C(30A)	35(5)	54(6)	44(6)	17(5)	26(4)	8(4)
C(30B)	26(4)	35(5)	37(5)	5(4)	16(4)	8(3)
C(31)	29(2)	43(2)	28(2)	9(2)	17(1)	16(2)
C(31A)	36(4)	75(6)	32(4)	7(4)	18(3)	-2(4)
C(31B)	38(4)	54(5)	35(4)	-3(4)	23(3)	-5(4)
C(32)	32(2)	63(3)	26(2)	-1(2)	16(2)	14(3)
C(32A)	40(5)	61(7)	58(5)	-1(5)	33(4)	-5(5)
C(32B)	40(4)	66(6)	55(5)	-12(5)	33(4)	-15(4)
C(33)	35(2)	79(3)	30(2)	13(2)	22(2)	27(2)
C(33A)	52(6)	62(7)	48(6)	8(6)	26(5)	14(7)
C(33B)	31(4)	72(6)	40(5)	-25(5)	22(4)	-19(5)
C(34)	32(2)	122(5)	28(2)	10(3)	18(2)	22(3)
C(34A)	65(6)	68(7)	35(5)	12(5)	32(4)	23(6)
C(34B)	33(4)	122(10)	38(5)	-16(6)	22(4)	-15(6)

Hydrogen coordinates (x 10^4) and isotropic displacement parameters (Å^{2}x 10^3) for **3.3c**.

	x	y	z	U(eq)
H(23)	8023	6720	7448	74
H(23A)	8109	5773	7473	74
H(2)	2970	5666	2479	41
H(3)	3498	3606	2694	41
H(4)	4540	3663	3123	38
H(9B)	6826	6151	3982	40
H(9A)	6849	6153	4020	40
H(13)	5854	9815	3671	37

H(14)	5226	11752	3373	39
H(15)	4187	11447	2902	41
H(20)	7655	5815	5223	28
H(20A)	7755	6204	5221	28
H(21)	8157	5856	6497	39
H(21A)	8228	6249	6521	39
H(24)	6539	7046	6198	59
H(24A)	6605	5583	6231	39
H(25)	6055	6925	4920	53
H(25A)	6109	5521	4947	30
H(29C)	7228	2213	3563	60
H(29D)	7489	1981	4427	60
H(29E)	7317	2450	3549	60
H(29F)	7342	1845	4251	60
H(29A)	7146	1980	3676	60
H(29B)	7628	2228	4550	60
H(30A)	7978	3981	3898	36
H(30B)	8220	3854	4760	36
H(30C)	8222	3595	5021	50
H(30D)	8399	2230	4759	50
H(30E)	8138	2204	3904	40
H(30F)	7751	3548	3445	40
H(31A)	8262	1655	3904	39
H(31B)	8482	1487	4751	39
H(31C)	8075	4908	4000	58
H(31D)	8075	3533	3580	58
H(31E)	8607	3422	5043	49
H(31F)	8185	4740	4623	49
H(32A)	9259	3251	5076	49
H(32B)	9080	3123	4242	49
H(32C)	9118	4460	4286	60
H(32D)	9122	4549	5017	60
H(32E)	8741	4815	3971	60
H(32F)	9110	5390	4812	60
H(33A)	9545	854	5278	55
H(33B)	9383	759	4452	55
H(33C)	9392	2257	5312	66
H(33D)	9170	1872	4478	66

H(33E)	9240	2720	4342	55
H(33F)	9421	2888	5174	55
H(34A)	10190	2247	4769	90
H(34B)	10454	995	5350	90
H(34C)	10336	2462	5583	90
H(34D)	10015	3092	4617	80
H(34E)	10305	2118	5333	80
H(34F)	10202	3722	5398	80
H(34G)	10004	4365	4584	95
H(34H)	10325	3169	5195	95
H(34I)	10169	4617	5404	95

Torsion angles [°] for **3.3c**.

O(10)-C(9)-C(19)-C(20)	-138.2(11)	C(2)-C(3)-C(4)-C(5)	0.0(2)
O(10)-C(9)-C(19)-C(25)	45.8(8)	C(3)-C(4)-C(5)-C(6)	-179.49(15)
O(10)-C(9)-C(19A)-C(20A)	-108.9(16)	C(3)-C(4)-C(5)-C(18)	-0.6(2)
O(10)-C(9)-C(19A)-C(25A)	64.8(8)	C(4)-C(5)-C(6)-N(7)	5.6(2)
O(10)-C(11)-C(12)-C(13)	-2.6(2)	C(4)-C(5)-C(6)-C(11)	-179.41(15)
O(10)-C(11)-C(12)-C(17)	176.74(13)	C(4)-C(5)-C(18)-N(1)	0.7(2)
O(23)-C(22)-C(24)-C(25)	-179.7(5)	C(4)-C(5)-C(18)-C(17)	-178.69(15)
O(23A)-C(22A)-C(24A)-C(25A)	-179.7(5)	C(5)-C(6)-C(11)-O(10)	-178.12(14)
		C(5)-C(6)-C(11)-C(12)	-2.0(2)
O(28)-C(29)-C(30)-C(31)	176.0(3)	C(6)-N(7)-C(8)-C(9)	6.0(2)
O(28)-C(29)-C(30A)-C(31A)	-80.0(9)	C(6)-N(7)-C(8)-C(26)	-175.86(13)
O(28)-C(29)-C(30B)-C(31B)	65.5(7)	C(6)-C(5)-C(18)-N(1)	179.63(14)
N(1)-C(2)-C(3)-C(4)	0.4(3)	C(6)-C(5)-C(18)-C(17)	0.3(2)
N(7)-C(6)-C(11)-O(10)	-3.3(2)	C(6)-C(11)-C(12)-C(13)	-178.89(15)
N(7)-C(6)-C(11)-C(12)	172.82(14)	C(6)-C(11)-C(12)-C(17)	0.4(2)
N(7)-C(8)-C(9)-O(10)	-27.4(2)	C(8)-N(7)-C(6)-C(5)	-174.18(14)
N(7)-C(8)-C(9)-C(19)	90.2(4)	C(8)-N(7)-C(6)-C(11)	10.9(2)
N(7)-C(8)-C(9)-C(19A)	103.6(5)	C(8)-C(9)-C(19)-C(20)	100.9(12)
N(7)-C(8)-C(26)-O(27)	-7.8(3)	C(8)-C(9)-C(19)-C(25)	-75.1(7)
N(7)-C(8)-C(26)-O(28)	171.60(14)	C(8)-C(9)-C(19A)-C(20A)	126.4(16)
N(16)-C(17)-C(18)-N(1)	-1.2(2)	C(8)-C(9)-C(19A)-C(25A)	-60.0(7)
N(16)-C(17)-C(18)-C(5)	178.18(14)	C(9)-O(10)-C(11)-C(6)	-20.6(2)
C(2)-N(1)-C(18)-C(5)	-0.2(2)	C(9)-O(10)-C(11)-C(12)	163.10(14)
C(2)-N(1)-C(18)-C(17)	179.14(15)	C(9)-C(8)-C(26)-O(27)	170.49(17)

C(9)-C(8)-C(26)-O(28)	-10.1(2)
C(9)-C(19)-C(20)-C(21)	-174.0(16)
C(9)-C(19)-C(25)-C(24)	174.7(5)
C(9)-C(19A)-C(20A)-C(21A)	170.5(19)
C(9)-C(19A)-C(25A)-C(24A)	-170.6(5)
C(11)-O(10)-C(9)-C(8)	32.97(18)
C(11)-O(10)-C(9)-C(19)	-91.8(5)
C(11)-O(10)-C(9)-C(19A)	-89.5(6)
C(11)-C(12)-C(13)-C(14)	178.48(15)
C(11)-C(12)-C(17)-N(16)	-178.51(14)
C(11)-C(12)-C(17)-C(18)	1.5(2)
C(12)-C(13)-C(14)-C(15)	-0.1(2)
C(12)-C(17)-C(18)-N(1)	178.76(14)
C(12)-C(17)-C(18)-C(5)	-1.9(2)
C(13)-C(12)-C(17)-N(16)	0.8(2)
C(13)-C(12)-C(17)-C(18)	-179.13(14)
C(13)-C(14)-C(15)-N(16)	1.3(3)
C(15)-N(16)-C(17)-C(12)	0.2(2)
C(15)-N(16)-C(17)-C(18)	-179.83(15)
C(17)-N(16)-C(15)-C(14)	-1.3(3)
C(17)-C(12)-C(13)-C(14)	-0.8(2)
C(18)-N(1)-C(2)-C(3)	-0.3(3)
C(18)-C(5)-C(6)-N(7)	-173.34(14)
C(18)-C(5)-C(6)-C(11)	1.7(2)
C(19)-C(20)-C(21)-C(22)	-1(3)
C(19A)-C(20A)-C(21A)-C(22A)	3(4)
C(20)-C(19)-C(25)-C(24)	-1.3(14)
C(20)-C(21)-C(22)-O(23)	-179.2(14)
C(20)-C(21)-C(22)-C(24)	-2(3)
C(20A)-C(19A)-C(25A)-C(24A)	3.2(17)
C(20A)-C(21A)-C(22A)-O(23A)	180(2)
C(20A)-C(21A)-C(22A)-C(24A)	-2(4)
C(21)-C(22)-C(24)-C(25)	2.7(15)
C(21A)-C(22A)-C(24A)-C(25A)	2(2)
C(22)-C(24)-C(25)-C(19)	-1.2(9)
C(22A)-C(24A)-C(25A)-C(19A)	-2.7(9)
C(25)-C(19)-C(20)-C(21)	2(2)
C(25A)-C(19A)-C(20A)-C(21A)	-3(3)
C(26)-O(28)-C(29)-C(30)	177.7(3)
C(26)-O(28)-C(29)-C(30A)	-159.8(4)
C(26)-O(28)-C(29)-C(30B)	151.2(4)
C(26)-C(8)-C(9)-O(10)	154.47(14)
C(26)-C(8)-C(9)-C(19)	-87.9(4)
C(26)-C(8)-C(9)-C(19A)	-74.5(5)
C(29)-O(28)-C(26)-O(27)	0.3(3)
C(29)-O(28)-C(26)-C(8)	-179.13(15)
C(29)-C(30)-C(31)-C(32)	-177.8(4)
C(29)-C(30A)-C(31A)-C(32A)	-166.0(9)
C(29)-C(30B)-C(31B)-C(32B)	-174.3(7)
C(30)-C(31)-C(32)-C(33)	169.2(4)
C(30A)-C(31A)-C(32A)-C(33A)	52.4(14)
C(30B)-C(31B)-C(32B)-C(33B)	-81.5(10)
C(31)-C(32)-C(33)-C(34)	-178.2(3)
C(31A)-C(32A)-C(33A)-C(34A)	159.7(11)
C(31B)-C(32B)-C(33B)-C(34B)	-157.6(8)

Hydrogen bonds for **3.3c** [Å and °].

D-H...A	d(D-H)	d(H...A)	d(D...A)	<(DHA)
O(23)-H(23)...N(1)#1	0.84	1.91	2.676(6)	151
O(23A)-H(23A)...N(1)#1	0.84	2.53	2.940(8)	111
O(23A)-H(23A)...N(16)#1	0.84	2.40	3.228(9)	170
C(14)-H(14)...O(27)#2	0.95	2.53	3.189(2)	127
C(21A)-H(21A)...O(10)#3	0.95	2.55	3.21(4)	126

Symmetry transformations used to generate equivalent atoms:

#1 x+1/2,-y+3/2,z+1/2 #2 x,y+1,z #3 -x+3/2,-y+3/2,-z+1

#4 -x+3/2,-y+1/2,-z+1

3.3e

A clear yellow plate-like specimen of $C_{33}H_{37}N_3O_4$, approximate dimensions 0.060 mm x 0.160 mm x 0.420 mm, was used for the X-ray crystallographic analysis. The X-ray intensity data were measured at 100(2)K on a Bruker D8 Quest ECO with an Oxford Cryostream low temperature device using a MiTeGen micromount. See Table 1 for collection parameters and exposure time. Bruker APEX software was used to correct for Lorentz and polarization effects.

A total of 1047 frames were collected. The total exposure time was 5.24 hours. The frames were integrated with the Bruker SAINT software package using a narrow-frame algorithm. The integration of the data using a monoclinic unit cell yielded a total of 53584 reflections to a maximum θ angle of 26.91° (0.79 Å resolution), of which 6045 were independent (average redundancy 8.864, completeness = 99.7%, R_{int} = 5.88%, R_{sig} = 3.06%) and 4665 (77.17%) were greater than $2\sigma(F^2)$. The final cell constants of a = 31.9437(14) Å, b = 9.7362(5) Å, c = 22.5164(10) Å, β = 126.9651(12)°, volume = 5595.3(5) $Å^3$, are based upon the refinement of the XYZ-centroids of 9927 reflections above 20 σ(I) with 5.434° < 2θ < 53.70°. Data were corrected for absorption effects using the Multi-Scan method (SADABS). The ratio of minimum to maximum apparent transmission was 0.924. The calculated minimum and maximum transmission coefficients (based on crystal size) are 0.6890 and 0.7454.

The structure was solved with the XT structure solution program using Intrinsic Phasing and refined with the XL refinement package using Least Squares minimisation with Olex2, using the space group C2/c, with Z = 8 for the formula unit, $C_{33}H_{37}N_3O_4$. The final anisotropic full-matrix least-squares refinement on F^2 with 351 variables converged at R1 = 4.67%, for the observed data and wR2 = 11.63% for all data. The goodness-of-fit was 1.053. The largest peak in the final difference electron density synthesis was 0.305 $e^-/Å^3$ and the largest hole was -0.276 $e^-/Å^3$ with an RMS deviation of 0.055 $e^-/Å^3$. On the basis of the final model, the calculated density was 1.281 g/cm^3 and F(000), 2304 e^-.

Crystal data and structure refinement for **3.3e**.

Empirical formula	$C_{33}H_{37}N_3O_4$	
Formula weight	539.65	
Temperature	100(2) K	
Wavelength	0.71073 Å	
Crystal system	Monoclinic	
Space group	C2/c	
Unit cell dimensions	a = 31.9437(14) Å	α= 90°.
	b = 9.7362(5) Å	β= 126.9651(12)°.
	c = 22.5164(10) Å	γ= 90°.
Volume	5595.3(5) $Å^3$	
Z	8	
Density (calculated)	1.281 Mg/m^3	
Absorption coefficient	0.085 mm^{-1}	
F(000)	2304	
Crystal size	0.42 x 0.16 x 0.06 mm^3	

Theta range for data collection	2.574 to 26.910°.
Index ranges	-40≤h≤40, -12≤k≤12, -28≤l≤28
Reflections collected	53584
Independent reflections	6045 [R(int) = 0.0588]
Completeness to theta = 25.242°	99.9 %
Absorption correction	Semi-empirical from equivalents
Max. and min. transmission	0.7454 and 0.6890
Refinement method	Full-matrix least-squares on F^2
Data / restraints / parameters	6045 / 0 / 351
Goodness-of-fit on F^2	1.053
Final R indices [I>2σ(I)]	R1 = 0.0467, wR2 = 0.1040
R indices (all data)	R1 = 0.0662, wR2 = 0.1163
Largest diff. peak and hole	0.305 and -0.276 e.$Å^{-3}$

Atomic coordinates (x 10^4) and equivalent isotropic displacement parameters ($Å^2$x 10^3) for **3.3e**. U(eq) is defined as one third of the trace of the orthogonalized U^{ij} tensor.

	x	y	z	U(eq)
O(10)	5167(1)	4691(1)	6428(1)	18(1)
O(23)	6570(1)	2959(2)	5389(1)	32(1)
O(27)	4831(1)	-190(1)	6131(1)	24(1)
O(28)	4595(1)	1252(1)	5192(1)	21(1)
N(1)	6282(1)	4376(1)	9482(1)	20(1)
N(7)	5333(1)	2077(1)	7079(1)	17(1)
N(16)	6050(1)	6857(1)	8806(1)	21(1)
C(2)	6389(1)	3162(2)	9807(1)	22(1)
C(3)	6228(1)	1913(2)	9425(1)	22(1)

C(4)	5947(1)	1926(2)	8665(1)	20(1)
C(5)	5835(1)	3191(2)	8298(1)	16(1)
C(6)	5546(1)	3286(2)	7502(1)	16(1)
C(8)	5103(1)	2186(2)	6380(1)	16(1)
C(9)	5093(1)	3470(2)	5993(1)	17(1)
C(11)	5446(1)	4543(2)	7174(1)	16(1)
C(12)	5600(1)	5798(2)	7593(1)	16(1)
C(13)	5471(1)	7108(2)	7261(1)	20(1)
C(14)	5632(1)	8249(2)	7704(1)	25(1)
C(15)	5922(1)	8069(2)	8473(1)	26(1)
C(17)	5888(1)	5720(2)	8375(1)	16(1)
C(18)	6009(1)	4391(2)	8734(1)	17(1)
C(19)	5493(1)	3383(2)	5842(1)	16(1)
C(20)	6015(1)	3036(2)	6397(1)	20(1)
C(21)	6372(1)	2920(2)	6243(1)	23(1)
C(22)	6213(1)	3134(2)	5523(1)	22(1)
C(24)	5693(1)	3472(2)	4963(1)	19(1)
C(25)	5340(1)	3588(2)	5125(1)	18(1)
C(26)	4834(1)	929(2)	5905(1)	18(1)
C(29)	4304(1)	171(2)	4640(1)	22(1)
C(30)	4091(1)	829(2)	3897(1)	24(1)
C(31)	3670(1)	1900(2)	3661(1)	26(1)
C(32)	3508(1)	2732(2)	2981(1)	27(1)
C(33)	3041(1)	3665(2)	2701(1)	31(1)
C(34)	2924(1)	4691(2)	2104(1)	33(1)
C(35)	2783(1)	4057(2)	1388(1)	28(1)
C(36)	2635(1)	5128(2)	798(1)	28(1)
C(37)	2492(1)	4518(2)	74(1)	29(1)
C(38)	2327(1)	5583(2)	-522(1)	27(1)
C(39)	2208(1)	4994(2)	-1232(1)	37(1)
C(40)	2012(1)	6053(2)	-1837(1)	43(1)

Bond lengths [Å] and angles [°] for **3.3e**.

O(10)-C(9)	1.4657(17)	O(27)-C(26)	1.2041(19)
O(10)-C(11)	1.3568(17)	O(28)-C(26)	1.3355(18)
O(23)-H(23)	0.8400	O(28)-C(29)	1.4588(18)
O(23)-C(22)	1.3533(19)	N(1)-C(2)	1.322(2)

N(1)-C(18)	1.3530(19)	C(29)-H(29B)	0.9900
N(7)-C(6)	1.4064(19)	C(29)-C(30)	1.517(2)
N(7)-C(8)	1.2814(19)	C(30)-H(30A)	0.9900
N(16)-C(15)	1.324(2)	C(30)-H(30B)	0.9900
N(16)-C(17)	1.354(2)	C(30)-C(31)	1.523(2)
C(2)-H(2)	0.9500	C(31)-H(31A)	0.9900
C(2)-C(3)	1.398(2)	C(31)-H(31B)	0.9900
C(3)-H(3)	0.9500	C(31)-C(32)	1.522(2)
C(3)-C(4)	1.373(2)	C(32)-H(32A)	0.9900
C(4)-H(4)	0.9500	C(32)-H(32B)	0.9900
C(4)-C(5)	1.404(2)	C(32)-C(33)	1.521(2)
C(5)-C(6)	1.442(2)	C(33)-H(33A)	0.9900
C(5)-C(18)	1.408(2)	C(33)-H(33B)	0.9900
C(6)-C(11)	1.364(2)	C(33)-C(34)	1.530(2)
C(8)-C(9)	1.512(2)	C(34)-H(34A)	0.9900
C(8)-C(26)	1.509(2)	C(34)-H(34B)	0.9900
C(9)-H(9)	1.0000	C(34)-C(35)	1.519(2)
C(9)-C(19)	1.509(2)	C(35)-H(35A)	0.9900
C(11)-C(12)	1.437(2)	C(35)-H(35B)	0.9900
C(12)-C(13)	1.408(2)	C(35)-C(36)	1.524(2)
C(12)-C(17)	1.415(2)	C(36)-H(36A)	0.9900
C(13)-H(13)	0.9500	C(36)-H(36B)	0.9900
C(13)-C(14)	1.370(2)	C(36)-C(37)	1.524(2)
C(14)-H(14)	0.9500	C(37)-H(37A)	0.9900
C(14)-C(15)	1.399(2)	C(37)-H(37B)	0.9900
C(15)-H(15)	0.9500	C(37)-C(38)	1.518(2)
C(17)-C(18)	1.450(2)	C(38)-H(38A)	0.9900
C(19)-C(20)	1.397(2)	C(38)-H(38B)	0.9900
C(19)-C(25)	1.392(2)	C(38)-C(39)	1.516(2)
C(20)-H(20)	0.9500	C(39)-H(39A)	0.9900
C(20)-C(21)	1.380(2)	C(39)-H(39B)	0.9900
C(21)-H(21)	0.9500	C(39)-C(40)	1.512(3)
C(21)-C(22)	1.393(2)	C(40)-H(40A)	0.9800
C(22)-C(24)	1.393(2)	C(40)-H(40B)	0.9800
C(24)-H(24)	0.9500	C(40)-H(40C)	0.9800
C(24)-C(25)	1.381(2)		
C(25)-H(25)	0.9500	C(11)-O(10)-C(9)	117.56(11)
C(29)-H(29A)	0.9900	C(22)-O(23)-H(23)	109.5

C(26)-O(28)-C(29)	117.75(12)	C(13)-C(14)-C(15)	118.59(15)
C(2)-N(1)-C(18)	117.23(14)	C(15)-C(14)-H(14)	120.7
C(8)-N(7)-C(6)	116.71(13)	N(16)-C(15)-C(14)	124.20(15)
C(15)-N(16)-C(17)	117.85(13)	N(16)-C(15)-H(15)	117.9
N(1)-C(2)-H(2)	118.0	C(14)-C(15)-H(15)	117.9
N(1)-C(2)-C(3)	124.07(14)	N(16)-C(17)-C(12)	122.07(14)
C(3)-C(2)-H(2)	118.0	N(16)-C(17)-C(18)	118.07(13)
C(2)-C(3)-H(3)	120.6	C(12)-C(17)-C(18)	119.85(14)
C(4)-C(3)-C(2)	118.80(15)	N(1)-C(18)-C(5)	123.21(14)
C(4)-C(3)-H(3)	120.6	N(1)-C(18)-C(17)	117.39(14)
C(3)-C(4)-H(4)	120.5	C(5)-C(18)-C(17)	119.39(13)
C(3)-C(4)-C(5)	119.07(15)	C(20)-C(19)-C(9)	121.92(13)
C(5)-C(4)-H(4)	120.5	C(25)-C(19)-C(9)	119.97(13)
C(4)-C(5)-C(6)	122.28(14)	C(25)-C(19)-C(20)	118.04(14)
C(4)-C(5)-C(18)	117.60(13)	C(19)-C(20)-H(20)	119.5
C(18)-C(5)-C(6)	120.11(13)	C(21)-C(20)-C(19)	121.07(14)
N(7)-C(6)-C(5)	118.35(13)	C(21)-C(20)-H(20)	119.5
C(11)-C(6)-N(7)	121.58(13)	C(20)-C(21)-H(21)	119.9
C(11)-C(6)-C(5)	119.82(13)	C(20)-C(21)-C(22)	120.20(15)
N(7)-C(8)-C(9)	125.06(14)	C(22)-C(21)-H(21)	119.9
N(7)-C(8)-C(26)	117.70(13)	O(23)-C(22)-C(21)	118.36(14)
C(26)-C(8)-C(9)	117.22(12)	O(23)-C(22)-C(24)	122.26(14)
O(10)-C(9)-C(8)	110.33(11)	C(24)-C(22)-C(21)	119.34(15)
O(10)-C(9)-H(9)	107.8	C(22)-C(24)-H(24)	120.0
O(10)-C(9)-C(19)	112.19(12)	C(25)-C(24)-C(22)	119.90(14)
C(8)-C(9)-H(9)	107.8	C(25)-C(24)-H(24)	120.0
C(19)-C(9)-C(8)	110.82(12)	C(19)-C(25)-H(25)	119.3
C(19)-C(9)-H(9)	107.8	C(24)-C(25)-C(19)	121.44(14)
O(10)-C(11)-C(6)	122.15(14)	C(24)-C(25)-H(25)	119.3
O(10)-C(11)-C(12)	115.65(13)	O(27)-C(26)-O(28)	125.20(14)
C(6)-C(11)-C(12)	122.07(13)	O(27)-C(26)-C(8)	125.49(13)
C(13)-C(12)-C(11)	123.15(13)	O(28)-C(26)-C(8)	109.31(13)
C(13)-C(12)-C(17)	118.17(14)	O(28)-C(29)-H(29A)	110.6
C(17)-C(12)-C(11)	118.67(13)	O(28)-C(29)-H(29B)	110.6
C(12)-C(13)-H(13)	120.4	O(28)-C(29)-C(30)	105.61(12)
C(14)-C(13)-C(12)	119.11(14)	H(29A)-C(29)-H(29B)	108.7
C(14)-C(13)-H(13)	120.4	C(30)-C(29)-H(29A)	110.6
C(13)-C(14)-H(14)	120.7	C(30)-C(29)-H(29B)	110.6

C(29)-C(30)-H(30A)	109.0	C(35)-C(36)-C(37)	113.73(15)
C(29)-C(30)-H(30B)	109.0	H(36A)-C(36)-H(36B)	107.7
C(29)-C(30)-C(31)	112.98(14)	C(37)-C(36)-H(36A)	108.8
H(30A)-C(30)-H(30B)	107.8	C(37)-C(36)-H(36B)	108.8
C(31)-C(30)-H(30A)	109.0	C(36)-C(37)-H(37A)	108.8
C(31)-C(30)-H(30B)	109.0	C(36)-C(37)-H(37B)	108.8
C(30)-C(31)-H(31A)	108.7	H(37A)-C(37)-H(37B)	107.7
C(30)-C(31)-H(31B)	108.7	C(38)-C(37)-C(36)	113.60(15)
H(31A)-C(31)-H(31B)	107.6	C(38)-C(37)-H(37A)	108.8
C(32)-C(31)-C(30)	114.21(14)	C(38)-C(37)-H(37B)	108.8
C(32)-C(31)-H(31A)	108.7	C(37)-C(38)-H(38A)	108.8
C(32)-C(31)-H(31B)	108.7	C(37)-C(38)-H(38B)	108.8
C(31)-C(32)-H(32A)	109.0	H(38A)-C(38)-H(38B)	107.6
C(31)-C(32)-H(32B)	109.0	C(39)-C(38)-C(37)	114.01(15)
H(32A)-C(32)-H(32B)	107.8	C(39)-C(38)-H(38A)	108.8
C(33)-C(32)-C(31)	113.01(14)	C(39)-C(38)-H(38B)	108.8
C(33)-C(32)-H(32A)	109.0	C(38)-C(39)-H(39A)	108.9
C(33)-C(32)-H(32B)	109.0	C(38)-C(39)-H(39B)	108.9
C(32)-C(33)-H(33A)	108.6	H(39A)-C(39)-H(39B)	107.7
C(32)-C(33)-H(33B)	108.6	C(40)-C(39)-C(38)	113.42(17)
C(32)-C(33)-C(34)	114.54(15)	C(40)-C(39)-H(39A)	108.9
H(33A)-C(33)-H(33B)	107.6	C(40)-C(39)-H(39B)	108.9
C(34)-C(33)-H(33A)	108.6	C(39)-C(40)-H(40A)	109.5
C(34)-C(33)-H(33B)	108.6	C(39)-C(40)-H(40B)	109.5
C(33)-C(34)-H(34A)	108.5	C(39)-C(40)-H(40C)	109.5
C(33)-C(34)-H(34B)	108.5	H(40A)-C(40)-H(40B)	109.5
H(34A)-C(34)-H(34B)	107.5	H(40A)-C(40)-H(40C)	109.5
C(35)-C(34)-C(33)	115.26(16)	H(40B)-C(40)-H(40C)	109.5
C(35)-C(34)-H(34A)	108.5		
C(35)-C(34)-H(34B)	108.5		
C(34)-C(35)-H(35A)	109.1		
C(34)-C(35)-H(35B)	109.1		
C(34)-C(35)-C(36)	112.69(15)		
H(35A)-C(35)-H(35B)	107.8		
C(36)-C(35)-H(35A)	109.1		
C(36)-C(35)-H(35B)	109.1		
C(35)-C(36)-H(36A)	108.8		
C(35)-C(36)-H(36B)	108.8		

Anisotropic displacement parameters ($Å^2 x\ 10^3$) for **3.3e**. The anisotropic displacement factor exponent takes the form: $-2\pi^2[\ h^2\ a^{*2}U^{11} + ...\ + 2\ h\ k\ a^*\ b^*\ U^{12}\ ]$

	U^{11}	U^{22}	U^{33}	U^{23}	U^{13}	U^{12}
O(10)	25(1)	17(1)	11(1)	1(1)	10(1)	3(1)
O(23)	24(1)	52(1)	24(1)	15(1)	17(1)	11(1)
O(27)	31(1)	18(1)	20(1)	1(1)	13(1)	0(1)
O(28)	25(1)	20(1)	14(1)	-1(1)	10(1)	-2(1)
N(1)	20(1)	27(1)	12(1)	2(1)	9(1)	1(1)
N(7)	18(1)	18(1)	16(1)	0(1)	10(1)	0(1)
N(16)	26(1)	21(1)	16(1)	-2(1)	13(1)	0(1)
C(2)	21(1)	32(1)	14(1)	4(1)	10(1)	2(1)
C(3)	23(1)	25(1)	20(1)	9(1)	13(1)	4(1)
C(4)	21(1)	21(1)	18(1)	2(1)	11(1)	1(1)
C(5)	16(1)	21(1)	14(1)	1(1)	10(1)	2(1)
C(6)	16(1)	18(1)	14(1)	-1(1)	10(1)	0(1)
C(8)	18(1)	17(1)	15(1)	1(1)	10(1)	2(1)
C(9)	20(1)	17(1)	12(1)	0(1)	8(1)	1(1)
C(11)	16(1)	23(1)	11(1)	1(1)	8(1)	2(1)
C(12)	16(1)	21(1)	14(1)	1(1)	10(1)	2(1)
C(13)	23(1)	22(1)	16(1)	2(1)	12(1)	2(1)
C(14)	33(1)	19(1)	22(1)	3(1)	17(1)	4(1)
C(15)	35(1)	20(1)	21(1)	-3(1)	16(1)	0(1)
C(17)	16(1)	21(1)	14(1)	1(1)	10(1)	2(1)
C(18)	16(1)	22(1)	14(1)	1(1)	10(1)	2(1)
C(19)	20(1)	14(1)	14(1)	0(1)	10(1)	-1(1)
C(20)	21(1)	24(1)	12(1)	2(1)	8(1)	0(1)
C(21)	18(1)	29(1)	17(1)	5(1)	8(1)	2(1)
C(22)	23(1)	24(1)	20(1)	5(1)	14(1)	2(1)
C(24)	23(1)	21(1)	14(1)	4(1)	11(1)	3(1)
C(25)	19(1)	17(1)	13(1)	2(1)	7(1)	2(1)
C(26)	18(1)	20(1)	15(1)	0(1)	9(1)	2(1)

C(29)	26(1)	20(1)	16(1)	-4(1)	10(1)	-2(1)
C(30)	28(1)	26(1)	16(1)	-3(1)	11(1)	0(1)
C(31)	24(1)	33(1)	18(1)	2(1)	12(1)	3(1)
C(32)	27(1)	32(1)	20(1)	2(1)	14(1)	3(1)
C(33)	30(1)	38(1)	24(1)	5(1)	16(1)	7(1)
C(34)	36(1)	32(1)	26(1)	4(1)	15(1)	8(1)
C(35)	25(1)	29(1)	22(1)	1(1)	10(1)	-2(1)
C(36)	28(1)	29(1)	22(1)	3(1)	12(1)	3(1)
C(37)	29(1)	28(1)	23(1)	2(1)	12(1)	0(1)
C(38)	23(1)	32(1)	24(1)	4(1)	12(1)	4(1)
C(39)	46(1)	33(1)	26(1)	2(1)	18(1)	2(1)
C(40)	49(1)	47(1)	29(1)	8(1)	21(1)	7(1)

Hydrogen coordinates (x 10^4) and isotropic displacement parameters (Å^{2}x 10^3) for **3.3e**.

	x	y	z	U(eq)
H(23)	6441	3222	4955	47
H(2)	6588	3138	10333	27
H(3)	6312	1069	9686	27
H(4)	5829	1091	8391	24
H(9)	4739	3535	5504	20
H(13)	5275	7199	6738	24
H(14)	5548	9144	7494	30
H(15)	6035	8867	8776	31
H(20)	6127	2876	6889	24
H(21)	6726	2694	6629	28
H(24)	5581	3623	4470	23
H(25)	4986	3813	4738	21
H(29A)	4015	-171	4645	27
H(29B)	4538	-608	4740	27
H(30A)	3943	104	3512	29
H(30B)	4383	1270	3928	29
H(31A)	3356	1429	3555	31
H(31B)	3800	2537	4081	31
H(32A)	3808	3300	3107	32

H(32B)	3419	2095	2578	32
H(33A)	3106	4182	3128	37
H(33B)	2727	3086	2497	37
H(34A)	2630	5286	1981	40
H(34B)	3234	5286	2314	40
H(35A)	2486	3417	1190	34
H(35B)	3086	3519	1499	34
H(36A)	2933	5768	999	34
H(36B)	2334	5668	691	34
H(37A)	2797	4005	178	35
H(37B)	2201	3855	-119	35
H(38A)	2012	6066	-642	33
H(38B)	2611	6272	-320	33
H(39A)	2530	4566	-1118	45
H(39B)	1941	4264	-1417	45
H(40A)	1962	5621	-2268	64
H(40B)	2268	6798	-1652	64
H(40C)	1677	6426	-1983	64

Torsion angles [°] for **3.3e**.

O(10)-C(9)-C(19)-C(20)	73.24(18)	C(2)-N(1)-C(18)-C(17)	179.57(14)
O(10)-C(9)-C(19)-C(25)	-109.86(15)	C(2)-C(3)-C(4)-C(5)	0.8(2)
O(10)-C(11)-C(12)-C(13)	0.4(2)	C(3)-C(4)-C(5)-C(6)	179.44(14)
O(10)-C(11)-C(12)-C(17)	179.34(13)	C(3)-C(4)-C(5)-C(18)	-1.6(2)
O(23)-C(22)-C(24)-C(25)	177.56(15)	C(4)-C(5)-C(6)-N(7)	5.3(2)
O(28)-C(29)-C(30)-C(31)	-68.47(17)	C(4)-C(5)-C(6)-C(11)	179.69(15)
N(1)-C(2)-C(3)-C(4)	0.8(3)	C(4)-C(5)-C(18)-N(1)	1.0(2)
N(7)-C(6)-C(11)-O(10)	-4.5(2)	C(4)-C(5)-C(18)-C(17)	-178.05(14)
N(7)-C(6)-C(11)-C(12)	171.21(14)	C(5)-C(6)-C(11)-O(10)	-178.65(13)
N(7)-C(8)-C(9)-O(10)	-24.9(2)	C(5)-C(6)-C(11)-C(12)	-3.0(2)
N(7)-C(8)-C(9)-C(19)	99.97(17)	C(6)-N(7)-C(8)-C(9)	6.6(2)
N(7)-C(8)-C(26)-O(27)	-2.8(2)	C(6)-N(7)-C(8)-C(26)	-175.20(13)
N(7)-C(8)-C(26)-O(28)	176.75(13)	C(6)-C(5)-C(18)-N(1)	179.99(14)
N(16)-C(17)-C(18)-N(1)	-0.6(2)	C(6)-C(5)-C(18)-C(17)	0.9(2)
N(16)-C(17)-C(18)-C(5)	178.49(14)	C(6)-C(11)-C(12)-C(13)	-175.53(15)
C(2)-N(1)-C(18)-C(5)	0.5(2)	C(6)-C(11)-C(12)-C(17)	3.4(2)

C(8)-N(7)-C(6)-C(5)	-176.23(13)
C(8)-N(7)-C(6)-C(11)	9.5(2)
C(8)-C(9)-C(19)-C(20)	-50.58(19)
C(8)-C(9)-C(19)-C(25)	126.32(15)
C(9)-O(10)-C(11)-C(6)	-16.2(2)
C(9)-O(10)-C(11)-C(12)	167.83(12)
C(9)-C(8)-C(26)-O(27)	175.61(15)
C(9)-C(8)-C(26)-O(28)	-4.87(18)
C(9)-C(19)-C(20)-C(21)	178.00(15)
C(9)-C(19)-C(25)-C(24)	-177.88(14)
C(11)-O(10)-C(9)-C(8)	28.23(17)
C(11)-O(10)-C(9)-C(19)	-95.86(15)
C(11)-C(12)-C(13)-C(14)	179.57(15)
C(11)-C(12)-C(17)-N(16)	179.49(14)
C(11)-C(12)-C(17)-C(18)	-1.6(2)
C(12)-C(13)-C(14)-C(15)	0.4(2)
C(12)-C(17)-C(18)-N(1)	-179.58(13)
C(12)-C(17)-C(18)-C(5)	-0.5(2)
C(13)-C(12)-C(17)-N(16)	-1.5(2)
C(13)-C(12)-C(17)-C(18)	177.37(14)
C(13)-C(14)-C(15)-N(16)	-0.7(3)
C(15)-N(16)-C(17)-C(12)	1.3(2)
C(15)-N(16)-C(17)-C(18)	-177.62(15)
C(17)-N(16)-C(15)-C(14)	-0.2(3)
C(17)-C(12)-C(13)-C(14)	0.6(2)
C(18)-N(1)-C(2)-C(3)	-1.4(2)
C(18)-C(5)-C(6)-N(7)	-173.60(13)
C(18)-C(5)-C(6)-C(11)	0.8(2)
C(19)-C(20)-C(21)-C(22)	-0.8(3)
C(20)-C(19)-C(25)-C(24)	-0.9(2)
C(20)-C(21)-C(22)-O(23)	-177.47(16)
C(20)-C(21)-C(22)-C(24)	0.3(3)
C(21)-C(22)-C(24)-C(25)	-0.1(2)
C(22)-C(24)-C(25)-C(19)	0.4(2)
C(25)-C(19)-C(20)-C(21)	1.0(2)
C(26)-O(28)-C(29)-C(30)	-178.72(13)
C(26)-C(8)-C(9)-O(10)	156.84(12)
C(26)-C(8)-C(9)-C(19)	-78.29(16)
C(29)-O(28)-C(26)-O(27)	0.3(2)
C(29)-O(28)-C(26)-C(8)	-179.19(12)
C(29)-C(30)-C(31)-C(32)	171.08(14)
C(30)-C(31)-C(32)-C(33)	172.80(15)
C(31)-C(32)-C(33)-C(34)	170.23(16)
C(32)-C(33)-C(34)-C(35)	61.8(2)
C(33)-C(34)-C(35)-C(36)	176.13(15)
C(34)-C(35)-C(36)-C(37)	-179.90(16)
C(35)-C(36)-C(37)-C(38)	178.11(15)
C(36)-C(37)-C(38)-C(39)	177.30(16)
C(37)-C(38)-C(39)-C(40)	176.31(17)

Hydrogen bonds for **3.3e** [Å and °].

D-H...A	d(D-H)	d(H...A)	d(D...A)	<(DHA)
O(23)-H(23)...N(1)#1	0.84	2.49	3.0806(19)	128
O(23)-H(23)...N(16)#1	0.84	2.09	2.8928(17)	160

Symmetry transformations used to generate equivalent atoms:
#1 x,-y+1,z-1/2

3.4a

A clear pale yellow plate-like specimen of $C_{22}H_{13}N_3O_3$, approximate dimensions 0.060 mm x 0.080 mm x 0.130 mm, was used for the X-ray crystallographic analysis. The X-ray intensity data were measured at 100(2)K on a Bruker D8 Quest ECO with an Oxford Cryostream low temperature device using a MiTeGen micromount. See Table 1 for collection parameters and exposure time. Bruker APEX software was used to correct for Lorentz and polarization effects.

A total of 424 frames were collected. The total exposure time was 7.07 hours. The frames were integrated with the Bruker SAINT software package using a narrow-frame algorithm. The integration of the data using a monoclinic unit cell yielded a total of 10619 reflections to a maximum θ angle of 25.69° (0.82 Å resolution), of which 3144 were independent (average redundancy 3.378, completeness = 99.8%, R_{int} = 11.23%, R_{sig} = 10.11%) and 1637 (52.07%) were greater than $2\sigma(F^2)$. The final cell constants of a = 11.2937(10) Å, b = 16.2786(15) Å, c = 9.2757(10) Å, β = 103.225(3)°, volume = 1660.1(3) $Å^3$, are based upon the refinement of the XYZ-centroids of 1647 reflections above 20 σ(I) with 5.718° < 2θ < 50.79°. Data were corrected for absorption effects using the Multi-Scan method (SADABS). The ratio of minimum to maximum apparent transmission was 0.909. The calculated minimum and maximum transmission coefficients (based on crystal size) are 0.6775 and 0.7453.

The structure was solved with the XT structure solution program using Intrinsic Phasing and refined with the XL refinement package using Least Squares minimisation with Olex2, using the space group $P2_1/c$, with Z = 4 for the formula unit, $C_{22}H_{13}N_3O_3$. The final anisotropic full-matrix least-squares refinement on F^2 with 254 variables converged at R1 = 6.03%, for the observed data and wR2 = 14.99% for all data. The goodness-of-fit was 0.993. The largest peak in the final difference electron density synthesis was 0.260 $e^-/Å^3$ and the largest hole was -0.275 $e^-/Å^3$ with an RMS deviation of 0.065 $e^-/Å^3$. On the basis of the final model, the calculated density was 1.470 g/cm^3 and F(000), 760 e^-.

Crystal Data for $C_{22}H_{13}N_3O_3$ (*M* =367.35 g/mol): monoclinic, space group $P2_1/c$ (no. 14), *a* = 11.2937(10) Å, *b* = 16.2786(15) Å, *c* = 9.2757(10) Å, *β* = 103.225(3)°, *V* = 1660.1(3) $Å^3$, *Z* = 4, *T* = 100(2) K, μ(MoKα) = 0.101 mm^{-1}, *Dcalc* = 1.470 g/cm^3, 10619 reflections measured (6.228° ≤ 2Θ ≤ 51.374°), 3144 unique (R_{int} = 0.1123, R_{sigma} = 0.1011) which were used in all calculations. The final R_1 was 0.0603 (I > 2σ(I)) and wR_2 was 0.1499 (all data).

Crystal data and structure refinement for **3.3e**.

Empirical formula	$C_{22}H_{13}N_3O_3$	
Formula weight	367.35	
Temperature	100(2) K	
Wavelength	0.71073 Å	
Crystal system	Monoclinic	
Space group	$P2_1/c$	
Unit cell dimensions	a = 11.2937(10) Å	α= 90°.
	b = 16.2786(15) Å	β= 103.225(3)°.
	c = 9.2757(10) Å	ɣ = 90°.
Volume	1660.1(3) $Å^3$	
Z	4	
Density (calculated)	1.470 Mg/m^3	

Absorption coefficient	0.101 mm^{-1}
F(000)	760
Crystal size	0.13 x 0.08 x 0.06 mm^3
Theta range for data collection	3.114 to 25.687°.
Index ranges	-13≤h≤13, -19≤k≤19, -11≤l≤11
Reflections collected	10619
Independent reflections	3144 [R(int) = 0.1123]
Completeness to theta = 25.242°	99.8 %
Absorption correction	Semi-empirical from equivalents
Max. and min. transmission	0.7453 and 0.6775
Refinement method	Full-matrix least-squares on F^2
Data / restraints / parameters	3144 / 0 / 254
Goodness-of-fit on F^2	0.993
Final R indices [I>2σ(I)]	R1 = 0.0603, wR2 = 0.1181
R indices (all data)	R1 = 0.1408, wR2 = 0.1499
Largest diff. peak and hole	0.260 and -0.275 e.$Å^{-3}$

Atomic coordinates (x 10^4) and equivalent isotropic displacement parameters ($Å^2$x 10^3) for **3.4a**. U(eq) is defined as one third of the trace of the orthogonalized U^{ij} tensor.

	x	y	z	U(eq)
C(2)	1238(3)	3461(2)	-2102(4)	31(1)
C(3)	1462(3)	2651(2)	-2363(4)	31(1)
C(4)	2497(3)	2292(2)	-1555(4)	27(1)

C(5)	3293(3)	2764(2)	-509(4)	20(1)
C(6)	4385(3)	2377(2)	445(4)	21(1)
C(7)	5154(3)	2906(2)	1601(4)	21(1)
C(8)	4896(3)	3756(2)	1639(4)	20(1)
C(9)	5681(3)	4249(2)	2683(4)	21(1)
C(10)	5412(3)	5095(2)	2702(4)	22(1)
C(11)	4441(3)	5389(2)	1689(4)	25(1)
C(13)	3878(3)	4125(2)	666(4)	21(1)
C(14)	3026(3)	3596(2)	-359(4)	21(1)
C(17)	6808(3)	3031(2)	3548(4)	19(1)
C(18)	6686(3)	3869(2)	3678(4)	20(1)
C(19)	7508(3)	4362(2)	4843(4)	22(1)
C(20)	7575(3)	4196(2)	6329(4)	25(1)
C(21)	8295(3)	4677(2)	7400(4)	29(1)
C(22)	8955(3)	5324(2)	7004(4)	29(1)
C(23)	8891(3)	5489(2)	5534(4)	29(1)
C(24)	8167(3)	5012(2)	4452(4)	25(1)
C(25)	7858(3)	2577(2)	4515(4)	22(1)
C(28)	8445(3)	1378(2)	5913(4)	27(1)
N(1)	1997(3)	3943(2)	-1146(3)	29(1)
N(12)	3673(2)	4924(2)	670(3)	25(1)
N(16)	6061(2)	2548(2)	2540(3)	21(1)
O(15)	4637(2)	1657(1)	293(3)	26(1)
O(26)	8899(2)	2806(1)	4771(3)	32(1)
O(27)	7491(2)	1872(1)	5009(3)	25(1)

Bond lengths [Å] and angles [°] for **3.4a**.

C(2)-H(2)	0.9500	C(6)-C(7)	1.490(5)
C(2)-C(3)	1.374(5)	C(6)-O(15)	1.222(4)
C(2)-N(1)	1.337(4)	C(7)-C(8)	1.415(4)
C(3)-H(3)	0.9500	C(7)-N(16)	1.319(4)
C(3)-C(4)	1.368(5)	C(8)-C(9)	1.406(4)
C(4)-H(4)	0.9500	C(8)-C(13)	1.422(4)
C(4)-C(5)	1.394(5)	C(9)-C(10)	1.411(4)
C(5)-C(6)	1.484(4)	C(9)-C(18)	1.429(4)
C(5)-C(14)	1.400(4)	C(10)-H(10)	0.9500

C(10)-C(11)	1.357(4)	C(4)-C(5)-C(14)	118.9(3)
C(11)-H(11)	0.9500	C(14)-C(5)-C(6)	121.3(3)
C(11)-N(12)	1.358(4)	C(5)-C(6)-C(7)	116.8(3)
C(13)-C(14)	1.467(4)	O(15)-C(6)-C(5)	121.5(3)
C(13)-N(12)	1.322(4)	O(15)-C(6)-C(7)	121.7(3)
C(14)-N(1)	1.347(4)	C(8)-C(7)-C(6)	119.6(3)
C(17)-C(18)	1.379(4)	N(16)-C(7)-C(6)	117.1(3)
C(17)-C(25)	1.507(4)	N(16)-C(7)-C(8)	123.3(3)
C(17)-N(16)	1.358(4)	C(7)-C(8)-C(13)	122.6(3)
C(18)-C(19)	1.489(4)	C(9)-C(8)-C(7)	118.3(3)
C(19)-C(20)	1.390(5)	C(9)-C(8)-C(13)	119.1(3)
C(19)-C(24)	1.387(5)	C(8)-C(9)-C(10)	117.5(3)
C(20)-H(20)	0.9500	C(8)-C(9)-C(18)	118.7(3)
C(20)-C(21)	1.375(5)	C(10)-C(9)-C(18)	123.8(3)
C(21)-H(21)	0.9500	C(9)-C(10)-H(10)	120.7
C(21)-C(22)	1.388(5)	C(11)-C(10)-C(9)	118.6(3)
C(22)-H(22)	0.9500	C(11)-C(10)-H(10)	120.7
C(22)-C(23)	1.375(5)	C(10)-C(11)-H(11)	117.6
C(23)-H(23)	0.9500	C(10)-C(11)-N(12)	124.9(3)
C(23)-C(24)	1.381(5)	N(12)-C(11)-H(11)	117.6
C(24)-H(24)	0.9500	C(8)-C(13)-C(14)	118.6(3)
C(25)-O(26)	1.203(4)	N(12)-C(13)-C(8)	122.1(3)
C(25)-O(27)	1.336(4)	N(12)-C(13)-C(14)	119.4(3)
C(28)-H(28A)	0.9800	C(5)-C(14)-C(13)	120.5(3)
C(28)-H(28B)	0.9800	N(1)-C(14)-C(5)	122.1(3)
C(28)-H(28C)	0.9800	N(1)-C(14)-C(13)	117.4(3)
C(28)-O(27)	1.447(4)	C(18)-C(17)-C(25)	120.9(3)
		N(16)-C(17)-C(18)	125.1(3)
C(3)-C(2)-H(2)	117.8	N(16)-C(17)-C(25)	114.0(3)
N(1)-C(2)-H(2)	117.8	C(9)-C(18)-C(19)	120.4(3)
N(1)-C(2)-C(3)	124.4(3)	C(17)-C(18)-C(9)	116.9(3)
C(2)-C(3)-H(3)	120.6	C(17)-C(18)-C(19)	122.6(3)
C(4)-C(3)-C(2)	118.9(3)	C(20)-C(19)-C(18)	119.9(3)
C(4)-C(3)-H(3)	120.6	C(24)-C(19)-C(18)	120.3(3)
C(3)-C(4)-H(4)	120.7	C(24)-C(19)-C(20)	119.8(3)
C(3)-C(4)-C(5)	118.6(3)	C(19)-C(20)-H(20)	120.2
C(5)-C(4)-H(4)	120.7	C(21)-C(20)-C(19)	119.6(3)
C(4)-C(5)-C(6)	119.7(3)	C(21)-C(20)-H(20)	120.2

C(20)-C(21)-H(21)	119.8
C(20)-C(21)-C(22)	120.4(4)
C(22)-C(21)-H(21)	119.8
C(21)-C(22)-H(22)	120.0
C(23)-C(22)-C(21)	120.1(3)
C(23)-C(22)-H(22)	120.0
C(22)-C(23)-H(23)	120.0
C(22)-C(23)-C(24)	119.9(3)
C(24)-C(23)-H(23)	120.0
C(19)-C(24)-H(24)	119.9
C(23)-C(24)-C(19)	120.2(3)
C(23)-C(24)-H(24)	119.9
O(26)-C(25)-C(17)	124.5(3)
O(26)-C(25)-O(27)	124.3(3)
O(27)-C(25)-C(17)	111.2(3)
H(28A)-C(28)-H(28B)	109.5
H(28A)-C(28)-H(28C)	109.5
H(28B)-C(28)-H(28C)	109.5
O(27)-C(28)-H(28A)	109.5
O(27)-C(28)-H(28B)	109.5
O(27)-C(28)-H(28C)	109.5
C(2)-N(1)-C(14)	117.0(3)
C(13)-N(12)-C(11)	117.8(3)
C(7)-N(16)-C(17)	117.7(3)
C(25)-O(27)-C(28)	115.3(2)

Anisotropic displacement parameters ($Å^2 x\ 10^3$) for **3.4a**. The anisotropic displacement factor exponent takes the form: $-2\pi^2[\ h^2\ a^{*2}U^{11} + ...\ + 2\ h\ k\ a^*\ b^*\ U^{12}\ ]$

	U^{11}	U^{22}	U^{33}	U^{23}	U^{13}	U^{12}
C(2)	18(2)	35(2)	37(2)	6(2)	-3(2)	0(2)
C(3)	22(2)	30(2)	34(2)	2(2)	-4(2)	-4(2)
C(4)	27(2)	19(2)	32(2)	1(2)	3(2)	-2(2)
C(5)	17(2)	20(2)	25(2)	1(2)	5(2)	1(1)
C(6)	23(2)	20(2)	20(2)	3(2)	3(2)	0(1)
C(7)	17(2)	21(2)	23(2)	1(2)	4(2)	1(1)
C(8)	20(2)	18(2)	22(2)	0(2)	6(2)	3(1)
C(9)	20(2)	21(2)	22(2)	3(2)	5(2)	-1(2)
C(10)	23(2)	17(2)	26(2)	-4(2)	5(2)	0(1)
C(11)	28(2)	18(2)	31(2)	-1(2)	7(2)	6(2)
C(13)	20(2)	20(2)	22(2)	1(2)	4(2)	4(2)
C(14)	17(2)	21(2)	22(2)	3(2)	1(2)	0(1)
C(17)	16(2)	17(2)	23(2)	2(2)	2(2)	1(1)
C(18)	20(2)	19(2)	21(2)	2(2)	5(2)	0(1)
C(19)	18(2)	15(2)	30(2)	-2(2)	2(2)	2(1)
C(20)	21(2)	23(2)	29(2)	2(2)	3(2)	-1(2)
C(21)	23(2)	36(2)	25(2)	3(2)	0(2)	2(2)
C(22)	19(2)	26(2)	38(2)	-11(2)	-2(2)	-1(2)
C(23)	27(2)	25(2)	34(2)	0(2)	2(2)	-5(2)
C(24)	26(2)	23(2)	24(2)	-2(2)	1(2)	0(2)
C(25)	20(2)	20(2)	25(2)	-1(2)	0(2)	0(2)
C(28)	27(2)	22(2)	27(2)	5(2)	-4(2)	3(2)
N(1)	24(2)	27(2)	31(2)	4(1)	-2(2)	2(1)
N(12)	24(2)	22(2)	29(2)	1(1)	6(1)	4(1)
N(16)	17(2)	18(1)	25(2)	1(1)	1(1)	0(1)
O(15)	27(1)	18(1)	31(2)	0(1)	1(1)	2(1)
O(26)	21(1)	25(1)	44(2)	7(1)	-2(1)	0(1)
O(27)	21(1)	21(1)	30(1)	6(1)	-1(1)	2(1)

Hydrogen coordinates (x 10^4) and isotropic displacement parameters ($Å^2$x 10^3) for **3.4a**.

	x	y	z	U(eq)
H(2)	496	3694	-2636	37
H(3)	906	2346	-3091	37
H(4)	2671	1731	-1705	32
H(10)	5899	5451	3407	27
H(11)	4287	5963	1694	31
H(20)	7126	3752	6603	30
H(21)	8341	4565	8417	35
H(22)	9452	5654	7749	34
H(23)	9344	5932	5264	35
H(24)	8119	5128	3436	30
H(28A)	9129	1337	5430	40
H(28B)	8130	828	6034	40
H(28C)	8720	1636	6887	40

Torsion angles [°] for **3.4a**.

C(2)-C(3)-C(4)-C(5)	-0.6(6)	C(6)-C(7)-C(8)-C(9)	-176.1(3)
C(3)-C(2)-N(1)-C(14)	-2.2(6)	C(6)-C(7)-C(8)-C(13)	4.0(5)
C(3)-C(4)-C(5)-C(6)	176.3(3)	C(6)-C(7)-N(16)-C(17)	176.5(3)
C(3)-C(4)-C(5)-C(14)	-2.3(5)	C(7)-C(8)-C(9)-C(10)	179.9(3)
C(4)-C(5)-C(6)-C(7)	-176.3(3)	C(7)-C(8)-C(9)-C(18)	-1.3(5)
C(4)-C(5)-C(6)-O(15)	3.3(5)	C(7)-C(8)-C(13)-C(14)	3.5(5)
C(4)-C(5)-C(14)-C(13)	-176.3(3)	C(7)-C(8)-C(13)-N(12)	-177.2(3)
C(4)-C(5)-C(14)-N(1)	3.1(5)	C(8)-C(7)-N(16)-C(17)	-2.8(5)
C(5)-C(6)-C(7)-C(8)	-6.7(5)	C(8)-C(9)-C(10)-C(11)	-2.1(5)
C(5)-C(6)-C(7)-N(16)	173.9(3)	C(8)-C(9)-C(18)-C(17)	-0.5(5)
C(5)-C(14)-N(1)-C(2)	-0.9(5)	C(8)-C(9)-C(18)-C(19)	-177.4(3)
C(6)-C(5)-C(14)-C(13)	5.2(5)	C(8)-C(13)-C(14)-C(5)	-8.1(5)
C(6)-C(5)-C(14)-N(1)	-175.4(3)	C(8)-C(13)-C(14)-N(1)	172.4(3)

C(8)-C(13)-N(12)-C(11)	-2.9(5)
C(9)-C(8)-C(13)-C(14)	-176.5(3)
C(9)-C(8)-C(13)-N(12)	2.8(5)
C(9)-C(10)-C(11)-N(12)	2.1(5)
C(9)-C(18)-C(19)-C(20)	116.0(4)
C(9)-C(18)-C(19)-C(24)	-61.0(4)
C(10)-C(9)-C(18)-C(17)	178.2(3)
C(10)-C(9)-C(18)-C(19)	1.3(5)
C(10)-C(11)-N(12)-C(13)	0.5(5)
C(13)-C(8)-C(9)-C(10)	-0.2(5)
C(13)-C(8)-C(9)-C(18)	178.6(3)
C(13)-C(14)-N(1)-C(2)	178.5(3)
C(14)-C(5)-C(6)-C(7)	2.2(5)
C(14)-C(5)-C(6)-O(15)	-178.2(3)
C(14)-C(13)-N(12)-C(11)	176.3(3)
C(17)-C(18)-C(19)-C(20)	-60.7(5)
C(17)-C(18)-C(19)-C(24)	122.3(4)
C(17)-C(25)-O(27)-C(28)	178.1(3)
C(18)-C(9)-C(10)-C(11)	179.2(3)
C(18)-C(17)-C(25)-O(26)	-44.9(5)
C(18)-C(17)-C(25)-O(27)	137.4(3)
C(18)-C(17)-N(16)-C(7)	0.7(5)
C(18)-C(19)-C(20)-C(21)	-177.1(3)
C(18)-C(19)-C(24)-C(23)	177.3(3)
C(19)-C(20)-C(21)-C(22)	-0.2(5)
C(20)-C(19)-C(24)-C(23)	0.3(5)
C(20)-C(21)-C(22)-C(23)	0.1(5)
C(21)-C(22)-C(23)-C(24)	0.1(5)
C(22)-C(23)-C(24)-C(19)	-0.4(5)
C(24)-C(19)-C(20)-C(21)	-0.1(5)
C(25)-C(17)-C(18)-C(9)	178.2(3)
C(25)-C(17)-C(18)-C(19)	-5.1(5)
C(25)-C(17)-N(16)-C(7)	-176.7(3)
N(1)-C(2)-C(3)-C(4)	3.1(6)
N(12)-C(13)-C(14)-C(5)	172.6(3)
N(12)-C(13)-C(14)-N(1)	-6.9(5)
N(16)-C(7)-C(8)-C(9)	3.2(5)
N(16)-C(7)-C(8)-C(13)	-176.7(3)
N(16)-C(17)-C(18)-C(9)	0.9(5)
N(16)-C(17)-C(18)-C(19)	177.7(3)
N(16)-C(17)-C(25)-O(26)	132.6(4)
N(16)-C(17)-C(25)-O(27)	-45.1(4)
O(15)-C(6)-C(7)-C(8)	173.7(3)
O(15)-C(6)-C(7)-N(16)	-5.7(5)
O(26)-C(25)-O(27)-C(28)	0.4(5)

Hydrogen bonds for **3.4a** [Å and °].

D-H...A	d(D-H)	d(H...A)	d(D...A)	<(DHA)
C(10)-H(10)...O(15)#1	0.95	2.45	3.158(4)	131

Symmetry transformations used to generate equivalent atoms:

#1 -x+1,y+1/2,-z+1/2

[Ag(**4.1**)(NO_3)]

A specimen of $C_{18}H_{11}AgN_6O_5$, approximate dimensions 0.050 mm x 0.120 mm x 0.130 mm, was used for the X-ray crystallographic analysis. The X-ray intensity data were measured at 100(2)K on a Bruker APEX Kappa Duo with an Oxford Cobra low temperature device using a MiTeGen micromount. See Table 1 for collection parameters and exposure time. Bruker APEX software was used to correct for Lorentz and polarization effects.

A total of 514 frames were collected. The total exposure time was 1.71 hours. The frames were integrated with the Bruker SAINT software package using a wide-frame algorithm. The integration of the data using a triclinic unit cell yielded a total of 11367 reflections to a maximum θ angle of 27.19° (0.78 Å resolution), of which 3790 were independent (average redundancy 2.999, completeness = 99.8%, R_{int} = 6.21%, R_{sig} = 7.59%) and 2908 (76.73%) were greater than $2\sigma(F^2)$. The final cell constants of a = 8.3219(15) Å, b = 10.3830(18) Å, c= 10.5249(19) Å, α = 73.092(2)°, β = 80.063(3)°, γ = 79.284(3)°, volume = 848.1(3) $Å^3$, are based upon the refinement of the XYZ-centroids of 3004 reflections above 20 σ(I) with 5.021° < 2θ < 54.12°. Data were corrected for absorption effects using the Multi-Scan method (SADABS). The ratio of minimum to maximum apparent transmission was 0.868. The calculated minimum and maximum transmission coefficients (based on crystal size) are 0.8560 and 0.9410.

The structure was solved with the XT structure solution program using Intrinsic Phasing and refined with the XL refinement package using Least Squares minimisation with Olex2, using the space group $P\bar{1}$, with Z = 2 for the formula unit, $C_{18}H_{11}AgN_6O_5$. The final anisotropic full-matrix least-squares refinement on F^2 with 275 variables converged at R1 = 4.19%, for the observed data and wR2 = 7.19% for all data. The goodness-of-fit was 1.025. The largest peak in the final difference electron density synthesis was 0.533 $e^-/Å^3$ and the largest hole was -0.875 $e^-/Å^3$ with an RMS deviation of 0.126 $e^-/Å^3$. On the basis of the final model, the calculated density was 1.955 g/cm^3 and F(000), 496 e^-.

Refinement Note: Amide hydrogen atom located and refined with restraints (DFIX). Refined distances: 2.6468 (0.0028) Å Ag1 - O28; 2.7822 (0.0027) Å Ag1 - O27.

Crystal Data for $C_{18}H_{11}AgN_6O_5$ (*M* =499.20 g/mol): triclinic, space group P-1 (no. 2), *a* = 8.3219(15) Å, *b* = 10.3830(18) Å, *c* = 10.5249(19) Å, *α* = 73.092(2)°, *β* = 80.063(3)°, *γ* = 79.284(3)°, *V* = 848.1(3) $Å^3$,*Z* = 2, *T* = 100(2) K, μ(MoKα) = 1.239 mm^{-1}, *Dcalc* = 1.955 g/cm^3, 11367 reflections measured (4.078° ≤ 2Θ ≤ 54.372°), 3790 unique (R_{int} = 0.0621, R_{sigma} = 0.0759) which were used in all calculations. The final R_1 was 0.0419 (I > 2σ(I)) and wR_2 was 0.0719 (all data).

Crystal data and structure refinement for [Ag(**4.1**)(NO_3)].

Empirical formula	$C_{18}H_{11}AgN_6O_5$
Formula weight	499.20
Temperature	100(2) K
Wavelength	0.71073 Å
Crystal system	Triclinic
Space group	$P\bar{1}$

Unit cell dimensions	a = 8.3219(15) Å	α= 73.092(2)°.
	b = 10.3830(18) Å	β= 80.063(3)°.
	c = 10.5249(19) Å	ɣ= 79.284(3)°.
Volume	848.1(3) $Å^3$	
Z	2	
Density (calculated)	1.955 Mg/m^3	
Absorption coefficient	1.239 mm^{-1}	
F(000)	496	
Crystal size	0.13 x 0.12 x 0.05 mm^3	
Theta range for data collection	2.039 to 27.186°.	
Index ranges	-10≤h≤10, -13≤k≤13, -13≤l≤13	
Reflections collected	11367	
Independent reflections	3790 [R(int) = 0.0621]	
Completeness to theta = 25.242°	100.0 %	
Absorption correction	Semi-empirical from equivalents	
Max. and min. transmission	0.7455 and 0.6472	
Refinement method	Full-matrix least-squares on F^2	
Data / restraints / parameters	3790 / 1 / 275	
Goodness-of-fit on F^2	1.025	
Final R indices [I>2σ(I)]	R1 = 0.0419, wR2 = 0.0659	
R indices (all data)	R1 = 0.0685, wR2 = 0.0719	
Largest diff. peak and hole	0.533 and -0.875 e.$Å^{-3}$	

Atomic coordinates (x 10^4) and equivalent isotropic displacement parameters

($Å^2 x\ 10^3$) for [Ag(**4.1**)(NO_3)]. U(eq) is defined as one third of the trace of the orthogonalized U^{ij} tensor.

	x	y	z	U(eq)
Ag(1)	105(1)	9396(1)	-2004(1)	20(1)
O(8)	5781(3)	8002(3)	2767(3)	25(1)
O(25)	5637(3)	3256(3)	3000(3)	26(1)
N(1)	2116(4)	8583(3)	-714(3)	16(1)
N(9)	5796(4)	5789(3)	2801(3)	18(1)
N(10)	6666(4)	5343(3)	3851(3)	18(1)
N(16)	9483(4)	1849(3)	7095(3)	16(1)
N(19)	8527(4)	-121(3)	6263(3)	17(1)
C(2)	2653(5)	9428(4)	-190(4)	17(1)
C(3)	3708(4)	8992(4)	786(3)	16(1)
C(4)	4284(4)	7605(4)	1219(3)	15(1)
C(5)	3764(4)	6729(4)	650(3)	17(1)
C(6)	2665(5)	7244(4)	-286(4)	17(1)
C(7)	5378(5)	7183(4)	2309(4)	18(1)
C(11)	7035(4)	4038(4)	4358(4)	16(1)
C(12)	8007(4)	3636(4)	5497(3)	15(1)
C(13)	8429(4)	4603(4)	6031(4)	18(1)
C(14)	9374(4)	4180(4)	7065(4)	17(1)
C(15)	9904(4)	2792(4)	7550(3)	17(1)
C(17)	8525(4)	2253(4)	6092(3)	14(1)
C(18)	8058(4)	1193(4)	5623(3)	16(1)
C(20)	8098(4)	-1094(4)	5848(4)	17(1)
C(21)	7215(4)	-841(4)	4771(4)	19(1)
C(22)	6718(4)	497(4)	4118(4)	19(1)
C(23)	7113(4)	1533(4)	4546(3)	16(1)
C(24)	6525(4)	2972(4)	3892(4)	17(1)
O(27)	-292(4)	6729(3)	-1758(3)	30(1)
O(28)	-1833(3)	7726(3)	-325(3)	30(1)
O(29)	-2245(4)	5747(3)	-374(3)	44(1)
N(26)	-1473(4)	6726(3)	-814(3)	23(1)

Bond lengths [Å] and angles [°] for [Ag(**4.1**)(NO_3)].

Ag(1)-N(1)	2.225(3)	C(20)-C(21)	1.391(5)
Ag(1)-N(16)#1	2.434(3)	C(21)-H(21)	0.9500
Ag(1)-N(19)#1	2.314(3)	C(21)-C(22)	1.379(5)
O(8)-C(7)	1.212(4)	C(22)-H(22)	0.9500
O(25)-C(24)	1.230(4)	C(22)-C(23)	1.391(5)
N(1)-C(2)	1.336(4)	C(23)-C(24)	1.480(5)
N(1)-C(6)	1.347(5)	O(27)-N(26)	1.271(4)
N(9)-N(10)	1.347(4)	O(28)-N(26)	1.255(4)
N(9)-C(7)	1.386(5)	O(29)-N(26)	1.236(4)
N(9)-H(9)	0.899(10)		
N(10)-C(11)	1.303(5)	N(1)-Ag(1)-N(16)#1	118.56(10)
N(16)-C(15)	1.331(4)	N(1)-Ag(1)-N(19)#1	163.08(10)
N(16)-C(17)	1.354(4)	N(19)#1-Ag(1)-N(16)#1	70.24(10)
N(19)-C(18)	1.351(4)	C(2)-N(1)-Ag(1)	118.8(2)
N(19)-C(20)	1.336(4)	C(2)-N(1)-C(6)	117.7(3)
C(2)-H(2)	0.9500	C(6)-N(1)-Ag(1)	122.8(2)
C(2)-C(3)	1.387(5)	N(10)-N(9)-C(7)	117.7(3)
C(3)-H(3)	0.9500	N(10)-N(9)-H(9)	121(2)
C(3)-C(4)	1.396(5)	C(7)-N(9)-H(9)	121(2)
C(4)-C(5)	1.388(5)	C(11)-N(10)-N(9)	119.0(3)
C(4)-C(7)	1.502(5)	C(15)-N(16)-Ag(1)#2	126.2(2)
C(5)-H(5)	0.9500	C(15)-N(16)-C(17)	118.7(3)
C(5)-C(6)	1.383(5)	C(17)-N(16)-Ag(1)#2	115.0(2)
C(6)-H(6)	0.9500	C(18)-N(19)-Ag(1)#2	118.9(2)
C(11)-C(12)	1.477(5)	C(20)-N(19)-Ag(1)#2	122.4(2)
C(11)-C(24)	1.487(5)	C(20)-N(19)-C(18)	118.7(3)
C(12)-C(13)	1.405(5)	N(1)-C(2)-H(2)	118.3
C(12)-C(17)	1.407(5)	N(1)-C(2)-C(3)	123.4(3)
C(13)-H(13)	0.9500	C(3)-C(2)-H(2)	118.3
C(13)-C(14)	1.373(5)	C(2)-C(3)-H(3)	120.7
C(14)-H(14)	0.9500	C(2)-C(3)-C(4)	118.6(3)
C(14)-C(15)	1.395(5)	C(4)-C(3)-H(3)	120.7
C(15)-H(15)	0.9500	C(3)-C(4)-C(7)	116.5(3)
C(17)-C(18)	1.466(5)	C(5)-C(4)-C(3)	118.1(3)
C(18)-C(23)	1.414(5)	C(5)-C(4)-C(7)	125.4(3)
C(20)-H(20)	0.9500	C(4)-C(5)-H(5)	120.3

C(6)-C(5)-C(4)	119.5(3)	C(18)-C(23)-C(24)	120.7(3)
C(6)-C(5)-H(5)	120.3	C(22)-C(23)-C(18)	119.2(3)
N(1)-C(6)-C(5)	122.6(3)	C(22)-C(23)-C(24)	120.1(3)
N(1)-C(6)-H(6)	118.7	O(25)-C(24)-C(11)	122.0(3)
C(5)-C(6)-H(6)	118.7	O(25)-C(24)-C(23)	120.3(3)
O(8)-C(7)-N(9)	123.0(3)	C(23)-C(24)-C(11)	117.8(3)
O(8)-C(7)-C(4)	122.1(3)	O(28)-N(26)-O(27)	119.1(3)
N(9)-C(7)-C(4)	114.8(3)	O(29)-N(26)-O(27)	120.5(3)
N(10)-C(11)-C(12)	115.5(3)	O(29)-N(26)-O(28)	120.4(4)
N(10)-C(11)-C(24)	124.9(3)		
C(12)-C(11)-C(24)	119.6(3)		
C(13)-C(12)-C(11)	121.8(3)		
C(13)-C(12)-C(17)	117.8(3)		
C(17)-C(12)-C(11)	120.3(3)		
C(12)-C(13)-H(13)	120.2		
C(14)-C(13)-C(12)	119.6(3)		
C(14)-C(13)-H(13)	120.2		
C(13)-C(14)-H(14)	120.6		
C(13)-C(14)-C(15)	118.7(3)		
C(15)-C(14)-H(14)	120.6		
N(16)-C(15)-C(14)	123.1(3)		
N(16)-C(15)-H(15)	118.5		
C(14)-C(15)-H(15)	118.5		
N(16)-C(17)-C(12)	122.0(3)		
N(16)-C(17)-C(18)	117.6(3)		
C(12)-C(17)-C(18)	120.5(3)		
N(19)-C(18)-C(17)	118.3(3)		
N(19)-C(18)-C(23)	120.7(3)		
C(23)-C(18)-C(17)	121.0(3)		
N(19)-C(20)-H(20)	118.0		
N(19)-C(20)-C(21)	124.0(3)		
C(21)-C(20)-H(20)	118.0		
C(20)-C(21)-H(21)	121.1		
C(22)-C(21)-C(20)	117.8(3)		
C(22)-C(21)-H(21)	121.1		
C(21)-C(22)-H(22)	120.2		
C(21)-C(22)-C(23)	119.6(3)		
C(23)-C(22)-H(22)	120.2		

Symmetry transformations used to generate equivalent atoms:
#1 x-1,y+1,z-1 #2 x+1,y-1,z+1

Anisotropic displacement parameters ($Å^2 x\ 10^3$) for [Ag(**4.1**)(NO_3)]. The anisotropic displacement factor exponent takes the form: $-2\pi^2[\ h^2\ a^{*2}U^{11} + ...\ + 2\ h\ k\ a^*\ b^*\ U^{12}\ ]$

	U^{11}	U^{22}	U^{33}	U^{23}	U^{13}	U^{12}
Ag(1)	22(1)	19(1)	20(1)	-2(1)	-12(1)	1(1)
O(8)	30(2)	21(2)	26(2)	-5(1)	-14(1)	-4(1)
O(25)	33(2)	24(2)	23(2)	-5(1)	-19(1)	2(1)
N(1)	16(2)	16(2)	15(2)	-1(1)	-6(1)	-2(1)
N(9)	19(2)	18(2)	14(2)	-1(1)	-7(1)	1(1)
N(10)	15(2)	23(2)	13(2)	-2(1)	-4(1)	0(1)
N(16)	17(2)	17(2)	14(2)	-4(1)	-6(1)	0(1)
N(19)	17(2)	18(2)	17(2)	-6(1)	-6(1)	0(1)
C(2)	20(2)	10(2)	18(2)	1(2)	-4(2)	-1(2)
C(3)	18(2)	18(2)	14(2)	-4(2)	-3(2)	-6(2)
C(4)	12(2)	18(2)	13(2)	-2(2)	-4(2)	-1(2)
C(5)	19(2)	13(2)	16(2)	-2(2)	-4(2)	4(2)
C(6)	19(2)	16(2)	19(2)	-6(2)	-4(2)	-3(2)
C(7)	18(2)	21(2)	15(2)	-6(2)	-3(2)	-1(2)
C(11)	13(2)	19(2)	16(2)	-4(2)	-3(2)	1(2)
C(12)	12(2)	20(2)	13(2)	-4(2)	-1(1)	-2(2)
C(13)	18(2)	17(2)	17(2)	1(2)	-2(2)	-3(2)
C(14)	15(2)	17(2)	20(2)	-6(2)	-3(2)	-3(2)
C(15)	15(2)	23(2)	10(2)	-1(2)	-4(2)	-2(2)
C(17)	8(2)	19(2)	13(2)	-4(2)	-4(1)	2(2)
C(18)	14(2)	19(2)	14(2)	-6(2)	1(2)	-2(2)
C(20)	18(2)	13(2)	20(2)	-5(2)	-3(2)	0(2)
C(21)	16(2)	22(2)	21(2)	-9(2)	-3(2)	-4(2)
C(22)	17(2)	26(2)	14(2)	-5(2)	-4(2)	-2(2)
C(23)	15(2)	21(2)	13(2)	-3(2)	-7(2)	0(2)
C(24)	16(2)	19(2)	14(2)	-3(2)	-3(2)	0(2)
O(27)	37(2)	26(2)	28(2)	-6(1)	-12(1)	-3(1)
O(28)	35(2)	26(2)	34(2)	-15(1)	-6(1)	-6(1)

O(29)	49(2)	20(2)	63(2)	-6(2)	-6(2)	-16(2)
N(26)	33(2)	13(2)	26(2)	-3(2)	-14(2)	-3(2)

Hydrogen coordinates (x 10^4) and isotropic displacement parameters ($Å^2$x 10^3) for [Ag(**4.1**)(NO_3)].

	x	y	z	U(eq)
H(2)	2293	10376	-502	21
H(3)	4033	9625	1152	19
H(5)	4159	5782	901	20
H(6)	2284	6630	-640	21
H(13)	8062	5544	5679	22
H(14)	9662	4820	7442	20
H(15)	10599	2506	8238	20
H(20)	8414	-2015	6316	20
H(21)	6964	-1566	4494	22
H(22)	6109	709	3380	23
H(9)	5520(40)	5210(30)	2420(30)	20(11)

Torsion angles [°] for [Ag(**4.1**)(NO_3)].

Ag(1)-N(1)-C(2)-C(3)	169.6(3)	N(10)-N(9)-C(7)-C(4)	-174.9(3)
Ag(1)-N(1)-C(6)-C(5)	-171.6(3)	N(10)-C(11)-C(12)-C(13)	3.0(5)
Ag(1)#2-N(16)-C(15)-C(14)	-173.8(3)	N(10)-C(11)-C(12)-C(17)	-177.8(3)
Ag(1)#2-N(16)-C(17)-C(12)	177.7(3)	N(10)-C(11)-C(24)-O(25)	-3.0(6)
Ag(1)#2-N(16)-C(17)-C(18)	-3.3(4)	N(10)-C(11)-C(24)-C(23)	177.5(3)
Ag(1)#2-N(19)-C(18)-C(17)	-2.2(4)	N(16)-C(17)-C(18)-N(19)	3.7(5)
Ag(1)#2-N(19)-C(18)-C(23)	179.1(3)	N(16)-C(17)-C(18)-C(23)	-177.6(3)
Ag(1)#2-N(19)-C(20)-C(21)	-176.9(3)	N(19)-C(18)-C(23)-C(22)	-2.3(5)
N(1)-C(2)-C(3)-C(4)	2.0(5)	N(19)-C(18)-C(23)-C(24)	176.8(3)
N(9)-N(10)-C(11)-C(12)	179.3(3)	N(19)-C(20)-C(21)-C(22)	-1.8(6)
N(9)-N(10)-C(11)-C(24)	-1.9(5)	C(2)-N(1)-C(6)-C(5)	-0.8(5)
N(10)-N(9)-C(7)-O(8)	1.2(5)	C(2)-C(3)-C(4)-C(5)	-0.2(5)

C(2)-C(3)-C(4)-C(7)	-178.1(3)	C(24)-C(11)-C(12)-C(17)	3.4(5)
C(3)-C(4)-C(5)-C(6)	-2.0(5)		
C(3)-C(4)-C(7)-O(8)	-1.9(5)		
C(3)-C(4)-C(7)-N(9)	174.1(3)		
C(4)-C(5)-C(6)-N(1)	2.6(6)		
C(5)-C(4)-C(7)-O(8)	-179.7(4)		
C(5)-C(4)-C(7)-N(9)	-3.6(5)		
C(6)-N(1)-C(2)-C(3)	-1.5(5)		
C(7)-N(9)-N(10)-C(11)	178.1(3)		
C(7)-C(4)-C(5)-C(6)	175.7(3)		
C(11)-C(12)-C(13)-C(14)	-178.1(3)		
C(11)-C(12)-C(17)-N(16)	176.8(3)		
C(11)-C(12)-C(17)-C(18)	-2.2(5)		
C(12)-C(11)-C(24)-O(25)	175.7(3)		
C(12)-C(11)-C(24)-C(23)	-3.8(5)		
C(12)-C(13)-C(14)-C(15)	0.6(5)		
C(12)-C(17)-C(18)-N(19)	-177.3(3)		
C(12)-C(17)-C(18)-C(23)	1.4(5)		
C(13)-C(12)-C(17)-N(16)	-3.9(5)		
C(13)-C(12)-C(17)-C(18)	177.1(3)		
C(13)-C(14)-C(15)-N(16)	-2.8(5)		
C(15)-N(16)-C(17)-C(12)	1.9(5)		
C(15)-N(16)-C(17)-C(18)	-179.1(3)		
C(17)-N(16)-C(15)-C(14)	1.6(5)		
C(17)-C(12)-C(13)-C(14)	2.6(5)		
C(17)-C(18)-C(23)-C(22)	179.0(3)		
C(17)-C(18)-C(23)-C(24)	-1.9(5)		
C(18)-N(19)-C(20)-C(21)	1.2(5)		
C(18)-C(23)-C(24)-O(25)	-176.4(3)		
C(18)-C(23)-C(24)-C(11)	3.1(5)		
C(20)-N(19)-C(18)-C(17)	179.6(3)		
C(20)-N(19)-C(18)-C(23)	0.9(5)		
C(20)-C(21)-C(22)-C(23)	0.2(5)		
C(21)-C(22)-C(23)-C(18)	1.7(5)		
C(21)-C(22)-C(23)-C(24)	-177.4(3)		
C(22)-C(23)-C(24)-O(25)	2.6(6)		
C(22)-C(23)-C(24)-C(11)	-177.8(3)		
C(24)-C(11)-C(12)-C(13)	-175.8(3)		

Symmetry transformations used to generate equivalent atoms:
#1 x-1,y+1,z-1 #2 x+1,y-1,z+1

Hydrogen bonds for [Ag(**4.1**)(NO_3)] [Å and °].

D-H...A	d(D-H)	d(H...A)	d(D...A)	<(DHA)
C(2)-H(2)...O(28)#3	0.95	2.32	3.090(5)	138
C(6)-H(6)...O(29)#4	0.95	2.39	3.053(5)	127
C(20)-H(20)...O(27)#2	0.95	2.38	3.159(5)	139
C(21)-H(21)...O(8)#5	0.95	2.39	3.192(4)	142

Symmetry transformations used to generate equivalent atoms:

#1 x-1,y+1,z-1 #2 x+1,y-1,z+1 #3 -x,-y+2,-z

#4 -x,-y+1,-z #5 x,y-1,z

4.3a.2$CHCl_3$

Crystal data

$C_{24}H_{14}N_6O_2 \cdot 2(CHCl_3)$	$F(000)$ = 664
M_r = 657.15	D_x = 1.604 Mg m^{-3}
Monoclinic, $P2_1/c$	Mo $K\alpha$ radiation, λ = 0.71073 Å
a = 5.9406 (7) Å	Cell parameters from 5155 reflections
b = 18.856 (2) Å	θ = 2.7–26.1°
c = 12.2375 (16) Å	μ = 0.67 mm^{-1}
β = 96.863 (4)°	T = 150 K
V = 1361.0 (3) $Å^3$	Lath, red
Z = 2	0.43 × 0.05 × 0.04 mm

Data collection

Bruker-Nonius X8APEX-II CCD diffractometer	2732 independent reflections
Radiation source: fine-focus sealed-tube	2068 reflections with $I > 2\sigma(I)$
Detector resolution: 9.1 pixels mm^{-1}	$R_{int} = 0.045$
thin–slice ω and ϕ scans	$\theta_{max} = 26.2°$, $\theta_{min} = 2.7°$
Absorption correction: multi-scan *SADABS* v2012/1, Sheldrick, G.M., (2012)	$h = -5 \rightarrow 7$
$T_{min} = 0.657$, $T_{max} = 0.745$	$k = -23 \rightarrow 23$
18529 measured reflections	$l = -15 \rightarrow 14$

Refinement

Refinement on F^2	Primary atom site location: dual
Least-squares matrix: full	Secondary atom site location: difference Fourier map
$R[F^2 > 2\sigma(F^2)] = 0.044$	Hydrogen site location: mixed
$wR(F^2) = 0.111$	H atoms treated by a mixture of independent and constrained refinement
$S = 1.02$	$w = 1/[\sigma^2(F_o^2) + (0.0444P)^2 + 1.8407P]$ where $P = (F_o^2 + 2F_c^2)/3$
2732 reflections	$(\Delta/\sigma)_{max} = 0.001$
184 parameters	$\Delta\rangle_{max} = 0.87$ e $Å^{-3}$
0 restraints	$\Delta\rangle_{min} = -0.59$ e $Å^{-3}$

Special details

Geometry. All esds (except the esd in the dihedral angle between two l.s. planes) are estimated using the full covariance matrix. The cell esds are taken into account individually in the estimation of esds in distances, angles and torsion angles; correlations between esds in cell parameters are only used when they are defined by crystal symmetry. An approximate (isotropic) treatment of cell esds is used for estimating esds involving l.s. planes.

Fractional atomic coordinates and isotropic or equivalent isotropic displacement parameters (Å^2) for **4.3a.**2$CHCl_3$

	x	*y*	*z*	U_{iso}*/U_{eq}
N1	0.3174 (4)	0.63628 (11)	0.66898 (18)	0.0216 (5)
C1	0.3648 (5)	0.69741 (14)	0.6234 (2)	0.0240 (6)
H1	0.269904	0.736919	0.632910	0.029*
C2	0.5456 (5)	0.70706 (14)	0.5623 (2)	0.0255 (6)
H2	0.572645	0.752054	0.531450	0.031*
C3	0.6846 (4)	0.65044 (14)	0.5473 (2)	0.0219 (6)
H3	0.810516	0.656051	0.507047	0.026*
C4	0.6383 (4)	0.58421 (13)	0.5923 (2)	0.0174 (5)
C5	0.7702 (4)	0.52078 (13)	0.5757 (2)	0.0177 (5)
N2	0.9396 (3)	0.52817 (11)	0.50912 (17)	0.0195 (5)
C6	0.7175 (4)	0.45623 (14)	0.6231 (2)	0.0195 (5)
O1	0.8303 (3)	0.39726 (10)	0.61010 (16)	0.0246 (4)
H1A	0.937 (6)	0.4088 (17)	0.569 (3)	0.037*
C7	0.5313 (4)	0.45226 (13)	0.6889 (2)	0.0191 (5)
C8	0.4726 (5)	0.38783 (14)	0.7366 (2)	0.0239 (6)
H8	0.554738	0.345644	0.726050	0.029*
C9	0.2948 (5)	0.38714 (15)	0.7985 (2)	0.0274 (6)

H9	0.251833	0.344474	0.831710	0.033*
C10	0.1781 (5)	0.45015 (15)	0.8118 (2)	0.0253 (6)
H10	0.057433	0.449191	0.856178	0.030*
N3	0.2257 (4)	0.51143 (12)	0.76615 (18)	0.0224 (5)
C11	0.4006 (4)	0.51294 (13)	0.7050 (2)	0.0182 (5)
C12	0.4522 (4)	0.58002 (13)	0.6541 (2)	0.0185 (5)
C21	0.0382 (5)	0.64497 (15)	0.8784 (2)	0.0271 (6)
H21	0.087592	0.621547	0.811921	0.032*
Cl1	-0.23375 (13)	0.61485 (6)	0.89683 (7)	0.0493 (3)
Cl2	0.03861 (18)	0.73803 (4)	0.85952 (7)	0.0508 (3)
Cl3	0.23081 (12)	0.62261 (4)	0.99506 (6)	0.0333 (2)

Atomic displacement parameters (Å^2) for **4.3a.**2$CHCl_3$

	U^{11}	U^{22}	U^{33}	U^{12}	U^{13}	U^{23}
N1	0.0234 (11)	0.0211 (12)	0.0208 (12)	0.0047 (9)	0.0050 (9)	-0.0007 (9)
C1	0.0290 (14)	0.0208 (15)	0.0229 (14)	0.0070 (11)	0.0065 (11)	-0.0003 (11)
C2	0.0330 (15)	0.0159 (13)	0.0279 (15)	0.0000 (11)	0.0054 (12)	0.0012 (11)
C3	0.0231 (13)	0.0216 (14)	0.0219 (14)	-0.0011 (11)	0.0064 (11)	-0.0016 (11)
C4	0.0192 (13)	0.0169 (13)	0.0160 (12)	0.0001 (10)	0.0008 (10)	-0.0016 (10)
C5	0.0158 (12)	0.0196 (13)	0.0169 (13)	0.0011 (10)	-0.0011 (10)	-0.0021 (10)
N2	0.0180	0.0213	0.0193	0.0023 (8)	0.0020 (9)	-0.0036

	(11)	(11)	(11)			(9)
C6	0.0192 (13)	0.0203 (14)	0.0180 (13)	0.0023 (10)	-0.0011 (10)	-0.0020 (10)
O1	0.0258 (10)	0.0197 (10)	0.0293 (11)	0.0053 (8)	0.0072 (8)	0.0007 (8)
C7	0.0212 (13)	0.0203 (13)	0.0151 (13)	0.0003 (10)	-0.0007 (10)	0.0007 (10)
C8	0.0277 (14)	0.0199 (14)	0.0236 (14)	0.0023 (11)	0.0004 (11)	0.0027 (11)
C9	0.0319 (15)	0.0274 (15)	0.0230 (14)	-0.0046 (12)	0.0036 (12)	0.0063 (12)
C10	0.0244 (14)	0.0290 (15)	0.0236 (14)	-0.0027 (11)	0.0077 (11)	0.0032 (12)
N3	0.0235 (11)	0.0250 (12)	0.0190 (11)	-0.0009 (9)	0.0039 (9)	0.0005 (9)
C11	0.0207 (13)	0.0198 (13)	0.0141 (12)	0.0010 (10)	0.0016 (10)	-0.0020 (10)
C12	0.0199 (13)	0.0196 (13)	0.0156 (13)	0.0008 (10)	0.0008 (10)	-0.0015 (10)
C21	0.0290 (15)	0.0290 (16)	0.0242 (15)	0.0014 (12)	0.0077 (12)	-0.0021 (12)
Cl1	0.0258 (4)	0.0875 (7)	0.0346 (5)	-0.0121 (4)	0.0037 (3)	-0.0095 (4)
Cl2	0.0818 (7)	0.0295 (4)	0.0438 (5)	0.0156 (4)	0.0196 (5)	0.0009 (4)
Cl3	0.0273 (4)	0.0379 (4)	0.0339 (4)	-0.0051 (3)	0.0008 (3)	0.0002 (3)

Geometric parameters (Å, º) for **4.3a.**2$CHCl_3$

N1—C1	1.326 (3)	O1—H1A	0.88 (3)
N1—C12	1.355 (3)	C7—C11	1.409 (4)
C1—C2	1.392 (4)	C7—C8	1.409 (4)
C1—H1	0.9500	C8—C9	1.371 (4)
C2—C3	1.375 (4)	C8—H8	0.9500
C2—H2	0.9500	C9—C10	1.395 (4)
C3—C4	1.405 (4)	C9—H9	0.9500
C3—H3	0.9500	C10—N3	1.328 (3)
C4—C12	1.414 (3)	C10—H10	0.9500
C4—C5	1.457 (3)	N3—C11	1.352 (3)
C5—N2	1.376 (3)	C11—C12	1.459 (4)
C5—C6	1.400 (4)	C21—Cl1	1.752 (3)
N2—N2^{i}	1.316 (4)	C21—Cl2	1.770 (3)
C6—O1	1.318 (3)	C21—Cl3	1.771 (3)
C6—C7	1.446 (4)	C21—H21	1.0000

C1—N1—C12	117.7 (2)	C8—C7—C6	121.2 (2)
N1—C1—C2	123.8 (2)	C9—C8—C7	118.8 (2)
N1—C1—H1	118.1	C9—C8—H8	120.6
C2—C1—H1	118.1	C7—C8—H8	120.6
C3—C2—C1	118.9 (3)	C8—C9—C10	118.9 (3)
C3—C2—H2	120.5	C8—C9—H9	120.6
C1—C2—H2	120.5	C10—C9—H9	120.6
C2—C3—C4	119.3 (2)	N3—C10—C9	123.9 (2)
C2—C3—H3	120.3	N3—C10—H10	118.0

C4—C3—H3	120.3	C9—C10—H10	118.0
C3—C4—C12	117.4 (2)	C10—N3—C11	117.9 (2)
C3—C4—C5	122.8 (2)	N3—C11—C7	122.2 (2)
C12—C4—C5	119.8 (2)	N3—C11—C12	118.0 (2)
N2—C5—C6	123.3 (2)	C7—C11—C12	119.8 (2)
N2—C5—C4	116.3 (2)	N1—C12—C4	122.7 (2)
C6—C5—C4	120.4 (2)	N1—C12—C11	117.6 (2)
$N2^{i}$—N2—C5	118.1 (3)	C4—C12—C11	119.6 (2)
O1—C6—C5	122.8 (2)	Cl1—C21—Cl2	110.73 (16)
O1—C6—C7	117.2 (2)	Cl1—C21—Cl3	109.64 (15)
C5—C6—C7	120.0 (2)	Cl2—C21—Cl3	109.29 (16)
C6—O1—H1A	106 (2)	Cl1—C21—H21	109.1
C11—C7—C8	118.3 (2)	Cl2—C21—H21	109.1
C11—C7—C6	120.4 (2)	Cl3—C21—H21	109.1

Symmetry code: (i) -*x*+2, -*y*+1, -*z*+1.

Hydrogen-bond geometry (Å, º) for **4.3a.**2$CHCl_3$

D—H···*A*	*D*—H	H···*A*	*D*···*A*	*D*—H···*A*
O1—H1*A*···$N2^{i}$	0.88 (3)	1.74 (3)	2.540 (3)	149 (3)
C21—H21···N1	1.00	2.36	3.219 (3)	143
C21—H21···N3	1.00	2.33	3.136 (4)	137

Symmetry code: (i) -*x*+2, -*y*+1, -*z*+1.

^{1}H NMR Spectral Data from Stability Testing of 4.2a1, 4.2a1, 4.2a1

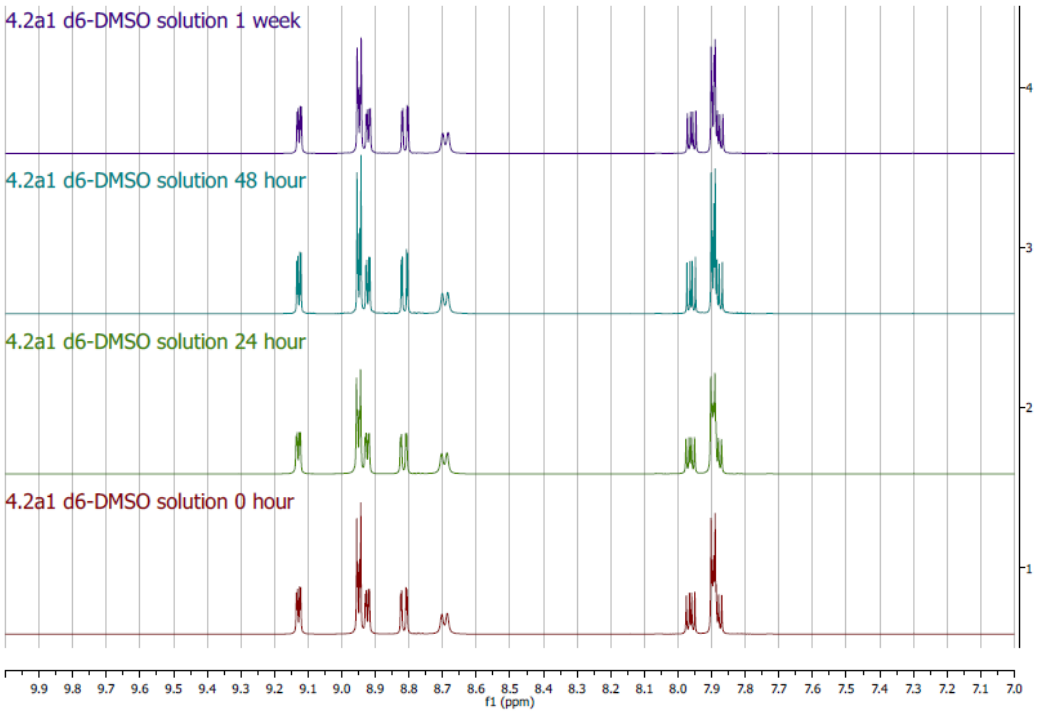

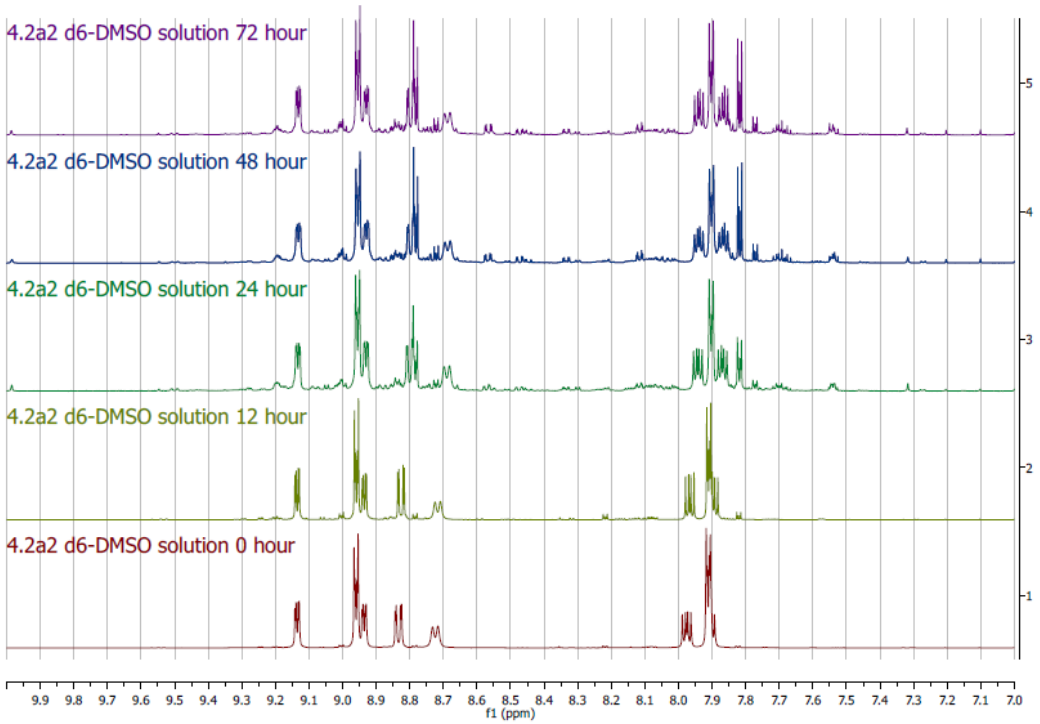

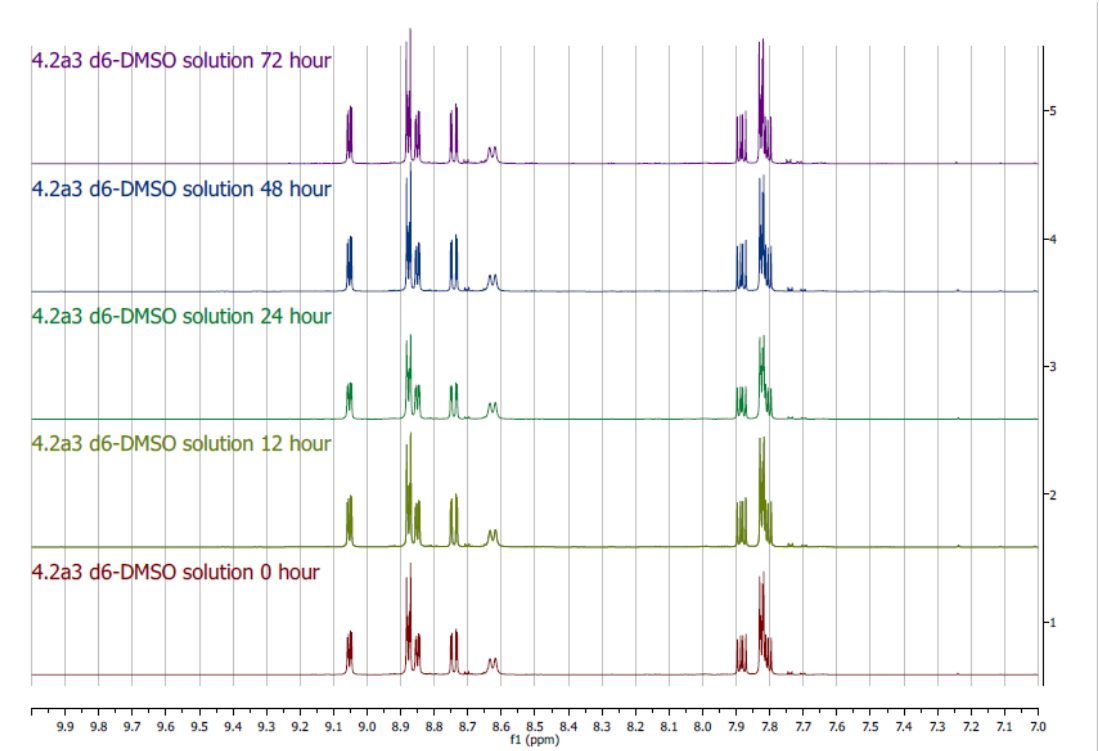
4.2a3 d6-DMSO solution 72 hour
4.2a3 d6-DMSO solution 48 hour
4.2a3 d6-DMSO solution 24 hour
4.2a3 d6-DMSO solution 12 hour
4.2a3 d6-DMSO solution 0 hour
5
4
3
2
1
9.9 9.8 9.7 9.6 9.5 9.4 9.3 9.2 9.1 9.0 8.9 8.8 8.7 8.6 8.5 8.4 8.3 8.2 8.1 8.0 7.9 7.8 7.7 7.6 7.5 7.4 7.3 7.2 7.1 7.0
f1 (ppm)